SKELETAL MUSCLE REMODELLING UNDER DISTINCT LOADING STATES

SKELETAL MUSCLE REMODELLING UNDER DISTINCT LOADING STATES IN

YOUNG MEN

By: TANNER STOKES, B.Sc. Kin (HONS)

A Thesis

Submitted to the School of Graduate Studies in Partial Fulfillment of the

Requirements for the Degree

Doctor of Philosophy

DOCTOR OF PHILOSOPHY (2022)　　　　　　　McMaster University

(Kinesiology)　　　　　　　　　　　　　　　Hamilton, Ontario

TITLE:　　　Skeletal muscle remodelling under distinct loading states in young men

AUTHOR:　　Tanner Stokes

　　　　　　Hons.B.Sc.Kin (McMaster University)

SUPERVISOR: Dr. Stuart M. Phillips, Ph.D.

NUMBER OF PAGES: xix, 155

LAY ABSTRACT

Adaptations of skeletal muscle to loading and unloading are variable between individuals. Herein, we employed a unilateral approach to better understand the drivers of this variability by assessing the influence of resistance training (RT) and disuse on muscle protein turnover and gene expression. First, we validated the use of ultrasound for measuring changes in muscle size in response to loading and unloading. We then identified thousands of genes regulated by loading status and discovered many that were correlated with lean mass gain – some of which would not have been detected without our model. We also demonstrated that RT-induced increases in muscle protein synthesis were not associated with changes in muscle size; however, reductions in muscle protein synthesis were associated with the degree of muscle atrophy observed in response to disuse. Together, these studies contribute significantly to our understanding of how skeletal muscle size is regulated by muscle loading and unloading.

ABSTRACT

Skeletal muscle is a plastic tissue capable of responding to environmental perturbations. Increased loading via resistance exercise (RE) activates muscle protein synthesis (MPS) and, to a lesser extent, muscle protein breakdown (MPB). The ingestion of protein further stimulates MPS and suppresses MPB, inducing a positive net protein balance and protein accretion – i.e., muscle hypertrophy. In contrast, muscle unloading reduces MPS, which is thought to be the key driver underpinning skeletal muscle atrophy. The degree of muscle hypertrophy and atrophy in response to loading and unloading varies significantly between individuals and provides an opportunity to investigate the molecular regulators of skeletal muscle remodelling. To that end, we developed a novel unilateral model in which one leg was subjected to RE to induce hypertrophy (Hyp) and the contralateral limb was immobilized to induce atrophy (At). In study 1, we characterized the morphological changes induced by our HypAt model and validated the use of ultrasonography to measure changes in muscle size in both limbs. We discovered that by assessing the differential change in muscle size between legs we reduced the coefficient of variation between subjects. This enabled a more in-depth means-based characterization of the molecular regulators of skeletal muscle remodelling. Indeed, we discovered significantly more genes regulated by muscle remodelling than similarly-sized studies. We also identified a transcriptional signature that scaled with lean mass gains in three independent cohorts and included RNA species that were only modulated at their untranslated regions. Finally, in study 3 we simultaneously measured MPS and MPB in response to short-term immobilization (4 days) and demonstrated for the first time that

MPB is statistically unchanged by unloading. Taken together, these studies contribute significantly to our understanding of skeletal muscle remodelling under different loading states and provide a valuable hypothesis-generating resource for future research in the field.

ACKNOWLEDGEMENTS

To Stu, I am deeply grateful for the opportunities you have given me. Your love of science is palpable and contagious. Being a curious person myself, I knew that I would thrive under your supervision. Your intelligence and relentless pursuit of excellence are only surpassed by your devotion to your trainees. I couldn't have asked for a better mentor. Thank you.

To Drs. Gibala and Ljubicic, thank you for your continued support, guidance, and insightful comments throughout my Ph.D. Your perspectives were invaluable and truly appreciated.

To Dr. Jamie Timmons, thank you for your patience in fielding countless questions relating to bioinformatics and computational biology. You are one of the most intelligent individuals I have ever met, and it was a privilege working with and learning from you.

To Todd, thank you for your assistance with all the logistical aspects of conducting research and for lending a helping hand on a day-to-day basis. You are the glue that holds the lab together.

To Chris, thank you for your mentorship as I found my footing as a scientist. Thank you for the countless hours you've spent over the years editing my work and helping me develop the soft skills necessary for success in academia and in life. More importantly, thank you for being a great friend.

To the EMRG group, past and present, including Sara, Rob, Michaela, Caoileann, Kirsten, Amy, Sophie, James, Everson, Tanya, Stefan, Dan, Changhyun, Brad, Jonathan, Aaron, Lauren, Sidney, Giulia, Alysha, Linda, and Mai, thank you for all the laughs, the helping hands, and the words of encouragement. I will cherish the experiences we've shared together.

To my family, thank you for your unconditional support of my academic pursuits and encouraging me to do things the right way – not the easy way. I am aware of the sacrifices you've made for me to have this opportunity and for that I will be forever greatful.

To Josie, thank you for always being there for me to lean on. Whether it was editing my work, watching my presentations, or getting me away from my computer when needed, your support has been unwavering.

TABLE OF CONTENTS

LIST OF FIGURES AND TABLES

FIGURES:

CHAPTER 4: Declines in muscle protein synthesis account for short-term muscle disuse atrophy in humans in the absence of increased muscle protein breakdown

CHAPTER 5: DISCUSSION

TABLES:

LIST OF ABBREVIATIONS

4EBP1	eIF4E Binding Protein 1
A-V Balance	Arteriovenous Balance
Akt	Protein Kinase B
ATF4	Activating Transcription Factor 4
ATP	Adenosine Triphosphate
B-mode	Brightness Mode
BCAT2	Branched Chain Amino Acid Transaminase 2
BIA	Bioelectrical Impedance Analysis
Ca	Calcium
COPD	Chronic Obstructive Pulmonary Disease
CS	Citrate Synthase
CSA	Cross Sectional Area
CT	Computed Tomography
D_2O	Deuterium Oxide
DDN	Data-Driven Network Analysis
DEG	Differentially Expressed Gene
DEPTOR	DEP Domain Containing mTOR Interacting Protein
DOCK1	Dedicator of Cytokinesis 1
DXA	Dual Energy X-ray Absorptiometry
ECM	Extracellular Matrix
eEF2	Eukaryotic Elongation Factor 2
eIF2	Eukaryotic Initiation Factor 2
eIF3F	Eukaryotic Initiation Factor 3F
eIF4A	Eukaryotic Initiation Factor 4A
eIF4B	Eukaryotic Initiation Factor 4B
eIF4E	Eukaryotic Initiation Factor 4E
eIF4F	Eukaryotic Initiation Factor 4F
eIF4G	Eukaryotic Initiation Factor 4G
EIF6	Eukaryotic Initiation Factor 6
EXT1	Exostosin-1
FAK	Focal Adhesion Kinase
FKBP1A	FKBP Prolyl Isomerase 1A
FOXO3	Forkhead Box O-3
GO	Gene Ontology
GTP	Guanosine Triphosphate
HypAt	Hypertrophy and Atrophy Model
ICC	Intra/Inter-class Correlation Coefficient
ICU	Intensive Care Unit
IPA	Ingenuity Pathway Analysis
ITM2A	Integral Membrane Protein 2A
MAFBx	Muscle Atrophy F-Box
MEF2C	Myocyte Enhancer Factor 2C

Met	Methionine
MIF	Muscle Intracellular Free Pool
MPB	Muscle Protein Breakdown
MPS	Muscle Protein Synthesis
MRI	Magnetic Resonance Imaging
mRNA	Messenger ribonucleic acid
MT	Muscle Thickness
mTORC1	Mechanistic target of Rapamycin Complex 1
MuRF1	Muscle RING Finger 1
NBAL	Net Balance
NDUFS3	NADH:Ubiquinone Oxidoreductase Core Subunit S3
NRA4A3	Nuclear Receptor Subfamily 4 Group A Member 3
P70S6K1	S6 Kinase 1
PCR	Polymerase Chain Reaction
PGC-1	Peroxisome Proliferator-Activated Receptor Gamma Coactivator 1-alpha
PIC	Pre-initiation Complex
rDNA	Ribosomal DNA
RE	Resistance Exercise
RNAi	RNA inhibition
rpS6	Ribosomal Protein S6
RT	Resistance Training
SC	Satellite Cells
SREBP1	Sterol Regulatory Element-Binding Protein 1
Thr389	Threonine Site 389
TIF-1A	Transcription Initiation Factor 1A
TM4SF18	Transmembrane 4 L Six Family Member 18
tRNA	Transfer ribonucleic acid
UBF	Upstream Binding Factor
UPS	Ubiquitin Proteasome System
US	Ultrasonography
UTR	Untranslated Region
VL CSA	*Vastus Lateralis* CSA

PREFACE:

DECLARATION OF ACADEMIC ACHEIVEMENT

FORMAT AND ORGANIZATION OF THESIS

This thesis is prepared in the "sandwich" format as outlined in the School of Graduate Studies Guide for the Preparation of Theses. It includes a general introduction, three original research papers prepared in journal article format, and a general discussion. The candidate is the first author on manuscripts 1 and 2, and joint first author on manuscript 3. At the time of thesis preparation Chapter 2, 3, and 4 were published in peer-reviewed journals.

CONTRIBUTION TO PAPERS WITH MULTIPLE AUTHORSHIPS

Chapter 1: Literature review (certain sections)

Introduction and Muscle Protein Turnover Sections:

Stokes, T., Hector, A.J., Morton, R.W., McGlory, C., Phillips, S.M. (2018). Recent perspectives regarding the role of dietary protein for the promotion of muscle hypertrophy with resistance exercise training. *Nutrients.* Feb 7;10(2):180.

Atrophy Section:

Nunes, E.A., **Stokes, T.**, McKendry, J., Currier, B.S., Phillips, S.M. (2022) Disuse-induced skeletal muscle atrophy in disease and non-disease states in humans: 2 mechanisms, prevention, and recovery strategies. Submitted to *Am. J. Physiol. Cell. Physiol.*

Omics Sections:

McKendry, J., **Stokes, T.**, Mcleod, J.C., Phillips, S.M. (2021) Resistance Exercise, Aging, Disuse, and Muscle Protein Metabolism. *Compr. Physiol.* Jun 30;11(3):2249-2278.

Contributions:

T.S. wrote the sections of the aforementioned review articles that are included in this thesis. All authors edited and approved the final version of the manuscripts.

Chapter 2:

Methodological considerations for and validation of the ultrasonographic determination of human skeletal muscle hypertrophy and atrophy. Published in *Physiological Reports.* 2021. 9(1): e14683

Contribution:

T.S., and S.M.P., designed the main validation study. R.W.M., S.Y.O., S.M.P., and M.J.M., designed the muscle thickness trial that investigated the influence of probe pressure on muscle thickness measurements. T.S., T.R.T., and K.M., collected and analyzed data for the validation study and R.W.M., S.Y.O., H.L.C., J.M., C.M., collected and analyzed data for the muscle thickness investigation. T.S., and S.M.P. wrote the manuscript. All authors edited and approved of the final manuscript.

Chapter 3:

Molecular Transducers of Human Skeletal Muscle Remodelling under Different Loading States. Published in *Cell Reports* 2020. 32(5): 107980

Contribution:

The project analysis strategy was established by J.A.T., T.S., and S.M.P. The HypAt clinical study was designed by T.S. and S.M.P., while the additional clinical studies were designed by S.M.P., J.A.T., B.P., and P.J.A. T.S., T.R.T., K.M., C.M., B.P., and S.B. conducted the clinical research and performed the sample collection. T.S., T.R.T., and K.M. performed the sample analysis. T.S., T.R.T., B.P., and S.M.P. analyzed the clinical data. H.C., J.A.T., and P.J.A. planned the cell biology work, and H.C. carried out that work. The transcriptome methods and primary statistical analysis was carried out by J.A.T. The custom chip definition file (CDF) method to quantify UTRs was conceived by J.A.T. and developed by J.A.T. The secondary data analysis and literature assessments were carried out by T.S., S.M.P., and J.A.T. The manuscript was drafted by T.S., J.A.T., and S.M.P., and all of the authors edited and approved the final version of the manuscript.

Chapter 4:

Declines in muscle protein synthesis account for short-term muscle disuse atrophy in humans in the absence of increased muscle protein breakdown. Accepted at the *Journal of Cachexia, Sarcopenia, and Muscle*.

Contribution:

T.S., M.S.B., S.H.M.G., S.M.P., K.S., and P.J.A designed the study. T.S., S.H.M., C.M., and S.M.P., performed data collection. T.S., M.S.B., S.H.M.G., J.J.B., J.C., D.J.W., B.E.W., K.S., S.M.P., and P.J.A. performed data analysis. M.S.B., and P.J.A. wrote the manscript. All authors edited and approved of the final manuscript.

CHAPTER 1:

INTRODUCTION

1.1 The importance of skeletal muscle

Skeletal muscle is critical for the promotion and maintenance of metabolic health and for providing the force necessary to complete activities of daily living. Although individual variation exists, skeletal muscle accounts for ~40% of total body mass[1] in humans and is one of the largest contributors to basal metabolic rate.[2] Skeletal muscle is also the primary depot site for blood-borne glucose in the postprandial state,[3] and is the largest reservoir of amino acids that can be liberated into the systemic circulation in the postabsorptive state. Therefore, it is unsurprising that depletion of skeletal muscle beyond a certain point is incompatible with life.

Skeletal muscle is hierarchically organized. The primary contractile units of muscle are sarcomeres, which are linked to one another in series to form myofibrils. Myofibrils, in turn, are suspended in a sarcoplasmic matrix and enveloped in a lipid bilayer membrane (i.e., sarcolemma) to form muscle fibres. Because of their unusually long length,[4] muscle fibers are multinucleated with each nuclei governing the transcription of a defined sarcoplasmic volume. Importantly, muscle fibers are post-mitotic, implying that their repair and regeneration rely on resident stem cells, called satellite cells,[5] that reside between the sarcolemma and basement membrane. Several other mononuclear cells (i.e., immune cells, fibroblasts, fibroadipogenic cells, endothelial cells, etc.) reside within and contribute to skeletal muscle homeostasis by responding to mechanical and/or humoral stimuli.

Muscle fibers are clustered into groups to form fascicles, which are bundled together to form the muscle. Each level of organization is enveloped in a connective

tissue layer: muscle fibers are surrounded by endomysium, fascicles by perimysium, and the whole muscle by epimysium. These connective tissue structures are important for the transmission of contractile force and are dynamically regulated to enable either the growth or loss of muscle mass in response to environmental perturbations including loading and unloading.

1.2 The influence of loading on skeletal muscle size

Skeletal muscle hypertrophy is a defining physiological adaptation following resistance training (RT). Intuitively, muscle hypertrophy results from exercise-induced contractile (i.e., myofibrillar) protein accretion; however, changes in myofibrillar protein concentrations are rarely measured in response to RT. Instead, changes in whole-muscle cross-sectional area (CSA), muscle volume, and/or muscle thickness are frequently quantified to assess the radial growth of the whole muscle, or immunohistochemical methods are used to measure individual muscle fibre CSA. These methods do not directly measure myofibrillar protein accretion *per se*, but a composite of connective tissue, sarcoplasmic, and myofibrillar protein accretion. For the purposes of this thesis, muscle hypertrophy will be defined as the radial expansion of skeletal muscle at a fibre- or whole-muscle level.

The rate of muscle hypertrophy is most rapid during the first 8 weeks of a resistance training (RT) program, proceding at progressively slower rates thereafter. Indeed, quadriceps CSA increases by ~5%, ~10%, and ~12% after 2, 4, and 6 months of progressive resistance training, respectively.[6] In bodybuilders with 5 years of RT experience, a 24-week training program failed to increase elbow flexor CSA further,[7]

indicating that a plateau in hypertrophic potential is eventually reached. Although protein accretion could conceivably occur following the first few RE bouts, the exact point in time when true muscle hypertrophy is detectable using current methods is debated. DeFreitas et al.[8] observed significant increases in quadriceps muscle CSA after only two RE bouts in untrained men, leading the authors to conclude that muscle hypertrophy occurs within the first 1-3 weeks of RT; however, our laboratory subsequently demonstrated that the 'hypertrophy' reported by DeFreitas and colleagues was actually due to edema and muscle swelling rather than muscle hypertrophy *per se*,[9] which is thought to occur after 3 weeks of RT.[10] In addition to changes in whole-muscle CSA, chronic RT alters the pennation angle of muscle fibres[11] and induces a fibre-type shift from type IIx to type IIa.[12] Together, these phenotypic adaptations alter the functional characteristics of skeletal muscle to enable a more efficient defence against future perturbations to homeostasis induced by resistance exercise (RE).

Although hypertrophy is consistently observed after RT on average, there is marked variability in the degree of response between individuals.[12-15] Hubal and colleagues were the first to formally study individual responses to 12 weeks of upper body RT in a large cohort in men and women and observed biceps brachii hypertrophy ranging from -2% to +59%, independent of sex.[15] Interindividual heterogeneity was also observed at the myofibre level in response to 16 weeks of knee extensor RT with the average change in myofibre CSA of -16 μm^2 ($\pm$ 99 μm^2), +1,111 μm^2 ($\pm$ 46 μm^2), and +2,475 μm^2 ($\pm$ 140 μm^2) in 'non-', 'moderate-', and 'extreme-responders', respectively.[16] Finally, our laboratory has observed a ~4-fold greater increase in lean body mass in

'higher' versus 'lower' responders following 12-weeks of whole-body resistance exercise.[17] Taken together, it is clear that RT leads to heterogeneous responses at the whole-body, whole-muscle and muscle fibre levels. It is common practice to 'collapse' these differences across participants and perform means-based comparisons on the data; however, response variability presents a unique opportunity to study the molecular regulators of muscle growth,[18] especially when combined with global 'omics' profiling technology.

1.3 The influence of unloading on skeletal muscle size

Muscle disuse occurs for several reasons, including clinically mandated bed rest, immobilization, limb suspension, or a voluntary reduction in physical activity (*i.e.,* sedentary behaviour). In contrast with muscle hypertrophy, which is a relatively slow and progressive process, muscle atrophy occurs within days of unloading and follows an exponential decay, reaching a plateau after several weeks.[19,20] Indeed, whole-quadriceps CSA is reduced by ~2.6%,[19] 3.9%,[21] and 7.2%[19] after 2, 5, and 7 days of limb immobilization, respectively, equating to ~0.8%-1.3% per day. When assessed after 2-4 weeks of limb immobilization, atrophy rates are approximately half of what they are during the first week, progressing at ~0.3 – 0.7% per day.[22-26] A similar pattern of atrophy is also observed when assessing quadriceps volume, albeit at marginally slower rates (0.7-0.85% per day during the first 2-7 days of unloading, and 0.2 – 0.6% in response to 2-5 weeks of unloading).[19,27,28] Finally, and per whole-muscle morphological data, myofibre atrophy proceeds more precipitously in response to 2 weeks vs. 5 weeks of

immobilization (~0.7% per day and ~0.5% per day, respectively), with minimal differences between fibre type.[22,27,29,30]

Disuse-induced muscle atrophy is also markedly heterogeneous between individuals.[23,31,32] For example, Chen and colleagues[32] observed an average decline of ~10% in medial gastrocnemius CSA following 4-6 weeks of ankle immobilization in young men and women who had sustained an injury to their lower limb. However, grouping participants into different responder categories using an *a priori*-defined criteria revealed non-significant muscle atrophy in designated 'low' responders (0.1 %) and ~15% atrophy in 'high' responders.[32] Resembling the heterogeneous responses to RT, the high- and low-responders to muscle disuse also demonstrated distinct molecular profiles, providing unique insight into the molecular regulation of muscle atrophy. Nonetheless, 'response' criteria was arbitrarily defined and included only participants at the extremes of adaptive responses – an approach that would not be feasible for invasive physiology studies that recruit a limited number of participants. Instead, a better approach would be to identify molecular events that scale with the degree of physiological response observed – i.e., considering all participant data.

1.4 Regulation of muscle protein turnover

Changes in muscle size are mediated, in part, by changes in muscle protein turnover, the rate of which is dependent on the balance between two opposing yet interrelated kinetic processes: MPS and MPB. In the fasted state, MPB predominates as intact muscle proteins are catabolized to supply amino acids for energy production and protein synthesis of acute phase proteins, resulting in skeletal muscle catabolism.[33]

Exposure to anabolic stimuli – namely dietary protein and skeletal muscle loading – acutely and chronically influences MPS, MPB and, eventually, skeletal muscle protein abundance.[34] Thus, quantifying these processes provides insight into the regulation of skeletal muscle size not possible with static molecular readouts.

1.4.1 Muscle protein synthesis

Muscle protein synthesis is the coordinated series of events in which messenger RNA (mRNA) is translated into a polypeptide chain. The translation process can be divided into three steps: initiation, elongation, and termination. Translation initiation involves the formation of a 43S preinitiation complex (PIC), consisting of the 40S ribosomal subunit, a ternary complex consisting of eIF2-GTP-Met-tRNA, and a suite of initiation factors.[35] Once formed, the 43S PIC is recruited to the 5'cap of mRNA through interactions with the eIF4F complex comprised of eIF4E, eIF4A, and eIF4G. Upon binding to the 5'cap, the 43S PIC scans the 5'UTR until encountering an AUG start codon, at which time eIF2-GTP is hydrolyzed and released along with several initiation factors.[35] The 60S subunit then binds to the 40S subunit, forming the 80S ribosomal complex. During elongation, the ribosome translocates along the mRNA one codon at a time and incorporates the corresponding amino acid into the growing polypeptide structure. This series of reactions proceeds until the ribosome encounters a stop codon, at which point termination factors trigger the release of the 80S ribosome from the mRNA template. Each step requires energy in the form GTP, however, translation initiation is considered a key rate-limiting step and thus a nodal point for regulation of MPS.[35]

At the molecular level, MPS can be altered by modulation of translational efficiency and/or translational capacity. Translational efficiency represents the rate at which mRNA is translated (initiation, elongation, and termination) into protein per ribosome. Increases in translational capacity are manifest as increases in the cellular machinery (predominantly ribosomes) available to synthesize proteins from mRNA template and so could increase the rate of MPS. Both translational efficiency and capacity are modulated primarily by the serine/threonine protein kinase known as the mechanistic target of rapamycin complex 1 (mTORC1). mTORC1 regulates several downstream effectors of anabolism and catabolism; however, the most relevant substrates for modulating translation efficiency include 4EBP1 and p70S6K1. Phosphorylation of 4EBP1 on Thr36/47 leads to its dissociation from eIF4E,[36,37] enabling the formation of the eIF4F complex and the recruitment of the 43S PIC to the 5'cap of mRNA. p70S6K1 is phosphorylated on Thr389 by mTORC1,[38] leading to inhibition of PDCD4[39] – an upstream inhibitor of eIF4A – and activation of eIF4B.[40] Collectively, these phosphorylation events increase translation initiation and elongation. mTORC1 also plays an important role in modulating translational capacity. Indeed, mTORC1 phosphorylates UBF[41] and TIF-1A,[42] leading to increased RNA polymerase-1-dependent rRNA transcription. Because an increase in ribosomal biogenesis requires purine and pyrimidine nucleotides, it is unsurprising that mTORC1 also regulates the synthesis of these molecules. Purine synthesis is regulated at the transcriptional level through mTORC1-mediated regulation of ATF4, which activates the mitochondrial tetrahydrofolate cycle leading to the production of precursors needed for purine synthesis.[43] Moreover,

p70S6K1 phosphorylates and activates carbamoyl-phosphate synthetase 2, aspartate transcarbamoylase, dihydroorotatase (CAD), which catalyzes the initial steps of pyrimidine synthesis needed for ribosome production.[44] Taken together, mTORC1 is a key regulatory hub that integrates signals from growth factors, amino acids, and mechanical stimuli to regulate downstream effectors of translational efficiency and capacity.

As myofibre hypertrophy ensues, the cytoplasmic volume governed by existing myonuclei expands. It is thought that the expansion of the 'myonuclear domain' results in a 'strain' on the capacity of existing myonuclei to provide mRNA templates to synthesize proteins. Continued myofibre growth beyond a certain point, therefore, is thought to require nuclear donation from resident muscle stem cells – i.e., satellite cells – to maintain a given myonuclear doman size. Indeed, once SCs become activated by mechanical and humoral signals, they proliferate and, depending on the transcriptional factors activated, can return to a quiescent state and/or undergo differentiation and donate their nuclei to muscle fibres. In this manner, the myonuclear domain can be maintained in the presence of myofibre hypertrophy. It has also been hypothesized that myonuclear accretion is required to supply rDNA substrate for ribosomal biogenesis;[45] however, this view has been challenged on the basis that each cell contains hundreds or even thousands of rDNA repeats, implying that copy number is not a limiting factor for ribosomal biogenesis.[46,47] SCs also communicate with other cell types in skeletal muscle, including endothelial cells and fibroblasts, implicating their involvement in angiogenesis and extracellular matrix remodelling, respectively.[48] Therefore, mTORC1 signalling,

ribosomal biogenesis, and satellite-cell mediated myonuclear accretion and signalling all appear to be important components involved in MPS and, by extension, muscle hypertrophy.

1.4.2 Muscle protein breakdown

Muscle protein breakdown (MPB) occurs via the coordinated activity of four interdependent proteolytic pathways. The ubiquitin-proteasome system (UPS) degrades the majority of cellular proteins.[49] Degradation by the UPS begins with the ATP-dependent activation of ubiquitin by a single ubiquitin-activating enzyme (E1), which is subsequently transferred to one of several ubiquitin carrier proteins (E2).[50] Finally, E3 ubiquitin ligase enzymes catalyze the transfer of ubiquitin to the lysine residue of the target protein.[50] Subsequent iterations of this cycle results in the polyubiquitination of target proteins, enabling their interaction with, and subsequent degradation by, the 26S proteasome. An estimated 500-1000 E3 ligases exist in humans;[51] however, research attention has primarily focused on MuRF1 and MAFBx (atrogin-1) because they are muscle-specific, and their genes are consistently expressed in several pre-clinical models of muscle wasting and atrophy.[52] Nonetheless, this myopic approach has hindered our understanding of muscle atrophy in contexts devoid of perturbations of these two E3 ligases.

Despite its centrality in protein breakdown, the UPS does not degrade intact myofibrillar proteins directly,[53] implying that a preceding step is required for their initial release from the structured lattice. Caspases are activated by pro-apoptotic stimuli and cleave actomyosin complexes *in vitro*, which significantly accelerates ATP-dependent

proteolysis.[54] Furthermore, the Ca^{2+}- dependent calpains are also important for the initial liberation of myofibrillar proteins because they degrade proteins that maintain the structural integrity of the sarcomere, including nebulin, titin, α-actinin and desmin.[55] Finally, the autophagy-lysosomal system is responsible for degrading damaged organelles (i.e., ribosomes, peroxisomes, and mitochondria), long-lived proteins, and protein aggregates.[56] Macroautophagy begins with the formation and nucleation of an isolation membrane, followed by its elongation and closure to form an autophagosome.[56] The autophagosome subsequently fuses with the lysosome, and cathepsin proteases degrade the engulfed protein cargo within the acidic lysosomal lumen. Selective breakdown of organelles, including the mitochondria (i.e., via mitophagy), is accomplished by specific adaptor proteins that interact with the autophagy machinery and molecules on the damaged organelle.[56] Although several investigations have probed individual components of these proteolytic pathways to infer changes in MPB, such approaches cannot adequately capture the dynamic nature of these processes during loading and unloading.

1.5 Measuring muscle protein turnover using stable isotopes

The ability to quantify the dynamic synthesis and degradation of proteins was made possible via the application of isotope tracers. An isotope of an element varies not in the number of protons contained within the nucleus but in the number of neutrons, resulting in mass variants that, when incorporated into certain chemical compounds (*i.e.,* amino acids), can be used to trace the metabolic fate of that compound into various macromolecular structures (*i.e.,* skeletal muscle protein). Prior to the pioneering work of Rudolf Schoenheimer in the 1930's, tissue proteins were thought to be inert in weight-

neutral adults. However, Schoenheimer demonstrated that amino acids containing the isotopes ^{15}N and ^{2}H were incorporated into the tissue protein of rats, which could only have occurred if peptide bonds were being broken and reformed.[57,58] Two years later, Hans Ussing measured protein synthesis rates in different organ tissues using deuterium oxide (D_2O) and demonstrated that the small intestine, liver and kidney incorporated deuterium more rapidly than proteins in the skin and skeletal muscle.[59] These pioneering studies revealed the underlying dynamic nature of proteins in mammalian organisms and sparked an interest in using radioactive and stable isotopes to study protein turnover in humans.

To measure MPS, isotope labels are introduced into the body using one of two strategies. The most frequently used approach, until recently, involves infusing an isotopically-labelled amino acid tracer into the circulation, which is then actively transported across the sarcolemma to enrich the muscle intracellular free (MIF) pool. Once isotopic steady-state is achieved in either the arterial or MIF pools, serial muscle biopsies are obtained, usually, several hours apart, and the change in protein-bound tracer enrichment is measured to calculate the fractional synthetic rate (the fraction of a pool synthesized per unit time; see Figure 1).[60] While this approach is highly sensitive to the acute stimulation of MPS in response to protein ingestion and muscle contraction, it is limited by a requirement for highly controlled laboratory conditions and may not generalize to free-living conditions.

A second approach that circumvents many of the above limitations involves introducing deuterium (^{2}H) into the body via orally ingested deuterated water (D_2O).[61]

Through intermediary reactions, deuterium is introduced into amino acids at carbon-hydrogen bonding sites. Although all amino acids become labelled at their alpha-hydrogens through transaminase reactions, alanine is the most frequently studied amino acid probe because it can be labelled at 4 positions, thus increasing analytical sensitivity. When compared to labelled amino acid tracer infusions, D_2O has the advantage of being relatively non-invasive and easily administered (i.e., via oral ingestion), which, when combined with its half-life of 7-11 days, enables assessments of free-living MPS (i.e., incorporating diet as well as periods of sedentary and increased activity). For these reasons, D_2O is increasingly employed to quantify MPS.
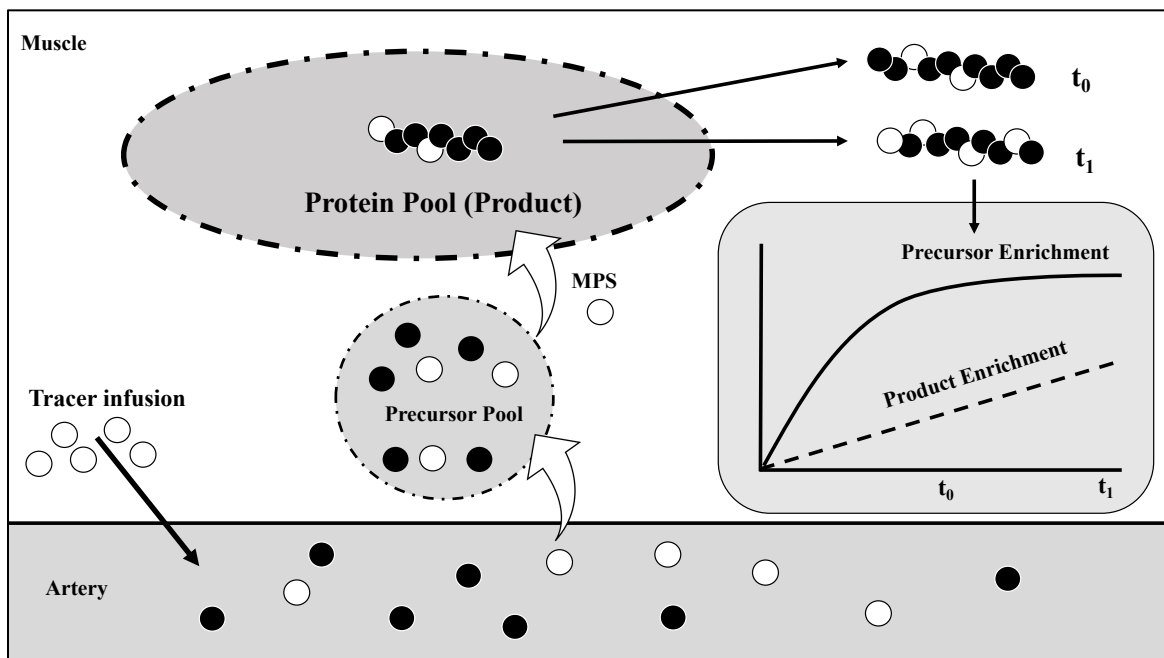
Figure 1. Schematic showing a simplified overview of how muscle protein synthesis is assessed using stable isotope tracers. A tracer is introduced into the system using either infused- (shown in the diagram) or orally-ingested stable isotopes. Isotope enriches the intracellular free amino acid pool in skeletal muscle ('Precursor Pool') and is incorporated into bound protein via protein synthesis. Muscle biopsies are taken at multiple time points (two are shown in the diagram inset, t0 and t1) after the precursor

pool had reached equilibrium. The change in protein-bound tracer enrichment relative to the precursor pool enrichment is calculated to derive a measure of MPS rates.

In contrast to MPS, the measurement of MPB is more complex. The precursor-product relationship that MPS measurements rely on is also applicable to the measurement of MPB, although the definitions are reversed. For MPS measurements, the muscle intracellular free amino acid (MIF) pool supplies the precursor that enriches bound proteins with tracer. When quantifying MPB, the dilution of tracer enrichment in the MIF pool is the measured 'product' (see Figure 2); however, because the pool is diluted from two principal sources (the arterial pool and protein breakdown), there is added complexity of the resultant calculations.[62,63] Furthermore, the method involves the pulsed injection of two additional amino acid tracers, which increases study cost, and requires multiple blood and muscle biopsy samples to model enrichment decay yielding rate of MPB. As a result of the technical complexity involved, few investigations have simultaneously measured the influence of increased or decreased muscle loading on rates of MPB and MPS, which is necessary if we are to develop an understanding of the relative contributions of each process to skeletal muscle adaptation.
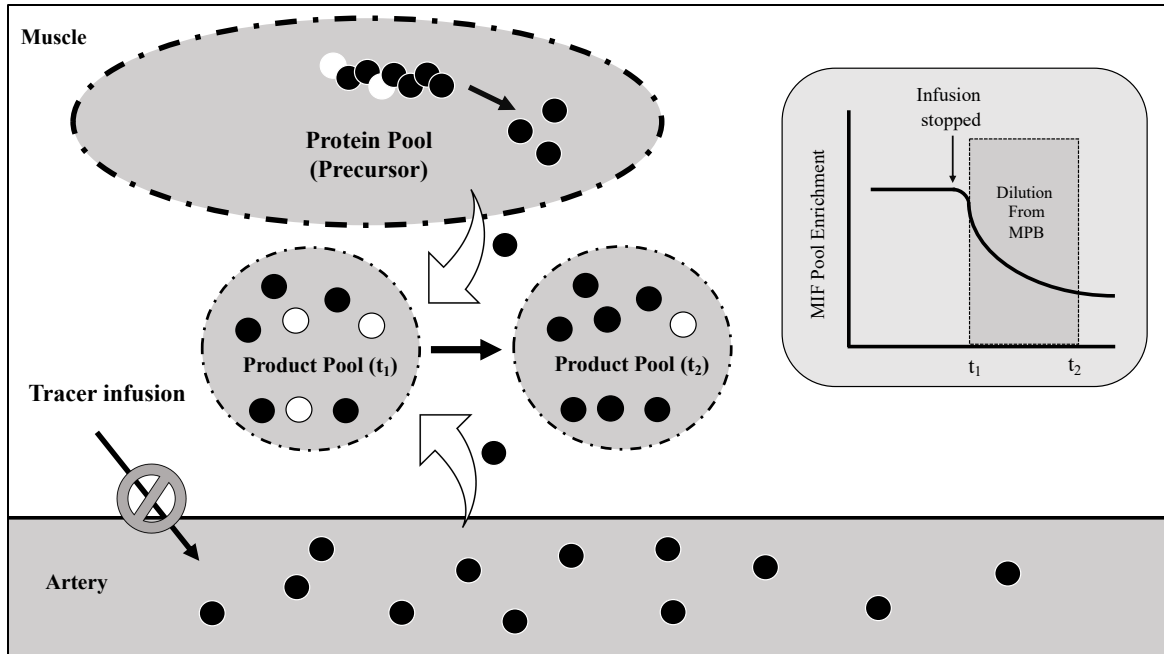
Figure 2. Schematic showing a simplified overview of the process of measuring muscle protein breakdown using stable isotope tracers. Tracer is first infused until enrichment in arterial and intracellular free amino acid pools reaches equilibrium. At this point, tracer infusion is stopped and the decay in tracer enrichment is monitored in the intracellular free amino acid pool ('Product Pool) and arterial pool at multiple time points (here, two times point, t1 and t2 are shown). Tracer decay occurs due to dilution from two sources: tracee release from protein breakdown and tracee being delivered from the arterial pool. Thus, by determining the decay of tracer in the intracellular free amino acid and arterial pools, the contribution from MPB can be estimated.

1.5.1 The influence of loading on muscle protein turnover

Resistance exercise potently stimulates MPS ~2-3 fold above basal levels,[64] which remains elevated for ~48 hours post-RE.[65] RE also induces a concomitant rise in MPB; however, the magnitude and duration of stimulation are less than half that of MPS. Nonetheless, in the fasted state, depite the anabolic nature of RE, net protein balance increases but remains negative in the absence of exogenous amino acid intake.[33] Protein ingestion, and the ensuing hyperaminoacidemia and hyperinsulinemia, transiently

stimulates MPS and suppresses MPB, respectively.[66,67] However, solely ingesting protein also does not result in muscle hypertrophy because MPS returns to basal levels within 2-3 hours after consumption, despite sustained hyperaminoacidemia (the 'tank-full' effect).[66,68] Combining protein consumption and RE results in an additive increase in MPS that effectively delays the 'tank-full' phenomenon for up to 24 hrs,[69] promotes a positive net protein balance and results in protein accretion over several weeks (i.e., muscle hypertrophy).

During the transition from exercise-naïve to 'resistance-trained', the MPS response to exercise is refined. In the untrained state, an acute bout of RE increases both myofibrillar and mitochondrial protein synthesis rates; however, only myofibrillar protein synthesis is increased after acute RE in the trained state.[70] Furthermore, the stimulation of MPS after acute RE is more pronounced in the trained state, but the overall response is shorter-lived.[71] A greater stimulation of MPS after acute RE in the untrained state may at first appear paradoxical, however, it ostensibly reflects the turnover of chemically-damaged or misfolded proteins in addition to myofibrillar proteins. Indeed, our laboratory has demonstrated that peri-workout MPS is highest following the first bout of RE, when muscle damage is greatest, and progressively wanes after the 3rd and 10th weeks of training.[72] MPB also exhibits a similar adaptive decline with continued resistance training, at least in the fasted state, rendering net protein balance less negative than pre-RT.[73] Taken together, increased protein turnover appears necessary, especially during the early resistance-training period, to facilitate skeletal muscle remodelling and to lay the foundation for subsequent muscle protein accretion with progressive training.

At the molecular level, translational efficiency and capacity are increased and contribute to the observed RE-induced increases in MPS. Chesley and colleagues were the first to demonstrate an increase in RNA activity (protein synthesized per unit of total RNA, the majority of which is ribosomal RNA or rRNA e.g., translational efficiency) 4hr and 24hr following acute RE without a change in RNA concentration (i.e., translational capacity).[74] Since then, numerous other investigations have demonstrated increased phosphorylation of mTORC1 substrates within hours following an acute bout of RE. Importantly, the acute rise in MPS following loading is partially inhibited by rapamycin administration,[75,76] implying some degree of dependency on mTORC1 activity. RE also enhances the peripheral colocalization of mTOR with eIF3f,[77] a key protein involved in assembly and docking of the 43S PIC on mRNA. Thus, RE enhances translational efficiency during the early post-exercise recovery period.

In constrast, changes in translational capacity are not immediate. The expression of 47S pre-rRNA, commonly used as a readout of ribosomal biogenesis, is increased within 4hr following a single bout of RE and remains elevated for 24-48 hours; however, there is not a corresponding increase in RNA content.[74] Given that rRNA comprises ~80-90% of total RNA, subtle changes in total RNA content driven by ribosomal biogenesis may not be detectable until several days following acute RE. Consistently, Bickel *et al.* observed an increase in total RNA content several days after the second bout of RE,[78] and others have observed increases after 4-12 weeks of progressive RT.[45,73,79-82] Importantly, the magnitude of increase in RNA content with RT may be quantitatively linked with subsequent muscle hypertrophy.[45,82]

1.5.2 The influence of unloading on muscle protein turnover

Muscle atrophy occurs due to an imbalance between MPS and MPB, favouring the net catabolism of muscle proteins. Accelerated catabolism may arise via the suppression of MPS, an increase of MPB, or a combination of both. The dominant mechanism underpinning disuse-induced skeletal muscle atrophy is an intensely debated topic.[83,84] The roots of this controversy may stem from conflicting observations from workers employing distinct models of muscle disuse (i.e., bed rest vs. limb immobilization) and metabolically distinct species (i.e. juvenile rodents vs. mature humans),[85] or inferences made from static measures of proteolytic gene markers.

Researchers employing surrogate models of human disuse (*i.e.* hindlimb suspension in rodents) have demonstrated increased proteolysis during muscle unloading.[86] In humans, however, proteolysis only appears to be a significant mechanism leading to muscle protein loss in pathological muscle wasting conditions (i.e., cancer cachexia, sepsis, burns, uremia) characterized by overt hypodynamia (bed-rest), hypercortisolemia and hypercytokinemia.[87] Indeed, work in *healthy* humans demonstrates that disuse-induced muscle loss can be mostly, if not entirely, accounted for by reductions in MPS. Seminal work[88] completed 30 years ago in young men undergoing 7 weeks of immobilization found a significant reduction in postabsorptive MPS rates (-25%). Considering the observed loss of muscle mass and the associated reductions in postabsorptive MPS, Gibson *et al*[88] concluded that MPB must have remained unchanged or even adaptively decreased during the immobilization period. Consistent with these findings, Paddon-Jones and colleagues detected a ~33% blunted postabsorptive MPS and

no observable change in MPB after 28 days of bed rest, using the A-V balance technique.[89] de Boer and colleagues demonstrated that the decrements in postabsorptive MPS occur within the first 10 days of disuse and remain depressed with prolonged disuse but without further reductions. Interestingly, recent work has demonstrated that disuse-induced reductions in MPS occur within days of unloading, being depressed by 16%, 41%, and 44% after 2, 5, and 7 days of lower-limb immobilization, respectively. These decrements in fasted MPS may be due to a concomitant reduction in translational capacity,[80,90] but reductions in RNA content are not always found in humans undergoing muscle disuse suggesting other mechanisms are involved.

Unloading also induces anabolic resistance to protein ingestion. Indeed, our laboratory has demonstrated an attenuated myofibrillar protein synthetic response to the infusion of both high- and low-dose amino acid infusion in young adults following 14 days of limb immobilization.[23] An impaired induction of myofibrillar protein synthesis has also been demonstrated in response to an oral protein bolus following 5 and 14 days of disuse (31% and 53% lower induction of MPS relative to control limb, respectively).[21,25] Taking the observed decrements of postabsorptive and postprandial MPS into account, combined with estimates of time spent in each phase throughout the day, reductions in MPS rates are considered to be responsible for the subsequent loss of muscle observed following muscle disuse.[91] To objectively support this assertion, however, more work is required exploring the association between integrative measurements of protein synthesis (i.e., methods that incorporate both fasting and fed periods) and the observed losses of skeletal muscle in response to disuse.

Despite convincing evidence implicating disuse-induced reductions in MPS as the key driver of muscle atrophy, transient activation of MPB within days of unloading cannot be definitively ruled out. Using tissue microdialysis, Tesch and colleagues observed a ~44% increase in interstitial 3-methylhistidine concentration,[92] which is a post-translationally modified breakdown product of actin and myosin, after 3 days of lower limb suspension. Furthermore, MAFBx and MuRF1 expression are increased after 3-5 days of immobilization,[21,93] potentially indicating an early induction of the UPS, and therefore MPB. However, it is equally likely that these factors do not stimulate bulk protein breakdown *per se* but rather selectively target specific initiation factors involved in MPS. As an example, MAFBx selectively degrades eIF3f,[94,95] which plays an important role in translation initiation and the assembly of the ternary complex, recruitment of eIF4G to the 5' m^7-GTP cap of mRNA molecules and as a scaffold linking mTORC1 and p70S6K1.[96,97] Thus, it is difficult to establish the role (if any) that MPB plays in the early disuse-induced atrophy programme from static readouts of purported genetic regulators of proteasomal activity. To address our knowledge gap on the role of MPB in atrophic muscle loss in response to disuse, there is a need to simultaneously quantify MPS and MPB after a unloading.

1.6 Mechanisms of muscle plasticity: insights from 'omics' technologies

In addition to the increased synthesis of myofibrillar protein, skeletal muscle plasticity involves remodelling the extracellular matrix to accommodate muscle fibre expansion, angiogenesis to ensure adequate oxygenation and nutrient provision, and satellite cell-mediated myonuclear accretion. However, the underlying molecular

regulators of these processes are still relatively undefined. Exercise regulates more than 2,000 gene transcripts in skeletal muscle[98] and alters the abundance[99] and ratio of post-translationally modified to native protein species.[100,101] These regulated molecules interact within larger network structures of hierarchical import[102,103] and are difficult to model using targeted analytical approaches (i.e. PCR and immunoblotting). Furthermore, mechanistic discoveries made using non-physiological mechanical stimuli in rodents often fail to translate to humans. Recently, 'omic' technologies have been employed in humans to overcome these limitations, as they provide a *theoretically* unbiased perspective of the molecular perturbations induced by the dynamic loading of skeletal muscle.

Although proteins are considered the biological workhorses of the cell, mRNA expression is commonly measured as a surrogate for protein abundance because it is easier to quantify on a global scale. Nonetheless, this approach has been challenged[104] based on experimental evidence demonstrating only a moderate relationship between these molecular species.[105] When properly modelled, however (i.e., when the method-specific error is taken into account), variation in mRNA expression can explain ~75% or more of the variance in protein abundance.[106] Furthermore, skeletal muscle is a complex tissue with only a limited proportion of its proteome currently quantifiable (i.e. <500 proteins reliably quantified in *all* participants[107]) compared to the ~30,000 RNA species that can be reliably measured using microarray technology.[108] Thus, many important regulatory molecules, including signalling proteins and transcription factors, are less likely to be identified.[109] For these reasons, transcriptome profiling represents a promising

strategy to uncover the molecular regulators of muscle plasticity when sensibly measured and linked to the degree of physiological changes that occur.

1.6.1   Effects of chronic RT on the skeletal muscle transcriptome

Endurance and resistance training induce divergent adaptations,[70] yet both phenotypes have substantial overlap in their respective transcriptional profiles.[110-112] One approach to identifying uniquely important regulators of muscle growth is to compare gene expression differences between individuals exhibiting variable degrees of muscle hypertrophy in response to RT.[18] While theoretically effective, existing studies using this approach[113] have employed small sample sizes (<30) that limit reliable correlational analysis,[114] in turn affecting the reproducibility of the results. For example, Raue and colleagues identified >600 genes that correlated with muscle growth and strength changes after 12 weeks of RT, including growth factor genes (i.e. *VEGFA, PDFGFA*), cell cycle-related genes (i.e. *CDK4, EIF4E)*, cytokine signalling genes (i.e. *MAP3K14, NFKBIA*) and several genes involved in UPS and substrate metabolism.[113] However, subsequent analysis by Phillips *et al.[110]* demonstrated that many of these 'growth' genes are actually generic features of exercise adaptation (i.e. also influenced by endurance training). This example highlights the importance of independently validating gene signatures, a process rarely attempted in exercise physiology research. As a result, the field lacks a reproducible signature of potential muscle growth-regulating genes.

Higher responders are also ostensibly 'primed' at baseline to mount an effective hypertrophic response to subsequent RT.[14] Specifically, higher responders have a greater expression of genes involved in myogenic signalling, including the satellite cell markers

PAX7 and *SOX8*,[14] which is consistent with the greater number of satellite cells observed at baseline in these individuals.[13] Other pathways differentially regulated between high and low responders to RT include fuel utilization, skeletal muscle development, ECM remodelling and transcriptional regulation.[14] Within these categories, expression of *NAP1L1* was >17-fold higher in skeletal muscle at baseline in high vs. low responders.[14] The protein product of *NAP1L1* regulates chromatin compaction, thus influencing transcription, but it also interacts with and regulates the nuclear shuttling[115] of another gene upregulated in high responders[14], *DGKZ*. *DGKZ* encodes a protein that is important for load-induced hypertrophy in rodents.[116] These examples demonstrate the utility of considering individual differences in responsiveness to RT when mining transcriptional profiles,[18] rather than averaging responses across a cohort of individuals.[98] Nonetheless, results derived from such analyses should be independently validated to ensure they are reproducible and not simply an artifact of the cohort that was studied.

1.6.2   Effects of muscle disuse on the skeletal muscle transcriptome

Muscle disuse rapidly alters both the size and metabolic characteristics of skeletal muscle to limit the inefficient consumption of cellular energy. Consistently, unloaded skeletal muscle exhibits a robust downregulation of mitochondrial transcripts and protein abundance.[32,117-122] Abadi *et al.* demonstrated that genes involved in oxidative phosphorylation, mitochondrial regulation and β-oxidation are rapidly suppressed within 48 hours of knee immobilization, implying a widespread impairment in mitochondrial function.[117] PGC-1α, an important regulator of mitochondrial biogenesis,[123] is consistently reduced in unloaded muscle[98,117,124], possibly via increased methylation in its

promoter region[119] or altered upstream activity of MEF2C.[121] Intriguingly, modulation of PGC-1α expression is important for preserving muscle mass during prolonged periods of muscle inactivity in hibernating mammals.[125] *NR4A3* is another transcriptional coactivator[126] that is consistently downregulated by inactivity and reduces basal and maximal oxygen consumption when silenced in myotubes.[98] These mitochondrial impairments are associated with reductions in fatty acid transporter and oxidative gene expression,[118,119] as well as increased SREBP1 expression[124] – the master controller of lipid synthesis. Together, these changes may lead to an increased synthesis of lipid intermediates (i.e. diacylglycerol and ceramides) linked to insulin resistance[127] and may also be related to the attenuation of MPS in response to protein ingestion that is observed in response to disuse.[23]

Muscle disuse is also associated with a reduction in myofibrillar protein content,[124] which can be attributed primarily to reductions in myofibrillar protein synthesis as described above.[27,103,128] Genes involved in MPB are not consistently featured in the transcriptional profile of unloaded skeletal muscle after 48 hours of unloading.[117] Only after 14 days of immobilization are protein degradation genes differentially regulated. After 14 days of immobilization, the unloaded transcriptional profile reflects impaired protein synthetic capacity, including downregulation of tRNA synthesizing enzymes, ribosomal subunits and translation initiation factors.[117] These transcript-level changes are largely consistent at the level of the proteome[129] and together argue against a *primary* role of protein breakdown in muscle disuse atrophy. Instead, it is likely that the early induction of atrogenes (i.e., MAFBx and MuRF1) during muscle

disuse may serve to reduce protein synthetic capacity. An example in support of this hypothesis described above is the targeted degradation of eIF3f by MAFBx.[130] Targeted profiling of skeletal muscle and measurement of MPB within the first few days of unloading will help address the more generalizable validity of this hypothesis.

1.6.3 Leveraging network analyses to understand muscle remodelling

An ongoing challenge with transcriptomic analyses is parsing through long lists of differentially expressed genes to identify those that are important mediators of adaptation. The discussion above has introduced several purported regulators of muscle hypertrophy and atrophy; however, these discoveries are often drawn from small sample sizes (<30), and, as a result, the reproducibility of existing signatures is currently low.[131] One approach to improve reproducibility is to perform gene expression meta-analyses, which leverage the growing repository of publicly available gene expression datasets.[131] Pillon and colleagues were the first to apply this approach to investigate the gene expression responses to acute and chronic endurance and resistance training studies; however, their analysis did not consider the divergent hypertrophic outcomes across participants and therefore collapsed many potentially important gene expression events to zero or non-significance. Therfore, an approach that considers response heterogeneity has the potential to increase our understanding of the molecular regulators of muscle remodelling.

Another approach to increase our understanding of skeletal muscle plasticity is to consider the broader context that genes function within. Instead of considering and ascribing importance to individual genes, we need to consider the network of interactions between several genes via network analysis (using tools such as Ingenuity pathway

analysis (IPA)). A drawback of tools like IPA, however, is that they rely on the function(s) of a gene product being known *a priori,* thus genes coding for proteins with an unknown function are essentially functional deadends.[132] This limitation can be overcome by using data-driven network (DDN) analysis, an approach that constructs networks based on experimentally derived gene co-expression similarities without any *a priori* knowledge of gene function. Clarke and colleagues [102] used this approach to construct gene networks from pre- and post-training muscle transcriptome samples obtained from the HERITAGE study[133] (endurance-based training) and identified *EIF6* as a highly interconnected exercise-responsive gene. EIF6 was therefore *predicted*, based on being highly connected to other regulated genes, to play an important role in the adaptation to endurance training. Indeed, the subsequent development of a mutant EIF6 murine model affected many of the same signalling pathways predicted by the HERITAGE study [102,133] that affect phenotype. At present, a DDN approach has not been employed to study how the molecular regulators of muscle remodelling might interact *in vivo*, possibly because of the large sample sizes required to construct reproducible networks, but there is tremendous potential for this approach to advance our understanding of skeletal muscle adaptation in response to loading and unloading.

1.7 Methods to assess changes in muscle size

Unravelling the mechanisms of muscle growth and atrophy also depends on the ability to accurately measure changes in muscle size. In theory, measuring changes in muscle size is a tractable research problem given the advancements in imaging technologies; however, uncertainties surrounding the exact definition of muscle

hypertrophy render the problem more nuanced. Indeed, Haun and colleagues critically examined the construct of muscle hypertrophy and suggested that what most researchers refer to as 'hypertrophy' is an umbrella term for three specific underlying processes: connective tissue, sarcoplasmic, and myofibrillar hypertrophy.[134] Although not explicitly covered by Haun and colleagues, the definition of muscle 'atrophy' could be similarly deconstructed. Thus, if different laboratories are using different methods to measure hypertrophy and atrophy, results may be discordant because the underlying construct being measured by each laboratory may be different. One approach to overcome this limitation is to combine methods to assess muscle size – i.e., at the whole-muscle and microscopic levels – to obtain a composite score of muscle growth and/or atrophy. Concordance between methods would suggest that the underlying changes are real and robust. However, this approach may not be feasible due to cost, equipment availability, and burden on research participants. Furthermore, different methods – such as myofibre CSA and whole-muscle CSA measurements – often yield different outcomes due to confounding factors such as regional hypertrophy/atrophy and fibre-type specific changes.[31] Thus, a method that is both sensitive to changes in muscle size and available for routine use by researchers outside of clinical settings is needed.

Commonly used methods to assess changes in muscle mass and/or size include bioelectrical impedance analysis (BIA), dual-energy x-ray absorptiometry (DXA), magnetic resonance imaging (MRI), computed tomography (CT) and, more recently, ultrasonography (US).[135] BIA measures the impedance of an electrical current as it passes through the body. Tissues with a high-water content (i.e., skeletal muscle) impede

electrical flow less than tissues with a low water content (i.e., adipose tissue), which is used in predictive equations to estimate body composition parameters, including lean soft tissue mass.[136] In contrast, DXA quantifies bone mineral and soft tissue mass (fat and fat-free mass) by measuring the differential absorption of two x-ray beams as they pass through an individual.[137] Although BIA and DXA have the advantage of being relatively low-cost and time-efficient methods, neither directly assesses skeletal muscle mass, and both are influenced by confounding factors such as hydration status.

MRI and CT are considered the gold-standard methods for assessing muscle cross-sectional area. Although both technologies produce high-quality images and data, MRI is generally preferred because it does not expose individuals to ionizing radiation and instead produces a signal based on interactions between hydrogen atoms present in tissues and an external magnetic field. However, MRI has a high operating cost combined with a limited availability and requirement for highly trained personnel limits its routine usage in physiology research. An alternative approach that overcomes many of the limitations of MRI is brightness-mode (B-mode) ultrasonography (US). In B-mode US, high frequency sound waves (i.e., ultrasound) are emitted from a handheld probe and travel through the tissue of interest. As the sound wave propagates throug a tissue, it encounters different boundaries (i.e., connective, adipose, and skeletal muscle tissues) that reflect sound waves to variable degrees (i.e., 'echoes'). The time taken for the sound wave to return to the probe is converted into a brightness signal that is then used to construct a two-dimensional image. Relative to MRI, which costs an estimated $424 per scan, an ultrasound scan costs ~$88.[138] Furthermore, US has been demonstrated to

accurately quantify skeletal muscle CSA compared to MRI (at single time points) in both young and older adults. Nonetheless, existing comparisons provide no insight on the ability of US to detect *changes* in muscle CSA.

The ability to quantify changes in muscle CSA is arguably more important than cross-sectional comparisons because the former allows researchers to test the efficacy of various interventions on muscle hypertrophy and/or atrophy. Franchi and colleagues demonstrated a significant correlation between unidimensional muscle thickness (MT) measurements obtained using US and changes in quadriceps CSA using MRI following 12 weeks of RT.[139] However, no relationship was observed between changes in MT and changes in quadriceps volume. It is possible that a two-dimensional US-based assessment of muscle CSA would more closely relate to changes in muscle CSA and muscle volume measured by MRI. Prior research using US to quantify muscle CSA has also not considered the influence of the probe pressure on changes in muscle size despite it being recognized as a potential confounding variable.[140] Thus, more work is needed to assess the suitability of B-mode US for measuring changes in muscle size induced by loading and unloading of skeletal muscle.

1.8 Objectives and Hypotheses:

The overarching objective of the experiments conducted as part of this thesis was to study the molecular regulators of skeletal muscle remodelling in response to increased (hypertrophy) and decreased (atrophy) loading. To accomplish this objective, we first validated a novel unilateral model whereby one limb resistance-trained to induce hypertrophy, and the other limb underwent a period of immobilization to induce atrophy

(study 1). This model provided us with a platform to study the molecular regulators of muscle remodelling by contrasting the response to these diverse loading states in the same individual, thus reducing variation associated with between-subjects' comparisons (study 2). Finally, to shed light on a possible role for MPB in short-term disuse atrophy, we employed an acute and chronic tracer approach that allowed us to quantify fasted MPS and MPB as well as integrated MPS (study 3).

Study 1: Methodological considerations for and validation of the ultrasonographic determination of human skeletal muscle hypertrophy and atrophy

We tested the validity of our HypAt model to measure changes in *vastus lateralis* CSA (VLCSA) in response to loading and unloading of skeletal muscle compared to MRI. Cross-sectional data has demonstrated a high correlation between US- and MRI-derived VLCSA in young and older adults. However, no data exists on the concordance between methods when assessing the change in VLCSA. Furthermore, it is likely that probe pressure – and the resultant depression of the skin and underlying muscle belly – significantly influences measurements obtained by US. However, no study has attempted to quantify the degree to which probe pressure influences measures of muscle size. We hypothesized that US-derived measurements of the change in VLCSA would show concordance with the criterion method in response to the loading and unloading of skeletal muscle. Secondly, we hypothesized that probe pressure would significantly affect the resultant measurements of muscle size.

Study 2: Molecular transducers of human skeletal muscle remodelling under different loading states

In study 2, we sought to investigate and uncover potential transcriptional regulators of muscle growth. Several studies have attempted to quantify the genes most important for muscle growth, but the results have not been reproducible.[110] The lack of reproducibility likely stems from the small sample sizes used, lack of independent validation, and collapsing of data across participants showing marked variability in the degree of muscle hypertrophy/atrophy observed. We employed the HypAt model from study 1, whereby one leg was subjected to a loading stimulus (Hyp) and the other to an unloading stimulus (At). We hypothesized that this model would reduce response variation and enable the discovery of a greater number of differentially expressed genes (DEGs) compared to similarly-sized clinical trials. Finally, we investigated which DEGs were correlated with muscle growth using 3 independent clinical cohorts to identify a transcriptional signature of muscle growth. Using several genes and in vitro cell culture, we then demonstrated that knocking down (using RNA inhibition - RNAi) genes supressed MPS and cellular signalling to a normally robust anabolic stimulus.

Study 3: Fasted/fed-state declines in muscle protein synthesis account for short-term muscle disuse atrophy in humans in the absence of increased muscle protein breakdown

In study 3, we investigated the effect of short-term muscle disuse on MPS and MPB. Despite extensive literature suggesting that decrements in MPS are the primary

driver of disuse-induced muscle loss in humans,[21,23,25-27,91] there is no evidence derived from studies directly measuring MPB within the first few days of unloading. However, markers of MPB are upregulated in some studies, which implies an early induction of proteolysis. Furthermore, having established the suitability of US to measure changes in muscle size, we employed US in conjunction with DXA-derived measures of lean mass to quantify changes in muscle size following 4 days of unloading. We hypothesized that fasted and integrated rates of MPS would be reduced with unloading and quantitatively related to changes in muscle size, with no significant change in rates of MPB.

1.9 References

1. Janssen I, Heymsfield SB, Wang Z, Ross R. Skeletal muscle mass and distribution in 468 men and women aged 18–88 yr. *Journal of Applied Physiology.* 2000;89:81-88.
2. Zurlo F, Larson K, Bogardus C, Ravussin E. Skeletal muscle metabolism is a major determinant of resting energy expenditure. *J Clin Invest.* 1990;86(5):1423-1427.
3. DeFronzo RA, Jacot E, Jequier E, Maeder E, Wahren J, Felber JP. The effect of insulin on the disposal of intravenous glucose. Results from indirect calorimetry and hepatic and femoral venous catheterization. *Diabetes.* 1981;30(12):1000-1007.
4. Arnold EM, Delp SL. Fibre operating lengths of human lower limb muscles during walking. *Philos Trans R Soc Lond B Biol Sci.* 2011;366(1570):1530-1539.
5. Schiaffino S, Bormioli SP, Aloisi M. Cell proliferation in rat skeletal muscle during early stages of compensatory hypertrophy. *Virchows Arch B Cell Pathol.* 1972;11(3):268-273.
6. Narici MV, Hoppeler H, Kayser B, et al. Human quadriceps cross-sectional area, torque and neural activation during 6 months strength training. *Acta Physiol Scand.* 1996;157(2):175-186.
7. Alway SE, Grumbt WH, Stray-Gundersen J, Gonyea WJ. Effects of resistance training on elbow flexors of highly competitive bodybuilders. *J Appl Physiol (1985).* 1992;72(4):1512-1521.
8. DeFreitas JM, Beck TW, Stock MS, Dillon MA, Kasishke PR, 2nd. An examination of the time course of training-induced skeletal muscle hypertrophy. *Eur J Appl Physiol.* 2011;111(11):2785-2790.
9. Damas F, Phillips SM, Lixandrao ME, et al. An inability to distinguish edematous swelling from true hypertrophy still prevents a completely accurate interpretation

of the time course of muscle hypertrophy. *Eur J Appl Physiol.* 2016;116(2):445-446.

10. Goreham C, Green HJ, Ball-Burnett M, Ranney D. High-resistance training and muscle metabolism during prolonged exercise. *Am J Physiol.* 1999;276(3):E489-496.

11. Seynnes OR, de Boer M, Narici MV. Early skeletal muscle hypertrophy and architectural changes in response to high-intensity resistance training. *J Appl Physiol (1985).* 2007;102(1):368-373.

12. Kosek DJ, Kim J-s, Petrella JK, Cross JM, Bamman MM. Efficacy of 3 days/wk resistance training on myofiber hypertrophy and myogenic mechanisms in young vs. older adults. *Journal of Applied Physiology.* 2006.

13. Petrella JK, Kim JS, Mayhew DL, Cross JM, Bamman MM. Potent myofiber hypertrophy during resistance training in humans is associated with satellite cell-mediated myonuclear addition: a cluster analysis. *J Appl Physiol (1985).* 2008;104(6):1736-1742.

14. Thalacker-Mercer A, Stec M, Cui X, Cross J, Windham S, Bamman M. Cluster analysis reveals differential transcript profiles associated with resistance training-induced human skeletal muscle hypertrophy. *Physiol Genomics.* 2013;45(12):499-507.

15. Hubal MJ, Gordish-Dressman H, Thompson PD, et al. Variability in muscle size and strength gain after unilateral resistance training. *Med Sci Sports Exerc.* 2005;37(6):964-972.

16. Bamman MM, Petrella JK, Kim JS, Mayhew DL, Cross JM. Cluster analysis tests the importance of myogenic gene expression during myofiber hypertrophy in humans. *J Appl Physiol (1985).* 2007;102(6):2232-2239.

17. Davidsen PKPKPK, Gallagher IJIJ, Hartman JWJWJW, et al. High responders to resistance exercise training demonstrate differential regulation of skeletal muscle microRNA expression. *Journal of Applied Physiology.* 2011;110:309-317.

18. Bamman MM, Roberts BM, Adams GR. Molecular Regulation of Exercise-Induced Muscle Fiber Hypertrophy. *Cold Spring Harb Perspect Med.* 2018;8(6).

19. Kilroe SP, Fulford J, Jackman SR, LJC VANL, Wall BT. Temporal Muscle-specific Disuse Atrophy during One Week of Leg Immobilization. *Med Sci Sports Exerc.* 2020;52(4):944-954.

20. Adams GR, Caiozzo VJ, Baldwin KM. Skeletal muscle unweighting: spaceflight and ground-based models. *Journal of applied physiology (Bethesda, Md : 1985).* 2003;95:2185-2201.

21. Wall BT, Dirks ML, Snijders T, et al. Short-term muscle disuse lowers myofibrillar protein synthesis rates and induces anabolic resistance to protein ingestion. *American Journal of Physiology Endocrinology and Metabolism.* 2015:ajpendo.00227.02015.

22. Oates BR, Glover EI, West DW, Fry JL, Tarnopolsky MA, Phillips SM. Low-volume resistance exercise attenuates the decline in strength and muscle mass associated with immobilization. *Muscle and Nerve.* 2010;42:539-546.

23. Glover EI, Phillips SM, Oates BR, et al. Immobilization induces anabolic resistance in human myofibrillar protein synthesis with low and high dose amino acid infusion. *Journal of Physiology.* 2008.

24. Skeletal muscle atrophy during short-term disuse: Implications for age-related sarcopenia, Ageing Research Reviews(2013).

25. Wall BT, Snijders T, Senden JMG, et al. Disuse impairs the muscle protein synthetic response to protein ingestion in healthy men. *Journal of Clinical Endocrinology and Metabolism.* 2013;98:4872-4881.

26. de Boer MD, Selby A, Atherton P, et al. The temporal responses of protein synthesis, gene expression and cell signalling in human quadriceps muscle and patellar tendon to disuse. *The Journal of physiology.* 2007;585:241-251.

27. Gibson JN, Halliday D, Morrison WL, et al. Decrease in human quadriceps muscle protein turnover consequent upon leg immobilization. *Clinical science.* 1987;72:503-509.

28. Suetta C, Hvid LG, Justesen L, et al. Effects of aging on human skeletal muscle after immobilization and retraining. *Journal of applied physiology (Bethesda, Md : 1985).* 2009;107:1172-1180.

29. Hvid L, Aagaard P, Justesen L, et al. Effects of aging on muscle mechanical function and muscle fiber morphology during short-term immobilization and subsequent retraining. *Journal of Applied Physiology.* 2010;109:1628-1634.

30. Hortobágyi T, Dempsey L, Fraser D, et al. Changes in muscle strength, muscle fibre size and myofibrillar gene expression after immobilization and retraining in humans. *The Journal of physiology.* 2000;524 Pt 1:293-304.

31. Yasuda N, Glover EI, Phillips SM, Isfort RJ, Tarnopolsky MA. Sex-based differences in skeletal muscle function and morphology with short-term limb immobilization. *Journal of Applied Physiology.* 2005.

32. Chen Y-W, Gregory C, Ye F, et al. Molecular signatures of differential responses to exercise trainings during rehabilitation. *Biomedical Genetics and Genomics.* 2017.

33. Biolo G, Fleming RYD, Maggi SP, Wolfe RR. Transmembrane transport and intracellular of amino acids in human skeletal muscle kinetics. *American Journal of Physiology Endocrinology and Metabolism.* 1995;268:E75-E84.

34. Burd Na, Tang JE, Moore DR, Phillips SM. Exercise training and protein metabolism: influences of contraction, protein intake, and sex-based differences. *Journal of applied physiology (Bethesda, Md : 1985).* 2009;106:1692-1701.

35. Jackson RJ, Hellen CU, Pestova TV. The mechanism of eukaryotic translation initiation and principles of its regulation. *Nat Rev Mol Cell Biol.* 2010;11(2):113-127.

36. Hara K, Yonezawa K, Kozlowski MT, et al. Regulation of eIF-4E BP1 phosphorylation by mTOR. *J Biol Chem.* 1997;272(42):26457-26463.

37. Gingras AC, Gygi SP, Raught B, et al. Regulation of 4E-BP1 phosphorylation: a novel two-step mechanism. *Genes Dev.* 1999;13(11):1422-1437.

38. Burnett PE, Barrow RK, Cohen NA, Snyder SH, Sabatini DM. RAFT1 phosphorylation of the translational regulators p70 S6 kinase and 4E-BP1. *Proc Natl Acad Sci U S A.* 1998;95(4):1432-1437.

39. Dorrello NV, Peschiaroli A, Guardavaccaro D, Colburn NH, Sherman NE, Pagano M. S6K1- and betaTRCP-mediated degradation of PDCD4 promotes protein translation and cell growth. *Science.* 2006;314(5798):467-471.

40. Dennis MD, Jefferson LS, Kimball SR. Role of p70S6K1-mediated phosphorylation of eIF4B and PDCD4 proteins in the regulation of protein synthesis. *J Biol Chem.* 2012;287(51):42890-42899.

41. Hannan KM, Brandenburger Y, Jenkins A, et al. mTOR-dependent regulation of ribosomal gene transcription requires S6K1 and is mediated by phosphorylation of the carboxy-terminal activation domain of the nucleolar transcription factor UBF. *Mol Cell Biol.* 2003;23(23):8862-8877.

42. Mayer C, Zhao J, Yuan X, Grummt I. mTOR-dependent activation of the transcription factor TIF-IA links rRNA synthesis to nutrient availability. *Genes Dev.* 2004;18(4):423-434.

43. Ben-Sahra I, Hoxhaj G, Ricoult SJH, Asara JM, Manning BD. mTORC1 induces purine synthesis through control of the mitochondrial tetrahydrofolate cycle. *Science.* 2016;351(6274):728-733.

44. Ben-Sahra I, Howell JJ, Asara JM, Manning BD. Stimulation of de novo pyrimidine synthesis by growth signaling through mTOR and S6K1. *Science.* 2013;339(6125):1323-1328.

45. Stec MJ, Kelly NA, Many GM, Windham ST, Tuggle SC, Bamman MM. Ribosome biogenesis may augment resistance training-induced myofiber hypertrophy and is required for myotube growth in vitro. *Am J Physiol Endocrinol Metab.* 2016;310(8):E652-E661.

46. Figueiredo VC, McCarthy JJ. Regulation of Ribosome Biogenesis in Skeletal Muscle Hypertrophy. *Physiology (Bethesda).* 2019;34(1):30-42.

47. Figueiredo VC, Wen Y, Alkner B, et al. Genetic and epigenetic regulation of skeletal muscle ribosome biogenesis with exercise. *J Physiol.* 2021;599(13):3363-3384.

48. Murach KA, Fry CS, Dupont-Versteegden EE, McCarthy JJ, Peterson CA. Fusion and beyond: Satellite cell contributions to loading-induced skeletal muscle adaptation. *FASEB J.* 2021;35(10):e21893.

49. Rock KL, Gramm C, Rothstein L, et al. Inhibitors of the proteasome block the degradation of most cell proteins and the generation of peptides presented on MHC class I molecules. *Cell.* 1994;78(5):761-771.

50. Schwartz AL, Ciechanover A. The ubiquitin-proteasome pathway and pathogenesis of human diseases. *Annu Rev Med.* 1999;50:57-74.

51. Nakayama KI, Nakayama K. Ubiquitin ligases: cell-cycle control and cancer. *Nat Rev Cancer.* 2006;6(5):369-381.

52. Bodine SC, Latres E, Baumhueter S, et al. Identification of ubiquitin ligases required for skeletal muscle atrophy. *Science (New York, NY).* 2001;294:1704-1708.

53.   Solomon V, Goldberg AL. Importance of the ATP-ubiquitin-proteasome pathway in the degradation of soluble and myofibrillar proteins in rabbit muscle extracts. *J Biol Chem.* 1996;271(43):26690-26697.

54.   Du J, Wang X, Miereles C, et al. Activation of caspase-3 is an initial step triggering accelerated muscle proteolysis in catabolic conditions. *J Clin Invest.* 2004;113(1):115-123.

55.   Volodin A, Kosti I, Goldberg AL, Cohen S. Myofibril breakdown during atrophy is a delayed response requiring the transcription factor PAX4 and desmin depolymerization. *Proc Natl Acad Sci U S A.* 2017;114(8):E1375-E1384.

56.   Mizushima N, Komatsu M. Autophagy: renovation of cells and tissues. *Cell.* 2011;147(4):728-741.

57.   Schoenheimer R, Ratner S, Rittenberg D. Studies in protein metabolism. X. The metabolic activity of body proteins investigated with l(-)-Leucine containing two isotopes. *J Biol Chem.* 1939;130:703-732.

58.   Schoenheimer R, Ratner S, Rittenberg D. The Process of Continuous Deamination and Reamination of Amino Acids in the Proteins of Normal Animals. *Science.* 1939;89(2308):272-273.

59.   Ussing HH. The Rate of Protein Renewal in Mice and Rats Studied by Means of Heavy Hydrogen. *Acta Physiologica Scandinavica.* 1941;2(3-4):209-221.

60.   Rennie MJ. An introduction to the use of tracers in nutrition and metabolism. *Proc Nutr Soc.* 1999;58(4):935-944.

61.   Gasier HG, Fluckey JD, Previs SF. The application of 2H2O to measure skeletal muscle protein synthesis. *Nutr Metab (Lond).* 2010;7:31.

62.   Zhang XJ, Chinkes DL, Wolfe RR. Measurement of muscle protein fractional synthesis and breakdown rates from a pulse tracer injection. *Am J Physiol Endocrinol Metab.* 2002;283(4):E753-764.

63.   Zhang XJ, Chinkes DL, Sakurai Y, Wolfe RR. An isotopic method for measurement of muscle protein fractional breakdown rate in vivo. *Am J Physiol.* 1996;270(5 Pt 1):E759-767.

64.   Kumar V, Atherton P, Smith K, Rennie MJ. Human muscle protein synthesis and breakdown during and after exercise. *J Appl Physiol (1985).* 2009;106(6):2026-2039.

65.   Phillips SM, Tipton KD, Aarsland A, Wolf SE, Wolfe RR. Mixed muscle protein synthesis and breakdown after resistance exercise in humans. *The American journal of physiology.* 1997;273:E99-107.

66.   Atherton PJ, Etheridge T, Watt PW, et al. Muscle full effect after oral protein: time-dependent concordance and discordance between human muscle protein synthesis and mTORC1 signaling. *Am J Clin Nutr.* 2010;92(5):1080-1088.

67.   Greenhaff PL, Karagounis LG, Peirce N, et al. Disassociation between the effects of amino acids and insulin on signaling, ubiquitin ligases, and protein turnover in human muscle. *Am J Physiol Endocrinol Metab.* 2008;295(3):E595-604.

68.   Bohe J, Low JF, Wolfe RR, Rennie MJ. Latency and duration of stimulation of human muscle protein synthesis during continuous infusion of amino acids. *J Physiol.* 2001;532(Pt 2):575-579.

69. Burd NA, West DW, Moore DR, et al. Enhanced amino acid sensitivity of myofibrillar protein synthesis persists for up to 24 h after resistance exercise in young men. *J Nutr.* 2011;141(4):568-573.

70. Wilkinson SB, Phillips SM, Atherton PJ, et al. Differential effects of resistance and endurance exercise in the fed state on signalling molecule phosphorylation and protein synthesis in human muscle. *Journal of Physiology.* 2008.

71. Tang JE, Perco JG, Moore DR, Wilkinson SB, Phillips SM. Resistance training alters the response of fed state mixed muscle protein synthesis in young men. *Am J Physiol Regul Integr Comp Physiol.* 2008;294(1):R172-178.

72. Damas F, Phillips SM, Libardi CA, et al. Resistance training-induced changes in integrated myofibrillar protein synthesis are related to hypertrophy only after attenuation of muscle damage. *Journal of Physiology.* 2016.

73. Reidy PT, Borack MS, Markofski MM, et al. Post-absorptive muscle protein turnover affects resistance training hypertrophy. *European Journal of Applied Physiology.* 2017.

74. Chesley A, MacDougall JD, Tarnopolsky Ma, Atkinson Sa, Smith K. Changes in human muscle protein synthesis after resistance exercise. *Journal of applied physiology.* 1992;73:1383-1388.

75. Gundermann DM, Walker DK, Reidy PT, et al. Activation of mTORC1 signaling and protein synthesis in human muscle following blood flow restriction exercise is inhibited by rapamycin. *Am J Physiol Endocrinol Metab.* 2014;306(10):E1198-1204.

76. Drummond MJ, Fry CS, Glynn EL, et al. Rapamycin administration in humans blocks the contraction-induced increase in skeletal muscle protein synthesis. *J Physiol.* 2009;587(Pt 7):1535-1546.

77. Song Z, Moore DR, Hodson N, et al. Resistance exercise initiates mechanistic target of rapamycin (mTOR) translocation and protein complex co-localisation in human skeletal muscle. *Sci Rep.* 2017;7(1):5028.

78. Bickel CS, Slade J, Mahoney E, Haddad F, Dudley GA, Adams GR. Time course of molecular responses of human skeletal muscle to acute bouts of resistance exercise. *J Appl Physiol (1985).* 2005;98(2):482-488.

79. Brook MS, Wilkinson DJ, Mitchell WK, et al. Skeletal muscle hypertrophy adaptations predominate in the early stages of resistance exercise training, matching deuterium oxide-derived measures of muscle protein synthesis and mechanistic target of rapamycin complex 1 signaling. *FASEB J.* 2015;29(11):4485-4496.

80. Haddad F, Baldwin KM, Tesch PA. Pretranslational markers of contractile protein expression in human skeletal muscle: effect of limb unloading plus resistance exercise. *J Appl Physiol (1985).* 2005;98(1):46-52.

81. Figueiredo VC, Caldow MK, Massie V, Markworth JF, Cameron-Smith D, Blazevich AJ. Ribosome biogenesis adaptation in resistance training-induced human skeletal muscle hypertrophy. *Am J Physiol Endocrinol Metab.* 2015;309(1):E72-83.

82. Mobley CB, Haun CT, Roberson PA, et al. Biomarkers associated with low, moderate, and high vastus lateralis muscle hypertrophy following 12 weeks of resistance training. *PLoS One.* 2018;13(4):e0195203.

83. Phillips SM, McGlory C. CrossTalk proposal: The dominant mechanism causing disuse muscle atrophy is decreased protein synthesis. *J Physiol.* 2014;592(24):5341-5343.

84. Reid MB, Judge AR, Bodine SC. CrossTalk opposing view: The dominant mechanism causing disuse muscle atrophy is proteolysis. *J Physiol.* 2014;592(24):5345-5347.

85. Rennie MJ, Selby A, Atherton P, et al. Facts, noise and wishful thinking: muscle protein turnover in aging and human disuse atrophy. *Scand J Med Sci Sports.* 2010;20(1):5-9.

86. Bodine SC, Latres E, Baumhueter S, et al. Identification of ubiquitin ligases required for skeletal muscle atrophy. *Science.* 2001;294(5547):1704-1708.

87. Schakman O, Kalista S, Barbe C, Loumaye A, Thissen JP. Glucocorticoid-induced skeletal muscle atrophy. *Int J Biochem Cell Biol.* 2013;45(10):2163-2172.

88. Gibson JN, Halliday D, Morrison WL, et al. Decrease in human quadriceps muscle protein turnover consequent upon leg immobilization. *Clin Sci (Lond).* 1987;72(4):503-509.

89. Paddon-Jones D, Sheffield-Moore M, Cree MG, et al. Atrophy and impaired muscle protein synthesis during prolonged inactivity and stress. *J Clin Endocrinol Metab.* 2006;91(12):4836-4841.

90. Figueiredo VC, D'Souza RF, Van Pelt DW, et al. Ribosome biogenesis and degradation regulate translational capacity during muscle disuse and reloading. *J Cachexia Sarcopenia Muscle.* 2021;12(1):130-143.

91. Phillips SM, Glover EI, Rennie MJ. Alterations of protein turnover underlying disuse atrophy in human skeletal muscle. *Journal of applied physiology (Bethesda, Md : 1985).* 2009;107:645-654.

92. Tesch PA, von Walden F, Gustafsson T, Linnehan RM, Trappe TA. Skeletal muscle proteolysis in response to short-term unloading in humans. *J Appl Physiol (1985).* 2008;105(3):902-906.

93. Gustafsson T, Osterlund T, Flanagan JN, et al. Effects of 3 days unloading on molecular regulators of muscle size in humans. *Journal of Applied Physiology.* 2010;109:721-727.

94. Lagirand-Cantaloube J, Offner N, Csibi A, et al. The initiation factor eIF3-f is a major target for atrogin1/MAFbx function in skeletal muscle atrophy. *The EMBO journal.* 2008;27:1266-1276.

95. Lagirand-Cantaloube J, Cornille K, Csibi A, Batonnet-Pichon S, Leibovitch MP, Leibovitch SA. Inhibition of atrogin-1/MAFbx mediated MyoD proteolysis prevents skeletal muscle atrophy in vivo. *PLoS One.* 2009;4(3):e4973.

96. Hinnebusch AG. eIF3: a versatile scaffold for translation initiation complexes. *Trends Biochem Sci.* 2006;31(10):553-562.

97. Csibi A, Cornille K, Leibovitch MP, et al. The translation regulatory subunit eIF3f controls the kinase-dependent mTOR signaling required for muscle differentiation and hypertrophy in mouse. *PLoS One.* 2010;5(2):e8994.

98. Pillon NJ, Gabriel BM, Dollet L, et al. Transcriptomic profiling of skeletal muscle adaptations to exercise and inactivity. *Nat Commun.* 2020;11(1):470.

99. Robinson MM, Dasari S, Konopka AR, et al. Enhanced Protein Translation Underlies Improved Metabolic and Physical Adaptations to Different Exercise Training Modes in Young and Old Humans. *Cell metabolism.* 2017;25:581-592.

100. Hoffman NJ, Parker BL, Chaudhuri R, et al. Global Phosphoproteomic Analysis of Human Skeletal Muscle Reveals a Network of Exercise-Regulated Kinases and AMPK Substrates. *Cell Metab.* 2015;22(5):922-935.

101. Potts GK, McNally RM, Blanco R, et al. A map of the phosphoproteomic alterations that occur after a bout of maximal-intensity contractions. *J Physiol.* 2017;595(15):5209-5226.

102. Clarke K, Ricciardi S, Pearson T, et al. The Role of Eif6 in Skeletal Muscle Homeostasis Revealed by Endurance Training Co-expression Networks. *Cell Rep.* 2017;21(6):1507-1520.

103. Stokes T, Timmons JA, Crossland H, et al. Molecular Transducers of Human Skeletal Muscle Remodeling under Different Loading States. *Cell Rep.* 2020;32(5):107980.

104. Miller BF, Konopka AR, Hamilton KL. The rigorous study of exercise adaptations: why mRNA might not be enough. *J Appl Physiol (1985).* 2016;121(2):594-596.

105. Schwanhausser B, Busse D, Li N, et al. Global quantification of mammalian gene expression control. *Nature.* 2011;473(7347):337-342.

106. Li JJ, Bickel PJ, Biggin MD. System wide analyses have underestimated protein abundances and the importance of transcription in mammals. *PeerJ.* 2014;2:e270.

107. Camera DM, Burniston JG, Pogson MA, Smiles WJ, Hawley JA. Dynamic proteome profiling of individual proteins in human skeletal muscle after a high-fat diet and resistance exercise. *FASEB J.* 2017;31(12):5478-5494.

108. Timmons JA, Atherton PJ, Larsson O, et al. A coding and non-coding transcriptomic perspective on the genomics of human metabolic disease. *Nucleic Acids Research.* 2018;46:7772-7792.

109. Srisawat K, Hesketh K, Cocks M, et al. Reliability of Protein Abundance and Synthesis Measurements in Human Skeletal Muscle. *Proteomics.* 2020;20(7):e1900194.

110. Phillips BE, Williams JP, Gustafsson T, et al. Molecular Networks of Human Muscle Adaptation to Exercise and Age. *PLoS Genetics.* 2013;9.

111. Stepto NK, Coffey VG, Carey AL, et al. Global gene expression in skeletal muscle from well-trained strength and endurance athletes. *Med Sci Sports Exerc.* 2009;41(3):546-565.

112. Chapman MA, Arif M, Emanuelsson EB, et al. Skeletal Muscle Transcriptomic Comparison between Long-Term Trained and Untrained Men and Women. *Cell Rep.* 2020;31(12):107808.

113. Raue U, Trappe TA, Estrem ST, et al. Transcriptome signature of resistance exercise adaptations: mixed muscle and fiber type specific profiles in young and old adults. *Journal of applied physiology (Bethesda, Md : 1985).* 2012;112:1625-1636.

114. Schönbrodt FD, Perugini M. At what sample size do correlations stabilize? *Journal of Research in Personality.* 2013;47:609-612.

115. Okada M, Hozumi Y, Ichimura T, et al. Interaction of nucleosome assembly proteins abolishes nuclear localization of DGKzeta by attenuating its association with importins. *Exp Cell Res.* 2011;317(20):2853-2863.

116. You JS, Dooley MS, Kim CR, et al. A DGKzeta-FoxO-ubiquitin proteolytic axis controls fiber size during skeletal muscle remodeling. *Sci Signal.* 2018;11(530).

117. Abadi A, Glover EI, Isfort RJ, et al. Limb immobilization induces a coordinate down-regulation of mitochondrial and other metabolic pathways in men and women. *PLoS ONE.* 2009.

118. Chopard A, Lecunff M, Danger R, et al. Large-scale mRNA analysis of female skeletal muscles during 60 days of bed rest with and without exercise or dietary protein supplementation as countermeasures. *Physiol Genomics.* 2009;38(3):291-302.

119. Alibegovic AC, Sonne MP, Hojbjerre L, et al. Insulin resistance induced by physical inactivity is associated with multiple transcriptional changes in skeletal muscle in young men. *Am J Physiol Endocrinol Metab.* 2010;299(5):E752-763.

120. McGlory C, Von Allmen MT, Stokes T, et al. Failed recovery of glycemic control and myofibrillar protein synthesis with 2 wk of physical inactivity in overweight, prediabetic older adults. *Journals of Gerontology - Series A Biological Sciences and Medical Sciences.* 2018;73.

121. Rullman E, Fernandez-Gonzalo R, Mekjavic IB, Gustafsson T, Eiken O. MEF2 as upstream regulator of the transcriptome signature in human skeletal muscle during unloading. *Am J Physiol Regul Integr Comp Physiol.* 2018;315(4):R799-R809.

122. Fernandez-Gonzalo R, Tesch PA, Lundberg TR, Alkner BA, Rullman E, Gustafsson T. Three months of bed rest induce a residual transcriptomic signature resilient to resistance exercise countermeasures. *FASEB J.* 2020;34(6):7958-7969.

123. Lin J, Handschin C, Spiegelman BM. Metabolic control through the PGC-1 family of transcription coactivators. *Cell Metab.* 2005;1(6):361-370.

124. Brocca L, Cannavino J, Coletto L, et al. The time course of the adaptations of human muscle proteome to bed rest and the underlying mechanisms. *J Physiol.* 2012;590(20):5211-5230.

125. Xu R, Andres-Mateos E, Mejias R, et al. Hibernating squirrel muscle activates the endurance exercise pathway despite prolonged immobilization. *Exp Neurol.* 2013;247:392-401.

126. Pearen MA, Muscat GE. Minireview: Nuclear hormone receptor 4A signaling: implications for metabolic disease. *Mol Endocrinol.* 2010;24(10):1891-1903.

127. Samuel VT, Shulman GI. Mechanisms for insulin resistance: common threads and missing links. *Cell.* 2012;148(5):852-871.

128. Phillips SM, McGlory C. CrossTalk proposal: The dominant mechanism causing disuse muscle atrophy is decreased protein synthesis. *The Journal of Physiology.* 2014;592:5341-5343.
129. Kenny HC, Tascher G, Ziemianin A, et al. Effectiveness of Resistive Vibration Exercise and Whey Protein Supplementation Plus Alkaline Salt on the Skeletal Muscle Proteome Following 21 Days of Bed Rest in Healthy Males. *J Proteome Res.* 2020.
130. Csibi A, Leibovitch MP, Cornille K, Tintignac LA, Leibovitch SA. MAFbx/Atrogin-1 controls the activity of the initiation factor eIF3-f in skeletal muscle atrophy by targeting multiple C-terminal lysines. *J Biol Chem.* 2009;284(7):4413-4421.
131. Sweeney TE, Haynes WA, Vallania F, Ioannidis JP, Khatri P. Methods to increase reproducibility in differential gene expression via meta-analysis. *Nucleic Acids Res.* 2017;45(1):e1.
132. Timmons JA, Szkop KJ, Gallagher IJ. Multiple sources of bias confound functional enrichment analysis of global -omics data. *Genome Biol.* 2015;16:186.
133. Timmons JA, Knudsen S, Rankinen T, et al. Using molecular classification to predict gains in maximal aerobic capacity following endurance exercise training in humans. *J Appl Physiol (1985).* 2010;108(6):1487-1496.
134. Haun CT, Vann CG, Roberts BM, Vigotsky AD, Schoenfeld BJ, Roberts MD. A Critical Evaluation of the Biological Construct Skeletal Muscle Hypertrophy: Size Matters but So Does the Measurement. *Front Physiol.* 2019;10:247.
135. Heymsfield SB, Adamek M, Gonzalez MC, Jia G, Thomas DM. Assessing skeletal muscle mass: historical overview and state of the art. *J Cachexia Sarcopenia Muscle.* 2014;5(1):9-18.
136. Janssen I, Heymsfield SB, Baumgartner RN, Ross R. Estimation of skeletal muscle mass by bioelectrical impedance analysis. *J Appl Physiol (1985).* 2000;89(2):465-471.
137. Proctor DN, O'Brien PC, Atkinson EJ, Nair KS. Comparison of techniques to estimate total body skeletal muscle mass in people of different age groups. *Am J Physiol.* 1999;277(3):E489-495.
138. Parker L, Nazarian LN, Carrino JA, et al. Musculoskeletal imaging: medicare use, costs, and potential for cost substitution. *J Am Coll Radiol.* 2008;5(3):182-188.
139. Franchi MV, Longo S, Mallinson J, et al. Muscle thickness correlates to muscle cross-sectional area in the assessment of strength training-induced hypertrophy. *Scandinavian Journal of Medicine and Science in Sports.* 2018.
140. Franchi MV, Raiteri BJ, Longo S, Sinha S, Narici MV, Csapo R. Muscle Architecture Assessment: Strengths, Shortcomings and New Frontiers of in Vivo Imaging Techniques. *Ultrasound Med Biol.* 2018;44(12):2492-2504.

CHAPTER 2:

Methodological considerations for and validation of the ultrasonographic determination of human skeletal muscle hypertrophy and atrophy.
Published in *Physiological Reports* 2021. 9(1): e14683

Published under the Creative Commons Attribution License 4.0

ORIGINAL RESEARCH

Physiological Reports

Methodological considerations for and validation of the ultrasonographic determination of human skeletal muscle hypertrophy and atrophy

Tanner Stokes[1] | **Thomas R. Tripp[1,2]** | **Kevin Murphy[1]** | **Robert W. Morton[1]** | **Sara Y. Oikawa[1]** | **Hon Lam Choi[1]** | **Jessica McGrath[1]** | **Chris McGlory[3]** | **Maureen J. MacDonald[1]** | **Stuart M. Phillips[1]**

[1]Department of Kinesiology, McMaster University, Hamilton, Ontario, Canada

[2]Faculty of Kinesiology, University of Calgary, Alberta, Canada

[3]School of Kinesiology and Health Sciences, Queen's University, Kingston, Ontario, Canada

Correspondence
Stuart Phillips, Department of Kinesiology, McMaster University, Hamilton, Ontario, Canada.
Email: phillis@mcmaster.ca

Funding information
National Science and Engineering Research Council

Abstract

Magnetic resonance imaging (MRI) is the current gold standard for measuring changes in muscle size (cross-sectional area [CSA] and volume) but can be cost-prohibitive and resource-intensive. We evaluated the validity of B-mode ultrasonography (US) as a low-cost alternative to MRI for measuring muscle hypertrophy and atrophy in response to resistance training and immobilization, respectively. Fourteen young men performed 10wk of unilateral resistance training (RT) to induce muscle hypertrophy. In the final two weeks of the 10wk, the subjects' contralateral leg was immobilized (IMB). The cross-sectional area of the *vastus lateralis* (VLCSA) was measured at the mid-thigh before and after each intervention using MRI (VLCSA$_{MRI}$) and US (VLCSA$_{US}$). The relationship and agreement between methods were assessed. Reliability of US measurements ranged from good to excellent in all comparisons (ICC >0.67). VLCSA significantly increased after 10 weeks of RT (VLCSA$_{US}$: $7.9 \pm 3.8\%$; VLCSA$_{MRI}$: $7.8 \pm 4.5\%$) and decreased after 2 weeks of IMB (VLCSA$_{US}$: $-8.2\% \pm 5.8\%$; VLCSA$_{MRI}$: $-8.7 \pm 6.1\%$). Significant correlations were identified between MRI and US at each time point measured (all $r > 0.85$) and, importantly, between MRI- and US-derived changes in VLCSA. Bland-Altman analysis revealed minimal bias in US measurements relative to the MRI ($-0.5 \pm 3.0\%$) and all measurements were within the upper and lower limits of agreement. Our data suggest that B-mode ultrasonography can be a suitable alternative to MRI for measuring changes in muscle size in response to increased and decreased muscle loading in young men.

KEYWORDS

exercise, human, imaging, immobilization

1 | INTRODUCTION

Skeletal muscle generates the forces necessary to perform activities of daily living and is a reservoir of amino acids that can be mobilized to supply gluconeogenic substrates during catabolic states (Wolfe, 2006). Muscle atrophy occurs with aging (Janssen et al., 2000, 2002), muscle disuse (Glover et al., 2008; Holloway et al., 2019; Yasuda et al., 2005), and/ or disease (Powers et al., 2016), and is associated with functional impairment and metabolic dysregulation. Resistance training (RT) is potently anabolic and results in hypertrophy (Stokes et al., 2020). Additionally, RT is an effective non-pharmacological strategy to prevent or attenuate muscle atrophy during catabolic conditions (Devries et al., 2015; Fernandez-Gonzalo et al., 2020; Moore et al., 2018; Oates et al., 2010), in part due to its potent hypertrophic effect on skeletal muscle.

A reproducible observation with both increased and decreased loading of skeletal muscle is the substantial inter-individual heterogeneity of the hypertrophic response with loading (Davidsen et al., 2011; Hubal et al., 2005; Stokes et al., 2020) and atrophy with unloading (Chen et al., 2017; Glover et al., 2008; Stokes et al., 2020; Yasuda et al., 2005). Interestingly, the ability to accurately quantify changes in muscle size in response to hypertrophy-inducing loading has recently been identified as being more complex than once thought, with substantial variability between methods (Haun et al., 2019). We propose a similar critique would be true when describing the response to unloading-induced atrophy. Microscopic assessments of myofiber cross-sectional area (CSA) are the only available method for the assessment of muscle fiber size; however, few laboratories have the capacity to obtain biopsy specimens and the invasive nature of the procedure may preclude measurements in certain populations (i.e., the frail elderly; (Wilson et al., 2018). These difficulties inevitably complicate the comparison of research findings between laboratories. Thus, cheaper and more readily accessible, non-invasive methods to assess muscle hypertrophy and atrophy are warranted.

Magnetic resonance imaging (MRI) is a non-invasive and non-radioactive means to determine muscle CSA (and volume) that offers unparalleled tissue differentiation capabilities and has a high correlation with the cadaver-measured determination of muscle (Mitsiopoulos et al., 1998). For these reasons, MRI is considered the gold standard for assessing changes in muscle size. However, obtaining MRI images requires highly specialized personnel and is otherwise limited by operation cost, availability, and time-consuming post-acquisition image processing. A potential low-cost and more readily available alternative to MRI is B-mode ultrasonography (US)(Parker et al., 2008). US has been shown to accurately quantify muscle CSA in both young (Franchi, Longo, et al., 2018; Lixandrao et al., 2014) and older adults

(Nijholt et al., 2017; Reeves et al., 2004) when measured at a single-time point. Moreover, changes in muscle thickness obtained by US correlated with MRI-derived changes in anatomical CSA, but not muscle volume, after 12 weeks of isokinetic RT (Franchi, Longo, et al., 2018).

No study, to date, has assessed the efficacy of US, relative to MRI, to accurately capture changes in *vastus lateralis* CSA (VLCSA)—a muscle routinely sampled by needle biopsy—before and after muscle hypertrophy and atrophy-inducing stimuli. It is plausible that a two-dimensional assessment of muscle size (i.e., VLCSA) will produce stronger correlations between MRI-derived measurements of VLCSA and, perhaps, muscle volume compared to unidimensional thickness measurements. Thus, the purpose of this study was to evaluate the relationship and methodological agreement between US and MRI measured *changes* in VLCSA after 10 weeks of unilateral RT and 2 weeks of brace-mediated immobilization (IMB). We hypothesized that US would show good concordance with the criterion measure for muscle size, MRI, showing similar changes in VLCSA in response to RT (hypertrophy) and immobilization (atrophy).

2 | METHODS

2.1 | Participants for methodological development

Prior to conducting the main study, we were interested in objectively quantifying the effect of applied force on an ultrasound probe to derive muscle thickness measurements. We studied 34 male participants from a previously published investigation (Age, 23 ± 3 yrs; Body Mass, 86.6 ± 13.5 kg; BMI, 26.4 ± 3.3 kg/m^2; (Morton et al., 2016)). Muscle thickness measurements were taken, as described below (see *Ultrasonography*), from the *vastus lateralis* prior to and upon the completion of 12 weeks of whole-body resistance training at four different applied probe forces (0.2, 0.5, 0.7, and 1.0 N).

2.2 | Participants for validation trial

For a detailed description of the participant recruitment strategy and screening procedures for the main trial, please refer to a previous report from the same participants (Stokes et al., 2020). Briefly, 14 recreationally active men (18–30 y) who were free of chronic disease and/or not currently taking medications known to influence protein metabolism volunteered to participate in the study. All procedures complied with the ethical standards outlined in the Tri-Council Policy statement for research involving humans and were approved by the Hamilton Integrated Research Ethics Board (REB Project

#14-333 and #2867 for the methodological and validation trials, respectively). Prior to participation, all subjects read and signed an informed consent form.

2.3 | Experimental protocol

For a schematic overview of the main experimental design, refer to Figure 1. Participants performed 10 weeks of unilateral resistance training, which consisted of thrice weekly leg press and leg extension training sessions under supervision. During the last two weeks of the study, a knee brace (DonJoy) was applied to the contralateral limb to induce immobilization as previously described (Holloway et al., 2019). Mid-thigh VLCSA was assessed before (day 0) and after the study (day 70) using B-mode ultrasonography (VLCSA$_{US}$) and MRI (VLCSA$_{MRI}$). An additional ultrasound scan of VLCSA was obtained at week 8 to confirm that no changes in muscle size had occurred in the free-living limb prior to undergoing immobilization. Muscle volume and peak quadriceps CSA were also measured using MRI at day 0 and day 70.

2.4 | Unilateral resistance exercise

Following a brief warmup on a cycle ergometer, participants performed three sets of unilateral leg extension followed by three sets of leg press. Loading was set at ~80% of 1-RM, which was predetermined using three successive familiarization sessions prior to commencing the study. This intensity led to muscle failure between 8 and 12 repetitions (defined as an inability to execute another repetition through a full range of motion). If the participant successfully completed less than 8 or more than 12 repetitions, the load for subsequent sessions was adjusted accordingly. After each exercise

session, participants ingested 25 g of whey protein isolate (Leprino Foods, Denver, CO, USA).

2.5 | Immobilization

Immobilization was accomplished by applying an X-ACT ROM knee brace (DonJoy, Vista, CA, USA) on the contralateral non-training leg during the last two weeks of the study (i.e., weeks 9 and 10). Prior to brace application, the leg randomly assigned to be immobilized was only subjected to activities of daily living. The angle of the brace was adjusted to permit toe clearance during ambulation with crutches without *active* hamstring flexion (~60° of flexion). The angle was subsequently locked into place with tabs provided by the manufacturer and secured with ties to prevent angle unlocking. Tape was wrapped around the brace and an investigator's signature was written such that if the brace was removed, the tape would be damaged. The brace was briefly removed at each exercise visit by an investigator and the (unweighted) leg was inspected for signs of a deep vein thrombosis following a procedure previously described (Oates et al., 2010). There were no reports of swelling or pain in the immobilized limb, and only minor skin chaffing occurred.

2.6 | Magnetic resonance imaging

Participants underwent a fasted MRI scan of both thighs on day 0 and upon study completion (day 70) for the assessment of mid-thigh VLCSA, peak quadriceps CSA and muscle volume. Each scan was performed in a 3-Tesla HD Scanner (SIGNA MRI System; GE Medical, Milwaukee, Wisconsin) at the Imaging Research Center (St. Joseph's Healthcare, Hamilton, ON). Participants rested in a supine position for ~10–15 minutes prior to scanning to normalize
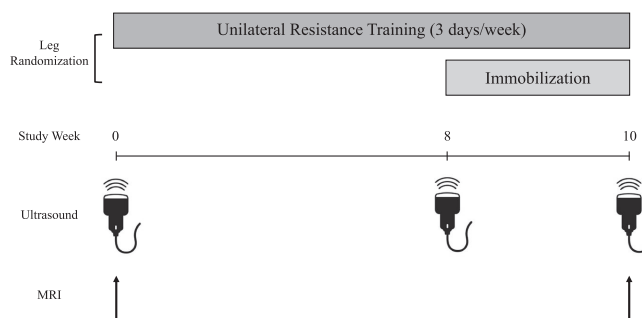

FIGURE 1 Schematic overview of the study. Subjects had one leg randomly assigned to perform 10 weeks of unilateral resistance exercise training three days per week. The contralateral leg performed habitual activities during the first 8 weeks of the study and was immobilized from week 8–10

fluid shifts in the body. Axial (transverse) MR images were obtained from both thighs from the distal end of the femur to greater trochanter. A fast-recovery, fast spin-echo pulse sequence was used, along with iterative decomposition of water and fat with echo asymmetry and least-squares estimation post-processing to obtain water-only, fat-only, in-phase, and out-of-phase images of the thighs. The following parameters were used: repetition time = 2000 msec, echo time=30 msec, refocusing flip angle = 111 degrees, echo train length = 6, Array coil spatial sensitivity encoding (parallel imaging factor) = 2, field of view = 42x21 cm, acquisition matrix = 512 × 256, 3 mm slice thickness, and 0 mm slice gap. An average of 140 slices was acquired from each participant. The acquisition was completed in two sections: a lower stage and an upper stage, which were subsequently stitched together by an MR technician. The total scan time for both stages was approximately 11 min.

Images were downloaded from a secure server and VLCSA was manually traced using the polygon selection tool in ImageJ. For comparisons with the ultrasound, mid-thigh VLCSA was analyzed from the image slice corresponding to 50% of the distance between the greater trochanter and lateral epicondyle of the femur, identified using a coronal image as a reference. Peak quadriceps CSA (i.e., the cross-sectional MRI image slice for which the quadriceps CSA was maximal) and quadriceps volume were quantified using semi-automatic software, Analyze 14.0 (AnalyzeDirect, Overland Park, NS) as previously described (Holloway et al., 2019). First, the distal 20% of thigh images and the proximal 30% of MRI images from each leg were excluded from analysis due to an increased difficulty to differentiate muscle groups at these extremes. Total quadriceps CSA was subsequently traced manually on every other image slice. The tracings were propagated to untraced images and used to train an algorithm to differentiate muscle from adipose and connective tissue. These images were in turn randomly checked for accuracy. Muscle volume (cm^3) was calculated as the sum of CSA values from all of the analyzed image slices multiplied by the slice thickness.

2.7 | Ultrasonography

Upon arrival to the laboratory after a ~ 10 h overnight fast, participants lied supine for 10 minutes to normalize fluid shifts in the body, while their feet were positioned in a custom foot-hold apparatus that prevented depression of the thigh against the bed. During the first assessment, a mark was made with permanent ink at a point equidistant between the greater trochanter of the femur and the lateral epicondyle of the knee that was identified by palpation. The medial border of the *vastus lateralis* was identified

along this point and a second mark was made on the leg. A straight line was then drawn down the leg perpendicular to the surface of the bed with horizontal markings made every 2 cm, which served as a guideline for ultrasound probe placement. Transparent paper was used to trace this guideline and any identifiable marks on the skin (moles, birthmarks, scars, etc.) that could be used as reference points for subsequent scans. To acquire images, a 50 mm 12.5 linear-array ultrasound probe (Vivid Q, GE Medical Systems, Horten, Norway) was positioned at the start of the *vastus lateralis*.

For the methodological trial, muscle thickness measurements were obtained with the probe oriented along the longitudinal axis of the *vastus lateralis*. To standardize the amount of force applied on the leg, the ultrasound probe was fixed—via a 90° angle bracket—to a strain gauge that displayed force (Dillon Model GL, Fairmont, MN, USA). This apparatus was in turn fixed to a vertical test stand with a movable clamp that could be modified based on the size of the participant. Four muscle thickness measurements were subsequently obtained from each participant (one at 0.2, 0.5, 0.7, and 1.0 Newtons (N) of applied force).

For the validation trial, a series of ~4–6 overlapping images were acquired from the start to the end of the *vastus lateralis*. To prevent depression of the muscle belly by the probe—in accordance with data generated in our pilot work—and to ensure adequate acoustic contact with the skin, a thick layer of water-based gel (~2 cm) was applied at the region of scanning and the probe was rested on top. Muscle thickness and muscle CSA images were converted from DICOM to.jpeg format using DICOM editing software (Sante DICOM Editor, version 3.1.2, Athens, Greece) and randomized by assigning to each image a letter and number identifier (i.e., "A56"). Muscle thickness was quantified as the linear distance from the superficial and deep fascial borders of the *vastus lateralis*. Images for CSA analysis were stitched together using open-source image editing software (GNU Image Manipulation Program v. 2.8.22, Mountain View, CA, USA) by aligning subcutaneous fat, superficial and deep aponeuroses, and intramuscular fat deposits between subsequent images and then traced using the polygon tool in ImageJ.

2.8 | Statistical analyses

All statistical analyses were performed using SPSS Statistics for Mac, version 23.0 (IBM Corp., Armonk, NY, USA) with the exception of sample size, which was calculated using "pwr.r.test" from the "pwr" package in R (version 4.02). Specifically, to achieve an effect size of 0.69 (Pearson's r obtained from Franchi, Longo, et al., 2018) at a significance level of 0.05 and power of 80%, 13 participants were

TABLE 1 Participant characteristics, n = 14

Parameter	Baseline	Week 5	Week 10
Age, y	21 ± 3	—	—
Height, m	1.72 ± 0.06	—	—
Mass, kg	72.4 ± 13.6	71.8 ± 14.0	72.2 ± 13.3
Daily Steps	10200 ± 4600	9000 ± 3000	8300 ± 3400
Activity, kcal·d^{-1}	1113 ± 667	986 ± 569	1049 ± 564
Energy intake, kcal·d^{-1}	2300 ± 550	2200 ± 850	2450 ± 820
Dietary Protein, g·kg·d^{-1}	1.5 ± 0.9	1.5 ± 0.6	1.6 ± 0.9
En% Protein	17 ± 6	18 ± 5	18 ± 4
En% CHO	49 ± 12	51 ± 8	52 ± 10
En% Fat	33 ± 11	32 ± 8	30 ± 10

required. Changes in muscle thickness over time and at different probe pressures were measured using a two-way repeated measures ANOVA. VLCSA$_{US}$ was analyzed using a two-way repeated-measures analysis of variance (ANOVA) with time (3) and leg (2) as within-subjects' factors. Changes in VLCSA$_{MRI}$ were analyzed using a two-way repeated measures ANOVA with time (2) and leg (2) as within-subjects' factor. If the ANOVA test revealed a significant interaction, a Tukey's HSD post hoc test was employed to interrogate pairwise differences between legs and across time points. Pearson's correlations were run to assess the relationship between the various measurements of muscle size (% change from pre- to post- intervention) obtained by ultrasonography and MRI. Bland-Altman plots were constructed to assess the agreement between ultrasonography with MRI. Inter- and intra-rater reliability of VLCSA$_{US}$ image analyses were examined using a random series of 36 images and a two-way random-effects model with absolute agreement [i.e., ICC(2,2)] (Koo & Li, 2016). Two investigators (T.S and T.T) independently stitched together and traced pre- and post-intervention images to assess inter-rater reliability. One investigator analyzed a randomized series of the same images from the same subjects ~8 weeks apart for the measurement of intra-rater reliability. Interpretation of the strength of each ICC was determined by referencing recommended threshold values (Koo & Li, 2016). We also calculated the 95% Minimal Detectable Change (MDC) using the equation discussed in (Weir, 2005):

$$MDC\,(95\%) = SEM * \sqrt{2} * 1.96$$

where *SEM* (Standard Error of the Measurement) and is equal to the standard deviation of the change score between the first and second stitching trial.

Data are plotted as box plots showing the group mean and median, interquartile range (box), and maximum and minimum (whiskers) values. Data are reported as means ±standard deviation (SD), and results were considered statistically significant when $p \leq 0.05$.

3 | RESULTS

3.1 | Methodological study

We could not *consistently* obtain forces of 0 N. That is, even resting the probe on a relatively thick (~2 cm) layer of gel produced variations in applied forces ranging from 0 N to 0.2 N. Thus, to standardize force measurements, we set 0.2 N as the baseline "reference" force which, importantly, did not visibly depress the skin overlying the *vastus lateralis* at the point of measurement but ensured sufficient acoustic contact with the gel for image quality. At this applied reference force, muscle thickness pre-RT was 28.8 ± 4.3 mm. However, muscle thickness values were significantly lower ($p < 0.05$) when 0.5 N (28.1 ± 4.4 mm), 0.7 N (27.6 ± 4.5), and 1.0 N (26.8 ± 4.4 mm) of force was applied. Moreover, significant differences in muscle thickness ($p < 0.05$) were observed when 1.0 N versus 0.2 N of force were applied at pre- and post- time points, respectively. We determined that this increase was likely due to the greater relative force (and thus the depression of the muscle) at the pre-RT time point because, in the subset of subjects studied, we did not observe a significant increase in muscle thickness when both pre- and post-RT measurements were obtained at a force of 0.2 N ($p > 0.05$). Thus, for the primary analysis (below) we elected to obtain CSA images by resting the ultrasound probe on the gel layer without depressing the underlying skin and muscle—which corresponded to an applied probe pressure of less than or equal to 0.2 N. Representative MRI and ultrasound images of the *vastus lateralis* are shown in Figure 2.

3.2 | Validation study

3.2.1 | Participant Characteristics

Participant characteristics are displayed in Table 1. Briefly, 14 participants completed the intervention (21 ± 3 years old). We ascertained that two participants from the 14 were

non-compliant with the immobilization protocol (changed flexion angle of the brace, which enabled partial weight-bearing, without authorization by study investigators), but were included in the analysis because we were only concerned with comparing muscle size measurements between US and MRI, not the degree of atrophy *per se*. Inclusion or removal of the non-compliant participants from the analysis did not change the conclusions drawn from the data.

3.2.2 | Ultrasound Reliability and MDC

Intra-rater reliability was good to excellent with an ICC of 0.940 (95% CI: 0.875 to 0.972). Inter-rater reliability was moderate to excellent (ICC=0.847; 95% CI: 0.666 – 0.926). The SEM and MDC for our image stitching technique were 1.09 cm^2 and 3.03 cm^2, respectively.

3.2.3 | Mid-thigh VLCSA$_{US}$

VLCSA$_{US}$ data are presented in Figure 3. VLCSA$_{US}$ did not differ between the RT and IMB limbs at baseline ($p > 0.05$). VLCSA$_{US}$ increased from 27.2 ± 4.4 to 29.4 ± 5.2 cm^2 after 10 weeks of RT ($7.9 \pm 3.8\%$; $p < 0.05$). There was no difference in VLCSA$_{US}$ in the IMB leg from weeks 1 to 8, but VLCSA$_{US}$ was significantly reduced from 27.6 ± 4.5 to 25.2 ± 3.6 cm^2 in response IMB (weeks 8 to 10) ($-8.2\% \pm 5.8\%$; $p < 0.05$).

3.2.4 | Mid-thigh VLCSA$_{MRI}$, peak VLCSA$_{MRI}$, and muscle volume

VLCSA$_{MRI}$ data are presented in Figure 4a. VLCSA$_{MRI}$ increased from 27.3 ± 5.3 to 29.6 ± 6.4 cm^2 after RT

($7.8 \pm 4.5\%$; $p < 0.05$) and decreased from 27.4 ± 5.3 to 24.9 ± 4.5 cm^2 after IMB ($-8.7 \pm 6.1\%$; $p < 0.05$). Peak quadriceps CSA (Figure 4b) and quadriceps volume (Figure 4c) increased significantly by $5.9 \pm 3.9\%$ and $6.4 \pm 3.7\%$ after RT, respectively. Relative to Pre-IM, peak quadriceps CSA ($-4.3 \pm 6.3\%$) and muscle volume ($-4.3 \pm 6.0\%$) were both significantly reduced in response to IMB ($p < 0.05$).

3.2.5 | Correlations

Statistically significant correlations were observed between VLCSA$_{US}$ and VLCSA$_{MRI}$ at baseline and 10 weeks in accordance with previous research(Franchi, Longo, et al., 2018; Lixandrao et al., 2014) (r > 0.85 for all comparisons; Figures 5a and b). Furthermore, there were strong correlations between the percentage change in VLCSA$_{US}$ and VLCSA$_{MRI}$ (r = 0.95; Figure 5c), peak quadriceps CSA (r = 0.82; data not shown), and quadriceps muscle volume (r = 0.83; data not shown) when the data from both legs were combined. When data were analyzed separately by intervention, the correlations between the percentage change in VLCSA$_{US}$ and VLCSA$_{MRI}$ (r = 0.85; Figure 5d), peak quadriceps CSA (r = 0.65; data not shown), and muscle volume (r = 0.67; data not shown) in the IMB limb remained significant. After RT, however, only the percentage change in VLCSA$_{US}$ remained significantly correlated with VLCSA$_{MRI}$ (r = 0.67; Figure 5e).

3.2.6 | Bland-Altman Plots

A Bland-Altman plot showing the agreement between percentage change in VLCSA$_{US}$ and VLCSA$_{MRI}$ in response to RT and IMB is displayed in Figure 6. There was minimal bias between methods for the measurement of the percentage
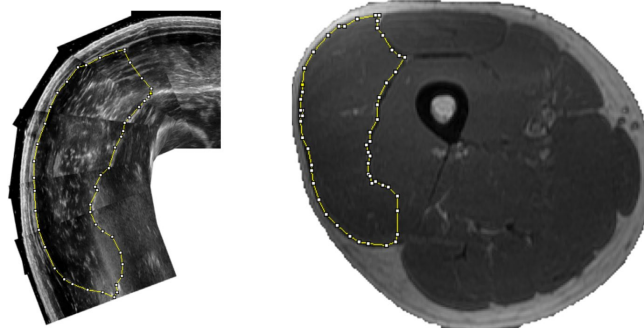

FIGURE 2 Representatives images of *vastus lateralis* CSA (VLCSA) obtained from (a) B-mode ultrasonography, and (b) Magnetic resonance. VLCSA was manually outlined in both images using open-source (ImageJ) software by the investigators in a randomized and blinded manner
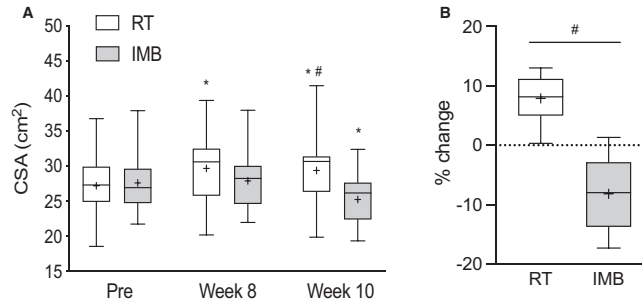
FIGURE 3 Box and whisker plots showing (a) absolute values of VLCSA and (b) percentage change in VLCSA after 10 weeks of RT and 2 weeks of IMB. Upper and lower boundaries of the boxes represent the 75th and 25th quartiles, respectively. The whiskers represent the maxima and minima. The central horizontal line represents the median and the cross represents the mean value. *denotes a statistical difference from Pre value in the respective leg and # denotes a significant difference between legs at a given time point ($p < 0.05$)

change in VLCSA ($-0.5 \pm 3.0\%$; $p > 0.05$). All measured values fell within the upper (5.4%) and lower (-6.5%) limits of agreement for both interventions with no evidence of bias within the range of measured values.

4 | DISCUSSION

We report for the first time that ultrasound-derived measurements of VLCSA hypertrophy and atrophy induced by resistance training and immobilization are significantly correlated with MRI-derived measurements when the appropriate care is taken to avoid depression of skin and muscle. Moreover, we showed that although changes in VLCSA$_{US}$ did not correlate with changes in muscle volume in response to RT, there was a significant relationship between these indices in response to immobilization. The reliability of our ultrasound assessment technique was in the range of good to excellent, and the bias compared to MRI was minimal. These results suggest that B-mode ultrasonography is a suitable alternative for the assessment of muscle hypertrophy and muscle atrophy under conditions of dynamic loading in young men.

MRI is considered to be the gold-standard for non-invasively measuring muscle size. However, it is cost-prohibitive, which has limited its routine use in physiological research. We report that, with practice and skilled operation, ultrasonography offers comparable tissue differentiation capabilities but it cannot quantify large muscles like the *vastus lateralis* in a single image because of the field of view limitation of US probes (Esformes et al., 2002; Franchi, Raiteri, et al., 2018). The introduction of the extended-field-of-view ultrasound technique (EFOV; also called panoramic ultrasound), which relies on algorithms to automatically overlap ultrasound images in real-time, has been proposed as a solution and alternative to the time-consuming process of stitching images together manually.

This method has demonstrated a high degree of concordance with MRI when measuring hamstrings CSA in an athletic cohort (Franchi et al., 2020), quadriceps muscle hypertrophy in response to RT (Ahtiainen et al., 2010), and muscle atrophy in response to bed rest (Scott et al., 2017). However, the EFOV method is limited by the relative difficulty in applying constant (and minimal) probe pressure throughout the scanning process (Ahtiainen et al., 2010; Franchi, Raiteri, et al., 2018), unless specially designed equipment is used to control probe trajectory (Noorkoiv et al., 2010). In our view, probe pressure is easier to control using the manual stitching technique that we elected to use, which allows the operator to reset his/her posture after capturing each image.

The technique of stitching several images together to overcome the small field of view of traditional ultrasound probes was developed ~15 years ago and was shown to provide valid measurements of VLCSA in a small, homogenous population of elderly adults (Reeves et al., 2004). Since this pioneering work, other research groups have confirmed the applicability and cross-sectional validity of this technique in larger sample cohorts with a wider range of *vastus lateralis* CSA (Franchi, Longo, et al., 2018; Lixandrao et al., 2014). Our data are in broad agreement with these data (Franchi, Longo, et al., 2018; Lixandrao et al., 2014), confirming the accuracy of a single assessment of muscle CSA using ultrasound. More recently, it was shown that obtaining one-dimensional muscle thickness measurements using ultrasound, obviating the need for serial image stitching, also correlates strongly with MRI-derived measurements of VLCSA and muscle volume (Franchi, Longo, et al., 2018). Together these findings provide support for the use of ultrasound to assess muscle size at a single-time point, which has important clinical utility such as effectively differentiating sarcopenic from non-sarcopenic older persons (Ismail et al., 2015). However, the ability to accurately measure *changes* in muscle size is arguably more
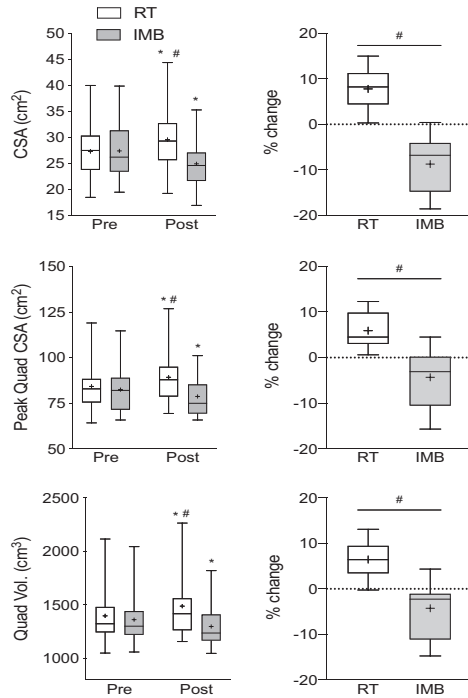
FIGURE 4 Box and whisker plots showing (a) VLCSA, (b) peak quadriceps CSA, and (c) quadriceps muscle volume before and after RT (open box and whisker plots) and IMB (gray box and whisker plots). Upper and lower boundaries of the boxes represent the 75th and 25th quartiles, respectively. The whiskers represent the maxima and minima. The central horizontal line represents the median and the cross represents the mean value. *denotes a statistical difference from Pre value in the respective leg and # denotes a significant difference between legs at a given time point ($p < 0.05$)

important, as doing so allows researchers to test the efficacy of dietary or exercise interventions or clinical conditions that result in either hypertrophy or atrophy.

The use of US to quantify muscle hypertrophy in response to resistance training is a relatively common practice and has led to important insights regarding regional hypertrophy and other morphological adaptations (i.e., changes in the pennation angle and fascicle length Earp et al., 2015; Mangine et al., 2018; Wells et al., 2014). However, very few studies have evaluated the validity of ultrasound against the reference standard to accurately measure muscle growth. Franchi *et al* demonstrated a significant correlation between changes in muscle thickness assessed by ultrasound after 12 weeks of unilateral RT and the corresponding changes in VLCSA measured by MRI, indicating that US-derived MT measurements could serve as a useful surrogate for

mid-thigh VLCSA hypertrophy (Franchi, Longo, et al., 2018). However, changes in MT were not correlated with changes in muscle volume (Franchi, Longo, et al., 2018). In accordance with these findings (Franchi, Longo, et al., 2018), we observed a significant correlation between ultrasound- and MRI-measured changes in mid-thigh VLCSA, but not between VLCSA and muscle volume in response to RT. The reasons for this lack of relationship are unclear but could be due to regional differences in muscle hypertrophy (Earp et al., 2015; Franchi et al., 2014; Franchi, Longo, et al., 2018; Mangine et al., 2018; Wells et al., 2014). Indeed, changes in fascicle length—which have been reported to occur—are more likely to affect the growth of distal regions of the muscle (Jorgenson et al., 2020) and would, therefore, be undetected by a single measurement at the mid-point of the thigh.

To circumvent the potential confounding influence of regional hypertrophy, and strengthen the association between ultrasound and MRI in future investigations, multiple images could be obtained along the length of the muscle and volume estimated using the Cavalieri principle (Infantolino et al., 2007). Indeed, the measurement of *vastus lateralis* muscle volume using ultrasound is largely concordant with volume estimates derived from the hydrostatic weighing of cadaver samples when applying this method (Infantolino et al., 2007). Again, however, these measurements were made at a single-time point (Infantolino et al., 2007) and the addition of repeated measurements to assess changes over time will inevitably introduce additional error and likely weaken the association. These errors are likely to be magnified by not taking into account the impact of probe pressure during serial image acquisition. Thus, future research is warranted to investigate whether the derivation of muscle volume from a series of US images would strengthen the relationship between US and MRI when assessing muscle hypertrophy.

In comparison to resistance exercise, there is a paucity of literature assessing the efficacy of ultrasound to detect, and accurately measure, changes in muscle size associated with disuse and muscle-wasting conditions. Puthucheary and colleagues showed that the loss of *rectus femoris* CSA measured by ultrasound correlated with the extent of organ failure and length of stay in critically ill patients admitted to the ICU (Puthucheary et al., 2013). Thus, although the authors did not formally assess the relationship between ultrasound and MRI measured muscle loss in these patients, the correlations identified between ultrasound-derived measurements of muscle size and clinically relevant outcomes provided evidence that ultrasound might be useful for quantifying skeletal muscle loss in a patient population (Paris et al., 2017; Puthucheary et al., 2013). Scott *et al* recently validated the use of panoramic ultrasound against MRI for measuring changes in VLCSA in response to bed-rest with or without an exercise counter-intervention reporting close agreement between methods (Scott et al.,
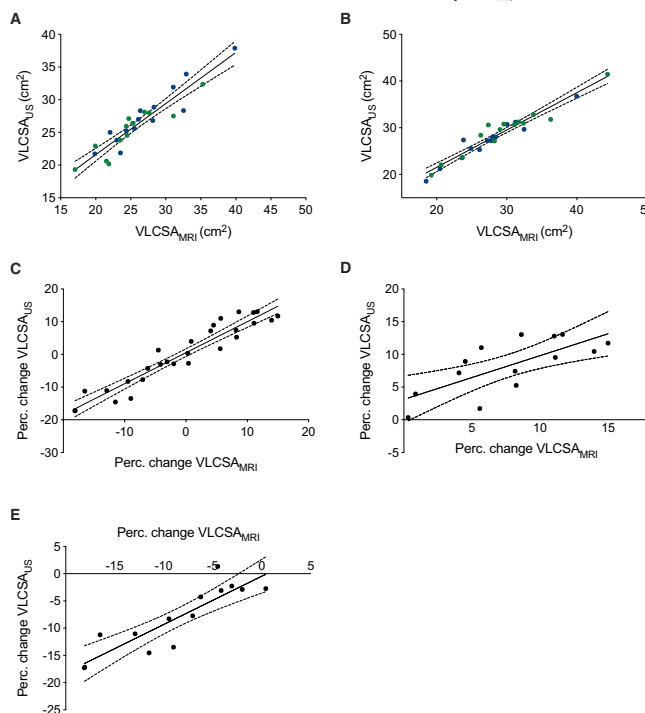
FIGURE 5 (a and b) Scatterplots showing the relationship between absolute VLCSA$_{US}$ and VLCSA$_{MRI}$ measurements taken from the IMB leg (a) and RT leg (b). Blue dots depict baseline values, whereas green dots represent values taken at week 10. (c-e) Scatterplots showing the relationship between the percentage change in (c) VLCSA$_{US}$ and VLCSA$_{MRI}$ including both RT and IMB limbs, (d) VLCSA$_{US}$ and VLCSA$_{MRI}$ in the limb subjected to resistance training (RT), and (e) VLCSA$_{US}$ and VLCSA$_{MRI}$ in the limb subjected to immobilization (IMB). The solid line and the dotted lines in Panels A through E represent the line of best fit and the 95% confidence intervals, respectively

2017). In line with their findings, we also observed a close association between methods using image-stitching using an ultrasound unit lacking automated panoramic capabilities. We also provide novel data showing that the loss of VLCSA in response to immobilization measured by US is correlated with the reduction in muscle volume measured by MRI. These data suggest that, in contrast to muscle hypertrophy, muscle atrophy appears to be more homogenous through the length of the muscle in response to immobilization. However, whether ultrasound can detect early stage smaller decreases in muscle size in response to shorter term disuse (i.e., 3–7 days) requires further investigation.

4.1 | Limitations

The primary limitation of the present study is that we only measured the *vastus lateralis* muscle at a single site using US.

There is evidence that the quadriceps muscle group exhibits regional muscle hypertrophy (Franchi et al., 2014; Franchi, Longo, et al., 2018; Mangine et al., 2018; Wells et al., 2014), which would be missed when only assessing the mid-thigh region of one muscle. Indeed, as we discussed above, this may be a major reason for the lack of correlation we observed between VLCSA measurements by US and MRI-derived assessments of muscle volume in response to RT. Obtaining multiple measurements of VLCSA at different regions of the thigh and deriving an estimate of muscle volume would, we hypothesize, strengthen the association between methods. Second, while the average changes in VLCSA observed in our study exceed the minimal detectable change of 3.03 cm^2 we calculated, our stitching technique may not be suitable to detect more subtle changes in muscle size that occur with other interventions that induce comparatively minor changes in VLCSA. Finally, our analysis included only younger, college-aged men, a population with a relatively thin layer
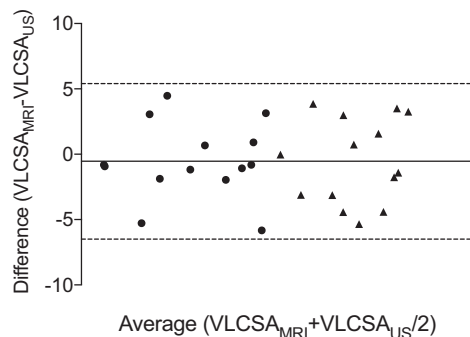
FIGURE 6 Bland-Altman plot showing the methodological agreement between the percentage change in VLCSA$_{US}$ and VLCSA$_{MRI}$ after 10 weeks of resistance training (triangles) and 2 weeks of immobilization (circles). Dotted horizontal lines represent the upper and lower limits of agreement and the solid horizontal line represents the bias of ultrasonography relative to MRI

of subcutaneous adipose tissue overlying the muscle. Future research is needed to determine how US compares to MRI in older populations and in overweight/obese individuals with thicker subcutaneous adipose depots that may reduce the accuracy of our image stitching technique.

5 | CONCLUSIONS

We show that B-mode ultrasonography provides a comparable alternative to magnetic resonance imaging for measuring changes in muscle size in response to loading-induced hypertrophy and immobilization-induced atrophy of the *vastus lateralis* in young men. In addition, we highlight that it is important to not depress the skin during image acquisition, and that caution is warranted when comparing ultrasound-derived muscle CSA and MRI-derived muscle volume. Further work is required to establish that this conclusion is valid in women and in older persons or other clinical scenarios.

CONFLICTS OF INTEREST
The authors declare no conflicts of interest.

ORCID
Stuart M. Phillips https://orcid.org/0000-0002-1956-4098

REFERENCES
Ahtiainen, J. P., Hoffren, M., Hulmi, J. J., Pietikainen, M., Mero, A. A., Avela, J., & Hakkinen, K. (2010). Panoramic ultrasonography is a valid method to measure changes in skeletal muscle cross-sectional area. *European Journal of Applied Physiology*, 108, 273–279.

Chen, Y. W., Gregory, C., Ye, F., Harafuji, N., Lott, D., Lai, S. H., Mathur, S., Scarborough, M., Gibbs, P., Baligand, C., & Vandenborne, K. (2017). Molecular signatures of differential responses to exercise trainings during rehabilitation. *Biomed Genet Genom*, 2.

Davidsen, P. K., Gallagher, I. J., Hartman, J. W., Tarnopolsky, M. A., Dela, F., Helge, J. W., Timmons, J. A., & Phillips, S. M. (2011). High responders to resistance exercise training demonstrate differential regulation of skeletal muscle microRNA expression. *Journal of Applied Physiology*, 1985(110), 309–317.

Devries, M. C., Breen, L., von Allmen, M., Macdonald, M. J., Moore, D. R., Offord, E. A., Horcajada, M. N., Breuillé, D., & Phillips, S. M. (2015). Low-load resistance training during step-reduction attenuates declines in muscle mass and strength and enhances anabolic sensitivity in older men. *Physiological Reports*, 3, e12493.

Earp, J. E., Newton, R. U., Cormie, P., & Blazevich, A. J. (2015). Inhomogeneous quadriceps femoris hypertrophy in response to strength and power training. *Medicine and Science in Sports and Exercise*, 47, 2389–2397.

Esformes, J. I., Narici, M. V., & Maganaris, C. N. (2002). Measurement of human muscle volume using ultrasonography. *European Journal of Applied Physiology*, 87, 90–92.

Fernandez-Gonzalo, R., Tesch, P. A., Lundberg, T. R., Alkner, B. A., Rullman, E., & Gustafsson, T. (2020). Three months of bed rest induce a residual transcriptomic signature resilient to resistance exercise countermeasures. *The FASEB Journal*, 34, 7958–7969.

Franchi, M. V., Atherton, P. J., Reeves, N. D., Fluck, M., Williams, J., Mitchell, W. K., Selby, A., Beltran Valls, R. M., & Narici, M. V. (2014). Architectural, functional and molecular responses to concentric and eccentric loading in human skeletal muscle. *Acta Psychologica*, 210, 642–654.

Franchi, M. V., Fitze, D. P., Hanimann, J., Sarto, F., & Sporri, J. (2020). Panoramic ultrasound vs. MRI for the assessment of hamstrings cross-sectional area and volume in a large athletic cohort. *Scientific Reports*, 10, 14144.

Franchi, M. V., Longo, S., Mallinson, J., Quinlan, J. I., Taylor, T., Greenhaff, P. L., & Narici, M. V. (2018). Muscle thickness correlates to muscle cross-sectional area in the assessment of strength training-induced hypertrophy. *Scandinavian Journal of Medicine and Science in Sports*, 28, 846–853.

Franchi, M. V., Raiteri, B. J., Longo, S., Sinha, S., Narici, M. V., & Csapo, R. (2018). Muscle architecture assessment: strengths, shortcomings and new frontiers of in vivo imaging techniques. *Ultrasound in Medicine and Biology*, *44*, 2492–2504.

Glover, E. I., Phillips, S. M., Oates, B. R., Tang, J. E., Tarnopolsky, M. A., Selby, A., Smith, K., & Rennie, M. J. (2008). Immobilization induces anabolic resistance in human myofibrillar protein synthesis with low and high dose amino acid infusion. *Journal of Physiology*, *586*, 6049–6061.

Haun, C. T., Vann, C. G., Roberts, B. M., Vigotsky, A. D., Schoenfeld, B. J., & Roberts, M. D. (2019). A critical evaluation of the biological construct skeletal muscle hypertrophy: size matters but so does the measurement. *Frontiers in Physiology*, *10*, 247.

Holloway, T. M., McGlory, C., McKellar, S., Morgan, A., Hamill, M., Afeyan, R., Comb, W., Confer, S., Zhao, P., Hinton, M., Kubassova, O., Chakravarthy, M. V., & Phillips, S. M. (2019). A novel amino acid composition ameliorates short-term muscle disuse atrophy in healthy young men. *Frontiers in Nutrition*, *6*, 105.

Hubal, M. J., Gordish-Dressman, H., Thompson, P. D., Price, T. B., Hoffman, E. P., Angelopoulos, T. J., Gordon, P. M., Moyna, N. M., Pescatello, L. S., Visich, P. S., Zoeller, R. F., Seip, R. L., & Clarkson, P. M. (2005). Variability in muscle size and strength gain after unilateral resistance training. *Medicine and Science in Sports and Exercise*, *37*, 964–972.

Infantolino, B. W., Gales, D. J., Winter, S. L., & Challis, J. H. (2007). The validity of ultrasound estimation of muscle volumes. *Journal of Applied Biomechanics*, *23*, 213–217.

Ismail, C., Zabal, J., Hernandez, H. J., Woletz, P., Manning, H., Teixeira, C., Dipietro, L., Blackman, M. R., & Harris-Love, M. O. (2015). Diagnostic ultrasound estimates of muscle mass and muscle quality discriminate between women with and without sarcopenia. *Frontiers in Physiology*, *6*, 302.

Janssen, I., Heymsfield, S. B., & Ross, R. (2002). Low relative skeletal muscle mass (sarcopenia) in older persons is associated with functional impairment and physical disability. *Journal of the American Geriatrics Society*, *50*, 889–896.

Janssen, I., Heymsfield, S. B., Wang, Z. M., & Ross, R. (2000). Skeletal muscle mass and distribution in 468 men and women aged 18–88 yr. *Journal of Applied Physiology*, *1985*(89), 81–88.

Jorgenson, K. W., Phillips, S. M., & Hornberger, T. A. (2020). Identifying the structural adaptations that drive the mechanical load-induced growth of skeletal muscle: A Scoping Review. *Cells*, *9*.

Koo, T. K., & Li, M. Y. (2016). A guideline of selecting and reporting intraclass correlation coefficients for reliability research. *Journal of Chiropractic Medicine*, *15*, 155–163.

Lixandrao, M. E., Ugrinowitsch, C., Bottaro, M., Chacon-Mikahil, M. P., Cavaglieri, C. R., Min, L. L., de Souza, E. O., Laurentino, G. C., & Libardi, C. A. (2014). Vastus lateralis muscle cross-sectional area ultrasonography validity for image fitting in humans. *Journal of Strength & Conditioning Research*, *28*, 3293–3297.

Mangine, G. T., Redd, M. J., Gonzalez, A. M., Townsend, J. R., Wells, A. J., Jajtner, A. R., Beyer, K. S., Boone, C. H., la Monica, M. B., Stout, J. R., Fukuda, D. H., Ratamess, N. A., & Hoffman, J. R. (2018). Resistance training does not induce uniform adaptations to quadriceps. *PLoS One*, *13*, e0198304.

Mitsiopoulos, N., Baumgartner, R. N., Heymsfield, S. B., Lyons, W., Gallagher, D., & Ross, R. (1998). Cadaver validation of skeletal muscle measurement by magnetic resonance imaging and computerized tomography. *Journal of Applied Physiology (1985)*, *85*, 115–122.

Moore, D. R., Kelly, R. P., Devries, M. C., Churchward-Venne, T. A., Phillips, S. M., Parise, G., & Johnston, A. P. (2018). Low-load resistance exercise during inactivity is associated with greater fibre area and satellite cell expression in older skeletal muscle. *Journal of Cachexia, Sarcopenia Muscle*, *9*, 747–754.

Morton, R. W., Oikawa, S. Y., Wavell, C. G., Mazara, N., McGlory, C., Quadrilatero, J., Baechler, B. L., Baker, S. K., & Phillips, S. M. (2016). Neither load nor systemic hormones determine resistance training-mediated hypertrophy or strength gains in resistance-trained young men. *Journal of Applied Physiology*, *121*(1), 129–138..

Nijholt, W., Scafoglieri, A., Jager-Wittenaar, H., Hobbelen, J. S. M., & van der Schans, C. P. (2017). The reliability and validity of ultrasound to quantify muscles in older adults: a systematic review. *J Cachexia Sarcopenia Muscle*, *8*, 702–712.

Oates, B. R., Glover, E. I., West, D. W., Fry, J. L., Tarnopolsky, M. A., & Phillips, S. M. (2010). Low-volume resistance exercise attenuates the decline in strength and muscle mass associated with immobilization. *Muscle and Nerve*, *42*, 539–546.

Paris, M. T., Lafleur, B., Dubin, J. A., & Mourtzakis, M. (2017). Development of a bedside viable ultrasound protocol to quantify appendicular lean tissue mass. *Journal of Cachexia Sarcopenia Muscle*, *8*, 713–726.

Parker, L., Nazarian, L. N., Carrino, J. A., Morrison, W. B., Grimaldi, G., Frangos, A. J., Levin, D. C., & Rao, V. M. (2008). Musculoskeletal imaging: medicare use, costs, and potential for cost substitution. *Journal of the American College of Radiology*, *5*, 182–188.

Powers, S. K., Lynch, G. S., Murphy, K. T., Reid, M. B., & Zijdewind, I. (2016). Disease-induced skeletal muscle atrophy and fatigue. *Medicine and Science in Sports and Exercise*, *48*, 2307–2319.

Puthucheary, Z. A., Rawal, J., McPhail, M., Connolly, B., Ratnayake, G., Chan, P., Hopkinson, N. S., Phadke, R., Dew, T., Sidhu, P. S., Velloso, C., Seymour, J., Agley, C. C., Selby, A., Limb, M., Edwards, L. M., Smith, K., Rowlerson, A., Rennie, M. J., … Montgomery, H. E. (2013). Acute skeletal muscle wasting in critical illness. *JAMA*, *310*, 1591–1600.

Reeves, N. D., Maganaris, C. N., & Narici, M. V. (2004). Ultrasonographic assessment of human skeletal muscle size. *European Journal of Applied Physiology*, *91*, 116–118.

Scott, J. M., Martin, D. S., Ploutz-Snyder, R., Matz, T., Caine, T., Downs, M., Hackney, K., Buxton, R., Ryder, J. W., & Ploutz-Snyder, L. (2017). Panoramic ultrasound: a novel and valid tool for monitoring change in muscle mass. *Journal of Cachexia, Sarcopenia and Muscle*, *8*, 475–481.

Stokes, T., Timmons, J. A., Crossland, H., Tripp, T. R., Murphy, K., McGlory, C., Mitchell, C. J., Oikawa, S. Y., Morton, R. W., Phillips, B. E., Baker, S. K., Atherton, P. J., Wahlestedt, C., & Phillips, S. M. (2020). Molecular transducers of human skeletal muscle remodeling under different loading states. *Cell Reports*, *32*, 107980.

Weir, J. P. (2005). Quantifying test-retest reliability using the intraclass correlation coefficient and the SEM. *Journal of Strength Conditioning Research*, *19*, 231–240.

Wells, A. J., Fukuda, D. H., Hoffman, J. R., Gonzalez, A. M., Jajtner, A. R., Townsend, J. R., Mangine, G. T., Fragala, M. S., & Stout, J. R. (2014). Vastus lateralis exhibits non-homogenous adaptation to resistance training. *Muscle and Nerve*, *50*, 785–793.

Wilson, D., Breen, L., Lord, J. M., & Sapey, E. (2018). The challenges of muscle biopsy in a community based geriatric population. *BMC Research Notes*, *11*, 830.

Wolfe, R. R. (2006). The underappreciated role of muscle in health and disease. *American Journal of Clinical Nutrition*, *84*, 475–482.

Yasuda, N., Glover, E. I., Phillips, S. M., Isfort, R. J., & Tarnopolsky, M. A. (2005). Sex-based differences in skeletal muscle function and morphology with short-term limb immobilization. *Journal of Applied Physiology*, *1985*(99), 1085–1092.

CHAPTER 3:

Molecular Transducers of Human Skeletal Muscle Remodelling under Different Loading States.
Published in *Cell Reports* 2020. 32(5): 107980

Cell Reports

Molecular Transducers of Human Skeletal Muscle Remodeling under Different Loading States

Graphical Abstract

Authors

Tanner Stokes, James A. Timmons, Hannah Crossland, ..., Phillip J. Atherton, Claes Wahlestedt, Stuart M. Phillips

Correspondence

phillis@mcmaster.ca

In Brief

Stokes et al. identify and validate a core set of genes that are regulated in proportion to the magnitude of muscle protein turnover with loading. Several of these genes correlate with muscle growth only at their 3′ or 5′ untranslated region, and a subset directly influences protein synthesis *in vitro*.

Highlights

- Muscle loading and unloading regulate the untranslated regions of mRNA

- Regulated genes form functional networks central to muscle plasticity

- 141 genes correlate with muscle growth in 3 independent validation cohorts

- Several growth-correlated network genes directly regulate myocyte protein synthesis

CellPress

Cell Reports

Resource

Molecular Transducers of Human Skeletal Muscle Remodeling under Different Loading States

Tanner Stokes,[1] James A. Timmons,[2] Hannah Crossland,[3] Thomas R. Tripp,[4] Kevin Murphy,[1] Chris McGlory,[5] Cameron J. Mitchell,[6] Sara Y. Oikawa,[1] Robert W. Morton,[1] Bethan E. Phillips,[3] Steven K. Baker,[7] Phillip J. Atherton,[3] Claes Wahlestedt,[2] and Stuart M. Phillips[1,8,*]

[1]Department of Kinesiology, McMaster University, Hamilton, ON, Canada
[2]Center for Therapeutic Innovation, University of Miami Miller School of Medicine, Miami, FL, USA
[3]School of Medicine, Royal Derby Hospital, University of Nottingham, Derby, UK
[4]Faculty of Kinesiology, University of Calgary, Calgary, AB, Canada
[5]School of Kinesiology and Health Studies, Queens University, Kingston, ON, Canada
[6]School of Kinesiology, University of British Columbia, BC, Canada
[7]Physical Medicine and Rehabilitation, Department of Medicine, McMaster University, Hamilton, Canada
[8]Lead Contact
*Correspondence: phillis@mcmaster.ca
https://doi.org/10.1016/j.celrep.2020.107980

SUMMARY

Loading of skeletal muscle changes the tissue phenotype reflecting altered metabolic and functional demands. In humans, heterogeneous adaptation to loading complicates the identification of the underpinning molecular regulators. A within-person differential loading and analysis strategy reduces heterogeneity for changes in muscle mass by ~40% and uses a genome-wide transcriptome method that models each mRNA from coding exons and 3′ and 5′ untranslated regions (UTRs). Our strategy detects ~3–4 times more regulated genes than similarly sized studies, including substantial UTR-selective regulation undetected by other methods. We discover a core of 141 genes correlated to muscle growth, which we validate from newly analyzed independent samples (n = 100). Further validating these identified genes via RNAi in primary muscle cells, we demonstrate that members of the core genes were regulators of protein synthesis. Using proteome-constrained networks and pathway analysis reveals notable relationships with the molecular characteristics of human muscle aging and insulin sensitivity, as well as potential drug therapies.

INTRODUCTION

Increased loading of skeletal muscle induces muscle fiber hypertrophy requiring the remodeling of myofibrillar and extracellular protein lattices. In contrast, unloading (UL) results in fiber atrophy, reductions in protein content, and a more fatigable tissue phenotype. In humans, voluntary loading (via resistance exercise training [RT]) leads to a highly heterogeneous physiological adaptation across individuals, which is associated with differential molecular response (Davidsen et al., 2011; Keller et al., 2011; Timmons et al., 2005). The implications of this heterogeneity are substantial, influencing muscle insulin sensitivity and age-related musculoskeletal frailty (Timmons et al., 2018; von Haehling et al., 2012) and potentially underpinning the compromised growth response in older individuals (Da Boit et al., 2016; Kosek et al., 2006). Less appreciated is the fact that the UL of human muscle also results in highly variable losses of muscle mass (Glover et al., 2008; Yasuda et al., 2005). The key regulators of heterogeneous muscle remodeling in response to loading and UL are unknown.

Collapsing data across individuals showing divergent physiological adaptation, as well as the use of small sample sizes, limits the reliable discovery of molecular regulators (Sweeney et al., 2017; Timmons, 2011). In contrast, accounting for physiological heterogeneity helps identify genes that regulate exercise adaptation in humans (Adami et al., 2018; Peter et al., 2014). Small-scale human physiology studies that focus on in-depth phenotyping limit reliable correlation modeling (Cohain et al., 2017; Schönbrodt and Perugini, 2013), particularly for genome-wide omics. The increasing use of omics has advanced our understanding of the molecular regulators of loading; however, proteomics applied to muscle tissue captures a very limited sample of the protein-coding genome (Camera et al., 2017), which limits the validity of pathway analysis (Timmons et al., 2015). Unbiased transcriptome profiling can be more reliable, and variation in RNA can explain up to 75% of the variation in protein abundance, with some exceptions (Li and Biggin, 2015). Nevertheless, it has been reported that RNA does not reliably predict changes in protein abundance during muscle loading (Robinson et al., 2017). Typically, RNA quantification relies on technology that averages across an otherwise complex set of transcripts from a gene (Shalek et al., 2013) or uses short-read RNA sequencing that misses significant proportions of the tissue transcriptome (Sood et al., 2016). Thus, suboptimal RNA profiling may contribute to a discordance between muscle RNA and protein abundance (Robinson et al., 2017).
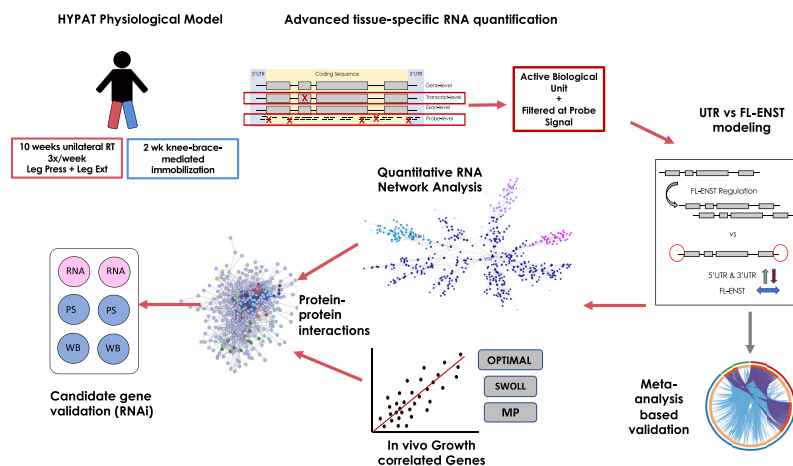
Figure 1. Experimental Workflow and Analysis Strategy
We used a paired unilateral loading (10 weeks of progressive RT) and unloading (UL; 2 weeks of UL) model in combination with genome-wide transcriptomic analysis (Timmons et al., 2018) to study differential expression of gene UTRs and protein coding regions. Probes were subjected to extensive filtering before downstream analysis (see STAR Methods). Significance analysis of microarrays implemented in the R programming environment (SAMR) was used to detect significantly regulated genes (Tusher et al., 2001), which were then used as an input list for quantitative network analysis using the MEGENA package for R (Song and Zhang, 2015). We also determined which genes played a role in regulating dynamic lean tissue growth in independent cohorts (total n = 100). Highly co-regulated genes and growth-correlated gene lists were used as input in metascape.org and https://www.networkanalyst.ca to characterize protein-protein interaction networks and drug signatures.

We hypothesized that a method that reduced physiological heterogeneity to loading states and improved the fidelity of RNA quantification (Figure 1) would allow the improved identification of the molecular regulators of adaptation. We contrasted muscle subjected to a loading hypertrophic stimulus with the paired (contralateral) muscle subjected to UL to induce atrophy (a model called HypAt). The aim of the HypAt model is to measure molecular responses to loading and UL within an individual to reduce heterogeneity and more readily reveal potential regulators. We characterized phenotypic responses to HypAt and implemented an approach to quantify both full-length mRNA transcripts (FL-ENST) and the untranslated regions (UTRs) of the same "gene," as they can regulate translational efficiency (Mayr, 2017). We established key genes regulated during gains in lean mass in three independent cohorts, some of which directly regulate protein synthesis *in vitro*. We used proteome-constrained network and pathway analyses to discover relationships between the transducers of dynamic muscle remodeling, muscle aging, and insulin resistance and match molecular signatures to potentially useful US Food and Drug Administration (FDA)-approved drugs.

RESULTS

Muscle Growth and Integrated Myofibrillar Protein Synthesis
Participant characteristics for the paired analysis (HypAt) are displayed in Table S1 (see STAR Methods for the demographics of the additional clinical studies). Dietary macronutrient intakes were stable during the study (17% ± 6% protein, 49% ± 15% carbohydrate, 32% ± 12% fat). The protein consumed was 1.5 ± 0.7 g · kg^{-1} · day and 1.7 ± 0.2 g · kg^{-1} on training days, sufficient to fully support muscle hypertrophy (Morton et al., 2018). At baseline, the daily step count averaged 9,900 ± 5,100 steps per day and remained unchanged throughout the study. The average changes in function were as expected—isometric maximal voluntary contraction torque (ISO-MVC) increased by 14% after RT (median: 5.6%; range: −2.5% to 50.1%; p < 0.05) and decreased by ~14% following UL (median: −12.7%; range: −1.3% to −28.3%; p < 0.05). Leg extension strength increased by 48% (median: 46%; range: 13%–100%) and leg press by 67% after RT (median: 72%; range: 13%–158%; p < 0.05). Orally administered deuterated water and muscle biopsies quantified integrated myofibrillar protein synthesis (iMyoPS) rates (Wilkinson et al., 2014) (deuterium enrichment in saliva over time is shown in Figure S1E). Pre-intervention iMyoPS was 1.37% ± 0.07% day^{-1}, consistent with earlier work (Brook et al., 2016). iMyoPS increased 12.6% after 10 weeks of RT and decreased 9.5% with 2 weeks of UL (p < 0.05; Figure 2A). In HypAt, leg lean mass (LLM; by dual-energy X-ray absorptiometry [DXA]) increased by ~5% (median: 4.2%; range: −1.2% to 14.0%; p < 0.05) in response to RT, while the immobilized leg demonstrated a 3.4% decrease (median: −3.0%; range: 0.5 to −8.4%; p < 0.05; Figure 2B). In addition, we found, using magnetic resonance imaging, that mid-thigh *vastus lateralis*

Figure 2. Dynamic Muscle Loading Alters Muscle Protein Synthesis (MPS) and Muscle Size

(A) Absolute change in integrated myofibrillar protein synthesis rates (n = 12).

(B) Percentage change in leg lean mass (LLM) after 10 weeks of unilateral RT and 2 weeks of UL, respectively (n = 12). *Statistically different from Pre (baseline value); #statistically different from RT value (p < 0.05).

In both panels, the boxes include the 25th, 50th, and 75th quartiles and whiskers represent the maximum and minimum values. The mean value is depicted by +.

See also Figure S1.

cross-sectional area (VLCSA) increased by 8.1% following RT (median: 8.2%; range: 0.9%–15%; p < 0.05), whereas VLCSA was reduced in the UL leg by 9.0% (median: −6.8%; range: 0.4 to −18.5%; p < 0.05; Figure S1A). Quadriceps volume (Figure S1B) and peak quadriceps CSA (Figure S1C) demonstrated a similar pattern. Calculating the individual physiological responses, as proposed (HypAt), reduced the inter-subject heterogeneity for change in muscle size by almost half (coefficient of variation [CoV] was 90%, 88%, and 49% for RT, UL, and HypAt, respectively). Thus, each subject provided a more consistent differential change in muscle mass, and hence improved the validity of any means-based analyses.

Functional RNA Networks Are in High Agreement with Established Proteome Responses to Exercise

Global muscle transcriptomes were generated from four independent clinical studies using the Affymetrix HTA 2.0 array. A probe set signal, based on ensemble identifiers (Dai et al., 2005), either represented a FL-ENST or the 5′ UTR or the 3′ UTR signal from a FL-ENST. For FL-ENST versus 3′ UTR comparisons, there were 32,307 probe sets, while for FL-ENST versus 5′ UTR, there were 28,291. This resulted in 44,358 largely protein-coding probe sets, representing 11,628 genes. For FL-ENST differential analysis, 18% of the 11,628 genes had at least 1 FL-ENST regulated (false discovery rate [FDR] <5%, fold change [FC] >1.2; 1,435 upregulated and 649 downregulated; Data S1). There were more genes regulated by measuring their 3′ UTR than the FL-ENST (Figure 3A; Data S1). There were 1,162 upregulated and 1,200 downregulated 3′ UTR (fewer 5′ UTRs were regulated; 553 genes upregulated and 206 downregulated; Data S1). Compared with clinical studies using interventions of similar duration (Damas et al., 2019; Melov et al., 2007; Phillips et al., 2013; Raue et al., 2012), our approach identified ~4 times more regulated molecular events. The regulated groups of genes had the expected roles in extracellular matrix remodeling, mitochondrial biology, and angiogenic processes (Figure 3B; Data S1).

The measurement of changes in the UTR signal allows for the identification of factors, beyond mRNA abundance, that influence translation. For example, a greater 3′ UTR:protein coding sequence (CDS) ratio can lead to lower protein production (Floor

and Doudna, 2016; Kocabas et al., 2015), presumably reflecting increased miRNA and RNA-binding protein target sites within the lengthened 3′ UTR. For HypAt upregulated genes, the pattern was >70% consistent between FL-ENST and the UTR signals; however, this consistency was reduced to 40% for downregulated genes (Data S1). There were >1,000 genes that were statistically "regulated" only at their UTR signal (Figure 3A; Data S1). We applied a heuristic method (see Method Details) to identify genes that demonstrated a distinct pattern of regulation across the 3 signals, revealing a subset of FL-ENST (n = 112 genes), 3′ UTR (n = 200 genes), and 5′ UTR transcripts (n = 62 genes), which demonstrated selective differential regulation *in vivo* (e.g., FL-ENST upregulated with reduced 5′ UTR signals or 3′ UTR signals reduced more than the FL-ENST signal, indicating a shift in the mRNA population; Data S1). For example, seven genes involved in the repair of double-strand DNA breaks (*HUS1B*, *LIG3*, *MRNIP*, *RAD51C*, *RIF1*, SPIDR, and *ZFYVE26*) had unchanged levels of mRNA, yet their 3′ UTR signal was substantially reduced. The 3′ UTR of branched-chain amino acid transaminase 2 (*BCAT2*), a mitochondrial branched-chain amino acid catabolism gene, increased on average, indicating that the BCAT2 population of mRNAs in muscle had longer 3′ UTRs during gains in lean mass. Furthermore, there were 275 discordantly regulated genes at the 3′ UTR versus 5′ UTR (Data S1). The biological processes carried out by these genes included developmental and peptide or K48-linked de-ubiquitination (Figure 3C).

We used quantitative network modeling (Song and Zhang, 2015) to demonstrate that the HypAt-regulated genes formed significant gene expression networks (Data S1). This method identifies groups of co-regulated genes and does so independently of any knowledge of gene function (i.e., it is data driven). The identification of known gene-gene relationships provides internal validation and a framework to assign genes of unknown function (van Dam et al., 2015). Analysis of the FL-ENST yielded networks centered around mitochondrial genes (e.g., NDUFS3, reflecting tight coordination of the mitochondrial transcriptome; Figure S2). The significant ontology categories, beyond tissue bias (Timmons et al., 2015), included Gene Ontology (GO):0055114 "oxidation-reduction process" (p < 1 × 10^{-15}) for the *NDUFS3* network. Another major network centered around Dedicator of Cytokinesis 1 (*DOCK1*) (a 312-gene network;
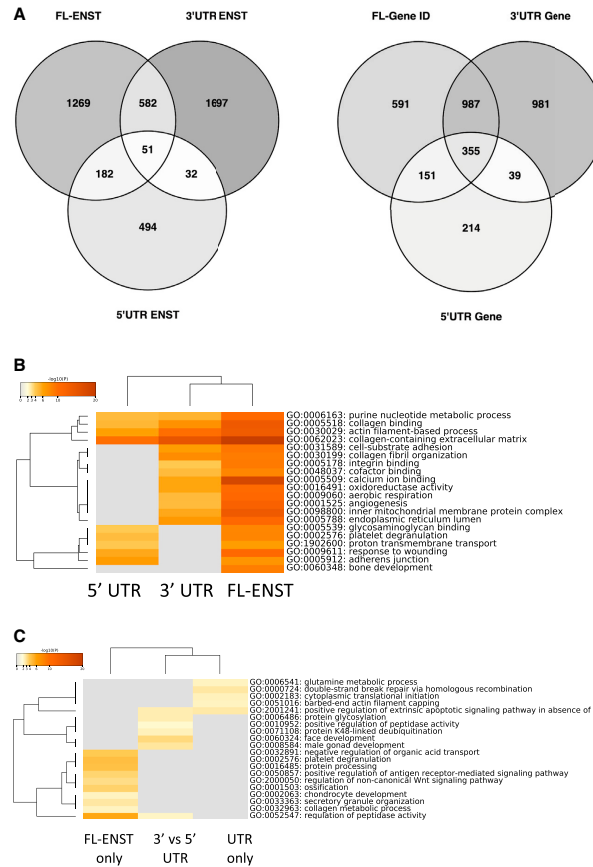
Figure 3. The Untranslated Regions (UTRs) of Genes Are Subject to Extensive Regulation by Dynamic Muscle Loading States

(A) Venn diagrams show the extent of overlap in FL-ENST, 3′ UTR, and 5′ UTR gene expression. More genes showed regulation at the 3′ UTR than at the FL-ENST level; however, there was substantial overlap.

(B and C) Heatmaps showing (B) functional pathway enrichment based on gene region (5′ UTR, 3′ UTR, or FL-ENST) and (C) the significance level of different Gene Ontology pathways by transcript type: FL-ENST only versus UTR only versus differential 3′ UTR/5′ UTR regulation only. The ontology enrichment scores are relatively modest after correction for tissue and platform bias. Heatmaps were generated using Metascape (metascape.org). The colors indicate the level of significance, with the darker colors being more significant. The gray boxes are non-significant results.

muscle mass. We used 3 independent studies (n = 100 individuals, 200 HTA 2.0 gene chips; Data S1), each with DXA-measured changes in LLM following exercise training (Mitchell et al., 2014; Morton et al., 2016; Phillips et al., 2017) to establish which of the ∼2,000 HypAt-regulated genes were potential regulators of growth. For reliable estimates, sample sizes of ≥30 are required for correlation analysis (Gobbi and Jurman, 2015; Schönbrodt and Perugini, 2013). We calculated pre-post training differential probe set signal and Spearman rank correlation across each study and then aggregated consistent (directionality) correlation coefficients and found that 141 genes were correlated in a consistent manner with muscle mass gains (either at the FL-ENST, 3′ UTR or 5′ UTR level) and were regulated in the HypAt model. Genes correlating with muscle growth coded for proteins involved in purine ribonucleoside monophosphate biosyn-

thesis (e.g., AMP, guanosine monophosphate [GMP], inosine monophosphate [IMP], and xanthosine monophosphate [XMP]), mitochondrial biology (Figure S3, inset) and included numerous positive regulators shown previously, such as the apelin receptor (APLNR, upregulated in HypAt, correlation coefficient (CC) = 0.34), a known mediator of hypertrophy (Hwangbo et al., 2017; Vinel et al., 2018). APLNR negatively co-varied with known negative regulators of hypertrophy (FOXO3, CC −0.4; PRKAA2, CC −0.3), which were negatively correlated with changes in LLM (CC −0.33 and −0.21, respectively). These in turn were strongly co-regulated, during muscle growth, with KDR, TIE1, and NRP1, which are potent regulators of angiogenesis.

Examination of the relationships between modulation of transcript 3′ UTR signals and the change in lean mass revealed

Figure S2), a Rho guanosine triphosphatase (GTPase)-related gene regulated by mechanical strain (Copley Salem et al., 2018) and genetically linked to cachexia (McDonald et al., 2017). The top ontology category of the DOCK1 network was GO:0040011 "self-propelled movement of a cell" (p < 1 × 10^{-11}). These analyses indicate that the molecules that we identified as regulated in the HypAt model reflect functional networks central to muscle tissue physiology, including many of the same features identified using proteome analysis (Robinson et al., 2017).

Proteome-Constrained Network Modeling Reveals Growth-Regulating Pathways

Genes regulated in a manner correlated with net muscle growth may be responsible for inter-subject variation in exercise-induced

Cell Reports
Resource

Table 1. Combining the Skeletal Muscle-Specific Proteome with the Core Transcriptional Signature from HypAt that Covaried with Gains in Muscle Mass across 3 Independent Studies Identified the Majority of Known Canonical Regulations of Cell Hypertrophy from Model Systems

Pathway	FDR
FOXO signaling	3E−14
MAPK signaling	3E−10
Neurotrophin signaling	1E−9
Mitophagy	6E−9
HIF-1 signaling	5E−8
Longevity regulating pathway	2E−7
AMPK signaling	3E−7
Hippo signaling	9E−7
PI3K-Akt signaling	1E−6
Apelin signaling	1E−6
Adipocytokine signaling	2E−6

FDR is −log value. FDR, false discovery rate.

several regulators of muscle growth (Data S1). The *BCAT2* 3′ UTR signal was strongly correlated (CC = 0.37, n = 100) to an increase in muscle mass, in which a greater *BCAT2* 3′ UTR signal means that more individual mRNAs had longer 3′ UTRs. This was in the absence of any relationship between the coding region signal and change in muscle mass. Another 3′ UTR-regulated gene, *TPI1* (triosephosphate isomerase 1), encodes a protein that plays a role in regulating the cytosolic redox state and is genetically linked to a muscle-wasting phenotype (Gnerer et al., 2006). Some 5′ UTR signals were also related to muscle growth (Data S1)—for example, the increase in 5′ UTR signal for exostosin glycosyltransferase 1 (*EXT1*) was strongly related to gain in lean mass (CC = 0.38, n = 100). *EXT1* is required for the biosynthesis of heparan sulfate, which in turn appears to be an essential factor for muscle remodeling and growth (Ghadiali et al., 2017).

One way to refine database-driven network analysis is to constrain the growth-correlated RNA networks by a muscle tissue-enriched proteome and model protein-protein interactions (PPIs) (https://www.networkanalyst.ca). Tissue-enriched PPI analysis of the growth-correlated RNAs (Figure S3; Data S1) yielded a list of pathways with known roles in cellular growth (Table 1), including ubiquitin protein ligase genes, apoptotic processes, and negative regulators of the nitrogen compound metabolic process. For example, *FOXO3* (negatively correlated with LLM changes during exercise training) was part of a PPI that contained 45 other *FOXO* signaling pathway members (Kyoto Encyclopedia of Genes and Genomes [KEGG] database, 1×10^{-14} FDR) and is a known regulator of cell growth (Sandri et al., 2013). The subset of genes found to be differentially regulated (Figure 3) and correlated with muscle growth are listed as an input file (Data S2) to allow for the generation of a 3-dimensional (3D) version of the proteome-constrained network model in Figure S3 (see Table S2 for instructions). The present analyses demonstrate that when measured in a sensitive and sophisticated manner, human muscle growth and dynamic changes in protein synthesis are accurately reflected in the pattern of responses observed in the human muscle transcriptome.

Identified Growth-Correlated Network Genes Directly Regulate Human Myocyte Protein Synthesis

We used puromycin-based measures of myocyte protein synthesis, in the presence of insulin growth factor 1 (IGF-1), with and without small interfering RNA (siRNA)-mediated downregulation of 4 genes identified from the list of regulated mRNA or 3′ UTR ENSTs that correlated with lean mass gains *in vivo* (*NID2*, *FKBP1A*, *BCAT2*, and *MBNL1*). As can be observed in Figure 4A, RNA interference (RNAi) effectively reduced RNA expression by >90% in differentiated myotubes after 3 days of treatment. There appeared to be some interaction between the loss of one gene and the expression of a second candidate regulator of muscle growth (Figure S4; see Discussion). In our analysis, the 3′ UTR signal of *FKBP1A* increased 20% in HypAt, and the change in 3′ UTR of the transcript variant ENST00000400137 strongly correlated with gains in lean mass *in vivo* (R = 0.31, n = 100). Knockdown (KD) of *FKBP1A in vitro* resulted in a reduction in puromycin signal, accompanied by an increase in eukaryotic elongation factor 2 (eEF2) phosphorylation (Figures 4B and S5) at Thr56 (the less active/inactive form), while the mammalian target of rapamycin (mTOR) Ser2448 (Figure 4B), P70 S6K1 Thr389, and 4E-BP1 Thr37/46 were not significantly altered (Figures S5 and S6). While the coding region of *FKBP1A* is clearly the "functional" entity, the importance of its regulation by altered 3′ UTR is further supported by the fact that it strongly covaried, with changes in >200 genes involved in extracellular matrix remodeling *in vivo* (bidirectionally), specifically with their 3′ UTR signals and not the signal from the entire mRNA (Data S1).

A core set of genes were both differentially regulated and quantitatively related to gains in lean mass, and there was evidence that these genes shared a number of common transcription factor binding sites (for KLF9, NF1A, and RBPJ) enriched (Gearing et al., 2019) over and above muscle-expressed genes or all HypAt-regulated genes (Figure 4C). The additional three genes chosen for RNAi targeting also validated our *in vivo* modeling. The loss of our proposed uncharacterized inhibitor of lean mass gains, MBNL1, was associated with an increase in protein synthesis and increased phosphorylation of mTOR Ser2448 (Figures 4A and 4B) and total protein (Figure S6). NID2—positively associated with lean mass gains—was effectively knocked down *in vitro* (Figures 4A and S7A), and this reduced global protein synthesis at 4 h (Figure S7B) and modestly suppressed total RNA (presumably rRNA), but not total protein content. Phosphorylation of p70 S6K1 and 4E-BP1, in response to IGF-1 treatment, was reduced when the *NID2* transcript was targeted (Figure S7D). The near-elimination of *BCAT2* expression also, as predicted, suppressed IGF-1-mediated protein synthesis at 4 h (Figures S7E and S7F) and reduced the phosphorylation of p70 S6K1 (Figure S7H), but it did not alter the total cell protein. It also resulted in an increase in eEF2 Thr56 phosphorylation (consistent with the inhibition of translation).

DISCUSSION

Implementing a within-person loading and analysis strategy facilitated the identification of the genome-wide molecular analysis of human muscle remodeling in a small human cohort. Combined with an updated RNA profiling strategy (to quantify 3′ or 5′

61
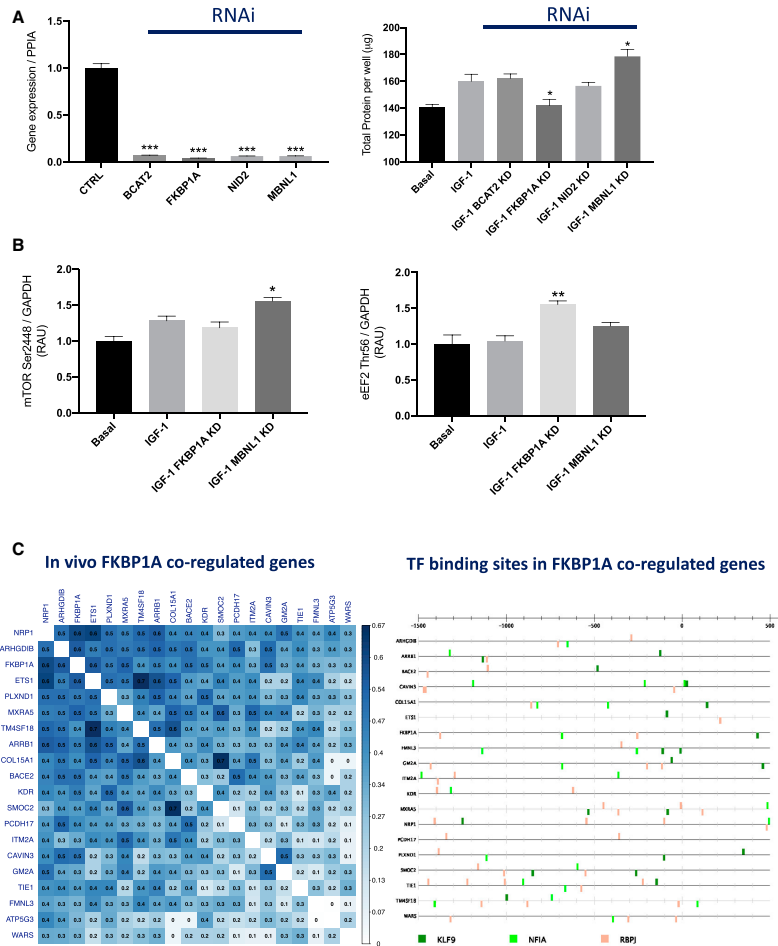
Figure 4. Growth-Regulated Genes Modulate Protein Synthesis and Anabolic Signaling in Human Muscle Cells

RNAi targeting of individual members of the muscle mass-related gene network.

(A) mRNA expression of BCAT2, FKBP1A, NID2, and MBNL1 relative to their own control (100%) following treatment with a pool of multiple siRNAs targeting each gene (BCAT2, FKBP1A, NID2, and MBNL1), with IGF-1 used to increase primary muscle cell protein synthesis. *p<0.05, **p<0.01, ***p<0.001.

(B) Calculation of relative arbitrary units (RAUs) for mTOR Ser2448 and eEF2 Thr56, using phosphospecific antibodies (IGF-1 treatment in primary muscle cell in the presence or absence of FKBP1A and MBNL1 RNAi). *p<0.05, **p<0.01, ***p<0.001.

(C) Correlation matrix of the *in vivo changes* in gene expression covarying with the change in FKBP1A. All of the genes were also correlated with exercise training-induced alterations in muscle lean mass (see Method Details). Transcription factor binding site enrichment analysis (−1,500 to +500 nt from the start codon using CiiiDER and controlled for bias in the muscle transcriptome) revealed that 3 transcription factors (KLF9, NFIA, and RBPJ) potentially coordinate this FKBP1A-angiogenesis related transcriptional "module" (i.e., they are not enriched in the larger lean-mass growth-related transcriptional signature).

regulatory ends of protein coding mRNA) enabled us to identify molecular transducers of muscle growth. A subset of transcripts was found to be regulated in proportion to the magnitude of human muscle growth, including members of validated growth and atrophy canonical pathways. We established that four of these genes regulated muscle protein synthesis (MPS) and canonical signaling events that regulate translational control. Overall, our analyses support the utility of using human models to identify relevant molecular transducers of muscle activity while reinforcing the view of Sweeney et al. (2017), and our own experience, that integrating multiple independent clinical datasets and accounting for variations in phenotypic adaptability are crucial for producing reliable molecular models of human physiology.

A Robust Molecular Model of Human Muscle during Changes in Mass

Many variables influence muscle responses to loading—age, biological sex, diet, and genetic variation (Roberts et al., 2018; Silventoinen et al., 2008). A within-subject study design enhanced the means-based statistical analysis and resulted in a far greater number of detected differentially expressed genes than comparably sized studies (Damas et al., 2019; Melov et al., 2007; Phillips et al., 2013; Raue et al., 2012). Our transcriptional analyses identified many genes with established roles in cell growth, but we discovered that they were regulated both by mRNA abundance and through differential modulation of their 5′ or 3′ UTR. Moreover, we demonstrate that UTR-specific regulatory events can covary with lean mass transitions in human muscle without corresponding changes to the full-length transcript. These regulatory events are missed by traditional transcriptomic analysis techniques that focus on the full transcript or gene-level regulation only. For instance, the recently curated database of transcriptional responses to acute and chronic exercise (Pillon et al., 2020) calculated only gene-level RNA regulation (from multiple different methods) and therefore erroneously considers many important growth-regulating genes as being unimportant in adaptation to exercise that we identified (e.g., BCAT2, KDR, NRP1). More generally, this type of database (Pillon et al., 2020) does not integrate physiological heterogeneity, and as such, any potential insights are obscured by the normalized means-based data analysis. In contrast, our unbiased analysis strategies yield a significant advance in our understanding of the molecular transducers of lean mass gain in response to RT.

Using our large multi-study tissue transcriptomic biobank and quantitative network analysis, we illustrated how HypAt-regulated genes may interact to influence skeletal muscle growth. Quantitative network analysis differs from database analysis as it reveals quantitative gene-gene interactions. In Figure S2, a multi-module mitochondrial network is presented that centers around well-recognized genes, such as NDUFS3 and SDHB, but it also reveals the regulation of less well-studied genes—for example, ChChd3, a mitochondrial membrane protein (Darshi et al., 2011). Underscoring the power of this approach, quantitative network analysis correctly localized a recently discovered long non-coding RNA LINC00116, to our mitochondrial network (Figure S2). Two recent publications demonstrated that a peptide called mitoregulin, originating from LINC00116, localizes to the inner mitochondrial membrane and regulates mitochon-

drial complex I activity (Chugunova et al., 2019; Stein et al., 2018). In fact, many genes with established mitochondrial roles were positively correlated with the degree of muscle growth. For instance, the apelin receptor (APLNR) was regulated at the FL-ENST level. Apelin plays an important role in the sarcopenia of aging and positively regulates inter-myofibrillar mitochondrial content in mice (Vinel et al., 2018). We observed that APLNR expression was positively related to numerous mitochondrial genes (e.g., ATP5G1, ATP5G3, BCAT2, COX7A2, NDUFB8, NDUFS2) as part of the mitochondrial gene expression network (Figure S2). The HypAt approach efficiently identified molecular transducers of dynamic muscle remodeling, and when combined with validation in multiple independent studies, the analysis provides unrivaled detail of the genome-wide responses.

Physiological Regulation of Human Muscle Protein Remodeling

The most conspicuous adaptation of protein turnover with immobilization-induced muscle UL is a rapid decline in MPS, first identified >30 years ago (Gibson et al., 1987) and that the loss of muscle mass can be explained completely by this reduction in rates of MPS (Phillips and McGlory, 2014). The analysis of the HypAt study demonstrated that reductions in iMyoPS represent a dominant feature of muscle mass changes during periods of disuse (Figure S1D), with muscle atrophy proceeding at a rate ~5 times faster during UL than corresponding RT-induced muscle growth. Notably, while myofibrillar protein synthesis was enhanced with RT, the extent of upregulation was not correlated with muscle growth. Our molecular analysis demonstrated abundant regulation of mitochondrial and microvascular gene networks, which we speculate support adaptive changes and contribute to and support an increased MPS signal. It has been reported that mitochondria support angiogenesis, the coordinated migration and proliferation of endothelial cells to form new blood vessel branches (Diebold et al., 2019), and the question arises whether components of the mitochondria also influence muscle hypertrophy.

Mitochondrial transcript abundance is sensitive to muscle UL (Abadi et al., 2009; Powers et al., 2012; Timmons et al., 2006). Moreover, we have shown that maximal ADP-stimulated respiration is impaired within days of UL, but in the absence of detectable mitochondrial protein content (Miotto et al., 2019). A loss of mitochondrial function therefore appears to be an earlier manifestation of muscle disuse (Miotto et al., 2019), and this is directly reflected in the present transcriptome model. In addition to the mitochondrial-dominated gene network, numerous angiogenesis-related genes were differentially regulated in our study. The angiogenic program is stimulated early in an RT program and appears temporally coupled with muscle growth (Holloway et al., 2018). In the present study, not only was the regulation of FKBP1A linked to protein synthesis (it is a prolyl isomerase, but also binds the immunosuppressants rapamycin and FK506; Aylett et al., 2016) and its expression tightly coordinated with a number of key angiogenetic genes but it also covaried with the degree of muscle hypertrophy, possibly through the activities of KLF9, NFIA, and RBPJ (Figure 4C). Clearly, muscle growth and remodeling are multifaceted processes, and it is thus unsurprising that any relationship between muscle growth and the

A Gene-level Overlap
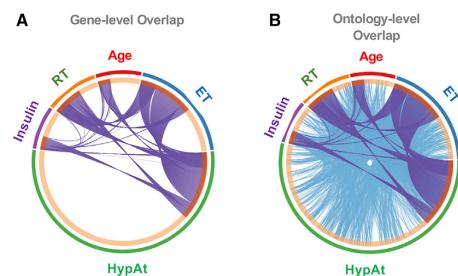
B Ontology-level Overlap

Figure 5. Genes Regulated by Potentially Related Physiological Conditions Show Substantial Pathway Overlap

(A and B) Circos plots showing the overlap in gene expression (A) and Gene Ontology (B) between the HypAt model and additional biological signatures of potentially related physiological conditions (e.g., insulin sensitivity; RT [resistance training]; age; ET [endurance training]). While the overlap in individual genes is modest (HYPAT versus ET = 338 genes; HYPAT versus RT = 160 genes; HYPAT versus insulin sensitivity = 73 genes; HYPAT versus age = 69 genes; see Data S1 for full lists), the overlap at the pathway level is substantial (highlighting at least one caveat of relying on only gene identifiers to compare and contrast molecular profiles). Notably, there are pathway features of insulin sensitivity and aging that do not appear in the ET and RT signatures (obtained from healthy subjects).

corresponding changes in iMyoPS would be complex, reflecting the precise composition of newly formed proteins.

Leveraging Transcriptional Networks to Investigate Chronic Disease and Identify Potential Therapies

Immobilization impairs the sensitivity of the protein synthetic machinery to hyperaminoacidemia (Glover et al., 2008), implicating anabolic resistance as a key process in atrophy. Here, we find that the average *BCAT2* transcript has longer 3′ UTRs and that this change was positively related to gains in lean mass in three independent studies (without our distinct RNA method, the importance of *BCAT2* in this context would have been missed). BCAT is a mitochondrial protein that catalyzes the transamination of leucine to α-ketoisocaproic acid, leading to TOR complex 1 (TORC1) activation (Moghei et al., 2016). In our *in vitro* studies, loss of *BCAT2* in primary muscle cells resulted in reduced (Figure S7H) p70 S6K1 phosphorylation and protein synthesis (in response to IGF-1) and an increase in eEF2 Thr56 phosphorylation (also consistent with the inhibition of protein translation). In tumor cells, global shortening of 3′ UTRs is a hallmark of mTORC1 activation and increased protein production (Chang et al., 2015a). This implies, as previously posited (Phillips et al., 2013), that mTOR activation will not be key to explaining the variation in muscle growth across individuals. The loss of *BCAT2* expression *in vitro* also resulted in the cell reducing other members of the core 141-gene signature we describe that was regulated in proportion to changes in lean mass (i.e., *FKBP1A* and *NID2*; Figure S7A), as well as increased eEF2 Thr56 phosphorylation (consistent with direct FKBP1A KD; Figure 4B). Thus, the loss of BCAT2 signals to the cell to downregulate several other modulators of muscle growth or protein synthesis and suggests

that leucine metabolism (Chawla et al., 1975; Escobar et al., 2010) and/or aspects of amino acid sensing in general regulate changes in human muscle mass in response to loading and UL.

While our approach identified numerous known and validated genes, we also discovered several less well-characterized molecular transducers of muscle adaptation in humans. The main power of genome-wide transcript modeling is that the signatures generated can be used as powerful tools to investigate chronic disease and identify potential treatments (Chang et al., 2015b; Subramanian et al., 2017; Timmons et al., 2005). At the level of individual genes, shared features common to aging or insulin resistance and exercise have been, to date, underwhelming (Melov et al., 2007; Phillips et al., 2013), and we also noted limited overlap between the HypAt-regulated genes and age- or insulin-sensitivity-regulated genes (Figure 5A; Data S1). However, at a pathway level, the overlap between our gene signature and these processes was considerable (Figure 5B). Specific hypotheses can be generated by overlaying the information of transcript signatures for each condition, using tissue-specific network analysis. Annotating quantitative networks in this way revealed various single-gene interactions between exercise, aging, and insulin signaling. For example, we show in Figure 6 an "age network" formed around *LAMTOR5*, a protein subunit of the pentameric Ragulator complex that tethers the Rag GTPases and, by extension, mTORC1, to the lysosomal membrane (Bar-Peled et al., 2012; Sancak et al., 2010). The expression of *LAMTOR5* was not regulated by exercise, yet Figure 6 reveals parts of the *LAMTOR5* "interactome" relate to muscle activity (e.g., *PRDX1* interacts with *TXNL1*, and *MTRF1* interacts with *LAMTOR5*). These interactions can be explored further using reverse genetic strategies and pharmacological tools in human primary cells (Crossland et al., 2017a).

Any RNA signature can be used to calculate a global "gene score" per sample (Sood et al., 2015; Timmons et al., 2010), and related to features of aging or frailty (i.e., used as a potential diagnostic) or the gene list can be used to direct targeted DNA sequencing. For example, we identified 141 gene expression responses that quantitatively related to the magnitude of muscle growth (Figure S3, see Table S2 for instructions on how to produce a 3D representation of this network). Several genes have already been extensively validated as regulators of growth and protein synthesis (e.g., *FOXO*, *MAPK*, *AMPK*, *PI3K-Akt*, and *APLNR*) (Ellis et al., 2014; Li et al., 2012; Sandri et al., 2013; Vinel et al., 2018), and we validated four additional genes (see above). There was no statistically significant overlap with the *in vitro* transcriptional signature for rapamycin in primary muscle cells (Timmons et al., 2019) and a rather limited overlap with the mTOR canonical pathway. However, when using the 141-gene signature to interrogate the L1000 drug signature database (Keenan et al., 2018), we did identify that a number of mTOR inhibitors could perturb the 141-gene signature. Unlike human muscle aging (Timmons et al., 2019), this list did not include rapamycin. The cMAP L1000 database also includes transcriptional signatures following gene KD or overexpression (OE), in 8 independent cell lines (Data S1). Overall, we identified 119 drugs that could either mimic or oppose the *in vivo* lean mass 141-gene signature (Data S1), including numerous cyclin-dependent kinase (CDK) inhibitors, which is consistent with our independent primary cell culture experiments, where we found that eEF2 Thr56

Direction with >Age   **Direction with >Insulin Sensitivity**   **Direction with HypAT (RT/UL)**
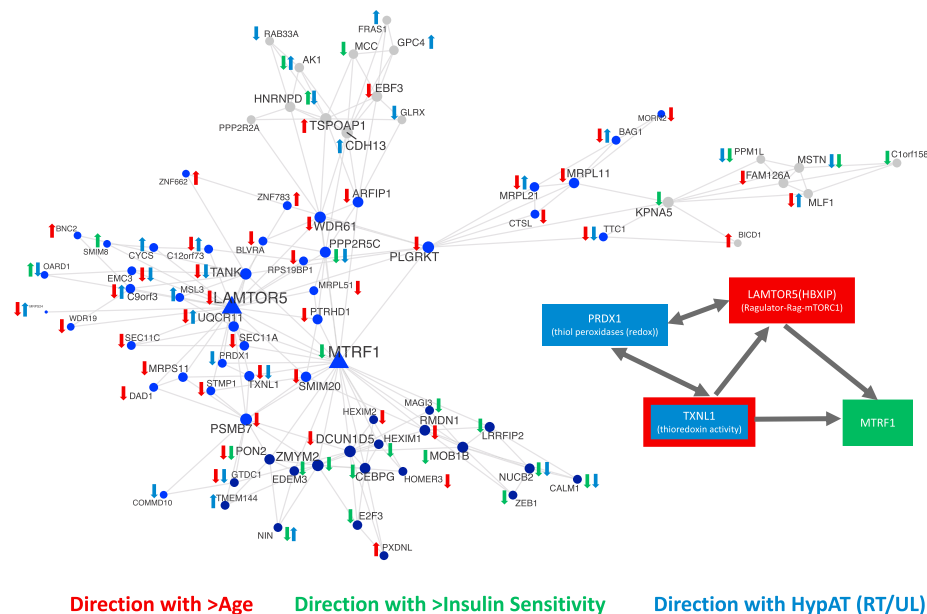
Figure 6. Quantitative Network Analysis Unveils Potentially Important Gene Interactions across Potentially Related Physiological Conditions
An example network of gene interactions across different, yet interrelated physiological conditions, constructed using HypAt-, age-, and insulin sensitivity-regulated transcripts (FDR < 5%) as input into Megena (FDR < 1% Spearman correlation; p < 0.01 for module significance, p < 0.01 for network connectivity, and 10,000 permutations for calculating FDR and connectivity p values). This example network is centered on LAMTOR5, a gene encoding a subunit of the pentameric Ragulator complex involved in mTORC1 activation. From these interactome networks, relationships between genes can be discovered and subsequently studied in model systems. Triangle symbols represent "hub genes," whereas circles represent non-hub network members. Node colors represent different subnetwork clusters, and node size is proportional to node degree.

phosphorylation status was influenced by *BCAT2* and *FKBP1A* expression. Future studies examining the potential of some of these 119 drugs to interact with exercise-induced muscle adaptation will shed light on whether the matching of transcriptional signatures is predictive of positive synergies or potential aggravation of age-related muscle frailty.

Limitations of Study
The present study lacked a parallel proteome analysis. To overcome this limitation, we used large-scale protein-protein interaction datasets to establish that our data generate significant networks containing proteins that belong to pathways known to regulate cell growth and protein synthesis. This allowed us to demonstrate strong agreement between our transcriptional approach and the proteome changes identified in a recent publication (Robinson et al., 2017). While our paired loading and UL modeling strategy recapitulated well-known RNA and proteome signatures, we only included men in the HypAt study. Women have shown, compared to men, a differing abundance of genes involved in fatty acid oxidation (Liu et al., 2010); perhaps this is of

limited concern, given that in a large (n = 178) analysis of muscle sex differences in physiologically matched subjects, only ~200 genes are differentially expressed (>1.2 FC, FDR < 1%), and only 2, *ATRNL1* and *TSPYL2*, are in the present analysis. Finally, our method identifies alterations in UTR signal, but it does not catalog the specific details, which can include losses and gains in microRNA (miRNA) target sites, mRNA stability, and alterations in transcript polyadenylation. For example, the increase in *FKBP1A* 3′ UTR signal reflects the increased production of up to 3 transcripts with the long 3′ UTR, each coding for ~100 amino acid protein.

Conclusion
We developed a powerful model and analytical tool to measure the within-individual paired tissue responses to loading and UL in human muscle tissue that reduces response heterogeneity by ~40%, meaning that lower sample sizes can be used to discover insightful transcriptional signatures (MacInnis et al., 2017) before independent validation. Using an innovative genome-wide analysis strategy, we also demonstrated significant regulation of gene expression occurring only at the UTRs,

CellPress
OPEN ACCESS

Cell Reports
Resource

thus providing some insight into the reported discordance between mRNA and corresponding protein levels. Moreover, we discovered that many of these UTR regulatory events covary with lean mass transitions in humans. The global pattern of gene expression was not mTOR dominant; however, we demonstrate some level of mTOR involvement occurring at the protein phosphorylation level. The extensive independent validation and close agreement with previous mechanistic studies supports the use of the HypAt model as a powerful tool to identify causal molecular determinants of muscle growth and atrophy directly in humans using a variety of molecular techniques and interventions.

STAR★METHODS

Detailed methods are provided in the online version of this paper and include the following:

- KEY RESOURCES TABLE
- RESOURCE AVAILABILITY
  - Lead Contact
  - Materials Availability
  - Data and Code Availability
- EXPERIMENTAL MODEL AND SUBJECT DETAILS
  - Human Participants
  - Human Primary Muscle Cell Culture
- METHOD DETAILS
  - Experimental Protocol
  - Pretesting
  - Dietary Records and Activity Monitoring
  - Unilateral Resistance Exercise - HypAt
  - Immobilization
  - Dual energy X-ray absorptiometry
  - Muscle Strength
  - Deuterium Oxide Protocol
  - Saliva Analysis
  - Magnetic Resonance Imaging
  - Muscle Tissue Extraction
  - RNA Extraction and Transcriptome Profiling
  - Myofibrillar Extraction
  - Calculations
  - Exercise Protocols used in Independent Studies
  - siRNA Transfection Experiments
  - Cell culture total RNA Extraction and RT-PCR
  - Cell culture Western Blotting
- QUANTIFICATION AND STATISTICAL ANALYSES
  - Physiological Data
  - Transcriptomic Data

SUPPLEMENTAL INFORMATION

Supplemental Information can be found online at https://doi.org/10.1016/j.celrep.2020.107980.

AUTHOR CONTRIBUTIONS

The project analysis strategy was established by J.A.T., T.S., and S.M.P. The HypAt clinical study was designed by T.S. and S.M.P., while the additional clinical studies were designed by S.M.P., J.A.T., B.P., and P.J.A. T.S., T.R.T., K.M., C.M., B.P., and S.B. conducted the clinical research and performed the sample collection. T.S., T.R.T., and K.M. performed the sample analysis. T.S., T.R.T., B.P., and S.M.P. analyzed the clinical data. H.C., J.A.T., and P.J.A. planned the cell biology work, and H.C. carried out that work. The transcriptome methods and primary statistical analysis was carried out by J.A.T. The custom chip definition file (CDF) method to quantify UTRs was conceived by J.A.T. and developed by J.A.T. The secondary data analysis and literature assessments were carried out by T.S., S.M.P., and J.A.T. The manuscript was drafted by T.S., J.A.T., and S.M.P., and all of the authors edited and approved the final version of the manuscript.

DECLARATION OF INTERESTS

The authors declare no competing interests.

REFERENCES

Abadi, A., Glover, E.I., Isfort, R.J., Raha, S., Safdar, A., Yasuda, N., Kaczor, J.J., Melov, S., Hubbard, A., Qu, X., et al. (2009). Limb immobilization induces a coordinate down-regulation of mitochondrial and other metabolic pathways in men and women. PLOS ONE 4, e6518.

Adami, A., Hobbs, B.D., McDonald, M.N., Casaburi, R., and Rossiter, H.B.; COPDGene Investigators (2018). Genetic variants predicting aerobic capacity response to training are also associated with skeletal muscle oxidative capacity in moderate-to-severe COPD. Physiol. Genomics 50, 688–690.

Aylett, C.H., Sauer, E., Imseng, S., Boehringer, D., Hall, M.N., Ban, N., and Maier, T. (2016). Architecture of human mTOR complex 1. Science 351, 48–52.

Bar-Peled, L., Schweitzer, L.D., Zoncu, R., and Sabatini, D.M. (2012). Ragulator is a GEF for the rag GTPases that signal amino acid levels to mTORC1. Cell 150, 1196–1208.

Bengtsson, H., Simpson, K., Bullard, J., and Hansen, K. (2008). aroma.affymetrix: a generic framework in R for analyzing small to very large Affymetrix data sets in bounded memory.https://statistics.berkeley.edu/sites/default/files/tech-reports/745.pdf.

Brook, M.S., Wilkinson, D.J., Mitchell, W.K., Lund, J.N., Phillips, B.E., Szewczyk, N.J., Greenhaff, P.L., Smith, K., and Atherton, P.J. (2016). Synchronous deficits in cumulative muscle protein synthesis and ribosomal biogenesis underlie age-related anabolic resistance to exercise in humans. Journal of Physiology 594, 7399–7417.

Camera, D.M., Burniston, J.G., Pogson, M.A., Smiles, W.J., and Hawley, J.A. (2017). Dynamic proteome profiling of individual proteins in human skeletal muscle after a high-fat diet and resistance exercise. FASEB J. 31, 5478–5494.

Chang, J.W., Zhang, W., Yeh, H.S., de Jong, E.P., Jun, S., Kim, K.H., Bae, S.S., Beckman, K., Hwang, T.H., Kim, K.S., et al. (2015a). mRNA 3'-UTR shortening is a molecular signature of mTORC1 activation. Nat. Commun. 6, 7218.

Chang, R., Karr, J.R., and Schadt, E.C. (2015b). Causal inference in biology networks with integrated belief propagation. Pac. Symp. Biocomput., 359–370.

Chawla, R.K., Stackhouse, W.J., and Wadsworth, A.D. (1975). Efficiency of alpha-ketoisocaproic acid as a substitute for leucine in the diet of the growing rat. J. Nutr. 105, 798–803.

Chugunova, A., Loseva, E., Mazin, P., Mitina, A., Navalayeu, T., Bilan, D., Vishnyakova, P., Marey, M., Golovina, A., Serebryakova, M., et al. (2019).

Cell Reports
Resource

LINC00116 codes for a mitochondrial peptide linking respiration and lipid metabolism. Proc. Natl. Acad. Sci. USA 116, 4940–4945.

Cohain, A., Divaraniya, A.A., Zhu, K., Scarpa, J.R., Kasarskis, A., Zhu, J., Chang, R., Dudley, J.T., and Schadt, E.E. (2017). Exploring the reproducibility of probabilistic causal molecular network models. Pac. Symp. Biocomput. 22, 120–131.

Copley Salem, C., Ulrich, C., Quilici, D., Schlauch, K., Buxton, I.L.O., and Burkin, H. (2018). Mechanical strain induced phospho-proteomic signaling in uterine smooth muscle cells. Journal of Biomechanics 73, 99–107.

Crossland, H., Atherton, P.J., Strömberg, A., Gustafsson, T., and Timmons, J.A. (2017a). A reverse genetics cell-based evaluation of genes linked to healthy human tissue age. FASEB J. 31, 96–108.

Crossland, H., Smith, K., Atherton, P.J., and Wilkinson, D.J. (2017b). A novel puromycin decorporation method to quantify skeletal muscle protein breakdown: a proof-of-concept study. Biochem. Biophys. Res. Commun. 494, 608–614.

Da Boit, M., Sibson, R., Meakin, J.R., Aspden, R.M., Thies, F., Mangoni, A.A., and Gray, S.R. (2016). Sex differences in the response to resistance exercise training in older people. Physiol. Rep. 4, e12834.

Dai, M., Wang, P., Boyd, A.D., Kostov, G., Athey, B., Jones, E.G., Bunney, W.E., Myers, R.M., Speed, T.P., Akil, H., et al. (2005). Evolving gene/transcript definitions significantly alter the interpretation of GeneChip data. Nucleic Acids Res. 33, e175.

Damas, F., Angleri, V., Phillips, S.M., Witard, O.C., Ugrinowitsch, C., Santanielo, N., Soligon, S.D., Costa, L.A.R., Lixandrão, M.E., Conceição, M.S., et al. (2019). Myofibrillar protein synthesis and muscle hypertrophy individualised responses to systematically changing resistance training variables in trained young men. J. Appl. Physiol. 127, 806–815.

Darshi, M., Mendiola, V.L., Mackey, M.R., Murphy, A.N., Koller, A., Perkins, G.A., Ellisman, M.H., and Taylor, S.S. (2011). ChChd3, an inner mitochondrial membrane protein, is essential for maintaining crista integrity and mitochondrial function. J. Biol. Chem. 286, 2918–2932.

Davidsen, P.K., Gallagher, I.J., Hartman, J.W., Tarnopolsky, M.A., Dela, F., Helge, J.W., Timmons, J.A., Phillips, S.M., et al. (2011). High responders to resistance exercise training demonstrate differential regulation of skeletal muscle microRNA expression. Journal of Applied Physiology 110, 309–317.

Diebold, L.P., Gil, H.J., Gao, P., Martinez, C.A., Weinberg, S.E., and Chandel, N.S. (2019). Mitochondrial complex III is necessary for endothelial cell proliferation during angiogenesis. Nat. Metab. 1, 158–171.

Ellis, B.C., Graham, L.D., and Molloy, P.L. (2014). CRNDE, a long non-coding RNA responsive to insulin/IGF signaling, regulates genes involved in central metabolism. Biochim. Biophys. Acta 1843, 372–386.

Escobar, J., Frank, J.W., Suryawan, A., Nguyen, H.V., Van Horn, C.G., Hutson, S.M., and Davis, T.A. (2010). Leucine and alpha-ketoisocaproic acid, but not norleucine, stimulate skeletal muscle protein synthesis in neonatal pigs. J. Nutr. 140, 1418–1424.

Floor, S.N., and Doudna, J.A. (2016). Tunable protein synthesis by transcript isoforms in human cells. eLife 5, e10921.

Gearing, L.J., Cumming, H.E., Chapman, R., Finkel, A.M., Woodhouse, I.B., Luu, K., Gould, J.A., Forster, S.C., and Hertzog, P.J. (2019). CiiiDER: a tool for predicting and analysing transcription factor binding sites. PLOS ONE 14, e0215495.

Gentleman, R.C., Carey, V.J., Bates, D.M., Bolstad, B., Dettling, M., Dudoit, S., Ellis, B., Gautier, L., Ge, Y., Gentry, J., et al. (2004). Bioconductor: open software development for computational biology and bioinformatics. Genome Biol. 5, R80.

Ghadiali, R.S., Guimond, S.E., Turnbull, J.E., and Pisconti, A. (2017). Dynamic changes in heparan sulfate during muscle differentiation and ageing regulate myoblast cell fate and FGF2 signalling. Matrix Biol. 59, 54–68.

Gibson, J.N., Halliday, D., Morrison, W.L., Stoward, P.J., Hornsby, G.A., Watt, P.W., Murdoch, G., and Rennie, M.J. (1987). Decrease in human quadriceps muscle protein turnover consequent upon leg immobilization. Clin. Sci. (Lond.) 72, 503–509.

Glover, E.I., Phillips, S.M., Oates, B.R., Tang, J.E., Tarnopolsky, M.A., Selby, A., Smith, K., and Rennie, M.J. (2008). Immobilization induces anabolic resis-

tance in human myofibrillar protein synthesis with low and high dose amino acid infusion. J. Physiol. 586, 6049–6061.

Gnerer, J.P., Kreber, R.A., and Ganetzky, B. (2006). Wasted away, a Drosophila mutation in triosephosphate isomerase, causes paralysis, neurodegeneration, and early death. Proc. Natl. Acad. Sci. USA 103, 14987–14993.

Gobbi, A., and Jurman, G. (2015). A null model for Pearson coexpression networks. PLOS ONE 10, e0128115.

Holloway, T.M., Snijders, T., Van Kranenburg, J., Van Loon, L.J.C., and Verdijk, L.B. (2018). Temporal Response of Angiogenesis and Hypertrophy to Resistance Training in Young Men. Med. Sci. Sports Exerc. 50, 36–45.

Hwangbo, C., Wu, J., Papangeli, I., Adachi, T., Sharma, B., Park, S., Zhao, L., Ju, H., Go, G.-w., Cui, G., et al. (2017). Endothelial APLNR regulates tissue fatty acid uptake and is essential for apelin's glucose-lowering effects. Sci. Transl. Med. 9, eaad4000.

Keenan, A.B., Jenkins, S.L., Jagodnik, K.M., Koplev, S., He, E., Torre, D., Wang, Z., Dohlman, A.B., Silverstein, M.C., Lachmann, A., et al. (2018). The Library of Integrated Network-Based Cellular Signatures NIH Program: System-Level Cataloging of Human Cells Response to Perturbations. Cell Syst. 6, 13–24.

Keller, P., Vollaard, N.B.J., Gustafsson, T., Gallagher, I.J., Sundberg, C.J., Rankinen, T., Britton, S.L., Bouchard, C., Koch, L.G., Timmons, J.A., et al. (2011). A transcriptional map of the impact of endurance exercise training on skeletal muscle phenotype. Journal of Applied Physiology 110, 46–59.

Kocabas, A., Duarte, T., Kumar, S., and Hynes, M.A. (2015). Widespread Differential Expression of Coding Region and 3′ UTR Sequences in Neurons and Other Tissues. Neuron 88, 1149–1156.

Kosek, D.J., Kim, J.S., Petrella, J.K., Cross, J.M., and Bamman, M.M. (2006). Efficacy of 3 days/wk resistance training on myofiber hypertrophy and myogenic mechanisms in young vs. older adults. J. Appl. Physiol. 101, 531–544.

Langmead, B., and Salzberg, S.L. (2012). Fast gapped-read alignment with Bowtie 2. Nat. Methods 9, 357–359.

Li, M., Verdijk, L.B., Sakamoto, K., Ely, B., van Loon, L.J.C.C., and Musi, N. (2012). Reduced AMPK-ACC and mTOR signaling in muscle from older men, and effect of resistance exercise. Mech. Ageing Dev. 133, 655–664.

Li, J.J., and Biggin, M.D. (2015). Gene expression. Statistics requantitates the central dogma. Science 347, 1066–1067.

Liu, D., Sartor, M.A., Nader, G.A., Gutmann, L., Treutelaar, M.K., Pistilli, E.E., Iglayreger, H.B., Burant, C.F., Hoffman, E.P., and Gordon, P.M. (2010). Skeletal muscle gene expression in response to resistance exercise: sex specific regulation. BMC Genomics 11, 659.

MacInnis, M.J., McGlory, C., Gibala, M.J., and Phillips, S.M. (2017). Investigating human skeletal muscle physiology with unilateral exercise models: when one limb is more powerful than two. Appl. Physiol. Nutr. Metab. 42, 563–570.

Mayr, C. (2017). Regulation by 3′-Untranslated Regions. Annu. Rev. Genet. 51, 171–194.

McDonald, M.L.N., Won, S., Mattheisen, M., Castaldi, P.J., Cho, M.H., Rutten, M., Yip, W., Rennard, S.I., Lomas, D.A., Wouters, E.F.M., et al. (2017). Body mass index change in gastrointestinal cancer and chronic obstructive pulmonary disease is associated with Dedicator of Cytokinesis 1. Journal of Cachexia Sarcopenia and Muscle 8, 428–436.

Melov, S., Tarnopolsky, M.A., Beckman, K., Felkey, K., and Hubbard, A. (2007). Resistance exercise reverses aging in human skeletal muscle. PLOS ONE 2, e465.

Miotto, P.M., McGlory, C., Bahniwal, R., Kamal, M., Phillips, S.M., and Holloway, G.P. (2019). Supplementation with dietary ω-3 mitigates immobilization-induced reductions in skeletal muscle mitochondrial respiration in young women. FASEB J. 33, 8232–8240.

Mitchell, C.J., Churchward-Venne, T.A., Parise, G., Bellamy, L., Baker, S.K., Smith, K., Atherton, P.J., and Phillips, S.M. (2014). Acute post-exercise myofibrillar protein synthesis is not correlated with resistance training-induced muscle hypertrophy in young men. PLOS ONE 9, e89431.

Moghei, M., Tavajohi-Fini, P., Beatty, B., and Adegoke, O.A.J. (2016). Ketoisocaproic acid, a metabolite of leucine, suppresses insulin-stimulated glucose

CellPress
OPEN ACCESS

Cell Reports
Resource

transport in skeletal muscle cells in a BCAT2-dependent manner. Am. J. Physiol. Cell Physiol. *311*, C518–C527.

Morton, R.W., Murphy, K.T., McKellar, S.R., Schoenfeld, B.J., Henselmans, M., Helms, E., Aragon, A.A., Devries, M.C., Banfield, L., Krieger, J.W., Phillips, S.M., et al. (2018). A systematic review, meta-analysis and meta-regression of the effect of protein supplementation on resistance training-induced gains in muscle mass and strength in healthy adults. British Journal of Sports Medicine *52*, 376–384.

Morton, R.W., Oikawa, S.Y., Wavell, C.G., Mazara, N., McGlory, C., Quadrilatero, J., Baechler, B.L., Baker, S.K., and Phillips, S.M. (2016). Neither load nor systemic hormones determine resistance training-mediated hypertrophy or strength gains in resistance-trained young men. J. Appl. Physiol. *121*, 129–138.

Peter, I., Papandonatos, G.D., Belalcazar, L.M., Yang, Y., Erar, B., Jakicic, J.M., Unick, J.L., Balasubramanyam, A., Lipkin, E.W., Delahanty, L.M., et al.; Look AHEAD Research Group (2014). Genetic modifiers of cardiorespiratory fitness response to lifestyle intervention. Med. Sci. Sports Exerc. *46*, 302–311.

Phillips, S.M., and McGlory, C. (2014). CrossTalk proposal: the dominant mechanism causing disuse muscle atrophy is decreased protein synthesis. J. Physiol. *592*, 5341–5343.

Phillips, B.E., Williams, J.P., Gustafsson, T., Bouchard, C., Rankinen, T., Knudsen, S., Smith, K., Timmons, J.A., and Atherton, P.J. (2013). Molecular networks of human muscle adaptation to exercise and age. PLOS Genet. *9*, e1003389.

Phillips, B., Kelly, B., Lilja, M., Ponce-González, J., Brogan, R., Morris, D., Gustafsson, T., Kraus, W., Atherton, P., Vollaard, N., et al. (2017). A practical and time-efficient high-intensity interval training programme modifies cardiometabolic risk-factors in adults with risk-factors for type II diabetes. Front. Endocrinol. *8*, 229.

Pillon, N.J., Gabriel, B.M., Dollet, L., Smith, J.A.B., Sardón Puig, L., Botella, J., Bishop, D.J., Krook, A., and Zierath, J.R. (2020). Transcriptomic profiling of skeletal muscle adaptations to exercise and inactivity. Nat. Commun. *11*, 470.

Powers, S.K., Wiggs, M.P., Duarte, J.A., Zergeroglu, A.M., and Demirel, H.A. (2012). Mitochondrial signaling contributes to disuse muscle atrophy. Am. J. Physiol. Endocrinol. Metab. *303*, E31–E39.

Raue, U., Trappe, T.A., Estrem, S.T., Qian, H.-R., Helvering, L.M., Smith, R.C., and Trappe, S. (2012). Transcriptome signature of resistance exercise adaptations: mixed muscle and fiber type specific profiles in young and old adults. J. Appl. Physiol (1985) *112*, 1625–1636.

Roberts, M.D., Haun, C.T., Mobley, C.B., Mumford, P.W., Romero, M.A., Roberson, P.A., Vann, C.G., and McCarthy, J.J. (2018). Physiological differences between low versus high skeletal muscle hypertrophic responders to resistance exercise training: current perspectives and future research directions. Front. Physiol. *9*, 834.

Robinson, M.M., Dasari, S., Konopka, A.R., Johnson, M.L., Manjunatha, S., Esponda, R.R., Carter, R.E., Lanza, I.R., and Nair, K.S. (2017). Enhanced Protein Translation Underlies Improved Metabolic and Physical Adaptations to Different Exercise Training Modes in Young and Old Humans. Cell Metab. *25*, 581–592.

Sancak, Y., Bar-Peled, L., Zoncu, R., Markhard, A.L., Nada, S., and Sabatini, D.M. (2010). Ragulator-Rag complex targets mTORC1 to the lysosomal surface and is necessary for its activation by amino acids. Cell *141*, 290–303.

Sandri, M., Barberi, L., Bijlsma, A.Y., Blaauw, B., Dyar, K.A., Milan, G., Mammucari, C., Meskers, C.G.M., Pallafacchina, G., Paoli, A., et al. (2013). Signalling pathways regulating muscle mass in ageing skeletal muscle: the role of the IGF1-Akt-mTOR-FoxO pathway. Biogerontology *14*, 303–323.

Schneider, C.A., Rasband, W.S., and Eliceiri, K.W. (2012). NIH Image to ImageJ: 25 years of Image Analysis. Nature Methods *9*, 671–675.

Schönbrodt, F.D., and Perugini, M. (2013). At what sample size do correlations stabilize? J. Res. Pers. *47*, 609–612.

Shalek, A.K., Satija, R., Adiconis, X., Gertner, R.S., Gaublomme, J.T., Raychowdhury, R., Schwartz, S., Yosef, N., Malboeuf, C., Lu, D., et al. (2013). Single-cell transcriptomics reveals bimodality in expression and splicing in immune cells. Nature *498*, 236–240.

Silventoinen, K., Magnusson, P.K.E., Tynelius, P., Kaprio, J., and Rasmussen, F. (2008). Heritability of body size and muscle strength in young adulthood: a study of one million Swedish men. Genet. Epidemiol. *32*, 341–349.

Song, W.M., and Zhang, B. (2015). Multiscale Embedded Gene Co-expression Network Analysis. PLOS Comput. Biol. *11*, e1004574.

Sood, S., Gallagher, I.J., Lunnon, K., Rullman, E., Keohane, A., Crossland, H., Phillips, B.E., Cederholm, T., Jensen, T., van Loon, L.J.C., et al. (2015). A novel multi-tissue RNA diagnostic of healthy ageing relates to cognitive health status. Genome Biol. *16*, 185.

Sood, S., Szkop, K.J., Nakhuda, A., Gallagher, I.J., Murie, C., Brogan, R.J., Kaprio, J., Kainulainen, H., Atherton, P.J., Kujala, U.M., et al. (2016). iGEMS: an integrated model for identification of alternative exon usage events. Nucleic Acids Res. *44*, e109.

Stein, C.S., Jadiya, P., Zhang, X., McLendon, J.M., Abouassaly, G.M., Witmer, N.H., Anderson, E.J., Elrod, J.W., and Boudreau, R.L. (2018). Mitoregulin: A lncRNA-Encoded Microprotein that Supports Mitochondrial Supercomplexes and Respiratory Efficiency. Cell Rep. *23*, 3710–3720.e8.

Subramanian, A., Narayan, R., Corsello, S.M., Peck, D.D., Natoli, T.E., Lu, X., Gould, J., Davis, J.F., Tubelli, A.A., Asiedu, J.K., et al. (2017). A Next Generation Connectivity Map: L1000 Platform and the First 1,000,000 Profiles. Cell *171*, 1437–1452.e17.

Sweeney, T.E., Haynes, W.A., Vallania, F., Ioannidis, J.P., and Khatri, P. (2017). Methods to increase reproducibility in differential gene expression via meta-analysis. Nucleic Acids Res. *45*, e1.

Timmons, J.A. (2011). Variability in training-induced skeletal muscle adaptation. J. Appl. Physiol. (1985) *110*, 846–853.

Timmons, J.A., Larsson, O., Jansson, E., Fischer, H., Gustafsson, T., Greenhaff, P.L., Ridden, J., Rachman, J., Peyrard-Janvid, M., Wahlestedt, C., and Sundberg, C.J. (2005). Human muscle gene expression responses to endurance training provide a novel perspective on Duchenne muscular dystrophy. FASEB J. *19*, 750–760.

Timmons, J.A., Norrbom, J., Schéele, C., Thonberg, H., Wahlestedt, C., and Tesch, P. (2006). Expression profiling following local muscle inactivity in humans provides new perspective on diabetes-related genes. Genomics *87*, 165–172.

Timmons, J.A., Knudsen, S., Rankinen, T., Koch, L.G., Sarzynski, M., Jensen, T., Keller, P., Scheele, C., Vollaard, N.B.J., Nielsen, S., et al. (2010). Using molecular classification to predict gains in maximal aerobic capacity following endurance exercise training in humans. J. Appl. Physiol. *108*, 1487–1496.

Timmons, J.A., Szkop, K.J., and Gallagher, I.J. (2015). Multiple sources of bias confound functional enrichment analysis of global -omics data. Genome Biol. *16*, 186.

Timmons, J.A., Atherton, P.J., Larsson, O., Sood, S., Blokhin, I.O., Brogan, R.J., Volmar, C.H., Josse, A.R., Slentz, C., Wahlestedt, C., et al. (2018). A coding and non-coding transcriptomic perspective on the genomics of human metabolic disease. Nucleic Acids Res. *46*, 7772–7792.

Timmons, J.A., Volmar, C.H., Crossland, H., Phillips, B.E., Sood, S., Janczura, K.J., Törmäkangas, T., Kujala, U.M., Kraus, W.E., Atherton, P.J., and Wahlestedt, C. (2019). Longevity-related molecular pathways are subject to midlife "switch" in humans. Aging Cell *18*, e12970.

Tusher, V.G., Tibshirani, R., and Chu, G. (2001). Significance analysis of microarrays applied to the ionizing radiation response. Proc. Natl. Acad. Sci. USA *98*, 5116–5121.

van Dam, S., Craig, T., and de Magalhães, J.P. (2015). GeneFriends: a human RNA-seq-based gene and transcript co-expression database. Nucleic Acids Res. *43*, D1124–D1132.

Vinel, C., Lukjanenko, L., Batut, A., Deleruyelle, S., Pradère, J.-P., Le Gonidec, S., Dortignac, A., Geoffre, N., Pereira, O., Karaz, S., et al. (2018). The exerkine apelin reverses age-associated sarcopenia. Nat. Med. *24*, 1360–1371.

68

Cell Reports
Resource

CellPress
OPEN ACCESS

von Haehling, S., Morley, J.E., and Anker, S.D. (2012). From muscle wasting to sarcopenia and myopenia: update 2012. J. Cachexia Sarcopenia Muscle *3*, 213–217.

Wang, X., Kang, D.D., Shen, K., Song, C., Lu, S., Chang, L.C., Liao, S.G., Huo, Z., Tang, S., Ding, Y., et al. (2012). An R package suite for microarray meta-analysis in quality control, differentially expressed gene analysis and pathway enrichment detection. Bioinformatics *28*, 2534–2536.

Wilkinson, D.J., Franchi, M.V., Brook, M.S., Narici, M.V., Williams, J.P., Mitchell, W.K., Szewczyk, N.J., Greenhaff, P.L., Atherton, P.J., and Smith, K. (2014). A validation of the application of D(2)O stable isotope tracer techniques for monitoring day-to-day changes in muscle protein subfraction synthesis in humans. Am. J. Physiol. Endocrinol. Metab. *306*, E571–E579.

Yasuda, N., Glover, E.I., Phillips, S.M., Isfort, R.J., and Tarnopolsky, M.A. (2005). Sex-based differences in skeletal muscle function and morphology with short-term limb immobilization. J. Appl. Physiol. *99*, 1085–1092.

CellPress
OPEN ACCESS

Cell Reports
Resource

STAR★METHODS

KEY RESOURCES TABLE

REAGENT or RESOURCE	SOURCE	IDENTIFIER
Antibodies		
Phospho-mTOR (Ser2448) (D9C2) XP® Rabbit mAb	Cell Signaling Technology	CAT: #5536; RRID: AB_10691552
Phospho-p70 S6 Kinase (Thr389) (108D2) Rabbit mAb	Cell Signaling Technology	CAT: #9234; RRID: AB_2269803
Phospho-eEF2 (Thr56) Antibody	Cell Signaling Technology	CAT: #2331; RRID:AB_10015204
Phospho-4E-BP1 (Thr37/46) (236B4) Rabbit mAb	Cell Signaling Technology	CAT: #2855; RRID:AB_10695878
Anti-Puromycin Antibody, clone 12D10	Merck Millipore	CAT: MABE343; RRID:AB_2566826
Biological Samples		
Human Muscle	Present article	NA
Human Muscle	Morton et al., 2016; Mitchell et al., 2014; Phillips et al., 2017	NA
Chemicals, Peptides, and Recombinant Proteins		
Deuterium oxide (D, 70%)	Cambridge Isotope Laboratories, Inc.	DLM-4-70-PK; CAS#7732-18-5
Dowex – 50WX8 – Hydrogen Form	Sigma Aldrich	AC335335000
PhosStop Phosphatase Inhibitor	Roche	04906837001
cOmplete Mini EDTA-free Protease Inhibitor Cocktail	Roche	11836170001
TRIzol Reagent	ThermoFisher Scientific	CAT: 15596018
CD56 Microbeads, human	Miltenyi Biotec	CAT: 130-097-042
Lipofectamine RNAiMAX Transfection Reagent	ThermoFisher Scientific	CAT: 13778030
LONG® R3 IGF-I human	Sigma-Aldrich	CAT: I1271
Puromycin dihydrochloride	Sigma-Aldrich	CAT: P8833
SYBR Select Master Mix	Applied Biosystems	CAT: 4472920
Critical Commercial Assays		
E.Z.N.A Total RNA Isolation Kit	Omega Bio-Tek	SKU: R6834-01
GeneChip WT Plus Reagent Kit	ThermoFisher Scientific	CAT: 902280
High-Capacity cDNA Reverse Transcription Kit	Applied Biosystems	CAT: 4368813
Deposited Data		
Raw and analyzed data	This study	GEO: GSE154846
Oligonucleotides		
esiRNA human BCAT2 (esiRNA1)	Sigma-Aldrich	CAT: EHU032991
esiRNA human NID2 (esiRNA1)	Sigma-Aldrich	CAT: EHU083781
esiRNA human FKBP1A (esiRNA1)	Sigma-Aldrich	CAT: EHU106961
esiRNA human MBNL1 (esiRNA1)	Sigma-Aldrich	CAT: EHU086561
Primer: BCAT2 Forward: GAGCTGAAGGAGATCCAGTACG	Sigma-Aldrich	N/A
Primer: BCAT2 Reverse: GAGTCATTGGTAGGGAGGCG	Sigma-Aldrich	N/A
Primer: NID2 Forward: TGGAAGCTACAGGTGTGAGTG	Sigma-Aldrich	N/A
Primer: NID2 Reverse: AGGTGGGGTGATCAAGATGCAA	Sigma-Aldrich	N/A
Primer: MBNL1 Forward: CTGCCCAATACCAGGTCAAC	Sigma-Aldrich	N/A
Primer: MBNL1 Reverse: GGGGAAGTACAGCTTGAGGA	Sigma-Aldrich	N/A
Primer: FKBP1A Forward: GGTGGAAACCATCTCCCCAG	Sigma-Aldrich	N/A
Primer: FKBP1A Reverse: TCAAGCATCCCGGTGTAGTG	Sigma-Aldrich	N/A

Cell Reports
Resource

CellPress
OPEN ACCESS

Continued

REAGENT or RESOURCE	SOURCE	IDENTIFIER
Software and Algorithms		
ImageJ	Schneider et al., 2012	https://imagej.nih.gov
Bowtie Alignment Tool	Langmead and Salzberg, 2012	http://bowtie-bio.sourceforge.net/index.shtml
Significance Analysis of Microarrays (SAM) implemented in the R programming environment (SAMR)	Tusher et al., 2001	https://cran.r-project.org/web/packages/samr/index.html
aroma.affymetrix	Bengtsson et al., 2008	https://cran.rstudio.com/web/packages/aroma.affymetrix/index.html
MEGENA	Song and Zhang, 2015	https://rdrr.io/cran/MEGENA/
Bioconductor	Gentleman et al., 2004	https://www.bioconductor.org/
CMap-L1000v1 database	Subramanian et al., 2017	https://clue.io/
Custom CDF protocol	Timmons et al., 2018	https://www.augurprecisionmedicine.com
Ciiider	Gearing et al., 2019	www.ciiider.org
Other		
GeneChip Human Transcriptome Array 2.0 and RT labeling kits	ThermoFisher Scientific	CAT: 902162
Raw and analyzed data	Timmons et al., 2018, 2019	GEO: GSE154846
Human reference genome NCBI build 38, GRCh38_82p3	Genome Reference Consortium	https://www.ncbi.nlm.nih.gov/projects/genome/assembly/grc/human/

RESOURCE AVAILABILITY

Lead Contact
Further information and requests for resources should be directed to and will be fulfilled by the Lead Contact, Dr. Stuart M. Phillips (phillis@mcmaster.ca)

Materials Availability
This study did not generate any unique reagents.

Data and Code Availability
The accession number for the newly generated gene expression data reported in this paper is GEO:GSE154846 . Code for the various informatics analyses can be readily obtained by contacting jamie.timmons@gmail.com.

EXPERIMENTAL MODEL AND SUBJECT DETAILS

Human Participants
Participants were recruited via local advertisements posted at McMaster University. Twelve recreationally-active men (18-30 y) volunteered to participate in the study. A medical history questionnaire was administered at screening to exclude any individuals taking medications known to affect protein metabolism (i.e., glucocorticoids, prescription-strength acne medication, or non-steroidal anti-inflammatories), those with a (family) history of deep vein thrombosis, or individuals with acute or chronic illnesses that interfered with the safe conduct of the study. All participants provided informed verbal and written consent prior to beginning the study. The experimental trial was approved by the Hamilton integrated Research Ethics Board (REB #2867) and complied with the ethical standards outlined in the Tri-Council Policy statement for use of humans in research. This study was registered on CinicalTrials.gov with the identifier NCT03046095.

Human Primary Muscle Cell Culture
Human primary skeletal muscle cells were isolated from muscle biopsies from healthy young adults and cultured as previously described (Crossland et al., 2017a, 2017b). Myogenic cell enrichment was carried out using magnetic-activated cell sorting (MACS), using anti-CD56 microbeads and myoblasts were used for experimentation at passage 5-6. MACS-sorted myoblasts were cultured on Collagen Type I-coated 6-well dishes in Dulbecco's Modified Eagle Medium/Nutrient Mixture F-12 (DMEM/F-12; Life Technologies) containing 20% (v/v) fetal bovine serum (FBS, Sigma-Aldrich), 1% (v/v) antibiotic-antimycotic (AbAm) solution and 4mM L-glutamine (Life Technologies). Once cells reached ~95% confluency, differentiation was induced by switching the

medium to DMEM/F-12 containing 2% (v/v) horse serum (Sigma-Aldrich), 4mM L-glutamine and 1% (v/v) AbAm solution (Life Technologies). Puromycin based measures of protein synthesis was determined as previously described (Crossland et al., 2017b).

METHOD DETAILS

Experimental Protocol
The total duration of the study, including familiarization sessions, was 11 weeks. We employed a within-subjects design whereby one leg was randomized to perform unilateral leg extension and leg press exercise $3 \, d \cdot wk^{-1}$ for 10 weeks. The contralateral leg had a knee brace applied during the last two weeks of the study, and otherwise remained untrained. Body composition and maximal strength assessments were performed before training (Pre-RT; day 0), before immobilization (Pre-UL; day 56), and upon completion of training and immobilization (Post-RT/UL; day 70). At each testing session, participants had their lean body mass (LBM), mid-thigh vastus lateralis cross sectional area (VLCSA), and ISO-MVC assessed. VLCSA, muscle volume, and whole-quadriceps CSA was quantified using magnetic resonance imaging (MRI) at time points Pre-RT and Post-RT. A total of 7 muscle biopsies were obtained from the *vastus lateralis* throughout and used, in conjunction with deuterium oxide, to measure integrated rates of muscle protein synthesis (see below).

Pretesting
Participants visited McMaster University on three separate occasions at least one week prior to beginning the study to be familiarized on the proper execution of an isometric maximal voluntary contraction (ISO-MVC) and unilateral leg extension and leg press exercises. One-repetition maximum (1-RM) was tested on visits 2 and 3. Proper execution of unilateral leg extension and leg press contractions was demonstrated, after which participants performed one set of non-exhaustive contractions while having their form critiqued and adjusted. Participants then completed 3 sets of leg extension followed by 3 sets of leg press, with each set separated by a 90 s rest period. On the final set of each exercise, participants were instructed to reach volitional failure, defined as an inability to complete a full contraction through the predefined range of motion. Weight lifted, and the number of repetitions completed for both leg extension and leg press exercises, was recorded and used to calculate estimated 1-RM using the following formula:

$$1 - RM(kg) = (Load(kg))/(1.0278 - (0.0278 x \# reps)) \qquad \text{(Equation 1)}$$

On the second visit (~48hr after visit 1), participants completed two submaximal sets of 8-12 repetitions on the leg extension machine at ~40%–60% of their estimated 1-RM. Participants then attempted to lift 90% of their 1-RM predicted from Equation 1. Weight was increased progressively until the participant could not complete a full repetition. This testing procedure was repeated on the leg press after ~10 mins of rest. On the third visit,1-RM load was retested and either verified or adjusted accordingly and used for the subsequent calculation of week 1 working loads.

Dietary Records and Activity Monitoring
Participants completed 3-d dietary records during week 1, week 5 and week 10 of the study. Each record consisted of two weekdays and one weekend day. A sample record was provided to each participant to permit the accurate estimation of portion sizes. Dietary records were analyzed using NutriBase software (Cybersoft Inc., version 11.5, Phoenix, AZ, USA). During dietary recording, participants were also asked to wear an ActiGraph wGT3X-BT activity monitor (ActiGraph, Pensacola, FL, USA) on their dominant wrist to track daily step count and other metrics of physical activity levels. Data were downloaded from the activity monitors and analyzed using ActiLife version 6 13.2 software (ActiGraph, Pensacola, FL, USA).

Unilateral Resistance Exercise - HypAt
Participants visited the laboratory every Monday, Wednesday, and Friday to complete unilateral leg extension and leg press exercise. Each session was supervised by a strength and conditioning coach and consisted of 3 sets of 8-12 repetitions of leg extensions and 3 sets of 8-12 repetitions on a 45-degree leg press. The last set of each exercise was performed to volitional failure, defined as an inability to complete a repetition through the full range of motion. If the participant successfully completed more than 12 or less than 8 repetitions, weight was adjusted accordingly. Following each exercise bout, participants ingested 25 g of whey protein isolate to maximize the protein synthesis response to each exercise bout.

Immobilization
A X-ACT ROM knee brace (DonJoy, Dallas, TX, USA) was applied to the contralateral non-training leg for a continuous period of 14 d during weeks 9 and 10. The angle of the brace was adjusted to permit toe clearance during crutch-assisted ambulation without active hamstring flexion and averaged ~60° flexion.

Dual energy X-ray absorptiometry
Leg lean mass was assessed using dual energy X-ray absorptiometry Pre-RT, Pre-UL, and Post-RT/UL. The DXA was calibrated daily prior to participant arrival using a three-compartment Universal Whole Body DXA Phantom (Orthometrix, Naples, Florida).

Participants also underwent a fasted MRI scan of both thighs on day 0 and upon study completion (day 70) for the assessment of mid-thigh and whole-quadriceps CSA (see below).

Muscle Strength

Isometric maximal voluntary contractions (ISO-MVC) were performed prior to exercise Pre-RT, Pre-UL, and after exercise completion to assess peak knee extensor torque using a Biodex dynamometer (Biodex System 3, Biodex Medical Systems, Shirley, NY, USA). Participants were familiarized on three separate occasions during the pretesting visits to avoid practice effects associated with device familiarity. During the pre-test familiarization sessions, chair settings were adjusted to each participant such that the knee joint was aligned with the axis of rotation of the machine. All chair settings were recorded for accurate replication during subsequent testing sessions. Each session consisted of five isometric contractions at 60° from the resting, 90° neutral position. Contractions lasted 5 s and were separated by a 2-min resting period. Both legs were tested at each session in randomized order. Participants were shown their force tracing and verbally encouraged during each effort to limit the influence of motivation on trial performance. Peak torque was recorded and used in subsequent analyses. The coefficient of variation between contractions did not exceed 5%.

Deuterium Oxide Protocol

The incorporation of deuterium oxide (D2O) into muscle protein-bound alanine was assessed to quantify muscle protein synthesis rates. Deuterium dosing began on day 52 and continued until day 70. The protocol consisted of one loading day and 17 maintenance days with the goal of enriching, and subsequently maintaining the body water pool at ∼0.5% 2H atom percent excess (APE). Participants reported to the laboratory at 0800 h after an overnight (∼10 h) fast on day 52 (Thursday) and were asked to void their bladder before undergoing a DXA body scan to determine lean body mass. Participants then ingested 8 doses (0.625 ml·kg-1 LBM) of 70% D2O (Cambridge Isotope Laboratories, Andover, MA, USA) evenly spaced every 1.5 h throughout the day. After 5 of the 8 doses were ingested, participants were sent home with the remaining 3 doses and instructed to ingest them 1.5 h apart. None of the participants reported any adverse side effects such as nausea or vertigo after consuming D2O. Blood samples were collected in EDTA blood tubes and saliva samples were obtained by gently chewing on a cotton swab for 2-3 min until completely saturated with saliva. Blood and saliva samples were centrifuged at 4000 rpm for 10 min at 4°C, after which aliquots of each were snap frozen in liquid nitrogen and stored at −80°C for subsequent analysis.

Saliva Analysis

Saliva samples were obtained at baseline prior to commencing deuterium oxide loading on day 52 and each morning thereafter until the end of the study. Salivettes were centrifuged at 4000 rpm for 10 min and diluted in doubly-distilled water. Deuterium enrichment was then measured using a Picarro L2130-*i* Cavity Ringdown Spectrometer run in high-throughput mode. Six injections were performed on each sample; the first readings were discarded to eliminate memory effects from previous sample injections. Internal lab standards containing low, medium, and high enrichments of ^{2}H were sampled in parallel prior to and following each participant's samples to account for drift in enrichment over time.

Magnetic Resonance Imaging

Participants underwent a fasted MRI scan of both thighs on day 0 and upon study completion (day 70) for the assessment of mid-thigh and whole-quadriceps CSA. Each scan was performed in a 3-Tesla HD Scanner (Signa MRI System; GE Medical, Milwaukee, Wisconsin) at the Imaging Research Center (St. Joseph's Healthcare, Hamilton, ON). Axial (transverse) MR images were obtained from both thighs from the distal end of the femur to greater trochanter. A fast-recovery, fast spin echo (FRFSE) pulse sequence was used, along with IDEAL (iterative decomposition of water and fat with echo asymmetry and least-squares estimation) post-processing to obtain water-only, fat-only, in-phase and out-of-phase images of the thighs. The following parameters were used: (TR) = 2000 msec, (TE) = 30 msec, refocusing flip angle = 111 degrees, echo train length = 6, ASSET (parallel imaging factor) = 2, field of view = 42x21 cm, acquisition matrix = 512x256, 3 mm slice thickness, and 0mm slice gap. A total of ∼160 slices were acquired from each participant. The acquisition was completed in two sections: a lower stage and an upper stage, which were subsequently stitched together by an MR technician. Total scan time for both stages was approximately 11 min. Images were downloaded from a secure server and analyzed using ImageJ (NIH, v 1.52). Mid-thigh vastus lateralis CSA was analyzed at 50% of the distance between the greater trochanter and lateral epicondyle of the femur. Peak-quadriceps CSA was the slice with the greatest measured quadriceps CSA. Finally, quadriceps muscle volume was calculated by summing the CSA measurements of a given slice multiplied by the slice thickness. Peak-quadriceps CSA and muscle volume were analyzed using semi-automatic image analysis software (AnalysisPro). The distal 20% of thigh images and the proximal 30% were not included in analyses. This data was not utilized as the additional three clinical studies only had DXA measures of muscle mass.

Muscle Tissue Extraction

Muscle biopsy samples (∼100 – 150 mg each) were obtained on 7 occasions under local anesthesia using a Bergstrom needle modified for manual suction. Biopsies were taken from the RT limb pre-RT (day 0), day 53, day 56 and day 70 and from the UL limb on day 53, 56, and 70. Blood and other non-muscle tissue were dissected from each specimen at bedside prior to being snap-frozen in liquid nitrogen (within ∼20 s) and stored at −80°C.

RNA Extraction and Transcriptome Profiling

Approximately 20 mg of muscle was used to extract RNA. Muscle samples and 1000 μL of TRIzol were added to Lysing Matrix D tubes containing ceramic microbeads (MP Biomedicals, Solon, OH, USA) and homogenized using a FastPrep tissue homogenizer (MP Biomedicals, Solon, OH, USA). 200 μL of chloroform was added and the tubes hand-shaken vigorously for 15 s and incubated at room temperature for 5 min. Samples were then centrifuged at 12 000 g for 10 min at 4°C and the upper aqueous phase containing RNA was transferred to an RNase-free tube. RNA was purified using E.Z.N.A Total RNA Isolation kit (Omega Bio-Tek, Norcross, GA, USA). RNA was processed for transcriptome profiling using the GeneChip WT Plus Reagent Kit according to manufacturer's instructions. Briefly, first and second strand cDNA synthesis was performed using 100 ng of RNA and a spike-in Poly-A control, which was then followed by reverse transcription into cRNA. cRNA was purified using magnetic beads and quantified using spectrophotometry (Nanodrop UV-Vis, Thermo Fisher Scientific). 15 μg of cRNA was then amplified and hydrolyzed using RNase H (leaving single-stranded cDNA) and purified with magnetic beads. cDNA (5.5 μg) was then fragmented and labeled. A hybridization master mix was prepared and added to the fragmented and labeled cDNA. 200 μL of the mixture was applied to the HTA 2.0 cartridge and hybridized at 45°C for 16 h rotating at 60 rpm. The cartridge was washed and stained using the FS450_001 fluidics protocol on the GeneChip Fluidics Station 450 (Thermo Fisher) and scanned using a GeneChip Scanner 3000 7G (Thermo Fisher).

Myofibrillar Extraction

Snap-frozen muscle samples were homogenized using buffer (10 μl·mg^{-1}) containing 25 mM Tris buffer (pH 7.2), 0.5% vol/vol Triton X-100, a phosphatase inhibitor (PhosStop) and a complete protease inhibitor tablet (Roche, Mississauga, ON, CA). Samples were centrifuged at 4500 rpm for 10 min at 4°C and the supernatant was removed. Collagen was precipitated with 1M NaOH and discarded leaving a myofibrillar-enriched supernatant fraction. Perchloric acid (1M) was added to the supernatant to precipitate the myofibrillar fraction. Proteins were then hydrolyzed by adding 1 mL of Dowex resin (50WX8-200) and 1 mL of 1M HCl to each sample followed by subsequent incubation for 72 hr at 110°C. Samples were vortexed every 24 hr. Free amino acids were then isolated using Dowex ion-exchange chromatography and the N-acetyl-*n*-propyl ester of alanine was prepared and analyzed by gas chromatography pyrolysis isotope ratio mass spectrometry.

Calculations

Saliva

Saliva deuterium enrichments were provided as a ratio (δ^{2}H), where:

$$\delta^2 H \ = \ \left(\frac{(2H/1H)\ sample}{(2H/1H)\ standard} - 1 \right) * 1000 \qquad \text{(Equation 2)}$$

Atom percent values were calculated as previously described:

$$AtomPercent \ = \frac{100 \text{ x AR x } (\delta 2H \text{ x } 0.001 + 1)}{1 + AR(\delta 2H \text{ x } 0.001 + 1)} \qquad \text{(Equation 3)}$$

Where AR is the absolute ratio constant for deuterium (0.00015595) based on the VSMOW standard. Atom percent excess was calculated by subtracting background deuterium enrichment (at time = 0) from each sample and multiplying the result by 35 to account for sample dilution.

Integrated Muscle Protein Synthesis Rates

Myofibrillar protein synthesis was calculated using the standard precursor-product equation:

$$\text{iMyoPS } (\% \cdot d^{-1}) = \left[\frac{(\varDelta \text{ APE}_{Ala})}{\text{APE}_{BW} \text{ x } 3.7 \text{ x } t} \right] \times 100 \qquad \text{(Equation 4)}$$

Where $\varDelta$ APE$_{Ala}$ is the change in protein-bound ^{2}H-alanine enrichment between biopsy sampling points, APE_{BW} is the body-water ^{2}H enrichment multiplied by 3.7 to correct for the number of carbon-hydrogen bonds labeled in alanine relative to total body water, and t is the incorporation time (in days) between biopsies. RT-induced change in iMyoPS was calculated using the muscle deuterium enrichment values calculated in the muscle specimen taken from the RT limb on day 70 and the UL limb on day 56 (i.e., rested limb). The effect of UL on iMyoPS was calculated using the muscle deuterium enrichment values calculated in the muscle specimens taken from the UL limb on day 70 and from the UL limb on day 56.

Exercise Protocols used in Independent Studies

Morton et al. (2016)

For a detailed description of the RT protocol used, refer to Morton et al. (2016). Participants were 23 ± 2 years old, with a BMI of 26.9 ± 2 kg/m^2 and had 4-5 y of resistance training experience. Briefly, participants performed full-body resistance training 4 days/week (Mon, Tues, Thurs, Fri) for 12 weeks that targeted all of the major muscle groups. Each session included 5 exercises, each of which were performed for 3 sets to volitional failure. Participants were randomly assigned to perform either high-repetition (20-25 reps per set @ 30%–50% 1-RM) or low-repetition training (8-12 reps per set @ 75%–90% 1-RM). Indices of muscle hypertrophy did not significantly differ between the groups post-RT, so group allocation was not considered in the present use of muscle tissue samples.

Cell Reports
Resource

Participants consumed 30 g of protein after each exercise bout. Muscle biopsies were taken from the *vastus lateralis* using the Bergstrom approach described above prior initiating the RT protocol and 72 h after the final RE bout at 12 weeks. RNA was extracted from whole muscle samples and analyzed on the HTA 2.0 platform using an identical method as described above (see RNA Extraction and Transcriptome Profiling).

Mitchell et al. (2014)

For a detailed description of the protocol used, refer to Mitchell et al. (2014). Participants were 24 ± 1 years old, with a BMI of 26.4 kg/m^2 and were recreationally active (not participating in an RT program). Participants performed full-body resistance training 4 days/week for 16 weeks consisting of two upper body and two lower body training sessions per week. The program progressed from 3 sets of 12 repetitions to 4 sets of 6 repetitions of each exercise. The last set of each exercise was performed to volitional failure. Participants consumed 30 g of protein immediately after each exercise session. Biopsies were obtained from the *vastus lateralis* using the Bergstrom approach described above prior to initiating 16 weeks of RT and ~48-72 h following the last RE bout. RNA was extracted from whole muscle samples as described above (see RNA Extraction and Transcriptome Profiling). Samples were dissolved in RNase-free water, processed to single-stranded sense fragmented DNA using the GeneChip® WT PLUS Reagent Kit, which relies on a reverse transcription priming strategy that primes both the poly-A and non-poly-A RNA. HTA 2.0 chips were processed according to the manufacturer's protocol. Fragmented (5 μg) end-labeled sense strand target cDNA was hybridized to each array and scanned using a Gene Chip Scanner 30007G (Affymetrix Core, MPI A/S, Denmark).

Phillips et al. (2017)

For a detailed description of the protocol used, refer to Phillips et al. (2017). Participants performed high-intensity interval training (HIIT) 3 days/week (Mon, Wed, and Fri) for 6 weeks. Each session consisted of a 2 min warmup at 50 W followed by 5 sets of high intensity cycling at ~125% VO$_2$max for 1 minute. Each set was separated by 90 s of rest. Biopsy tissue was available at pre and post time points for 47 participants, including 16 males and 31 females with an average age of 39 years (range 20-51 years) and a BMI of 31 kg/m^2 (27-43 kg/m^2). RNA was extracted using TRizol® (Life Technologies), dissolved in RNase-free water, processed to single-stranded sense fragmented DNA using the GeneChip® WT PLUS Reagent Kit, which relies on a reverse transcription priming strategy that primes both the poly-A and non-poly-A RNA. HTA 2.0 chips were processed according to the manufacturer's protocol. Fragmented (5 μg) end-labeled sense strand target cDNA was hybridized to each array and scanned using a Gene Chip Scanner 30007G (Affymetrix Core, MPI A/S, Denmark).

siRNA Transfection Experiments

Four days following initiation of myocyte differentiation, siRNA transfection was carried out following a media change, using lipofectamine RNAiMAX (Invitrogen), according to the manufacturer's instructions. Gene-specific knockdown was achieved using 500ng human Mission® esiRNA (Sigma-Aldrich) for the following genes: BCAT2 (EHU032991), NID2 (EHU083781), FKBP1A (EHU106961) and MBNL1 (EHU086561). Thirty-six hours following transfection, a media change was carried out and long R3 IGF-1 (50 ng/ml; Sigma-Aldrich) was added to each well. Cells were harvested after 4h in TRIzol (Life Technologies) for RNA extraction (n = 2), or homogenization buffer (50 mM Tris-HCl, pH7.5, 1 mM EDTA, 1 mM EGTA, 10 mM β-glycerophosphate, 50 mM NaF and complete protease inhibitor cocktail tablet (Roche, West Sussex, UK)) for protein extraction (n = 4). A subset of cells was also collected after 48h in 0.3 mol/l NaOH for total protein, RNA and DNA extraction and quantification (n = 5). For 4h experiments, 0.5 μM puromycin (Sigma-Aldrich, UK) was added to each well at the point of IGF-1 addition.

Cell culture total RNA Extraction and RT-PCR

Total RNA was extracted using TRIzol (Life Technologies) according to the manufacturer's protocol. RNA was resuspended in 20 μl of RNase-free water and quantified using a NanoDrop (Thermo Scientific). cDNA was synthesized by reverse transcription using the High Capacity cDNA synthesis kit (Applied Biosystems) with 500 ng RNA. Samples were subsequently diluted 1:5 using RNase-free water and real-time PCR was performed using 1 μl cDNA in duplicate and 6 μl master mix containing SYBR Select Master Mix (Life Technologies) with primers targeting the following genes: BCAT2 (Fwd: GAGCTGAAGGAGATCCAGTACG, Rev: GAGTCATTGGTAGGGAGGCG), NID2 (Fwd: TGGAAGCTACAGGTGTGAGTG, Rev: AGGTGGGGTGATCAAGATGCAA), MBNL1 (Fwd: CTGCCCAATACCAGGTCAAC, Rev: GGGGAAGTACAGCTTGAGGA), and FKBP1A (Fwd: GGTGGAAACCATCTCCCCAG, Rev: TCAAGCATCCCGGTGTAGTG). RPL13A was used for as a housekeeping gene since it was stable between each group. PCR was performed using a Viia 7 real-time PCR machine (Life Technologies) using the following thermal cycling conditions: 2 min at 50°C, 10 min at 95°C and 40 cycles of 15 s at 95oC and 1 min at 60°C.

Cell culture Western Blotting

Protein extraction from cells was performed by repeatedly passing samples through gel-loading pipette tips. Samples were centrifuged at 13,000 g for 10 min at 4°C. Protein samples (5 μg) were loaded onto Criterion XT 12% Bis-Tris gels (Bio-Rad) at 200V for 1h, then transferred to PVDF membrane for 45 min at 100V. After this, membranes were blocked using 5% (w/v) milk for 1h at room temperature, then incubated with primary antibodies all diluted 1:2000 (phosphorylated mTOR Ser2448 (#5536), phosphorylated p70 S6K1 Thr389 (#9234), phosphorylated eEF2 Thr56 (#2331), and phosphorylated 4E-BP1 Thr37/46 (#2855); all from Cell Signaling

Technology), except for anti-puromycin (Millipore), which was diluted 1:5000. Membranes were incubated overnight at 4°C. The following day, membranes were washed 3x5 min with 1x TBS-Tween, then incubated with HRP-conjugated anti-rabbit secondary antibody (New England) 1:2000 for 1h at room temperature. Bands were detected by incubating with enhanced chemiluminescence detection reagent (Millipore) and exposing in a Chemidoc XRS system (Bio-Rad). Bands were normalized against GAPDH levels. For total Protein, RNA and DNA measurements (48h) cells were harvested in 0.3 mol/L NaOH and then incubated at 37°C for 20 minutes (extraction of total alkaline-soluble protein). After protein quantification, 1 mol/L PCA was added to each sample, which were then left at 4oC for 30 minutes. After centrifugation, the supernatant was quantified for RNA. Finally, to the pellet, 2 mol/L PCA was added and samples were incubated at 70°C for 1h. The resultant supernatant was used to quantify DNA.

QUANTIFICATION AND STATISTICAL ANALYSES

Physiological Data

Physiological data were assessed for normality using the Shapiro-Wilk test and visually inspected using Q-Q plots. Paired-samples t tests were conducted to test for baseline differences in leg lean mass, mid-thigh CSA, and ISO-MVC between the trained and immobilized legs. Changes in physical activity and macronutrient intake over the duration of the study were analyzed using a one-way repeated-measures ANOVA. Changes in ISO-MVC, mid-thigh CSA and body composition variables obtained via DEXA were analyzed using a two-way repeated-measures analysis of variance (ANOVA) with time (2) and leg (2) as the within-subjects' factors. Muscle protein synthesis was analyzed using a one-way ANOVA with repeated-measures. In all cases, the statistical procedures were conducted on 12 young men (n). Results are presented as mean response plus/minus SD and, where appropriate, the median and range is included to emphasize variation in response. A Tukey's HSD post hoc test was employed to probe for pairwise differences between legs and across time points where warranted. In all analyses, statistical significance was set at $p \leq 0.05$.

Transcriptomic Data

All of the new HTA 2.0 array data has been deposited along with existing array data and are available at GEO (GSE154846). Standard quality control processes were performed for each study (NUSE plots and PCA). While the array offers advantages in terms of reproducibility, standard pre-processing approaches do not account for study specific probe-performance, and we have developed a study-specific pipeline that scans the 7 million short probes prior to assembly of transcripts using the following criteria:

  a) specific to one location on the genome
  b) the probe signal is above background noise in the particular dataset

   Data analysis methods utilized numerous informatics resources (Bengtsson et al., 2008; Dai et al., 2005; Gentleman et al., 2004; Wang et al., 2012). Each transcriptional 'unit' of expression was defined by establishing which of the ~6.9 million probes, from the HTA 2.0 chip, were detectable, and then assembling the signal from GC corrected 'active' probes into probe-sets (defined by ensembl ENST identifiers, http://www.ensembl.org//useast.ensembl.org/?redirectsrc=//www.ensembl.org%2F). The custom chip definition file (CDF) used to summarize the transcript level data is deposited at GEO. Our method provides an enhanced signal by removing individual probes, from probe-sets, that approximate to background noise. To create each CDF, the ~6.9 million probe sequences (Affymetrix website) were aligned to the genome build e.g., GRCh38_82p3 (e.g., see http://brainarray.mbni.med.umich.edu for a description) using bowtie alignment tool (Langmead and Salzberg, 2012). Probes which map to more then one part of the genome are discarded. There are ~50,000 probes on the HTA 2.0 array which have an extreme GC content (i.e., < 20%, > 80%) and these were removed as the adjustment model used to correct GC content is not effective at these extreme values. Older-generation transcriptomic data was re-processed to use the same transcript identifiers from the updated HTA pipeline (Timmons et al., 2018).

   Most studies of human muscle to date have used RNA detection technology that is unable to accurately measure exon-specific transcripts (Shalek et al., 2013) or provides partial and skewed coverage of the transcriptome. Our process allows us to define which part of the transcript we wish to quantify and in the present study, we apply the custom CDF approach to study differential expression of specific regions of transcripts through comparing the differential expression (DE) response of the entire ('full length') ensembl defined transcript unit, with the responses of only the untranslated regions – regions critical for regulating protein translational efficiency and hence a key component of the cell hypertrophy response. For DE analysis, we utilized paired SAMR analysis using a cut off of 5% FDR and 1.2-fold difference to generate the initial transcript lists - before applying a number of down-stream approaches to subset the data (See Results). For network analysis, we used the R-package MEGENA (Song and Zhang, 2015) to identify network structures (FDR < 1% for spearman correlation; p < 0.01 for module significance and p < 0.01 for network connectivity) and 10,000 permutations for calculating FDR and connectivity p values. Network data-plots were produced using Fruchterman-Reingold force directed plotting within MEGENA (Song and Zhang, 2015). CiiiDER was used to identify potential regulatory transcription factors (Gearing et al., 2019).

To estimate if a UTR signal was regulated in a manner distinct from the full length (FL) ENST's the following heuristic was utilized:

1) A "gene" was considered if it was significantly regulated in any one of the three statistical analysis comparisons between RT and UL (FL-ENST, 3′UTR and 5′UTR values, FDR < 5%, > 1.2FC)

AND

2) the FL-ENST was neither statistically regulated, nor the absolute numerical FC values were > 30% different from the matching *statistically* significant UTR response

OR

3) the FL-ENST was *statistically* regulated but the absolute numerical FC values were > 30% different from the *numerical* UTR response e.g., to include discordant patterns

Supplemental Information

Molecular Transducers of Human Skeletal Muscle

Remodeling under Different Loading States

Tanner Stokes, James A. Timmons, Hannah Crossland, Thomas R. Tripp, Kevin Murphy, Chris McGlory, Cameron J. Mitchell, Sara Y. Oikawa, Robert W. Morton, Bethan E. Phillips, Steven K. Baker, Phillip J. Atherton, Claes Wahlestedt, and Stuart M. Phillips

Supplementary Figures and Tables
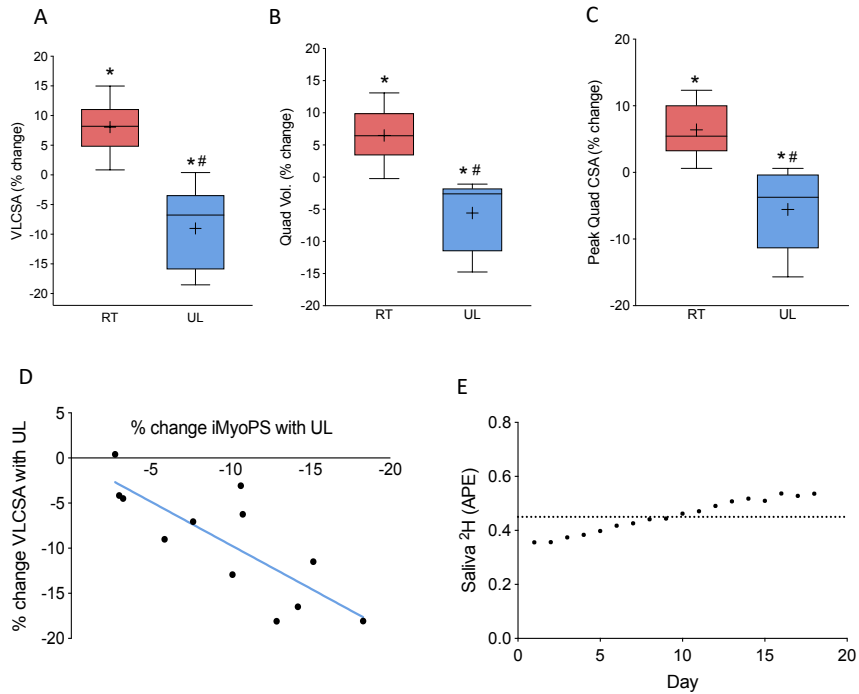
Figure S1. Muscle atrophy proceeds much more rapidly than muscle hypertrophy and is related to the change in muscle protein synthesis, related to Figure 2.
(A) Percentage change in mid-thigh *vastus lateralis* cross sectional area (VLCSA) following 10 weeks of resistance training (RT) and 2 weeks of unloading (UL); n=12.
(B) Percentage change in quadriceps volume following 10 weeks of RT and 2 weeks of UL, n=12.
(C) Percentage change in peak-quadriceps CSA following 10 weeks of RT and 2 weeks of UL, n=12.
(D) The linear relationship between changes in iMyoPS in response to 2 weeks of UL and the corresponding reduction of VLCSA in the same limb (Pearson's r=0.8, p<0.05, caveat with small sample size acknowledged despite the high probability of a causal relationship between these two variables); n=12.
(E) Average deuterium enrichment in saliva during the periods over which iMyoPS was assessed. The horizontal dotted line shows the global average from day 1 (i.e. after loading) until day 20; n=12.
For box and whisker plots, the boxes include the 25th, 50th and 75th quartiles and whiskers represent the maximum and minimum values. The mean value is depicted by the '+' symbol.
*denotes statistically different from Pre; # statistically different from RT value (p<0.05).
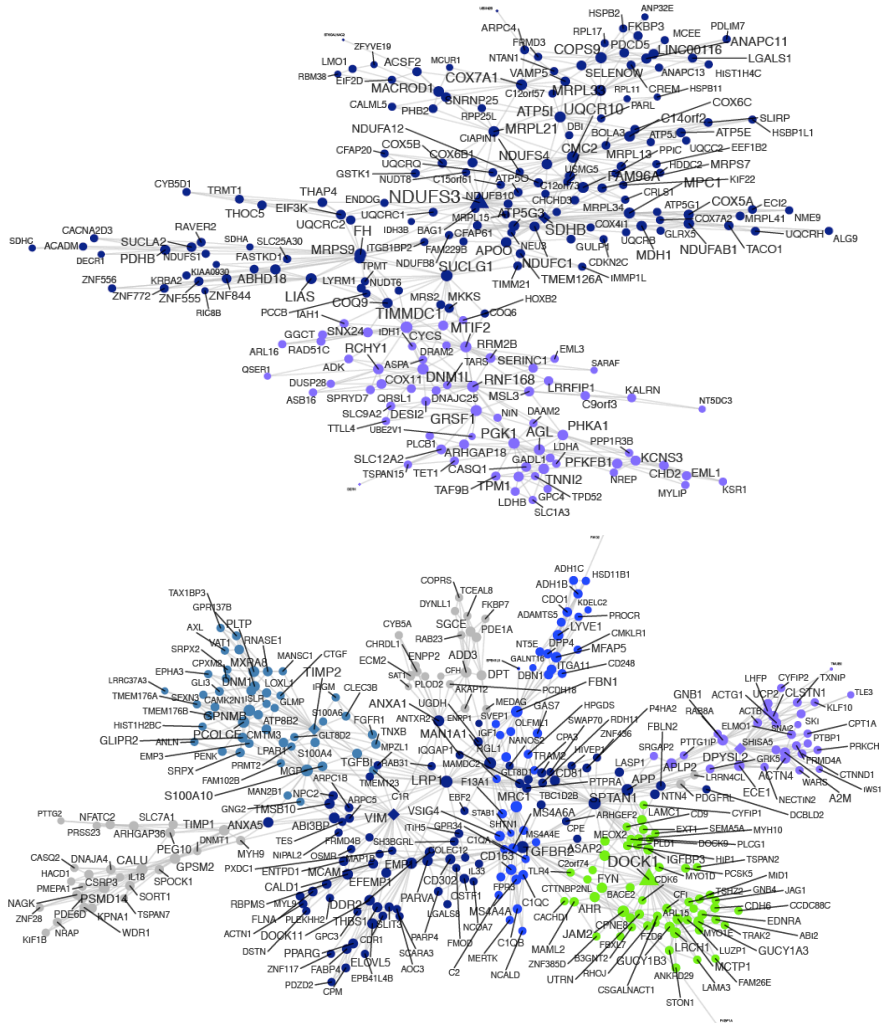
Figure S2. HypAt-regulated genes form functional networks in a large human muscle tissue biobank, related to Supplemental Data S1 and Figure 3.

Using the HypAT FL-ENST regulated transcripts (FDR <5%) as input into Megena (FDR <1% spearman correlation; p<0.01 for module significance, p<0.01 for network connectivity and 10,000 permutations for calculating FDR and connectivity p-values), top distinct planar filtered networks were identified that centered around NDUFS3 (top panel; enriched in genes relating to mitochondrial biology) and around DOCK1 (bottom

panel, enriched in genes related to extracellular matrix remodeling) using a large independent skeletal muscle data set (n=187).
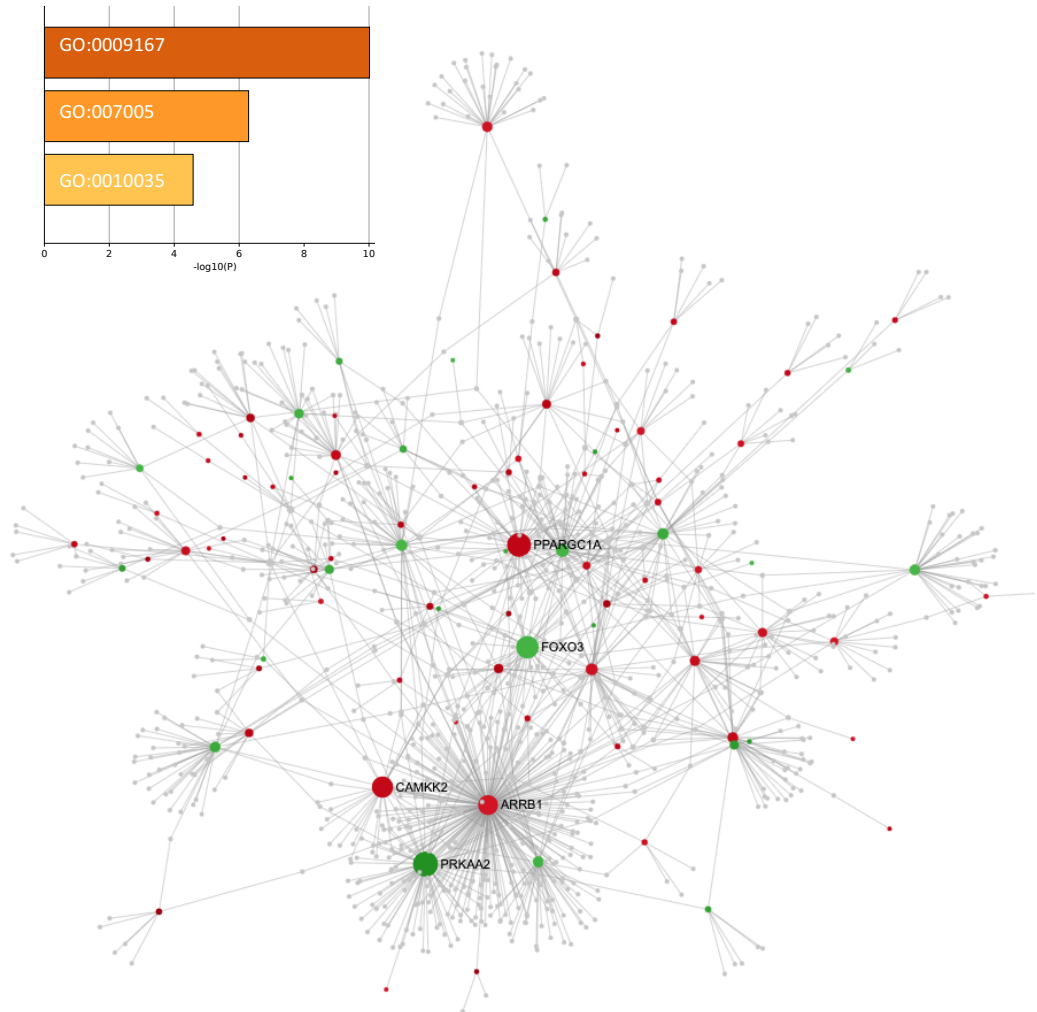
Figure S3. Proteome constrained network modeling reveals growth regulating pathways, related to Figure 3 and Table S2.

HypAT genes that correlated with lean mass gains in independent cohorts were used as input to characterize tissue-specific protein-protein interactions (PPI) using www.networkanalyst.ca and a 10th percentile threshold. A first-order network of protein-protein interactions is presented. FOXO3 was negatively correlated with leg lean mass changes and the PPI contained 45 FOXO signaling pathway members (Kegg database), 1×10^{-13} FDR. Green circles represent negatively- and red, positively-correlated genes. Grey genes are members of the protein-protein interactome acting on the 141 HypAT genes regulated in proportion to gains in lean mass. **Inset**: bar graph generated using Metascape showing top enrichment clusters derived from the list of growth correlated genes. GO Terms: GO:0009167, Purine ribonucleoside monophosphate metabolic process; GO:0007005, Mitochondrion

organization; GO:0010035, Response to inorganic substance. Color of bars indicates the level of significance of the corresponding cluster. Genes related to muscle growth in independent data sets were found to be dominated by proteins related to mitochondrial biology and ribonucleoside monophosphate synthesis.
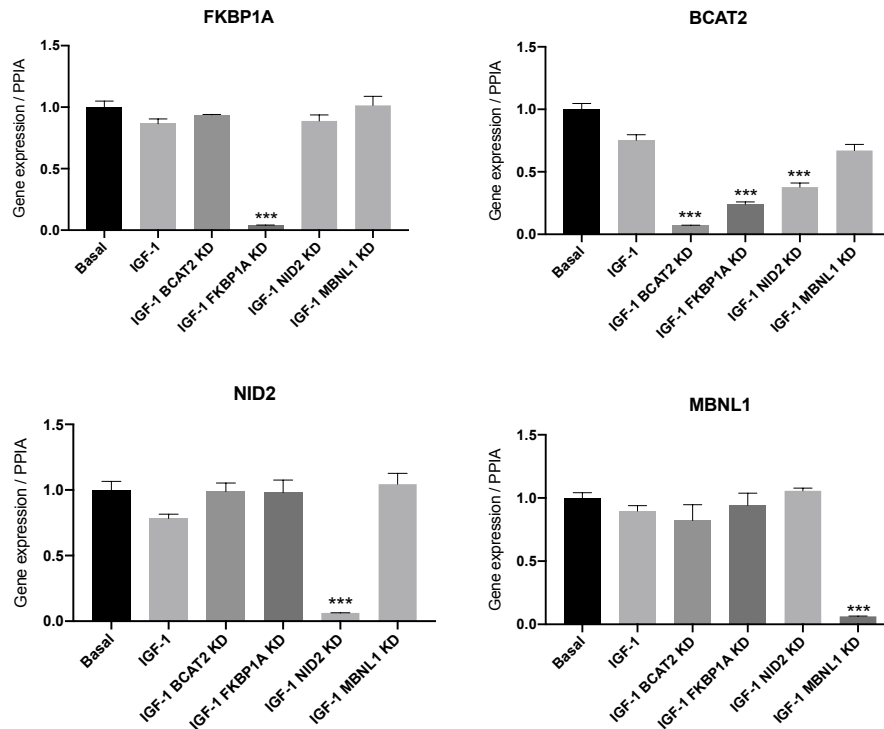
Figure S4. RNAi effectively reduced RNA expression of selected growth-correlated target genes by >90% in differentiated myotubes, related to Figure 4.
Normalized gene expression data from myotubes after knockdown with siRNA species against: FKBP1, BCAT2, MBNL1 and NID2. Cells were either untreated (set to 100%), treated with IGF-1 only, or treated with IGF-1 and with a pool of siRNA targeted against the gene listed. n=4; one-way ANOVA (*P<0.05, **P<0.01, ***P<0.001 versus IGF-1)
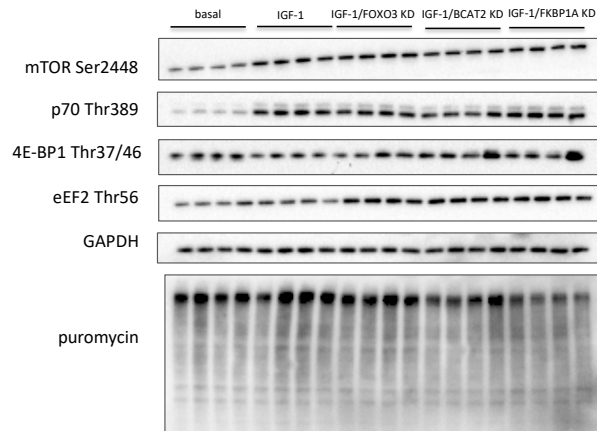
Lane order (n=4): basal, IGF-1, IGF-1/FOXO3 KD, IGF-1/BCAT2 KD, IGF-1/FKBP1A KD
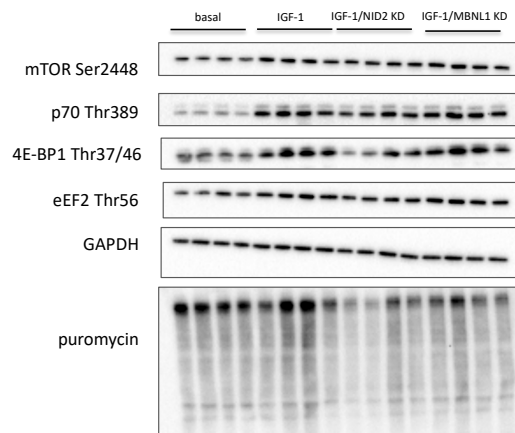
Lane order (n=4): basal, IGF-1, IGF-1/NID2 KD, IGF-1/MNBNL1 KD

Figure S5. Representative western blots of protein signaling data, related to Figure 4.
Lane order (n=4): basal (untreated), IGF-1, IGF-1/FOXO KD, IGF-1/BCAT2 KD, IGF-1/FKBP1a KD. Note: the RNAi tool against FOXO3 was inactive and so we did not, as originally planned, study FOXO3 as a control. However, western analyses were carried out prior to the discovery that FOXO3 siRNA was defective and thus included in the original gels.
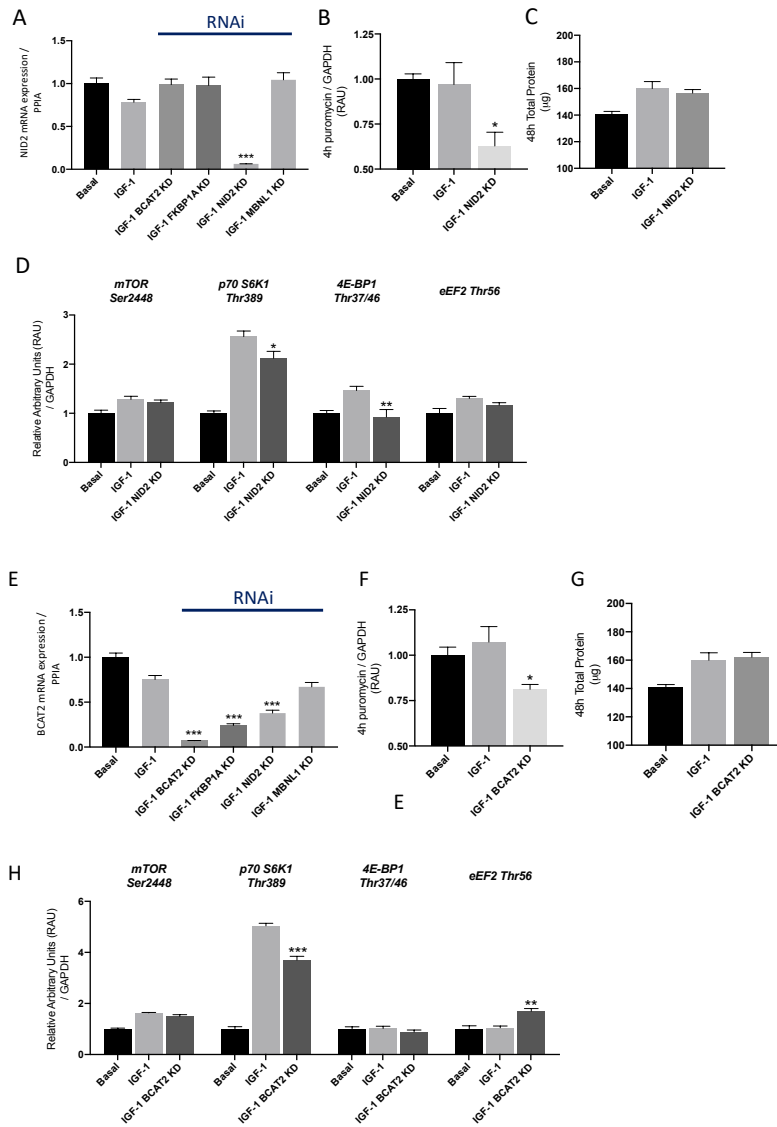
Figure S7. Knockdown of growth-correlated genes in myotubes alters protein synthesis and regulates signaling cascades that influence protein translation, related to Figure 4.
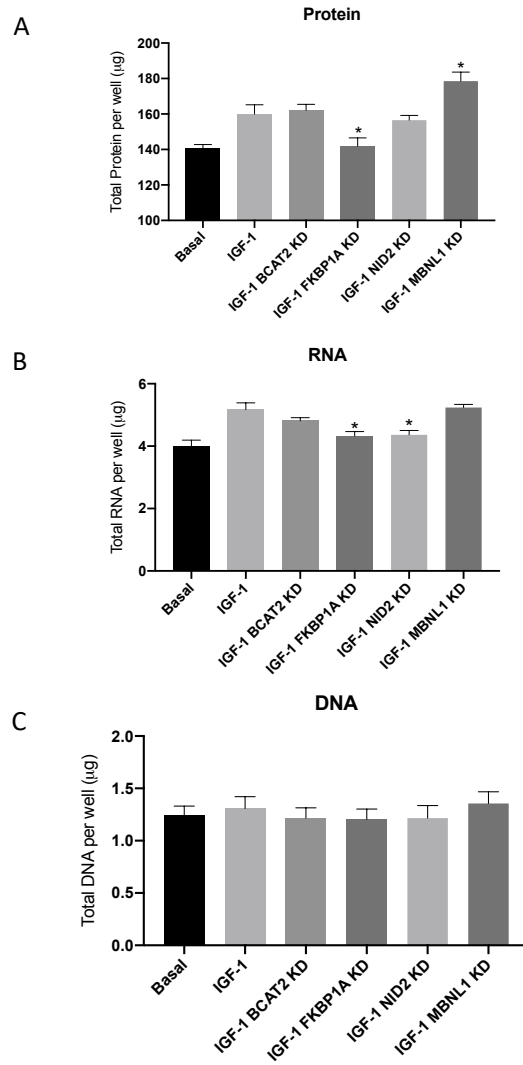
Figure S6. Total protein, RNA and DNA content after myotube treatment with or without IGF-1 and siRNA against selected gene targets, related to Figure 4.
Total protein (A), RNA (B) and DNA (C) after myotube treatment with IGF-1 in isolation or combined with siRNA against BCAT2, FKBP1A, NID2 or MBNL1. n=5; one-way ANOVA (*$P<0.05$, versus IGF-1).
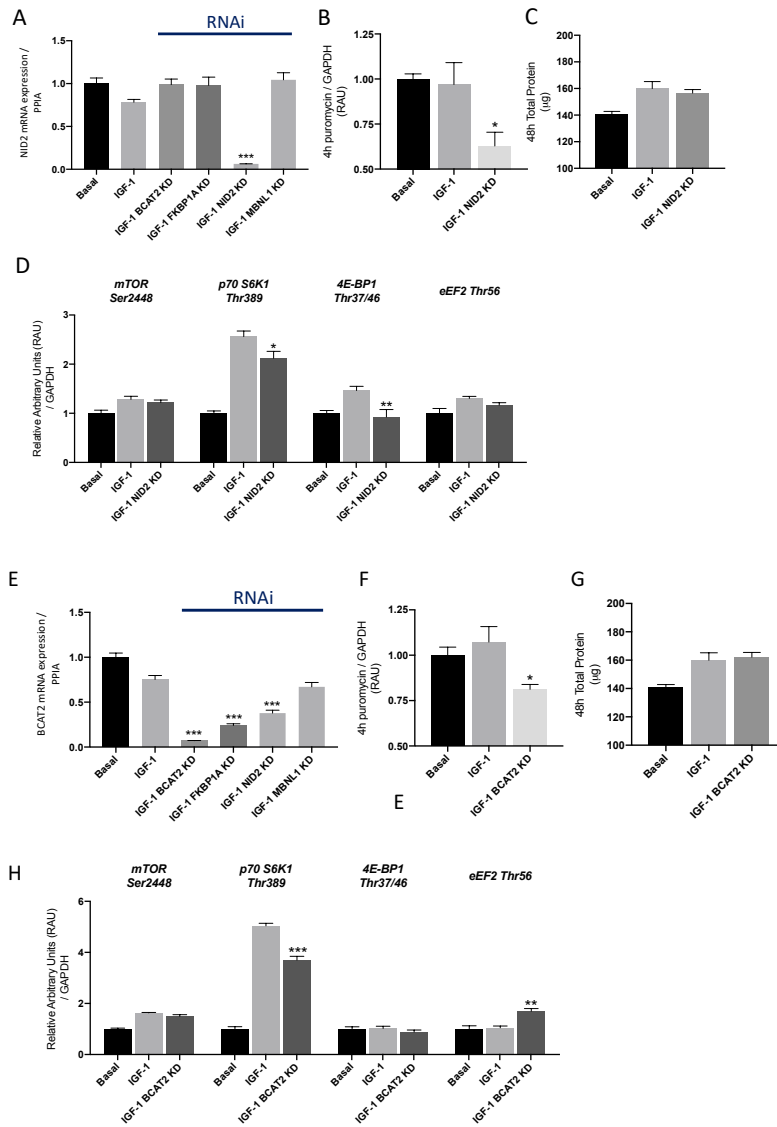
Figure S7. Knockdown of growth-correlated genes in myotubes alters protein synthesis and regulates signaling cascades that influence protein translation, related to Figure 4.

(A – D) The effects of targeting NID2 with siRNA on NID2 mRNA expression (A), 4hr puromycin signal (B), 48hr total protein (C) and protein content of various proteins thought to be involved in muscle growth.
(E – H) The effects of targeting BCAT2 with siRNA on BCAT2 mRNA expression (A), 4hr puromycin signal (B), 48hr total protein (C) and protein content of various proteins thought to be involved in muscle growth.

Supplementary Tables

Table S1. HypAt Participant Characteristics, related to Figure 1, 2, S1 and STAR Methods.

Parameter	Baseline	Week 5	Week 10
Age, y	20±3	-	-
Height, m	1.7±0.1	-	-
Mass, kg	71.2±12.2	71.2±11.4	70.8±11.2
BMI, $kg \cdot m^{-2}$	23.8±3.1	23.9±2.9	23.7±2.8
Leg Ext 1-RM, kg	53±12	-	77±12*
Leg Press 1-RM, kg	120±32	-	190±35*
Daily Steps	9900±5100	9100±2800	8000±3600
Activity, $kcal \cdot d^{-1}$	1012±477	970±403	965±437
Dietary Protein, $g \cdot kg \cdot d^{-1}$	1.5±0.9	1.4±0.7	1.6±0.9
En% Protein	17±6	19±5	18±4
En% CHO	49±15	52±7	54±10
En% Fat	32±12	31±7	28±10

Abbreviations: BMI, body mass index; 1-RM, one-repetition maximum; En%, energy percentage. CHO, carbohydrates. * significantly different from baseline, $p<0.05$. All data are presented as mean±SD.

Table S2. Steps for generating a proteome-constrained network plot, related to Table 1, STAR Methods, Figure S3 and Supplemental Data S2.

Steps	Link/File
Get list of genes for uploading to web-site	URL to Supplemental Data S2
Browse to network tool home page	www.networkanalyst.ca
Select 'Gene List Input' option	https://www.networkanalyst.ca/NetworkAnalyst/uploads/ListUploadView.xhtml
Select 'Human' and Official Gene Symbol	Pull-down lists
Open file containing gene list	Browse to location of 'Supplementary Data S2' file on your computer and open in text editor or Excel - then copy both columns
Upload gene list	Paste gene list and press upload and then press proceed
Choose Tissue-Specific PPI	Select 'skeletal muscle' from the pull-down menu and set the filter to 10
Define Network	Press proceed https://www.networkanalyst.ca/NetworkAnalyst/Secure/network/NetworkBuilder.xhtml)
Define network structure	Press 3D option within network plotting window. Then set 'view' to 'expression' and 'shading' = 'none'.
View 3D network	Place mouse cursor on any black space, hold-down mouse button and drag to rotate. Type any gene name into the 'search' function to highlight that gene. Zoom in and out to view network connections.
Explore pathway biology	Select database to query from top right-hand side of web page. E.g. Kegg. Choose all nodes and press submit

A step by step guide to generating a 3-dimentional plot of the 141 HypAT genes that correlated with lean mass gains across independent cohorts within the context of a muscle tissue-specific protein-protein interactions (PPI) network. Note, in November 2019, the analysis indicates FOXO3 was negatively correlated with leg lean mass changes and the PPI contains 45 FOXO signaling pathway members (Kegg database, 1×10^{-13} FDR). Green represents negatively and red positively correlated genes with in vivo changes in lean mass. Grey circles are members of the protein-protein interactome, acting on the 141 HypAt genes regulated in proportion to gains in lean mass, but themselves were not regulated at the RNA level in the present analysis. Any regulated gene, from the 141 identified, that was not part of the protein-protein interactome would not appear in this analysis as evidence for protein level interaction was a prerequisite for inclusion.

CHAPTER 4:

Declines in muscle protein synthesis account for short-term disuse atrophy in humans in the absence of increased muscle protein breakdown.
Published in the *Journal of Cachexia, Sarcopenia, and Muscle.* May 23. 2022. Doi: 10.1002/jcsm.13005. Online ahead of print

Declines in muscle protein synthesis account for short-term muscle disuse atrophy in humans in the absence of increased muscle protein breakdown

Matthew S. Brook[1,2] ⓘ, Tanner Stokes[3], Stefan H.M. Gorissen[3], Joseph J. Bass[1] ⓘ, Chris McGlory[4] ⓘ, Jessica Cegielski[1], Daniel J. Wilkinson[1] ⓘ, Bethan E. Phillips[1] ⓘ, Ken Smith[1], Stuart M. Phillips[3] ⓘ & Philip J. Atherton[1]* ⓘ

[1]MRC-Versus Arthritis Centre for Musculoskeletal Ageing Research and NIHR Nottingham BRC, Centre Of Metabolism, Ageing and Physiology (COMAP), School of Medicine, University of Nottingham, Derby, UK; [2]School of Life Sciences, University of Nottingham, Nottingham, UK; [3]Department of Kinesiology, McMaster University, Hamilton, ON, Canada; [4]School of Kinesiology and Health Studies, Queen's University, Kingston, ON, Canada

Abstract

Background We determined the short-term (i.e. 4 days) impacts of disuse atrophy in relation to muscle protein turnover [acute fasted-fed muscle protein synthesis (MPS)/muscle protein breakdown (MPB) and integrated MPS/estimated MPB].

Methods Healthy men ($N = 9$, 22 ± 2 years, body mass index 24 ± 3 kg m^{-2}) underwent 4 day unilateral leg immobilization. *Vastus lateralis* (VL) muscle thickness (MT) and extensor strength and thigh lean mass (TLM) were measured. Bilateral VL muscle biopsies were collected on Day 4 at $t = -120$, 0, 90, and 180 min to determine integrated MPS, estimated MPB, acute fasted-fed MPS (L-[ring-$^{13}C_6$]-phe), and acute fasted tracer decay rate representative of MPB (L-[^{15}N]-phe and L-[$^2H_8$]-phe). Protein turnover cell signalling was measured by immunoblotting.

Results Immobilization decreased TLM [pre: 7477 ± 1196 g, post: 7352 ± 1209 g ($P < 0.01$)], MT [pre: 2.67 ± 0.50 cm, post: 2.55 ± 0.51 cm ($P < 0.05$)], and strength [pre: 260 ± 43 N m, post: 229 ± 37 N m ($P < 0.05$)] with no change in control legs. Integrated MPS decreased in immob vs. control legs [control: $1.55 \pm 0.21\%$ day^{-1}, immob: $1.29 \pm 0.17\%$ day^{-1} ($P < 0.01$)], while tracer decay rate (i.e. MPB) (control: 0.02 ± 0.006, immob: 0.015 ± 0.015) and fractional breakdown rate (FBR) remained unchanged [control: $1.44 \pm 0.51\%$ day^{-1}, immob: $1.73 \pm 0.35\%$ day^{-1} ($P = 0.21$)]. Changes in MT correlated with those in MPS but not FBR. MPS increased in the control leg following feeding [fasted: $0.043 \pm 0.012\%$ h^{-1}, fed: $0.065 \pm 0.017\%$ h^{-1} ($P < 0.05$)] but not in immob [fasted: $0.034 \pm 0.014\%$ h^{-1}, fed: $0.049 \pm 0.023\%$ h^{-1} ($P = 0.09$)]. There were no changes in markers of MPB with immob ($P > 0.05$).

Conclusions Human skeletal muscle disuse atrophy is driven by declines in MPS, not increases in MPB. Pro-anabolic therapies to mitigate disuse atrophy would likely be more effective than therapies aimed at attenuating protein degradation.

Keywords Immobilization; Atrophy; Muscle; Protein synthesis; Protein breakdown

Introduction

Periods of skeletal muscle atrophy due to general ill-health, immobility, sedentary behaviours, trauma, disease, or age-ing punctuate the age-related declines in skeletal muscle mass.[1] While the aetiology of muscle atrophy depends on the underlying cause, a major component of all-cause muscle atrophy is physical inactivity. Inactivity may occur slowly, through sedentarism/immobility, or more rapidly due to enforced bed rest or limb casting after trauma or elective surgery.[2–4] It follows that a significant body of research has, and continues to focus upon, the mechanisms of muscle atrophy and mitigation strategies.[5] In terms of the temporal nature of muscle atrophy upon immobilization, there is growing evidence of rapidity over short time frames ($<$1 week).[4,6] The average UK NHS hospital stay is ~4.5 days (Source: NHS HES 2018–2019) and time off work due to flu related illness ~3 days.[7] However, the mechanisms of atrophy during short-term immobilization remain unclear in humans.[8]

Muscle mass is regulated by the balance between muscle protein synthesis (MPS) and muscle protein breakdown (MPB) rates. These rates exist in dynamic equilibrium resulting from fasted-fed cycles whereby dietary protein intake replenishes amino acids released from muscle for extra-muscular processes in between meals.[1] Theoretically, muscle disuse atrophy could be driven by declines in MPS, increases in MPB, or both. Early studies using stable isotopically labelled amino acid (AA) tracer infusions have shown that declines in post-absorptive MPS rates are a consistent feature of human disuse atrophy.[9,10] Similarly, MPS responses to protein intake during immobilization are also blunted, albeit through mechanisms not easily explained by classical AA sensing.[11] Nonetheless, it is clear that blunted rates of fasted and fed MPS are key players in human disuse atrophy.[9,12]

In contrast to MPS, the role of MPB in human disuse atrophy remains poorly defined, despite decades of work generated in animal models suggesting that MPB is a major driver of disuse atrophy. The lack of MPB data in humans is in part due to the technical challenges of quantifying MPB *in vivo*. Indeed, while MPS is readily measurable using 'direct incorporation (into muscle biopsy)' tracer techniques, such a gold standard does not exist for MPB. The arterio-venous (A-V) balance technique is one approach to quantify tracer rate of appearance/disappearance, although this requires limb—typically femoral—venous cannulation and is reliant upon assumptions and accurate and timely measures of blood flow.[13] Another approach is the 'pulse-chase' technique, capitalizing on the ratio of dilution between two tracers over time.[14] Of the few studies that have quantified MPB, one showed no effect on MPB (using A-V balance technique) after 14 day bed rest in the face of decreased MPS and whole-body protein synthesis.[15] Moreover, short-term studies measuring dynamic MPB are lacking, despite reports of heightened static biomarkers of MPB in the early phase of disuse atrophy.[4,16,17] Therefore, a major gap remains in our understanding of the relative roles of MPS/MPB and the technical challenges to quantifying these dynamic processes over an entire disuse period.

In the present study, we aimed to address each of these knowledge gaps by determining the short-term (4 days) impact of disuse atrophy using the knee brace immobilization model[9] in humans in relation to: MPS (acute fasted-fed via L-[ring-$^{13}C_6$]-phenylalanine and cumulative MPS via D_2O), acute pulse-chase tracer decay rate representative of MPB, and estimated 4d FBR, in addition to regulatory pathways of MPS/MPB. We hypothesized that declines in acute fasted and fed, and thus cumulative MPS would account for short-term disuse atrophy. We further hypothesized that MPB would not be playing a major role in human disuse atrophy.

Methods

Participant characteristics

Nine young, healthy male participants[11] (mean ± SD: age, 22 ± 2 years; body mass index, 24 ± 3 kg m^{-2}) volunteered to take part in this study. A sample size of nine in each group was determined to have a power of 95% and a significance level of 5%, based on previously published data showing a lower post-prandial stimulation of MPS in the immobilized vs. control limb (0.02 ± 0.007 vs. 0.044 ± 0.010% h^{-1}).[17] Participants were initially screened by medical questionnaire, with exclusions for history of any neuromuscular disorder or muscle/bone wasting disease, acute or chronic metabolic, respiratory or cardiovascular disorder, or any other signs of ill health. All participants were performing activities of daily living or recreation upon entry to the study but were not routinely undertaking heavy, structured exercise. Participants did not use tobacco-containing products or consume excessive alcohol ($>$21 units per week). The experimental procedures were approved by the Hamilton Integrated Research Ethics Board (HiREB #2192) and conformed to the Declaration of Helsinki. Written informed consent was obtained from all participants prior to their participation.

Experimental procedures

This study involved a bilateral leg protocol, with one leg randomly assigned to be immobilized and the contralateral limb used as a co-temporal control. Upon inclusion, participants were asked to visit the laboratory on two separate occasions, both of which followed an overnight fast (*Figure* 1).

On the first visit, participants had the thigh lean mass of both legs measured using dual-energy X-ray absorptiometry (DXA) (Lunar iDXA; GE Medical Systems, Mississauga, ON), before ingesting a bolus dose of D_2O (3 mL kg^{-1}) for the measurement of integrated MPS rates. A saliva and blood sample was obtained prior to and 2 h following D_2O consumption for measurement of deuterium enrichment in body water. *Vastus lateralis* (VL) muscle thickness (MT) was assessed using B-mode ultrasonography (Vivid Q, GE Medical Systems, Horten, Norway). During the first assessment, a mark was made with permanent marker 50% of the distance between the greater trochanter of the femur and the lateral epicondyle of the knee, identified by palpation. A thick layer of acoustic gel was applied on the leg at the area of measurement, and care was taken to avoid depressing the muscle belly during image acquisition. The test–retest intraclass correlation coefficient for VL MT was 0.96. Maximal voluntary isometric contraction torque (MVC) of each leg was assessed using Biodex dynamometer (Biodex System 3; Biodex Medical Systems, Shirley, New York). The test–retest intraclass correlation coefficient for Biodex measures was 0.92. Thereafter, a knee brace (X-Act ROM; DonJoy, Dallas, TX, USA) was fitted to the immobilization randomized leg and fixed at an angle of 60° of knee flexion. Participants continued to wear the knee brace as described for a duration of 3 days, collecting a saliva sample each day, before returning to the laboratory for their second visit exactly 4 days after the first visit. Upon arrival for Visit 2, participants had their knee brace removed, DXA thigh lean mass measured, ultrasound scan, and a further saliva sample was obtained. Participants were transported between stations in a wheelchair to prevent weight bearing in the immobilized leg prior to undergoing the infusion trial described below.

Infusion protocol

Participants reported to the laboratory in the overnight fasting state (at least 10 h fasted). The knee brace was removed, and participants remained in a supine position on a laboratory bed for the entire duration of the infusion trial. A catheter was placed in an antecubital vein for AA and dextrose infusions. A second catheter was inserted into an antecubital vein of the contralateral arm and placed in a heated blanket for arterialized blood sampling. After obtaining a baseline blood sample ($t = -210$ min), a primed constant infusion of L-[ring-$^{13}C_6$]-phenylalanine (0.4 mg kg^{-1} prime; 0.6 mg kg h^{-1} infusion) was initiated for the assessment of MPS. Additional blood samples were collected regularly throughout (*Figure* 2). At $t = -120$ min, a saliva sample was collected, and the first muscle biopsies were taken from both the immobilized and control leg for measurement of integrated MPS. Further muscle biopsies were collected from both legs at $t = 0$ min to determine basal MPS based on L-[ring-$^{13}C_6$]-phenylalanine incorporation. Pulse injections of L-[$^2H_8$]-phenylalanine at $t = -90$ min (5.53 mg kg^{-1}) and L-[^{15}N]-phenylalanine at $t = -30$ min (5.4 mg kg^{-1}) for the determination of MPB rates (represented by tracer decay rate over time) were applied in the fasted state, calculated from muscle biopsies at $t = 0$ min. After collecting the muscle biopsies, primed constant infusions of AAs (34 mg kg^{-1} prime; 102 mg kg h^{-1} infusion; PRIMENE 10%, Baxter Corporation, Mississauga, Ontario, Canada) and dextrose (blood glucose clamped at 7.0–7.5 mM) were started to mimic a post-prandial state for the remainder of the infusion trial. During the post-prandial state, the L-[ring-$^{13}C_6$]-phenylalanine infusion rate was increased to 0.86 mg kg h^{-1} to account for unlabelled phenylalanine entering the free AA pool and prevent dilution of the precursor pool. At $t = 90$ and
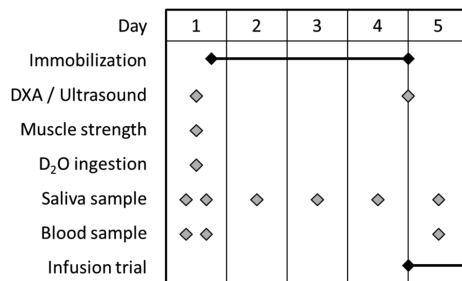

Figure 1 Schematic representation of study design.
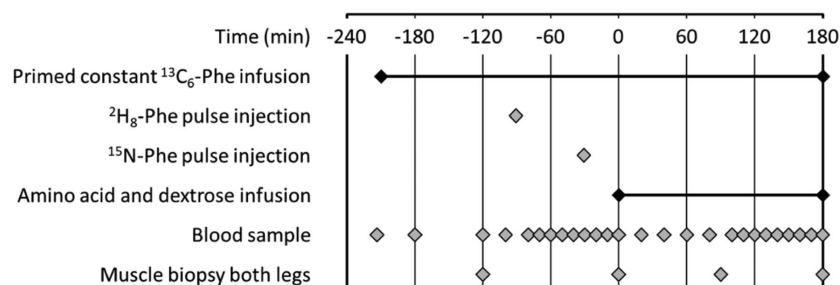
Figure 2 Schematic representation of infusion trial.

t = 180 min, muscle biopsies were collected from the immobilized and control legs. After the final biopsies, participants were provided with juice and a snack, the dextrose infusion was gradually decreased, and other infusions were stopped. Plasma glucose was monitored for another 30 min in order to prevent hypoglycaemia. Blood samples were collected in EDTA containing tubes and centrifuged at 1800g for 10 min at 4°C. Aliquots of plasma were frozen in liquid nitrogen and stored at −20°C. Biopsies were collected from the middle region of the *m. vastus lateralis*, approximately 15 cm above the patella and 3 cm below entry through the fascia, using the percutaneous needle biopsy technique. Muscle samples were dissected carefully, freed from any visible non-muscle material, immediately frozen in liquid nitrogen, and stored at −80°C until further analysis. A schematic representation of the infusion trial can be seen in *Figure* 2.

Glucose clamp

During the infusion trial, starting at t = 0 min, a glucose clamp was initiated to mimic a post-prandial state. Dextrose (25%) was infused according to a priming infusion protocol adapted from DeFronzo *et al*.[18] for the first 14 min until a steady-state blood glucose concentration of 7.0–7.5 mM was obtained. Steady-state blood glucose was maintained by measuring blood glucose concentrations every 5 min and adjusting the infusion rate accordingly. Blood glucose concentrations over the course of the dextrose infusion were measured using the YSI STAT 2300 glucose analyser. At the end of the infusion trial, participants consumed juice and a snack while the dextrose infusion rate was gradually decreased in order to prevent hypoglycaemia. Blood glucose was monitored for another 30 min.

Body water, muscle protein bound alanine, and intracellular free amino acid enrichments

Body water enrichment was measured as previously described.[19] Briefly, saliva was heated in a vial at 100°C, then cooled rapidly on ice and the condensate transferred to a clean vial ready for analysis. Deuterium enrichment was measured on a high-temperature conversion elemental analyser connected to an isotope ratio mass spectrometer (TC/EA-IRMS Thermo Finnigan, Hemel Hempstead, UK). For isolation of myofibrillar and sarcoplasmic fractions, 30–50 mg of muscle was used. Muscle samples were homogenized in ice-cold homogenization buffer [50 mM Tris–HCl (pH 7.4), 50 mM NaF, 10 mM $^{\beta}$-glycerophosphate disodium salt, 1 mM EDTA, 1 mM EGTA, and 1 mM activated Na_3VO_4 (all from Sigma-Aldrich)] and a complete protease inhibitor cocktail tablet (Roche, West Sussex, UK) at 10 μL μg^{-1} tissue. Homogenates were rotated for 10 min, and the supernatant (sarcoplasmic fraction) was collected by centrifugation at 1000g for 15 min at 4°C. The pellet was resuspended in 500 μL mitochondrial extraction buffer, dounce homogenized, and the supernatant removed after centrifugation at 1000g for 5 min at 4°C. The myofibrillar pellet was solubilized in 0.3 M NaOH and separated from the insoluble collagen by centrifugation, and the myofibrillar protein was precipitated in 1 M perchloric acid. The myofibrillar protein was then precipitated, hydrolysed in 0.1 M HCL for 24 h, and the free AAs purified and derivatized as their *n*-methoxycarbonyl methyl esters. Incorporation of deuterium into protein bound alanine was determined by gas chromatography-pyrolysis-isotope ratio mass spectrometry (GC-pyrolysis-IRMS, Delta V Advantage; Thermo Finnigan, Hemel Hempstead, UK) alongside a standard curve of known DL-alanine-2,3,3,3-D_4 enrichment to validate measurement accuracy. MPS, fractional growth rate (FGR), and fractional breakdown rate (FBR) were calculated

as previously described.[20] The incorporation of L-[ring-$^{13}C_6$]-phenylalanine was determined by gas chromatography-combustion-isotope ratio mass spectrometry (Delta plus XP; Thermo Fisher Scientific, Hemel Hempstead, United Kingdom) with muscle intracellular L-[ring-$^{13}C_6$]-phenylalanine, L-[^{15}N]-phenylalanine, and L-[$^2H_8$]-phenylalanine enrichment measured by gas chromatography-tandem mass spectrometry (TSQ 8000; Thermo Scientific) following precipitation of the sarcoplasmic fraction and purification of the supernatant using Dowex H$^+$ resin as described above, with AAs converted to their m*ethoxycarbonyl ethyl esters*. The fractional synthesis rate of the myofibrillar proteins was calculated using the precursor-product equation as previously described.[21] The tracer decay rate or MPB was calculated using pulse-chase methods (*n* = 5). From muscle biopsies collected at *t* = 0 min, the enrichment of L-[^{15}N]-phenylalanine and L-[$^2H_8$]-phenylalanine was calculated. Pulse injections of L-[^{15}N]-phenylalanine and L-[$^2H_8$]-phenylalanine were administered at *t* = −90 min and *t* = −30 min respectively, the tracer dilution within the intracellular pools enables a decay rate representing MPB to be calculated.[22–24] The exponential tracer decay rate was determined from the difference in intracellular enrichment of L-[^{15}N]-phenylalanine and L-[$^2H_8$]-phenylalanine at *t* = 0 biopsy over 1 h.

Immunoblotting for muscle signalling pathway activity

Immunoblotting was performed as previously described[25] using the sarcoplasmic fraction isolated from myofibrillar preparation (*n* = 8). Sarcoplasmic protein concentrations were analysed using a NanoDrop ND1000 spectrophotometer (NanoDrop Technologies, Inc., Wilmington, DE-US) and sample concentrations adjusted to 1 μg μL^{-1} in 3× Laemmli buffer to ensure equivalent protein loading in pre-cast 12% Bis-Tris Criterion XT gels (Bio-Rad, Hemel Hempstead, UK) of 10 μg/lane. Samples were separated electrophoretically at 200 V for 1 h, followed by transfer of proteins to PVDF membrane at 100 V for 45 min and subsequent blocking in 2.5% non-fat milk in Tris-buffered saline/Tween 20 (TBST) for 1 h. Membranes were incubated in primary antibodies (1:2000 dilution in 2.5% BSA in TBST) overnight at 4°C; *p*-mTOR Ser 2448 (#2972), *p*-4E-BP1 Thr 37/46 (#2855), *p*-eEF2 Thr 56 (#2331), *p*-AKT Ser 473 (#4060), *p*-rpS6 Ser 235/236 (#2211), *p*-eIF4E Ser 209 (#9741), *p*-eIF4B Ser 422 (#3591), Ubiquitin (1:1000; #3933, New England Biolabs, Hertfordshire, UK), Calpain (1:1000; ab3589, Abcam, Cambridge, UK), and MAFbx (1:1000; #AP2041, ECM Biosciences, Versailles, KY, USA). Membranes were subsequently washed and incubated in HRP conjugated anti-rabbit secondary antibody (#7074, New England Biolabs, Hertfordshire, UK; 1:2000 in 2.5% BSA in TBST) at ambient temperature for 1 h, before exposure to chemiluminescent HRP Substrate

(Millipore Corporation, Billerica, MA, USA) for 5 min. Bands were quantified by Chemidoc XRS (Bio-Rad, Hertfordshire, UK). All signals were within the linear range of detection; loading was corrected to Coomassie [34]. Fed (*t* = 90 min) data were normalized to control mean and transformed using $Y = (\log(1 + Y))$.

Statistical analyses

Data are presented as means ± standard deviation (SD) or as individual data points with paired samples connected by a line. Data were tested for normal distribution using a Kolmogorov–Smirnov test. DXA lean mass, VL MT, MVC, and acute MPS were analysed using a repeated measures two-way ANOVA. Immunoblotting values were normalized to control and transformed using $Y = (\log(1 + Y))$ prior to analysis using a repeated measures two-way ANOVA. Integrated MPS, FGR, FBR, and tracer decay rate were analysed using a paired *t*-test. All data analysis was performed using GraphPad Prism (GraphPad Software Inc., San Diego, CA); correlations were assessed using Pearson's product moment correlation coefficient. Cohen's *d* effect size (*d*) was calculated for paired samples. The alpha level of significance was set at $P < 0.05$.

Results

Muscle mass, vastus lateralis thickness, and strength

At baseline, there was no difference in TLM, VL MT, or strength between legs. Over the 4 day study period, the control leg showed no change in TLM [pre: 7476 ± 1341 g, post: 7501 ± 1349 g (*d* = 0.26)], VL MT [pre: 2.68 ± 0.54 cm, post: 2.65 ± 0.52 cm (*d* = 0.23)] or MVC [pre: 253 ± 48 N m^{-1}, post: 264 ± 68 N m^{-1} (*d* = 0.36)]. The immobilized leg showed a decrease from baseline in TLM [pre: 7477 ± 1196 g, post: 7352 ± 1209 g, ($P < 0.01$, *d* = 1.1) (main effect of interaction: *P* = 0.01, time: *P* = 0.06, intervention: *P* = 0.09), *Figure* 3A], VL MT [pre: 2.67 ± 0.50 cm, post: 2.55 ± 0.51 cm, ($P < 0.05$, *d* = 1.45) (main effect of interaction: *P* = 0.16, time: *P* = 0.01, intervention *P* = 0.8), *Figure* 3B], and MVC [pre: 260 ± 43 N m^{-1}, post: 229 ± 37 N m^{-1}, ($P < 0.05$, *d* = 0.93) (main effect of interaction: *P* = 0.02, time: *P* = 0.22, intervention *P* = 0.54), *Figure* 3C].

Integrated muscle protein synthesis, fractional growth and breakdown rates

Over the study period, 4 day integrated MPS was decreased in the immobilized vs. the control leg [control: 1.55 ± 0.21% day^{-1}, immob: 1.29 ± 0.17% day^{-1}, ($P < 0.01$
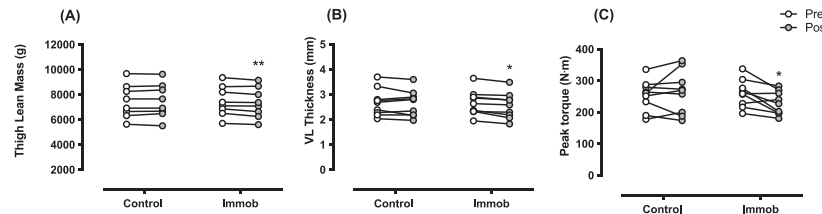
Figure 3 Thigh lean mass (*A*), vastus lateralis (VL) muscle thickness (*B*), and maximal voluntary isometric contraction torque (*C*) of the control and immobilized (immob) leg pre and post 4 days of single leg immobilization in health young men. **P < 0.01, *P < 0.05.
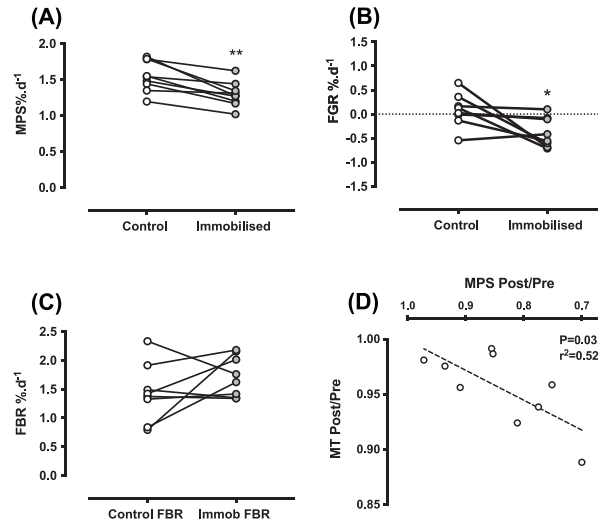
Figure 4 Over the 4 day study period in control and immobilized legs (*A*) muscle protein synthesis in % day^{-1}, (*B*) fractional growth rate in % day^{-1}, (*C*) fractional breakdown rate in % day^{-1}, and (*D*) correlation between the change in MPS and change in VL MT. **P < 0.01, *P < 0.05.

d = 1.35), *Figure* 4A]. Similarly, the FGR was decreased in the immobilized leg [control: 0.08 ± 0.34% day^{-1}, immob: −0.38 ± 0.31% day^{-1}, (*P* < 0.05, *d* = 0.77) *Figure* 4B], while the FBR remained unchanged [control: 1.44 ± 0.51% day^{-1}, immob: 1.73 ± 0.35% day^{-1}, (*P* = 0.21 *d* = 0.39), *Figure* 4C]. The change in MT was correlated with the change in MPS (*P* = 0.03, r^2 = 0.52, *Figure* 4D) and was not correlated with the change in FBR (*P* = 0.17, r^2 = 0.29, not shown).

Acute muscle protein turnover

After 4 days of immobilization, there was an overall trend for decreased MPS, yet fasted and fed rates of acute MPS re-

mained unchanged (*Figure* 5A) (main effect of interaction: *P* = 0.53, time: *P* = 0.008, intervention *P* = 0.07). However, only the control leg increased MPS in response to feeding [fasted: 0.043 ± 0.012% h^{-1}, fed: 0.065 ± 0.017% h^{-1}, (*P* < 0.05, *d* = 1.38)] with no change in the immobilized leg [fasted: 0.034 ± 0.014% h^{-1}, fed: 0.049 ± 0.023% h^{-1} (*P* = 0.09, *d* = 0.90) *Figure* 5A]. The absolute decrease in integrated or acute MPS was similar [integrated: −0.25 ± 0.16% day^{-1}, acute: −0.26 ± 0.38% day^{-1} (assuming two-thirds of the day is spent fasted and one-third fed) (*d* = 0.004), *Figure* 5B]. The acute fasted tracer decay rate representing MPB did not differ between control and immobilization legs [control: 0.02 ± 0.006, immob: 0.015 ± 0.015, (*d* = 0.89) *Figure* 5C]. The change in MPS was not correlated
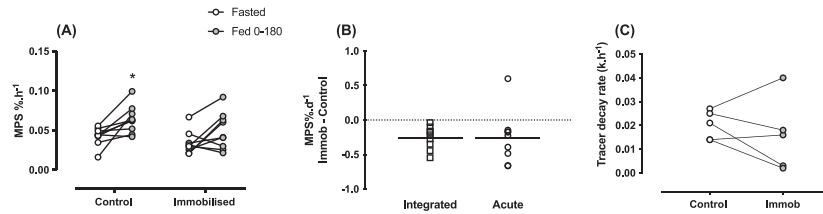
Figure 5 (*A*) Acute fasted and fed MPS rates in % h^{-1} in control and immobilized legs. (*B*) The absolute change in integrated or acute muscle protein synthesis in % day^{-1} (assuming two-thirds of the day is spent fasted and one-third fed). (*C*) Acute fasted tracer decay rate (k h^{-1} value). *$P < 0.05$.
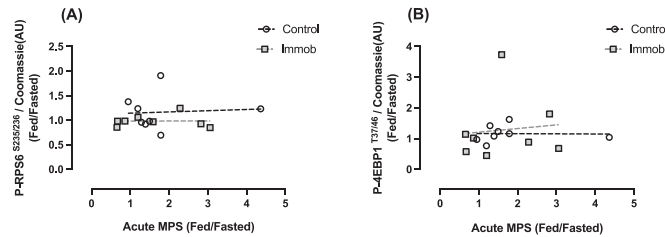
Figure 6 Correlation between change in fasted to fed muscle protein synthesis vs. (*A*) change in fasted to fed p-rpS6 and (*B*) change in in fasted to fed p-4E-BP1.

with either the change in rpS6 or 4E-BP1 phosphorylation from fasted to fed states (*Figure* 6A,B). Overall, both anabolic and catabolic markers were similar between control and immob, with no effect of immobilization on markers of MPB (*Table* 1) (*Figure* 7).

Discussion

Muscle disuse through lifestyle changes, injury, illness, or short-term hospitalization results in loss of skeletal muscle mass and strength.[2,3,26] This muscle wasting is particularly evident with long-term immobilization,[27] yet there is growing evidence that muscle mass loss proceeds most rapidly during the early stages of disuse.[4,28] Substantial muscle wasting occurs after 4 days of immobilization,[29] likely having critical consequences for many individuals undergoing short-term inactivity through acute hospitalization [~4.5 days (Source: NHS HES 2018–2019)] or illness (~3 days[7]). On this basis, it has been speculated that repeated short-term periods of immobilization may accelerate an older individual's trajectory to frailty.[30] Nevertheless, the proteostasis underpinnings of human disuse muscle atrophy and strength declines remain unclear, leaving us without effective countermeasures. Here, we discovered that reduction in muscle size and strength follow-

ing 4 days of immobilization was driven by declines in MPS and no change in D$_2$O-derived FBR. In addition, declines in MT correlated with change in MPS but not FBR. Feeding-induced hyperaminoacidemia showed a main effect of feeding with no significant interaction. However, there was a more robust and expected stimulation of MPS in the control leg, that was ablated in the immobilized leg, highlighting anabolic resistance as key element in muscle disuse atrophy. Finally, we observed no change in acute tracer decay, representative of MPB, or intracellular markers of MPB. Our results point to the prominent role of declines in MPS and not elevated proteolysis as the dominant mechanism of early muscle disuse atrophy.

There are numerous models of human muscle disuse atrophy (e.g. bed rest, casting, unilateral lower-limb suspension) that vary in mobility restrictions and clinical relevance, yet they all share common outcomes of decreased muscle mass and strength.[5] For instance, reductions in strength of 9% have been reported with 5 days of leg casting[4] and 25% with 14 days of unilateral lower-limb suspension.[10] Here, we report losses of ~11% in just 4 days, adding to previous literature of rapid losses of muscle strength.[29] Loss of strength is accompanied by muscle mass declines, with losses in muscle volume of 1.7% by 2 days and 6.7% by 7 days reported via MRI.[28] In addition to muscle wasting varying across individual muscles,[6] the extent of atrophy likely depends on the method

Table 1 Muscle anabolic and catabolic signalling in control and immobilized legs

		Fasted	Fed	
P-mTOR^{S2448}	C	0.60 ± 0.45	0.61 ± 0.24	Time = 0.89
	I	0.56 ± 0.48	0.52 ± 0.26	Intervention = 0.69
				Interaction = 0.84
P-4EBP1$^{T37/46}$	C	0.67 ± 0.21	0.72 ± 0.17	Time = 0.73
	I	0.84 ± 0.29	0.84 ± 0.24	Intervention = 0.09
				Interaction = 0.54
P-AKT^{S473}	C	0.67 ± 0.21	1.02 ± 0.48	Time = 0.006
	I	0.60 ± 0.21	1.12 ± 0.59*	Intervention = 0.94
				Interaction = 0.56
P-RPS6$^{S235/236}$	C	0.52 ± 0.60	1.78 ± 0.52*	Time = 0.001
	I	0.57 ± 0.47	1.62 ± 0.96*	Intervention = 0.81
				Interaction = 0.77
P-eIF4E^{S209}	C	0.66 ± 0.27	0.66 ± 0.22	Time = 0.21
	I	0.78 ± 0.28	0.59 ± 0.19	Intervention = 0.85
				Interaction = 0.15
P-eIF4B^{S422}	C	0.69 ± 0.13	0.88 ± 0.42	Time = 0.05
	I	0.59 ± 0.28	0.77 ± 0.36	Intervention = 0.46
				Interaction = 0.88
P-eEF2^{T56}	C	0.68 ± 0.17	0.65 ± 0.16	Time = 0.88
	I	0.66 ± 0.12	0.71 ± 0.11	Tntervention = 0.76
				Interaction = 0.36
Calpain 1	C	0.69 ± 0.12	0.74 ± 0.11	Time = 0.52
	I	0.78 ± 0.10	0.77 ± 0.09	Intervention = 0.17
				Interaction = 0.30
MAFbx	C	0.63 ± 0.36	0.76 ± 0.23	Time = 0.45
	I	0.74 ± 0.43	0.72 ± 0.32	Intervention = 0.83
				Interaction = 0.28
Ubiquitin	C	0.69 ± 0.09	0.76 ± 0.16	Time = 0.92
	I	0.70 ± 0.08	0.64 ± 0.09	Intervention = 0.20
				Interaction = 0.15

Data were normalized to control mean and transformed using $Y = (\log(1 + Y))$.
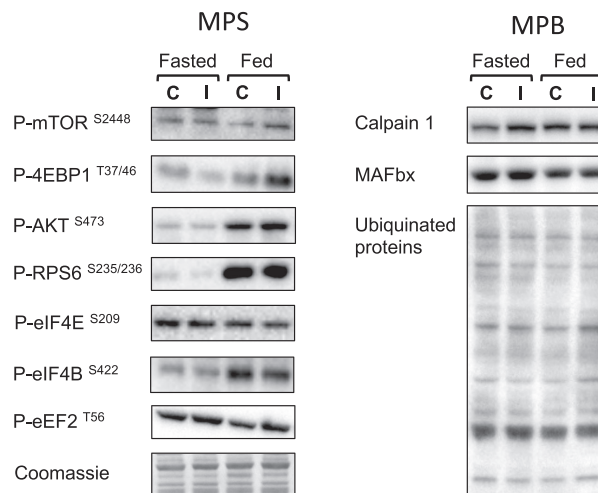*$P < 0.05$.

Figure 7 Representative immunoblots for muscle signalling pathway activity.

of assessment and immobilization model used.[5] For instance, while ~10% declines in fibre cross-sectional area (CSA) were reported after 4 days of knee-bracing,[29] 5 days of leg-casting showed no measurable decline in fibre CSA, despite ~3.5% decreases in whole muscle CSA.[4] In the present study, using independent measurement techniques, we show significant declines in DXA derived thigh lean mass loss of ~1.7% which correlated with significant declines in VL MT of ~4%. Our data therefore agree with previous literature highlighting that muscle mass loss occurs rapidly at the onset of immobilization. Further, these results support the use of ultrasound as an indicator of muscle size[31] at least in healthy individuals; the reduced invasiveness and cost offering a potential tool to increase measurement frequency during early atrophy.

Muscle mass is controlled by the balance between MPS and MPB. Earlier studies of MPS during immobilization utilized AA tracers representing the gold standard in assessing acute fasted-state MPS and/or MPS responses to external stimuli (nutrition/inactivity etc.). These studies revealed that immobilization results in declines in both fasted and fed-state MPS, that is, inducing a state of 'anabolic resistance'.[9,10,32] Despite calculations from these studies suggesting that declines in muscle mass may be entirely explained by declines in MPS,[10] the very nature of acute intravenous AA tracer studies means they provide only a 'snapshot' of proteostasis.[33] In contrast, the use of oral D_2O provides an effective tool to quantify integrated MPS, capturing anabolic responses over the entire measurement period.[34,35] Here, we combined integrated D_2O MPS measures along acute AA tracer approaches to capture both early changes in integrated MPS and acute feeding responses. We show that MPS is sustainably depressed over 4 days of immobilization and that this was correlated with loss of VL MT. Similarly, declines in MPS over 7 days of immobilization correlated with declines in quadriceps muscle volume determined by MRI. Together, these results provide good evidence that declines in MPS dominate the muscle atrophy process. Previous similar integrated measures of MPS have shown substantial declines over 14 and 7 days of immobilization,[28,35] with no significant changes over 2 days.[28] As such, we have shown the earliest declines in integrated MPS to date. Further, we show that by Day 4, this is primarily a result of impaired feeding responses and thus reduced MPS in both the fasted and fed states (also the earliest observation of immobilization induced anabolic resistance albeit congruent with longer term results). Intriguingly, we also estimated similar declines in daily integrated MPS from both our D_2O measures and our daily acute MPS when assuming that post-absorptive periods represent two-thirds of a diurnal cycle. These findings further substantiate that MPS alone can explain declines in muscle mass, in the absence of rises in 'bulk' MPB.

Increased markers of MPB during the early stages of immobilization have resulted in MPB having a proposed role in early disuse atrophy.[16,36] Previously, A-V balance techniques showed no difference in whole-body protein breakdown after 2 weeks of immobilization.[15] Another study showed that with 21 days of bed rest, there was no increase in MPB.[37] In contrast, indirect indicators of contractile protein breakdown (3-methylhistidine) have been shown to be elevated during the early stages of immobilization (3 days)[38]; however, the validity of this result has been questioned[39] given e.g. non-skeletal muscle sources of 3-methylhistidine. More recently, MPB was determined to be lower during a period of immobilization vs. re-training,[40] yet this study was not designed to compare with a control period, limiting conclusions that may be drawn. In contrast to measures of dynamic MPB, increased markers of MPB early with immobilization have been reported, most noticeably, those of ubiquitin proteasome pathway (e.g. MAFbx). However, eIF3f, a key initiation factor in protein synthesis, is a major target for MAFbx and subsequent degradation.[41] As such, we posit that increased markers of MPB act to degrade key components of the protein synthetic machinery rather than bulk myofibrillar contractile elements. To determine the role of bulk MPB in muscle atrophy, we adopted a pulse-chase tracer technique to assess dynamic rates of MPB[14] in addition to applying robust extrapolations from the D_2O tracer. Firstly, we found no differences in the rate of tracer decay between the immobilized vs. the control leg over 60 min in the fasted state, indicating MPB was not increased in the immobilized leg. Secondly, to assimilate MPB over the 4 day period, we combined rates of MPS with the net change in muscle mass per day (FGR) to calculate FBR. With the difficulties in accurately measuring FBR during atrophy/hypertrophy, these equations have shown to provide an accurate estimation of FBR in response to various interventions.[20,42,43] Using these validated equations, we observed no increases in FBR during immobilization. Furthermore, changes in FBR did not correlate with declines in muscle mass, with no change in the expression of key markers of MPB. For that reason, our data fully support MPB having a minimal role in driving immobilization induced human muscle atrophy.

Accompanying dynamic measures of MPS and MPB, we quantified the phosphorylation and abundance of proteins involved in proteostasis. Despite decreased cumulative MPS, owing to deficits in fed (and perhaps fasted) state MPS, anabolic responses to feeding (P-AKT^{S473} and P-RPS6$^{S235/236}$) were not reduced with immobilization. A lack of alignment between muscle anabolic signalling and fractional synthesis rate has been reported previously.[44,45] While providing valuable mechanistic insight, these measures represent a snapshot of intramuscular signalling, with peak responses likely occurring earlier in the feeding response.[44] Furthermore, these samples were collected under a glucose clamp, with insulin signalling potentially swamping any effects of AA.[46] Finally, we measured proteins that play a key role in both calcium activated and ubiquitin proteasome MPB pathways;

agreeing with our measures showing a lack of increase in FBR or MPB, we observed no clear induction of intracellular signalling markers of MPB.

While adding novel insights into the effects of immobilization on muscle protein turnover at the onset of immobilization induced muscle atrophy, our study is not without limitations. With the paucity of data on rates of MPB in early immobilization, we calculated study power on previous reports of declines in post-prandial MPS.[17] Expectedly, we found consistent and robust declines in MPS, and using balance equations, we showed no change in FBR, despite a heightened numerical average over 4 days (notably, such calculations rely on accurate scan-to-scan measures over a short study period and utilize whole changes in TFFM resulting in increased variability). Given limitations of retrospective power calculations,[47] we also report that effect sizes are far stronger for declines in MPS than in supporting any increase in FBR. Further supporting these data, we measured tracer decay rates within the VL, again, showing no change in MPB (although these dynamic measures of MPB were only performed at a single time point in the fasted stated and limited by subject number). Finally, we found only MPS and not FBR correlated with VL MT declines, with similar correlations having been independently reported by others.[28]

In conclusion, short-term immobilization results in significant loss of skeletal muscle mass that is driven by, and which correlates with sustained declines in MPS. A lack of increase in acute tracer decay, markers of MPB, and calculated FBR suggest that bulk MPB has a minor, if any, role at the onset of leg immobilization induced muscle atrophy in humans; a time at which muscle is rapidly lost. We also demonstrate in agreement to previous work that decreased integrated MPS is accompanied by a rapid blunting of acute anabolic responses to hyperaminoacidemia and hyperinsulinemia, with acute fasted/fed MPS reflective of declines in 4 day integrated MPS. As such, we contend the development of effective 'anti-catabolic' therapeutics should be targeted at enhancing basal MPS and anabolic responses to feeding.

Conflict of interest

None declared

References

1. Brook MS, Wilkinson DJ, Phillips BE, Perez-Schindler J, Philp A, Smith K, et al. Skeletal muscle homeostasis and plasticity in youth and ageing: impact of nutrition and exercise. *Acta Physiol* 2016;**216**:15–41.
2. Puthucheary ZA, Rawal J, Mcphail M, Connolly B, Ratnayake G, Chan P, et al. Acute skeletal muscle wasting in critical illness. *JAMA* 2013;**310**:1–10.
3. Kouw IWK, Groen BBL, Smeets JSJ, Kramer IF, van Kranenburg JMX, Nilwik R, et al. One week of hospitalization following elective hip surgery induces substantial muscle atrophy in older patients. *J Am Med Dir Assoc* 2019;**20**:35–42.
4. Wall BT, Dirks ML, Snijders T, Senden JMGG, Dolmans J, van Loon LJCC. Substantial skeletal muscle loss occurs during only 5 days of disuse. *Acta Physiol (Oxf)* 2014;**210**:600–611.
5. Rudrappa SS, Wilkinson DJ, Greenhaff PL, Smith K, Idris I, Atherton PJ. Human skeletal muscle disuse atrophy: effects on muscle protein synthesis, breakdown, and insulin resistance—a qualitative review. *Front Physiol* 2016;**7**:1–10.
6. Kilroe SP, Fulford J, Jackman SR, van Loon LJC, Wall BT. Temporal muscle-specific disuse atrophy during one week of leg immobilization. *Med Sci Sports Exerc* 2020;**52**:944–954.
7. Fragaszy EB, Warren-Gash C, White PJ, Zambon M, Edmunds WJ, Nguyen-Van-Tam JS, et al. Effects of seasonal and pandemic influenza on health-related quality of life, work and school absence in England: results from the Flu Watch cohort study. *In-fluenza Other Respi Viruses* 2018;**12**:171–182.
8. Phillips SM, McGlory C. CrossTalk proposal: the dominant mechanism causing disuse muscle atrophy is decreased protein synthesis. *J Physiol* 2014;**592**:5341–5343.
9. Glover EI, Phillips SM, Oates BR, Tang JE, Tarnopolsky MA, Selby A, et al. Immobilization induces anabolic resistance in human myofibrillar protein synthesis with low and high dose amino acid infusion. *J Physiol* 2008;**586**:6049–6061.
10. de Boer MD, Selby A, Atherton P, Smith K, Seynnes OR, Maganaris CN, et al. The temporal responses of protein synthesis, gene expression and cell signalling in human quadriceps muscle and patellar tendon to disuse. *J Physiol* 2007;**585**:241–251.

11. Willis CRG, Gallagher IJ, Wilkinson DJ, Brook MS, Bass JJ, Phillips BE, et al. Transcriptomic links to muscle mass loss and declines in cumulative muscle protein synthesis during short-term disuse in healthy younger humans. *FASEB J* 2021; **35**:e21830.

12. Drummond MJ, Dickinson JM, Fry CS, Walker DK, Gundermann DM, Reidy PT, et al. Bed rest impairs skeletal muscle amino acid transporter expression, mTORC1 signaling, and protein synthesis in response to essential amino acids in older adults. *Am J Physiol Endocrinol Metab* 2012;**302**:E1113–E1122.

13. Wilkinson DJ, Brook MS, Smith K, Atherton PJ. Stable isotope tracers and exercise physiology: past, present and future. *J Physiol* 2016;**1**:1–10.

14. Zhang XJ, Chinkes DL, Sakurai Y, Wolfe RR. An isotopic method for measurement of muscle protein fractional breakdown rate in vivo. *Am J Physiol* 1996;**270**: E759–E767.

15. Ferrando AA, Lane HW, Stuart CA, Davis-Street J, Wolfe RR. Prolonged bed rest decreases skeletal muscle and whole body protein synthesis. *Am J Physiol* 1996;**270**: E627–E633.

16. Gustafsson T, Osterlund T, Flanagan JN, Von Waldén F, Trappe TA, Linnehan RM, et al. Effects of 3 days unloading on molecular regulators of muscle size in humans. *J Appl Physiol* 2010;**109**:721–727.

17. Wall BT, Dirks ML, Snijders T, van Dijk J-W, Fritsch M, Verdijk LB, et al. Short-term muscle disuse lowers myofibrillar protein synthesis rates and induces anabolic resistance to protein ingestion. *Am J Physiol Endocrinol Metab* 2016;**310**:E137–E147.

18. DeFronzo RA, Tobin JD, Andres R. Glucose clamp technique: a method for quantifying insulin secretion and resistance. *Am J Physiol* 1979;**237**:E214–E223.

19. Wilkinson DJ, Franchi MV, Brook MS, Narici MV, Williams JP, Mitchell WK, et al. A validation of the application of D₂O stable isotope tracer techniques for monitoring day-to-day changes in muscle protein subfraction synthesis in humans. *Am J Physiol Endocrinol Metab* 2014;**306**: E571–E579.

20. Gharahdaghi N, Rudrappa S, Brook MS, Idris I, Crossland H, Hamrock C, et al. Testosterone therapy induces molecular programming augmenting physiological adaptations to resistance exercise in older men. *J Cachexia Sarcopenia Muscle* 2019; **10**:1276–1294.

21. Bukhari SSI, Phillips BE, Wilkinson DJ, Limb MC, Rankin D, Mitchell WK, et al. Intake of low-dose leucine-rich essential amino acids stimulates muscle anabolism equivalently to bolus whey protein in older women at rest and after exercise. *Am J Physiol Endocrinol Metab* 2015;**308**:E1056–E1065.

22. Sheffield-Moore M, Dillon EL, Randolph KM, Casperson SL, White GR, Jennings K, et al. Isotopic decay of urinary or plasma 3-methylhistidine as a potential biomarker of pathologic skeletal muscle loss. *J Cachexia Sarcopenia Muscle* 2014;**5**:19–25.

23. Holm L, ORourke B, Ebenstein D, Toth MJ, Bechshoeft R, Holstein-Rathlou N-H, et al. Determination of steady-state protein breakdown rate in vivo by the disappearance of protein-bound tracer-labeled amino acids: a method applicable in humans. *Am J Physiol Endocrinol Metab* 2013;**304**:E895–E907.

24. Zhang X-J, Chinkes DL, Wolfe RR. Measurement of muscle protein fractional synthesis and breakdown rates from a pulse tracer injection. *Am J Physiol Endocrinol Metab* 2002;**283**:E753–E764.

25. Atherton PJ, Smith K, Etheridge T, Rankin D, Rennie MJ. Distinct anabolic signalling responses to amino acids in C2C12 skeletal muscle cells. *Amino Acids* 2010;**38**: 1533–1539.

26. Breen L, Stokes KA, Churchward-Venne TA, Moore DR, Baker SK, Smith K, et al. Two weeks of reduced activity decreases leg lean mass and induces 'anabolic resistance' of myofibrillar protein synthesis in healthy elderly. *J Clin Endocrinol Metab* 2013;**98**: 2604–2612.

27. Trappe TA, Burd NA, Louis ES, Lee GA, Trappe SW. Influence of concurrent exercise or nutrition countermeasures on thigh and calf muscle size and function during 60 days of bed rest in women. *Acta Physiol* 2007;**191**:147–159.

28. Kilroe SP, Fulford J, Holwerda AM, Jackman SR, Lee BP, Gijsen AP, et al. Short-term muscle disuse induces a rapid and sustained decline in daily myofibrillar protein synthesis rates. *Am J Physiol Endocrinol Metab* 2020;**318**: E117–E130.

29. Suetta C, Frandsen U, Jensen L, Jensen MM, Jespersen JG, Hvid LG, et al. Aging affects the transcriptional regulation of human skeletal muscle disuse atrophy. *PLoS One* 2012;**7**:e51238.

30. Oikawa SY, Holloway TM, Phillips SM. The impact of step reduction on muscle health in aging: protein and exercise as countermeasures. *Front Nutr* 2019;**6**:1–11.

31. Franchi MV, Longo S, Mallinson J, Quinlan JI, Taylor T, Greenhaff PL, et al. Muscle thickness correlates to muscle cross-sectional area in the assessment of strength training-induced hypertrophy. *Scand J Med Sci Sports* 2018;**28**:846–853.

32. Wall BT, Snijders T, Senden JMGG, Ottenbros CLPP, Gijsen AP, Verdijk LB, et al. Disuse impairs the muscle protein synthetic response to protein ingestion in healthy men. *J Clin Endocrinol Metab* 2013;**98**:4872–4881.

33. Atherton PJ, Miller BF, a BN, Macnaughton LS, Murton AJ, Camera DM, et al. Commentaries on viewpoint: what is the relationship between acute measure of muscle protein synthesis and changes in muscle mass? *J Appl Physiol* 2015;**118**:498–503.

34. Brook M, Wilkinson D, Mitchell W, Lund J, Szewczyk NJ, Greenhaff P, et al. Skeletal muscle hypertrophy is most active during early resistance exercise training responses, matching long term

deuterium oxide (D₂O)-derived measures of muscle protein synthesis and mTORc1-signaling. *FASEB J* 2015;**29**: 4485–4496.

35. Mcglory C, Gorissen SHM, Kamal M, Bahniwal R, Hector AJ, Baker SK, et al. Omega-3 fatty acid supplementation attenuates skeletal muscle disuse atrophy during two weeks of unilateral leg immobilization in healthy young women. *FASEB J* 2019;**33**:4586–4597.

36. Urso ML, Scrimgeour AG, Chen YW, Thompson PD, Clarkson PM. Analysis of human skeletal muscle after 48 h immobilization reveals alterations in mRNA and protein for extracellular matrix components. *J Appl Physiol* 2006;**101**: 1136–1148.

37. Symons TB, Sheffield-Moore M, Chinkes DL, Ferrando AA, Paddon-Jones D. Artificial gravity maintains skeletal muscle protein synthesis during 21 days of simulated microgravity. *J Appl Physiol* 2009; **107**:34–38.

38. Tesch PA, Von Walden F, Gustafsson T, Linnehan RM, Trappe TA. Skeletal muscle proteolysis in response to short-term unloading in humans. *J Appl Physiol* 2008; **105**:902–906.

39. Rennie MJ, Phillips S, Smith K. Reliability of results and interpretation of measures of 3-methylhistidine in muscle interstitium as marker of muscle proteolysis. *J Appl Physiol* 2008;**105**:1380–1381.

40. Dideriksen K, Reitelseder S, Agergaard J, Boesen AP, Aas SN, Raastad T, et al. Muscle protein breakdown is impaired during immobilization compared to during a subsequent retraining period in older men: no effect of anti-inflammatory medication. *Pflugers Arch Eur J Physiol* 2020;**472**: 281–292.

41. Lagirand-Cantaloube J, Offner N, Csibi A, Leibovitch MP, Batonnet-Pichon S, Tintignac LA, et al. The initiation factor eIF3-f is a major target for atrogin1/MAFbx function in skeletal muscle atrophy. *EMBO J* 2008;**27**:1266–1276.

42. Garlick PJ, Millward DJ, James WP, Waterlow JC. The effect of protein deprivation and starvation on the rate of protein synthesis in tissues of the rat. *Biochim Biophys Acta* 1975;**414**: 71–84.

43. Hector AJ, McGlory C, Damas F, Mazara N, Baker SK, Phillips SM. Pronounced energy restriction with elevated protein intake results in no change in proteolysis and reductions in skeletal muscle protein synthesis that are mitigated by resistance exercise. *FASEB J* 2018;**32**:265–275.

44. Atherton PJ, Etheridge T, Watt PW, Wilkinson D, Selby A, Rankin D, et al. Muscle full effect after oral protein: time-dependent concordance and discordance between human muscle protein synthesis and mTORC1. *Am J Clin Nutr* 2010;**92**: 1080–1088.

45. Greenhaff PL, Karagounis LG, Peirce N, Simpson EJ, Hazell M, Layfield R, et al. Disassociation between the effects of amino acids and insulin on signaling, ubiquitin li-

103

gases, and protein turnover in human muscle. *Am J Physiol Endocrinol Metab* 2008; **295**:E595–E604.

46. Glynn EL, Fry CS, Timmerman KL, Drummond MJ, Volpi E, Rasmussen BB. Addition of carbohydrate or alanine to an essential amino acid mixture does not enhance human skeletal muscle protein anabolism. *J Nutr* 2013;**143**:307–314.

47. Walters SJ. Consultants forum: should post hoc sample size calculations be done? *Pharm Stat* 2009;**8**:163–169.

48. von Haehling S, Morley JE, Coats AJS, Anker SD. Ethical guidelines for publishing in the journal of cachexia, sarcopenia and muscle: update 2021. *J Cachexia Sarcopenia Muscle* 2021;**12**: 2259–2261.

CHAPTER 5:

GENERAL DISCUSSION

5.1 Introduction

Skeletal muscle is a plastic tissue capable of adapting to perturbations in its contractile and nutritional environment through alterations in both size and function.[141] These adaptations influence glycemia, amino acid homeostasis, and the ability to perform activities of daily living;[142] therefore, understanding the mechanisms regulating muscle remodelling is clinically important. To that end, the present thesis sought to characterize important molecular events that are influenced by and potentially drive loading- and unloading-induced changes in muscle size. We developed and validated a novel unilateral model in which one leg was subjected to RE to induce hypertrophy (Hyp) and the contralateral limb was immobilized to induce atrophy (At). In study 1, we characterized the morphological changes induced by our HypAt model and validated the use of ultrasonography to measure changes in muscle size in both limbs. We discovered that by assessing the differential change in muscle size between legs we reduced the coefficient of variation between subjects. This enabled a more in-depth means-based characterization of the molecular regulators of skeletal muscle remodelling in study 2. We also identified a transcriptional signature that scaled with lean mass gains in three independent cohorts and included RNA species that were only modulated at their untranslated regions. Finally, in study 3, we addressed a long-standing question regarding the mechanisms of muscle disuse atrophy by demonstrating no significant change in MPB in the first few days of muscle unloading. In the discussion that follows, the primary findings of each study will be elaborated on in the context of prior research, and the strengths, weaknesses, and avenues for future research will be explored.

5.2. Measuring changes in skeletal muscle size

Three general conditions must be met to advance our understanding of the mechanisms regulating muscle growth and atrophy. First, changes in muscle size must be accurately measured. Second, the technique employed to measure muscle size should be affordable, easy to use, and accessible so that results obtained from different laboratories can be interpreted relative to each other. This condition is also important for overcoming the limitation of small sample sizes in individual studies by enabling meta-analysis of gene expression data.[131] Third, assessing the purported regulators of muscle remodelling with high accuracy is required. In study 1, we developed an ultrasound method for measuring changes in muscle size following loading and unloading that, we believe, satisfies conditions 1 and 2, with certain caveats. In study 2, we accomplished the third objective by implementing the within-subjects model from study 1 with a pre-processing pipeline that enabled the profiling of the muscle transcriptional response to loading and unloading with high fidelity.

MRI and CT are considered the gold-standard methods for assessing changes in muscle size because both offer unparalleled tissue differentiation capabilities.[135] However, both have high operating costs, require skilled technicians to conduct analyses, and, in the case of CT, result in exposure to ionizing radiation. These factors limit the routine use of MRI and CT in physiological research. In contrast, many research laboratories are equipped with DXA units that are comparatively easier to operate and have lower per-scan operating costs. However, DXA also exposes participants to ionizing radiation, albeit low-dose, and, perhaps of greater importance, does not directly measure

skeletal muscle mass.[143] In many respects, ultrasonography (US) has advantages over DXA, MRI, and CT. Primarily, US does not emit ionizing radiation, rendering it safe for implementation in longitudinal research studies involving multiple assessments. Furthermore, US is cheap, relatively easy to use, and is highly portable. Indeed, point-of-care US units now plug directly into mobile phones and show promise as screening tools for sarcopenia in clinical settings.[144] Additionally, US also enables the non-invasive quantification of architectural parameters, including fascicle length and pennation angle, thus offering a more nuanced understanding of skeletal muscle remodelling.[140] Together, these characteristics position ultrasonography as a potentially viable alternative to DXA, MRI, and CT for scalable analysis of skeletal muscle hypertrophy and atrophy.

Numerous investigations have demonstrated ultrasound's cross-sectional (i.e., single time point) validity in various populations. Indeed, US-derived measurements of muscle thickness and/or CSA are valid when compared to DXA-derived lean body mass assessments in older adults,[145] different array/transducer combinations in COPD patients,[146] MRI-derived quadriceps CSA in healthy older and younger adults,[139,147,148] and CT-derived quadriceps CSA in trained and untrained older women.[149] In study 1, we confirmed the utility of US by demonstrating high concordance between US- and MRI-derived measurements of VL CSA in young adult men at pre- and post-loading and unloading time points. However, it is arguably more important from a clinical standpoint to measure changes in muscle mass rather than at single point-in-time assessments. For example, Rutten and colleagues demonstrated that *loss* of skeletal muscle in cancer patients treated with chemotherapy is prognostic for overall survival whereas single time

point measurements are not.[150] Furthermore, Puthucheary and colleagues showed a correlation between the degree of *rectus femoris* atrophy and the extent of organ failure and length of stay in ICU patients.[151] Relevant to the present thesis, valid techniques to assess changes in muscle size are required to test the effectiveness of nutritional and/or loading interventions in the context of slowing muscle loss during disuse or aging. Taken together, US has been extensively validated against criterion techniques at single-time points; however, few studies have evaluated the ability of US to detect changes in muscle size with loading and unloading.

5.2.1 Resistance exercise-induced changes in muscle size

Prior to the present thesis, few studies have quantified the validity of US-derived changes in muscle size in response to RT against the current gold standard, MRI. Ahtiainen *et al.,* studied a cohort of young men before and after 21 weeks of RT and found excellent agreement between VL CSA measurements obtained from panoramic US and MRI and high intra-day repeatability (ICC=0.997).[152] However, the authors showed consistently lower VL CSA values compared to MRI, which is probably related to a difficulty in maintaining constant and minimal probe pressure during longitudinal scanning using panoramic US.[140] Indeed, we demonstrated a subtle yet significant influence of probe pressure on measurements of muscle size in study 1, such that minimal changes in applied force led to significant differences in pre- and post-loading comparisons. Thus, despite the high concordance between panoramic US and MRI, operator training may impede its widespread use without skilled operator training.[153,154]

Using a simpler approach, Franchi and colleagues observed a significant correlation between US-derived changes in *vastus lateralis* MT and VL CSA measured by MRI in healthy young men who completed 12 weeks of knee-extensor RT.[139] However, they did not detect a relationship between changes in muscle volume obtained by MRI and MT measurements.[139] In study 1, we hypothesized that a two-dimensional US image (i.e., VL CSA) would more closely align with MRI-derived muscle volume than unidimensional thickness measurements. However, despite observing a significant relationship between changes in VL CSA measured using US and MRI, we did not detect a significant relationship between RT-induced changes in muscle volume and US-derived changes in VL CSA. Thus, data from study 1 and Dr. Franchi's laboratory[139] collectively suggest that while US is suitable for measuring changes in muscle CSA at the mid-thigh in response to RT, more images may be required to accurately capture changes in muscle volume.

5.2.2 Muscle disuse-induced changes in muscle size

In contrast with RT studies, no research has been conducted assessing the validity of US for measuring changes in muscle size that occur in response to immobilization. Using panoramic US, Scott and colleagues demonstrated close agreement between US and MRI for measuring changes in quadriceps and gastrocnemius CSA in response to bed rest.[155,156] Furthermore, the authors calculated muscle volume by taking several images of the quadriceps along the thigh and observed high concordance with MRI-derived measurements.[155,156] Nonetheless, the authors used custom-designed templates that ensured alignment of the probe during continuous scanning. Without templates, it would

be likely be difficult to maintain constant pressure on the probe and perpendicular alignment throughout the scanning process, resulting in image artifacts. In study 1, we demonstrated a significant relationship and close agreement between US- and MRI-derived measurements of VL CSA atrophy when measured at the mid-thigh. Importantly, we are also the first to demonstrate a significant relationship between US-derived changes in VL CSA and muscle volume changes measured by MRI. These data suggest that small field-of-view ultrasound units can be a suitable alternative to MRI for measuring changes in VL CSA and providing estimates of muscle volume changes induced by muscle unloading. These data also suggest that, in contrast to muscle hypertrophy, muscle atrophy is more homogenous along the length of the muscle.

5.2.3 Future directions

In study 1, we did not observe a significant relationship between RT-induced changes in muscle volume measured by MRI and US-derived changes in VL CSA. This lack of relationship suggests that the *vastus lateralis* may hypertrophy unevenly along its length in response to RT, as observed in previous reports.[157-159] Therefore, to obtain a more representative measurement of VL muscle volume using US, multiple images could be obtained along the length of the VL muscle and integrated using the Cavalieri principle to estimate muscle volume.[160,161] Scott and colleagues used this approach and observed high concordance between panoramic US- and MRI-derived changes in muscle volume following a period of bed rest.[156] However, ~8 custom-made templates were constructed to fit around each participant's leg to guide the ultrasound probe throughout the measurement and total scanning time lasted ~40 minutes per leg. Such a long image

acquisition period may be burdensome when multiple other time-sensitive outcome measurements are included in addition to US. Therefore, future work should investigate whether fewer images could be obtained along the length of the thigh – using the image stitching technique we employed – to obtain accurate measurements of muscle volume.

Study 1 was also limited by the homogeneous population studied – i.e., healthy young men. In general, young men have low intramuscular and subcutaneous adipose tissue depots, allowing for easy identification of superficial and deep aponeuroses and the outline of the *vastus lateralis* muscle belly. The infiltration of adipose tissue into skeletal muscle – which occurs in insulin-resistant,[162] obese,[163] and aging[164] individuals – may obscure these borders, thereby reducing the concordance between US- and MRI-derived changes in muscle mass. This discordance is an important knowledge gap considering that many nutritional and exercise interventions target such populations for potential therapeutic benefit; thus, future work should assess the suitability for measuring changes in muscle size in populations with significant adipose tissue infiltration.

Finally, more work is needed to assess whether US can accurately detect changes in muscle size in response to short-term muscle unloading. In study 3, we identified a significant reduction in muscle thickness following 4 days of immobilization that was quantitatively linked with the reduction in integrated MPS. However, no study has compared US-derived changes in VL CSA or muscle thickness to a reference method such as MRI or CT within the first few days of unloading. Changes in muscle size occur rapidly upon onset of disuse,[19] but it is unclear whether the US method we employed in study 1 is sensitive enough to detect these changes with comparable accuracy as the MRI.

Using the approach we developed, the minimal detectable change in VL CSA was ~2.15 cm^2, implying that smaller changes would be difficult to accurately detect using US; however, added resolution may be gained if more images are acquired and analyzed.

Taken together, in study 1 we developed and validated a within-subjects model of loading and unloading. Importantly, we also showed that muscle mass was unaltered in the free-living limb at week 8, prior to immobilization. This was an important finding because if the unilateral RT intervention influenced muscle mass in the contralateral limb prior to immobilization, it would have confounded the measurement of muscle atrophy and thus downstream molecular analyses in study 2. The lack of crossover effect we observed is consistent with previous reports demonstrating that while myofibre CSA,[30,71] thigh lean mass,[79,165] muscle thickness,[79,165] and whole-muscle CSA[166,167] increase with unilateral training, none of these variables are altered in the contralateral leg. We also observed a similar degree of between-subjects variability in pre-post changes for muscle hypertrophy and muscle atrophy compared to previous research. This variability normally complicates omics analyses because many important regulatory events are collapsed across participants showing divergent physiological responses (i.e., if the fold-change of 'gene x' is increased by RT in 'higher' responders but decreased or unchanged in 'lower' responders, then the mean change may be non-significant and thus mask important information). However, we found that response variability between subjects was reduced in our model when assessing the differential change in muscle size between legs (i.e., change in RT leg – change in immobilized leg). This finding enabled an optimized

means-based analytical approach in study 2 that ultimately led to the discovery of the first

reproducible loading-responsive gene expression signature.

5.3 Molecular regulators of muscle remodelling

Skeletal muscle loading and unloading induces muscle hypertrophy and atrophy,

respectively; however, the variability in responsiveness between individuals is

substantial.[15-17] This variability offers a unique opportunity to study the underlying

regulators of skeletal muscle adaptation, which, once understood, can potentially inform

the development of therapeutic strategies to offset the loss of muscle mass that occurs

with aging and disease.[18,168] Several laboratories have taken advantage of this approach to

uncover the purported regulators of muscle mass. For example, the Bamman laboratory

used a statistical clustering approach to group participants in low, moderate, and extreme

responders based on the degree of myofiber hypertrophy following RT. Profiling the

skeletal muscle transcriptome from these participants revealed greater myogenin,[16]

mechano-growth factor,[16] and cyclin D1 expression,[169] greater SC abundance at

baseline,[13] greater myonuclear accretion throughout RT,[13] and a greater increase in rRNA

content in extreme responders relative to low responders.[45] Furthermore, work from Dr.

Trappe's lab identified more than 600 genes that were correlated with muscle growth

following 12 weeks of RT, including genes involved in cell cycling, cytokine signalling,

growth factor signalling, and substrate metabolism.[113] Follow-up analyses, however,

showed that many of these RT-responsive genes could not be independently replicated or

represented generic exercise responses (i.e., they were regulated by aerobic and resistance

exercise alike).[110] This lack of reproducibility is likely due to a confluence of factors,

most relevant of which are the small sample sizes employed in exercise physiology research and few/no attempts to validate gene candidates in independent cohorts.

To overcome the limitations of prior work, we leveraged the differential responsiveness to RT and muscle disuse to interrogate the molecular regulators of muscle remodelling. Specifically, we employed the unilateral model developed in study 1 where one limb performed resistance training and the contralateral leg was immobilized. We combined this model with an optimized bioinformatics pipeline[108] that enabled a high fidelity interrogation of both the full-length mRNA transcript and its untranslated regions. By contrasting the differential expression of genes under distinct loading states, we identified >2000 regulatory events – the largest of any study to date – including significant regulation of the 5' and 3'UTRs. Many of the mechanically sensitive events we identified are broadly consistent with previous work (i.e., similar at the pathway level but distinct at the transcript level); however, we are the first to identify and independently validate a transcriptional growth signature that correlated with lean mass gain in 3 independent cohorts (n=100). Furthermore, we are the first to employ a data-driven network approach to gain a more thorough understanding of how the encoded proteins of regulated transcripts might interact *in vivo* in response to loading and unloading to drive adaptation.

5.3.1 New insights provided by data-driven network analysis

A common application of transcriptomics is the detection of differentially expressed genes (DEGs). However, the number of loading-regulated genes is usually extensive (>1000-2000)[98,110] and problematic to manually make sense of biologically.

Fortunately, user-friendly software has made it possible to categorize DEGs based on enrichment in biological function, reducing the dimensional space from thousands of DEGs to dozens of regulated pathways. In study 2, we observed an enrichment of transcripts involved in ECM organization, integrin binding, angiogenesis, and aerobic respiration – corroborating previous research on skeletal muscle remodelling.[98,110] While informative, enrichment analyses overlook the potential interaction between genes belonging to the same or different functional pathways.

A strength of study 2, compared to previous investigations, was our use of quantitative network modelling. Networks are constructed mathematically (i.e., unbiased) to show interactions between genes and therefore provide more information on biological context (i.e., they provide a framework to understand how molecules may interact when perturbed).[102] We identified two large network structures using full-length transcripts as input – the first of which was centred around the hub gene *NDUFS3*. This network was enriched in transcripts involved in oxidation-reduction and respiration processes. Several members of this network were modulated by our HypAt protocol and have also been identified as being load-sensitive in previous research. Indeed, mitochondrial gene expression, protein content and function are rapidly reduced with unloading.[117,170] By examining the *NDUFS3* network, it is easy to see how the modulation of one molecule (i.e., a central hub transcript) could influence other mitochondrial components and result in a reduction in mitochondrial-associated functions. In a companion paper to study 3, we also demonstrated for the first time that changes in certain mitochondrial transcripts (and their associated network of interactions) were associated with reductions in skeletal

muscle mass with short-term disuse.[171] The role(s) that mitochondrial adaptations play in load-induced muscle growth, however, are less clear.

Our laboratory has demonstrated a significant increase in mitochondrial protein synthesis after a bout of exhaustive RE in untrained young men but an attenuated stimulation in the trained state.[70] Robinson and colleagues also demonstrated increased mitochondrial protein synthesis after 12 weeks of RT, but only in older individuals, suggesting an age-specific response.[99] Analyses of mitochondrial content have yielded similarly equivocal results, showing either reductions,[172] no change,[70,173] or elevations[174] following RT. Thus, rather than reflecting a change in global mitochondrial content *per se*, our transcriptomic data might instead point to specific changes that alter the intrinsic function and/or organization of existing mitochondria in response to loading and unloading.

Few studies have analyzed the intrinsic respiratory function of mitochondria before and after RT. Porter and colleagues reported an increase in maximal coupled respiration from complexes 1 and 2 after 12 weeks of RT in permeabilized myofibers,[173] consistent with cross-sectional results obtained from trained vs. untrained participants.[175] However, neither study observed significant changes in CS activity (a marker of mitochondrial content[176]), implying that intrinsic mitochondrial function, and not content, was altered. It is also possible that loading-induced perturbations of the mitochondrial network coordinate non-bioenergetic processes that are important for muscle remodelling. For example, *in vitro* data suggests that mitochondrial respiratory complexes play an important role in regulating angiogenesis in endothelial cells.[177] Indeed, when complex III

is chemically silenced in human umbilical vein endothelial cells, proliferation and angiogenesis are significantly impaired due to a disruption in the cellular NAD+/NADH balance.[177] Likewise, our transcriptomic growth signature identified covariation between mitochondrial and angiogenic transcripts. Angiogenesis has been shown to be temporally linked with muscle hypertrophy in younger adults,[178] and capillary density is a key determinant of the hypertrophic response to RT in older adults.[179] These proposed relationships are also consistent with proteomic data from Robinson and colleagues, who demonstrated a significant increase in numerous mitochondrial proteins and angiogenic transcripts, but no change in mitochondrial respiration in young adults following RT.[99] Thus, our work may suggest an important role for mitochondrial signalling in loading-induced angiogenesis, rather than a strict bioenergetic function *per se*. More work is now needed to investigate whether perturbation of the mitochondrial network leads to these hypothesized changes.

We also identified a second network centered on *DOCK1*, a relatively uncharacterized gene in human skeletal muscle. This large network (312 gene members) was enriched in transcripts involved in 'cell migration,' consistent with DOCK1's role *in vitro* work. Indeed, the protein encoded by *DOCK1* is phosphorylated following mechanical strain,[180] likely through activation of FAK,[181] subsequently leading to GTP loading and activation of Rac1.[182,183] These signalling events cause a rearrangement of the actin cytoskeleton and increased activity of matrix metalloproteinases in cancer cells – enabling the local degradation of the ECM and migration of the cell.[181] Interestingly, *DOCK1* was also shown to play a critical role in fast-twitch myoblast fusion in

zebrafish[184] and *in vivo* in mice. Based on these findings, it is conceivable that modulation of the DOCK1 network may play a role in loading-induced growth through ECM remodelling, SC dynamics, and myonuclear accretion. Consistently, many of the nearest neighbors of this network have established roles in matrix remodelling and cell cycle regulation and were also perturbed by our HypAt model. How perturbation of the *DOCK1* network influences muscle remodelling during unloading is less clear; however, *DOCK1* expression is reduced by microgravity[185] and has been genetically linked to cancer cachexia.[186] It is also possible that modulating the *DOCK1* network regulates skeletal muscle remodelling through angiogenesis, given that Rac1 and several other network members are important for adhesion and angiogenic sprouting in endothelial cells.[187,188]

Described above are examples of how data-driven network analysis can be useful for generating hypotheses of implied gene product *interactions* and for visualizing how changes in one or a set of transcripts could regulate connected molecules and pathways. Networks can also be integrated with data from distinct populations and/or interventions. We provided an example of this approach in study 2, in which transcripts regulated by aging, insulin sensitivity, and loading (i.e., HypAt) were combined into a single network to demonstrate possible interactions between these physiological states. Hypotheses can be generated from the implied interactions and studied using reverse genetic techniques *in vitro* to elucidate the nature of the interaction further.[189] While study 2 underscores the advantages of network analysis, it is important to note that reproducible network construction requires >100 samples,[190] which is rare in exercise physiology research. Thus, the networks constructed in study 2 – integrating information from a large biobank

of skeletal muscle samples (n=187 samples) – represents the largest analysis of its kind and will undoubtedly be a useful hypothesis-generating resource for exercise physiologists and a tool for providing context to genes that are regulated by loading and unloading.

5.3.2 A novel role for UTR length in skeletal muscle remodelling

In addition to identifying the largest number of load-responsive transcripts relative to studies of similar size and duration, we are also the first to demonstrate extensive regulation at the UTRs of mRNA in response to loading and unloading. Although not inherently protein-coding, the 3' and 5'UTRs significantly influence the translation of mRNA into protein. The 3'UTR spans the nucleotide sequence between the stop codon and poly-A tail of an mRNA transcript and can be lengthened or shortened through alternative cleavage and polyadenylation in genes with multiple polyadenylation sites (PAS; estimated to be present in >50% of human genes).[191] Changes in 3'UTR length influence mRNA stability, translational efficiency, and localization in the cell and therefore have implications for subsequent protein production.[192] In study 2, we demonstrated that more genes were statistically regulated at their 3'UTR than at the full-length transcript level. Nonetheless, isolated regulation of the 3'UTR was only observed in ~200 genes, many of which were significantly correlated with lean mass gains (i.e., *BCAT2* and *FKBP1A*). Interestingly, the 3'UTR signal of *FKBP1A* covaried with the increase in lean mass and with >200 other transcripts. This 'module' was enriched for transcripts involved in angiogenesis, suggesting that modulation of the 3'UTR of *FKBP1A* may influence lean mass gain through expansion or reorganization of capillary

networks. We also discovered that knockdown of *BCAT2* and *FKBP1A* resulted in a

significant reduction in puromycin incorporation *in vitro*, ostensibly through impaired

elongation signalling. These findings underscore an important role for these genes in the

regulation of protein synthesis; however, the specific influence of 3'UTR

lengthening/shortening remains to be determined.

In contrast with the 3'UTR, the implications of 5'UTR lengthening/shortening are

less clear. Genes that are tightly regulated in the cell (including proto-oncogenes and

transcription factors) often contain longer 5'UTRs, with more extensive secondary

structure,[193] that effects translational efficiency. In addition to the physical barriers

introduced by stable secondary structures, 5'UTR length *per se* can also influence

translation through modulation of ribosome scanning time. Bohlen and colleagues

demonstrated that the scanning step of translation initiation is cap-tethered, which means

that the 40S ribosome remains bound to eIF4E (and other initiation factors) until

encountering the AUG start codon.[194] Lengthening of the 5'UTR therefore constrains

translational efficiency because only one ribosome can bind the 5'cap and scan for the

start codon at a time. In study 2, loading and unloading modulated the 5'UTR signal of

>700 genes, 16 of which were correlated with lean mass gains. Notable members include

ITM2A, which encodes a transmembrane protein involved in myogenic differentiation and

autophagy,[195,196] and two factors with known roles in angiogenesis – *TM4SF18* and

EXT1.[197,198] Collectively, modifying UTR length may be a mechanism for muscle cells to

selectively regulate the stability and/or translational efficiency of certain mRNA

molecules in response to loading and unloading. Regulation of UTR length may also

explain some of the reported discrepancies between RNA and protein species observed by Robinson and colleagues.[99] Nonetheless, our transcriptional data qualitatively align with the RT-responsive proteomic dataset identified by Robinson and colleagues, suggesting that the inconsistencies observed in their analyses may have been due to technical issues with RNA sequencing instead of true biological differences.[99]

A limitation of our UTR analyses is that we did not characterize the functional impact of the modifications we observed. Prior research has shown that lengthening of the 3'UTR is associated with reduced protein production via translational repression by miRNAs;[199] however, this finding is not universal.[200] Therefore, to experimentally determine the role of 3'UTR lengthening or shortening in our study, the sequence information from UTR-regulated transcripts in study 2 could be extracted and searched for structural features in the 3'UTR (i.e., via miRbase, https://www.mirbase.org). Subsequently, a score could be calculated that informs on how changes in UTR length would impact the gain or loss of a miRNA- or RBP-binding site and the predicted effect this would have on translation into protein.[201] Finally, because our data represents the first characterization of loading-induced changes in UTR lengthening, confirmation of our findings should be sought in high or low lean mass responders using methods that preferentially sequence UTRs[202] such as 3' region extraction and deep sequencing (3' READS).[203] Nonetheless, our UTR data represents an exciting and novel avenue of future inquiry and underscores the importance of considering transcript- rather than gene-level changes that occur in response to loading and unloading of skeletal muscle.

5.3.3 Individual responses to identify a transcriptional growth signature

The discussion thus far has mainly focussed on the transcripts regulated by muscle *remodelling* (i.e., loading and unloading). However, we also identified a transcriptional signature of lean mass gain from the list of regulated transcripts and subsequently validated it in 3 independent study cohorts. Interestingly, ~60 of these regulatory events (~43%) were associated with lean mass gain only at the UTR, without significant regulation of the full-length mRNA transcript. This result emphasizes the additional information gained from quantifying expression at the transcript- rather than gene-level. In a highly cited analysis, Pillon and colleagues meta-analyzed studies investigating the transcriptomic responses of skeletal muscle to acute and chronic exercise and disuse in an attempt to identify important loading-responsive genes.[98] However, because their analysis was conducted at the gene level, they overlooked the UTR-specific events we identified as important for muscle growth in study 2. For example, the signal from the 3'UTR of *BCAT2* was significantly correlated with lean mass gain in study 2 and covaried with several other growth-associated transcripts. In contrast, the MetaMEx output concludes that *BCAT2* is unresponsive to RT at the gene level (n=302, logFC=-0.01).[98] Another limitation of the MetaMEx database is a failure to consider individual differences in muscle hypertrophy/atrophy induced by RT training and disuse, respectively. For these reasons, our analysis has significant advantages over previous attempts to characterize loading-responsive and growth-associated molecular events.

The transcriptional growth signature in study 2 featured several known, and novel, regulators of muscle growth including FOXO3a, AMPK, and the apelin receptor. The

latter finding was particularly interesting because a recent pre-clinical analysis identified apelin as an exercise-sensitive myokine that exerts autocrine effects on skeletal muscle through the apelin receptor.[204] Indeed, apelin was shown to stimulate muscle protein synthesis via the mTOR-p70S6K1-4EBP1 axis, repress proteolysis by inhibiting FOXO3a, facilate repair and regeneration of skeletal muscle through an increase in SC number and activation, and stimulate mitochondrial biogenesis.[204] More recently, apelin was shown to mimic the effects of maternal exercise on the skeletal muscle health of the offspring through a mechanism involving the demethylation and increased expression of PGC-1a.[205] Many of these same signaling molecules were present in the transcriptional growth signature and/or the proteome-enriched network analysis in study 2 and, importantly, their expression levels were co-regulated with that of the apelin receptor. Together, these data suggest that modulation of apelin signaling may play a central role in skeletal muscle growth in response to resistance exercise and future work should interrogate this signaling axis in greater detail in humans.

To gain further insight into the functions of the transcriptional growth signature, we also conducted a background-corrected gene ontology (GO) analysis. This analysis revealed an enrichment of mitochondrial transcripts, corroborating the analysis of DEGs and our network analysis described earlier, and also identified an enrichment in genes involved in purine biosynthesis. The importance of purine synthesis for muscle growth may be related to enhanced rRNA synthesis and a subsequent increase in ribosome formation (i.e., ribosome biogenesis). Indeed mTORC1, which is downstream of many of the pathways regulated in our proteome-constrained analysis, plays a critical role in

purine biosynthesis at the transcriptional level.[43] Furthermore, small molecule inhibitors of mTORC1 were predicted to oppose our transcriptional growth signature, which could conceivably occur through a blunting of ribosome biogenesis and/or other anabolic processes controlled by mTORC1. In the absence of increased ribosomal degradation, ribosome biogenesis augments translational capacity, which may partially explain the observed increase in MPS we and others have observed following RT in the basal state.[73] Stec and colleagues, and more recently a group in Norway, also demonstrated that increases in total muscle RNA and rRNA content are associated with a greater hypertrophic response to RT in young and older adults.[45,206] Taken together, although we did not directly measure RNA content, the enrichment of purine biosynthetic transcripts in our growth signature suggests that ribosomal biogenesis plays an important role in muscle growth following RT.

Other growth-correlated transcripts were found to have roles in cell contact (i.e., adherens junction and tight junction) and cell-cycling, which may play a role in SC-mediated myonuclear accretion during muscle growth. Indeed, several cadherin transcripts were identified as being associated with lean mass gain in study 2, and have been shown to be involved in tethering quiescent satellite cells to myofibers in previous research.[207] The disruption of these contacts (i.e., by mechanical forces) induces SC activation and proliferation,[207] consistent with the enrichment of cell cycling transcripts we observed. Together these findings suggest that SC dynamics are important for muscle growth, possibly through their role in myonuclear accretion. In support of this hypothesis, Lundberg and colleagues observed a strong association (r>0.8) between muscle fibre

hypertrophy and changes in myonuclei per fibre following 5 weeks of combined aerobic and resistance exercise.[208] Furthermore, work from the Bamman laboratory demonstrated that satellite cell content prior to RT, and the capacity to add myonuclei during 16 weeks of RT in exercise-naïve subjects, differentiated high- from lower-responders.[13] More recently, Angleri *et al.* also demonstrated a relationship between myofiber hypertrophy and SC content and myonuclear accretion in trained individuals.[209] The addition of myonuclei during RT would presumably limit myonuclear domain expansion as the muscle fibre increases in size, thus minimizing mRNA diffusion distances. It would also increase the template DNA available for rRNA synthesis and ribosomal biogenesis. While both physiological adaptations would theoretically be important for muscle growth, their relative contribution remains to be determined.

Finally, the transcriptional growth signature was enriched in angiogenic transcripts. Indeed, *FKBP1A*, regulated only at its 3'UTR, was correlated with the expression of >200 transcripts, collectively involved in angiogenesis. Of note, *KDR,* which encodes a receptor for VEGF, was co-regulated with several other transcriptional growth genes in study 2 and was identified in a recent meta-analysis as a central regulatory hub of the exercise training response. As mentioned above, angiogenesis appears critical for loading-induced muscle growth,[178] potentially through an increased capacity to deliver nutrients (glucose and amino acids) and/or through communication with satellite cells. As a group, the angiogenic gene module was enriched in binding sites for three transcription factors – KLF9, NF1A, and RBPJ – which are relatively uncharacterized in skeletal muscle; however, RBPJ is critical for vascular homeostasis in

adult mice, acting downstream of Notch signalling.[210] Collectively, study 2 identified

several pathways known to be involved in skeletal muscle remodelling. We are also the

first to establish a reproducible signature of muscle growth that significantly contributes

to our understanding of how muscle size is regulated at the transcriptional level by

loading (Figure 1). As researchers continue to mine the extensive resource of loading-

responsive transcripts, our understanding of the key drivers of muscle adaptation will

only deepen, potentially paving the way for the development of therapeutic strategies to

combat muscle atrophy with age, disease, and disuse.
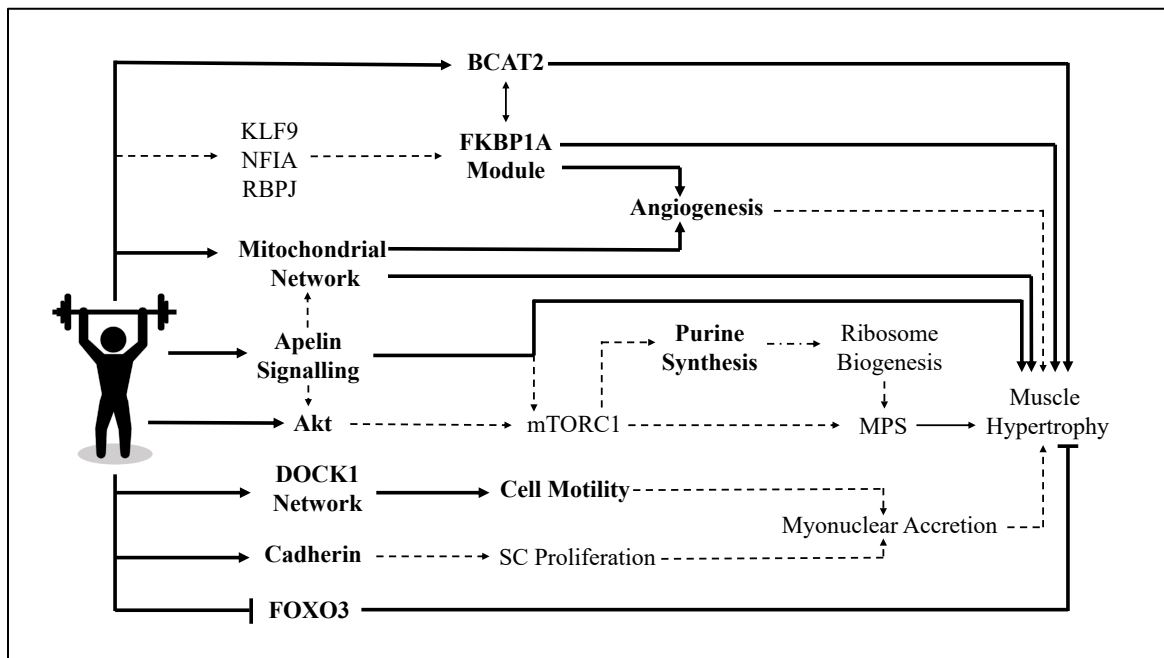
Figure 1. An incomplete map of the signalling mechanisms that induce muscle hypertrophy in response to resistance training. Bolded components and solid lines indicate relationships that were observed in study 2. Non-bolded components and dashed lines show relationships that have been identified by previous research, but were not directly assessed in the present thesis. Note: the present diagram omits several other regulators of muscle hypertrophy discovered in study 2 including, but not limited to, ECM remodelling and other well-established signalling axis (see Table 1 in Study 2) due to space limitations.

5.4 The influence of loading on muscle size and protein turnover

Resistance exercise induces skeletal muscle hypertrophy and augments muscle strength. In studies 1 and 2, we observed an ~8% increase in mid-thigh VL CSA and a ~5% increase in leg lean mass with substantial variability between subjects. In addition to the transcriptional changes noted above, these increases in muscle size result from a chronic elevation of MPS over MPB, leading to protein accretion during the training program. Although RT perturbs MPB,[73] we elected to quantify integrated rates of MPS in study 2 for two reasons. First, MPS is more sensitive to amino acid concentration changes compared to MPB.[211-213] Second, MPS is stimulated to a significantly greater extent by RE compared to MPB.[65,214] From these observations, it has been suggested that changes in MPS induced by RT play a disproportionately greater role in determining loading-induced changes in muscle size.[215]

RT induced a ~13% increase in integrated myofibrillar protein synthesis in study 2. In contrast, previous work from our laboratory and that of others, has demonstrated either no change or an increase in MPS in the trained vs. untrained state.[70,71,73,214,216,217] These discrepancies may be explained by the different muscle protein subfractions sampled and/or the use of different tracer techniques (i.e., acute isotope infusions vs. integrated measurements). Indeed, previous research focused primarily on MPS differences in the fasted- or fed-state over a brief time interval (1-4 hours), whereas we measured the integrated MPS response over two weeks. Surprisingly, the RT-induced enhancement of MPS that we observed was also uncorrelated to RT-induced muscle growth. This observation contrasts with work by Damas and colleagues, who identified an

association between the peri-workout stimulation of MPS at weeks 3 and 10 of an RT program and subsequent myofiber hypertrophy.[72]

The lack of association in study 2 may again, however, be related to the fact that our method captured protein synthesis over two weeks (as opposed to 48 h) and averaged across 6 RE bouts and 8 resting days. In this situation, a greater proportion of the weighted average MPS measurement came from resting days, therefore diluting the contribution of the peri-workout period shown to be correlated with muscle hypertrophy.[72,218] It is also possible that during the 8- to 10-week phase of an RT program (the period when MPS was measured), muscle growth was related to mechanisms other than MPS, such as SC-mediated myonuclear accretion, ribosomal biogenesis, ECM remodelling, and angiogenesis. Indeed, the transcriptional growth signature identified in study 2 suggested that these pathways are important determinants of the hypertrophic response to RT.

5.5 The influence of unloading on muscle size and protein turnover

Periods of muscle disuse are unavoidable and occur throughout life due to illness, injury, disease, and/or voluntary sedentarism. One of the objectives of the studies presented in this thesis was to gain a better understanding of how simple muscle disuse (i.e., a non-inflammatory, hypercatabolic, hypercytokinemic state) perturbs skeletal muscle protein turnover. At the morphological level, we observed that disuse-induced muscle atrophy occurred at a rate ~5 times faster than RT-induced muscle hypertrophy (studies 1 and 2); however, the degree of atrophy varied substantially between individuals. Indeed, we observed an average reduction in mid-thigh VL CSA of 8.2% in

response to 2 weeks of unloading, comparable in magnitude to 10 weeks of loading, but at the individual level, there was a range of loss between 0.4 to 18.5%. A similar degree of variability was evident when leg lean mass was assessed using DXA. In study 3, thigh lean mass was reduced by 0.4 to 4% in response to four days of unloading. These findings confirm the differential responsiveness previously shown to occur in response to short and moderate periods of unloading.[23,31,32]

Prior work has demonstrated that simple disuse-induced muscle atrophy in humans can be mostly, if not entirely, explained by reductions in MPS.[23,26,27] In the fasted state, MPS is reduced ~25-50% in response to periods of limb immobilization lasting 5-35 days.[21,23,25-27,219] In study 3, four days of unloading did not alter fasted-state MPS, however, the stimulation of MPS by amino acid infusion was attenuated in the immobilized limb. This finding extends previous work from our laboratory that demonstrated a reduced stimulation of MPS in response to both high and low dose amino acid infusion after two weeks of immobilization.[23] In study 3, we also demonstrated a ~16% reduction in integrated myofibrillar protein synthesis rates – identical in magnitude to what Kilroe and colleagues reported.[220] Notably, the change in MPS was quantitatively related to the observed loss of muscle mass in both short-term investigations (Kilroe et al.,[220] and study 3) and remained associated over two weeks of immobilization (study 1). Collectively, our data add to the existing literature on disuse-induced perturbations to protein synthesis by demonstrating that reductions in integrated MPS occur within days of unloading, are sustained at later time points, and are quantitatively linked to muscle atrophy.

Despite strong links between MPS and disuse-induced muscle loss, prior research has been unable to definitively ascribe a role for MPB in muscle atrophy in humans. For example, Ferrando and colleagues observed a ~50% reduction in MPS after 15 days of bed rest, but no change in protein breakdown assessed using A-V balance techniques.[221] Symons and colleagues were the first to employ the tracer dilution technique to measure MPB, and they found no significant changes in response to 21 days of bed rest.[222] These observations,[221,222] in combination with the observed changes in MPS noted above, suggest that longer-term unloading-induced atrophy is driven entirely by changes in MPS and that, if anything, MPB is adaptively reduced to match MPS.[91,128] Nonetheless, this view has been challenged[223] based on findings in rodents and from short-term investigations in humans that have found an upregulation of biomarkers associated with proteolysis in skeletal muscle. Indeed, Urso and colleagues identified 25 differentially expressed genes (most upregulated) in response to 48h of unloading that have established roles in the ubiquitin-proteasome pathway.[224] The most upregulated functional pathway was ubiquitin conjugation[224] – a finding consistent with the increase in protein ubiquitination observed by others in response to 48 hrs of unloading.[117] Finally, two canonical 'atrogenes,' MAFBx and MuRF1, are also increased in response to short-term muscle disuse.[219,220] These observations collectively suggest an early upregulation of proteolysis, but without directly measuring MPB these conclusions are supported only by static markers and not the dynamic process of MPB.

To directly measure MPB, the tracer decay rate in the muscle intracellular free amino acid pool is measured.[63] The technique involves the infusion of stable isotope

tracers until a steady-state enrichment is obtained in the arterial and intracellular free pool. Once achieved, the infusion is stopped – at which point the enrichment in the intracellular free pool begins to exponentially decay as tracee enters from the arterial pool and protein breakdown. A measurement of fractional breakdown rate is obtained by sampling the arterial pool, the intracellular free pool, and the protein-bound pool sequentially over 60-90 minutes.[63] In study 3, we used a modified version of this protocol that involved the staggered infusion of two amino acid tracers differing only in the isotope label used (i.e., L-^{2}H$_8$-phenylalanine and L-^{15}N-phenylalanine). By measuring the ratio of their respective dilutions in a single muscle sample, we obtained tracer decay and thus estimated MPB.[62] Using this approach, we demonstrated that fasted MPB was unchanged following 4 days of unloading. Furthermore, because we simultaneously measured integrated MPS and changes in leg lean mass, we obtained a pseudo-integrated rate of MPB over the 4-day unloading period (using the relationship: *Fractional Growth Rate = Fractional Synthesis Rate – Fractional Breakdown Rate)*. This analysis also revealed no change in daily protein breakdown for the duration of muscle disuse. Consistently, we also observed no changes in the expression of biomarkers associated with protein breakdown (i.e., calpain 1, MAFBx, or ubiquitin). Collectively, these findings significantly advance our understanding of how muscle protein turnover is regulated in response to short-term muscle disuse and suggest, consistent with prior views, that efforts to attenuate or prevent muscle atrophy should focus on modulating MPS. Future research, employing dynamic proteome profiling, is now needed to

determine whether specific proteins are subjected to increased degradation in response to disuse.

Given the lack of activation of MPB in study 3, the increased expression of biomarkers associated with proteolysis observed by others (see above) is nonetheless surprising. These seemingly contradictory findings may, however, highlight a more nuanced control over muscle protein turnover during periods of disuse. Indeed, as reviewed in the introduction of this thesis, the eukaryotic initiation factor eIF3f is known to be a substrate of MAFBx/atrogin-1 that plays a critical role in translation initiation.[94,130] The targeted polyubiquitination of eIF3f by MAFBx, and its subsequent degradation, could therefore significantly impair cellular protein synthetic capacity. Using muscle samples obtained from participants in study 3, we provided preliminary support for this hypothesis. Using data-driven network analysis, we identified several network modules quantitatively related either to the reduction in MPS or muscle size following 4 days of unloading.[171] Interestingly, MAFBx was identified as a hub gene of one network significantly associated with reductions in MPS.[171] While the nature of this relationship is unclear, these data support a hypothesis in which 'atrogenes' are increased within the first few days of unloading to induce the selective degradation of translational components rather than bulk proteolysis *per se.* Taken together, our data underscore the difficulty in drawing conclusions of dynamic processes on the basis of static measurements of gene and/or protein expression.

5.6 Mechanisms of disuse-induced reductions in MPS

While reductions in MPS ostensibly drive disuse-induced muscle atrophy (studies 2 and 3), the underlying mechanisms mediating these reductions remain obscure. MAFBx may play an important role, as described above, but several other pathways are also thought to be involved. The canonical 'conductor' of anabolic and catabolic processes – mTORC1 – regulates ribosomal biogenesis and protein translation and is therefore considered a key regulator of disuse-induced reductions in MPS;[225] however, existing data are equivocal. Our laboratory demonstrated significantly lower fasted and fed-state MPS without changes in the Akt-mTORC1 signalling pathway after 14d of immobilization.[23] These data are supported by a recent comprehensive analysis of hindlimb unloading in rodents which failed to link attenuated mTORC1 signaling activity (or any phosphoproteomic changes) to the observed reductions in MPS after 6 and 24hr of unloading.[226] Nonetheless, reduced phosphorylation of various mTORC1 substrates has been reported after 5 or 14 days of immobilization[21,25] or 10 days of bed rest in humans.[227] Furthermore, Urso and colleagues demonstrated a 25% decrease in p-Akt[Ser473] after only 3 days of unloading.[224]

In study 3 we observed minimal changes in the phosphorylation status of mTOR, 4EBP1, Akt, rpS6, eIF4E, eIF4B, or eEF2 following four 4 days of disuse. The corresponding transcriptomic data from the same participants did, however, uncover *DEPTOR* as a hub gene related to the declines in MPS observed. DEPTOR is a known inhibitor of both mTORC1 and mTORC2,[228] and its knockdown in C2C12 cells leads to increased phosphorylation of S6K1 and 4EBP1, and increased protein synthesis.[229]

However, DEPTOR has also been shown to be involved in several other processes (i.e., inflammation, apoptosis, and autophagy) that could influence protein synthesis and muscle mass regulation with disuse.[230] Thus, while it is possible that muscle unloading reduces signalling through the Akt-mTORC1 axis, the evidence is far from conclusive in humans and suggests – if anything – only a mild dysregulation of mTORC1 signalling. Moreover, 'snapshot' measurements of a few signalling molecules cannot capture the integrated responses that occur in response to disuse. In this regard, it is arguably more informative to study the effects of unloading on gene networks that integrate information from interacting pathways.

In a companion paper to study 3,[171] separate tissue samples were obtained pre- and post-immobilization to analyze the transcriptional responses to unloading. While the analysis was based on a small sample and would be exploratory, it is unique in being the first to investigate the signalling networks perturbed by short-term unloading. When analyzing gene-level changes, short-term unloading led to a downregulation of genes involved in muscle contraction and energy metabolism,[171] consistent with previous reports,[98,117] and other known regulators of muscle atrophy (i.e., FOXO3). However, when analyzed at the network level, additional pathways were revealed, including upregulation of ubiquitin-dependent catabolism, mRNA processing and ribosomal biogenesis.[171] The upregulation of genes involved in ribosomal biogenesis conflicts with data obtained from rodents subjected to hindlimb unloading[90] but aligns with observations made in unloaded human skeletal muscle.[90] Nonetheless, total RNA content (an index of translational capacity) is reduced in response to limb immobilization in humans,[90,231]

implying that ribosomal degradation supersedes ribosomal biogenesis during unloading. Future research should examine unloading-induced perturbations in RNA turnover in greater detail, preferably through a combination of techniques including PCR, Western Blotting, and D_2O-derived measurements of RNA synthesis.[165]

Another prominent molecular feature of short-term unloading potentially linked to reductions in MPS is mitochondrial dysregulation. Abadi and colleagues demonstrated a dominant mitochondrial signature following 48 hrs of unloading that remained repressed after 14 days.[117] In general, changes in mitochondrial transcripts precede the reduction in transcripts involved in protein translation, suggesting that it is one of the earliest detectable molecular features of unloading.[117] In the molecular complement to study 3, we also identified a prominent mitochondrial signature. We are also the first to demonstrate a quantitative link between the perturbation of a mitochondrial network and the loss of lean mass in response to 4 days of immobilization.[171] These findings are consistent, at least qualitatively, with muscle samples obtained from hibernating mammals in which the preservation of muscle mass is linked with increased expression of mitochondrial-related genes.[232] The question of how an early reduction in mitochondrial transcript expression might lead to, or is a consequence of, reduced MPS is unclear; however, research in worms and rodents provides some evidence of a link between the cytosolic and mitochondrial translational machinery.[233]

In nematodes, the RNAi-mediated knockdown of *mrps-5*, a gene encoding a mitochondrial ribosomal protein involved in mitochondrial translation, causes a shift in mRNA population from polysomes to monosomes, indicating a suppression of cytosolic

translation.[233] Probing further using a suite of omics techniques and complementary molecular analysis, it was discovered that genes showing a significant reduction in translational efficiency in response to *mrps-5* knockdown largely coded for proteins involved in ribosome biogenesis and protein translation.[233] Interestingly, in a meta-analysis of disuse studies (albeit *n=3* studies), a mitochondrial ribosomal protein (*MRPL12)* was predicted to be a hub gene. In addition to being downregulated by disuse, *MRPL12* was discovered to interact with a network of genes involved in mitochondrial respiration, oxidation-reduction processes, and angiogenesis,[234] which are many of the same pathways we found to be regulated in muscle samples taken from participants in study 2 and 3. Furthermore, the mitochondrial network we identified in study 2 supports an interaction between mitochondrial complex 1, several mitochondrial ribosomal protein encoding genes, and eIF3K implying – as hypothesized – that reductions in mitochondrial translation can influence cytoplasmic protein synthesis. Future research using stable isotopes should investigate whether disuse impairs mitochondrial protein synthesis and whether these changes precede, and are related to, reductions in myofibrillar or mixed muscle protein synthesis. Furthermore, the proposed mediator of the link between the mitochondrial and cytoplasmic molecualr machinery in worms – ATF4 – should be investigated in humans, given that it is implicated in disuse muscle atrophy in rodents.[235,236]
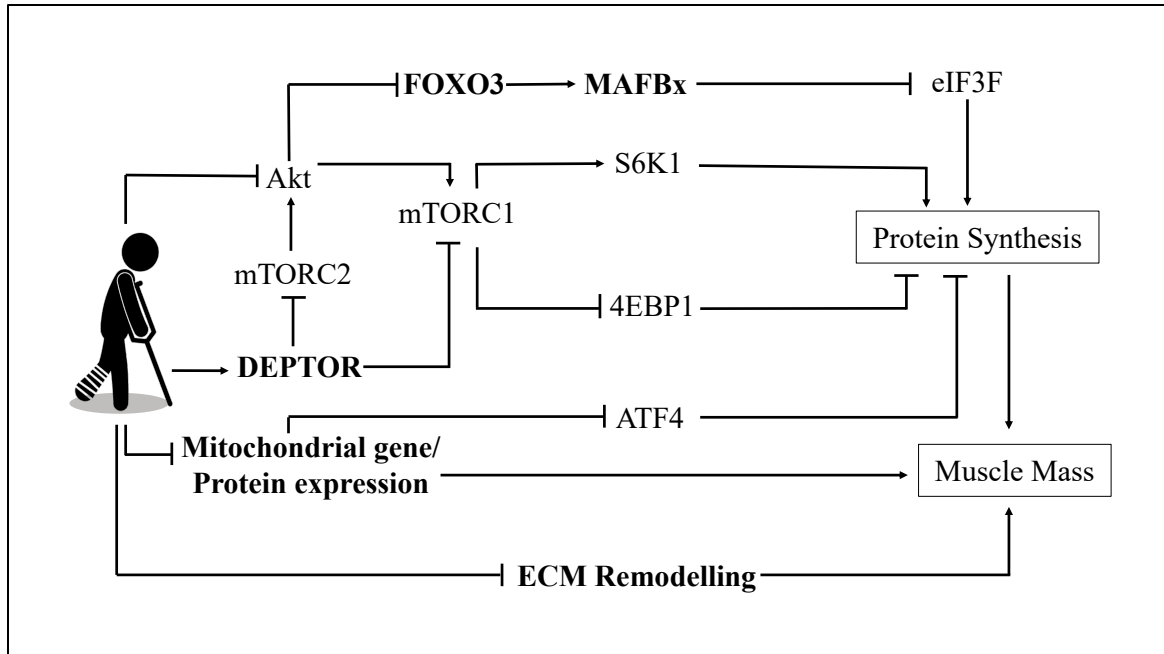
Figure 2. Proposed mechanisms of disuse-induced reductions in MPS and muscle mass. Bolded components are factors that were discovered in this thesis to be related to either the reduction in MPS or muscle mass, or both. Factors that are not bolded were not statistically affected in the studies that comprised this thesis (or were not measured), but have been shown in previous research to be modulated by inactivity or have established links with other model components.

5.7 Summary and main contributions of thesis

Loading and unloading alter the structure and function of skeletal muscle to a variable degree in humans through incompletely understood mechanisms. Fundamentally, changes in muscle size are driven by a chronic imbalance between MPS and MPB, leading to either net protein accrual or breakdown and, consequently, muscle hypertrophy or atrophy. These processes are supported, or in some cases thought to be driven by myonuclear and/or ribosomal accretion, ECM remodelling, and angiogenesis. The present thesis significantly contributes to our understanding of these processes. In study 1, we validated the use of ultrasonography for measuring changes in muscle size induced by

loading and unloading – an important finding for research laboratories not equipped with or capable of accessing MRI or CT. In so doing, we also developed a powerful within-subjects model to gain a better understanding of how loading and unloading influence skeletal muscle at a molecular level. Using this model, and an optimized bioinformatics pipeline, we identified and validated a transcriptional signature of lean muscle mass gain and provided the first evidence of loading-induced UTR-specific regulation in humans. Study 2, therefore, serves as a important and useful resource that can be interrogated by researchers and used to generate hypotheses. Finally, study 3 significantly advances our understanding of unloading-induced changes in muscle protein turnover. We provided novel data demonstrating a lack of change in MPB within the first few days of unloading, thus addressing a long-standing question in the field. We also provided further support for the hypothesis that disuse-induced muscle atrophy is primarily driven by reductions in MPS. Future research is now needed to identify the mechanism by which muscle unloading mediates these reductions in MPS, although we provided several possibilities. In conclusion, muscle remodelling is a complex process requiring the coordination of several molecular pathways. This complexity is best understood by considering differential responsiveness to loading and unloading and using thoughtful approaches to analyzing protein turnover and global gene expression responses.

5.8 References

1. Janssen I, Heymsfield SB, Wang Z, Ross R. Skeletal muscle mass and distribution in 468 men and women aged 18–88 yr. *Journal of Applied Physiology.* 2000;89:81-88.

2. Zurlo F, Larson K, Bogardus C, Ravussin E. Skeletal muscle metabolism is a major determinant of resting energy expenditure. *J Clin Invest.* 1990;86(5):1423-1427.

3. DeFronzo RA, Jacot E, Jequier E, Maeder E, Wahren J, Felber JP. The effect of insulin on the disposal of intravenous glucose. Results from indirect calorimetry and hepatic and femoral venous catheterization. *Diabetes.* 1981;30(12):1000-1007.

4. Arnold EM, Delp SL. Fibre operating lengths of human lower limb muscles during walking. *Philos Trans R Soc Lond B Biol Sci.* 2011;366(1570):1530-1539.

5. Schiaffino S, Bormioli SP, Aloisi M. Cell proliferation in rat skeletal muscle during early stages of compensatory hypertrophy. *Virchows Arch B Cell Pathol.* 1972;11(3):268-273.

6. Narici MV, Hoppeler H, Kayser B, et al. Human quadriceps cross-sectional area, torque and neural activation during 6 months strength training. *Acta Physiol Scand.* 1996;157(2):175-186.

7. Alway SE, Grumbt WH, Stray-Gundersen J, Gonyea WJ. Effects of resistance training on elbow flexors of highly competitive bodybuilders. *J Appl Physiol (1985).* 1992;72(4):1512-1521.

8. DeFreitas JM, Beck TW, Stock MS, Dillon MA, Kasishke PR, 2nd. An examination of the time course of training-induced skeletal muscle hypertrophy. *Eur J Appl Physiol.* 2011;111(11):2785-2790.

9. Damas F, Phillips SM, Lixandrao ME, et al. An inability to distinguish edematous swelling from true hypertrophy still prevents a completely accurate interpretation of the time course of muscle hypertrophy. *Eur J Appl Physiol.* 2016;116(2):445-446.

10. Goreham C, Green HJ, Ball-Burnett M, Ranney D. High-resistance training and muscle metabolism during prolonged exercise. *Am J Physiol.* 1999;276(3):E489-496.

11. Seynnes OR, de Boer M, Narici MV. Early skeletal muscle hypertrophy and architectural changes in response to high-intensity resistance training. *J Appl Physiol (1985).* 2007;102(1):368-373.

12. Kosek DJ, Kim J-s, Petrella JK, Cross JM, Bamman MM. Efficacy of 3 days/wk resistance training on myofiber hypertrophy and myogenic mechanisms in young vs. older adults. *Journal of Applied Physiology.* 2006.

13. Petrella JK, Kim JS, Mayhew DL, Cross JM, Bamman MM. Potent myofiber hypertrophy during resistance training in humans is associated with satellite cell-mediated myonuclear addition: a cluster analysis. *J Appl Physiol (1985).* 2008;104(6):1736-1742.

14. Thalacker-Mercer A, Stec M, Cui X, Cross J, Windham S, Bamman M. Cluster analysis reveals differential transcript profiles associated with resistance training-induced human skeletal muscle hypertrophy. *Physiol Genomics.* 2013;45(12):499-507.

15. Hubal MJ, Gordish-Dressman H, Thompson PD, et al. Variability in muscle size and strength gain after unilateral resistance training. *Med Sci Sports Exerc.* 2005;37(6):964-972.

16. Bamman MM, Petrella JK, Kim JS, Mayhew DL, Cross JM. Cluster analysis tests the importance of myogenic gene expression during myofiber hypertrophy in humans. *J Appl Physiol (1985).* 2007;102(6):2232-2239.

17. Davidsen PKPKPK, Gallagher IJIJ, Hartman JWJWJW, et al. High responders to resistance exercise training demonstrate differential regulation of skeletal muscle microRNA expression. *Journal of Applied Physiology.* 2011;110:309-317.

18. Bamman MM, Roberts BM, Adams GR. Molecular Regulation of Exercise-Induced Muscle Fiber Hypertrophy. *Cold Spring Harb Perspect Med.* 2018;8(6).

19. Kilroe SP, Fulford J, Jackman SR, LJC VANL, Wall BT. Temporal Muscle-specific Disuse Atrophy during One Week of Leg Immobilization. *Med Sci Sports Exerc.* 2020;52(4):944-954.

20. Adams GR, Caiozzo VJ, Baldwin KM. Skeletal muscle unweighting: spaceflight and ground-based models. *Journal of applied physiology (Bethesda, Md : 1985).* 2003;95:2185-2201.

21. Wall BT, Dirks ML, Snijders T, et al. Short-term muscle disuse lowers myofibrillar protein synthesis rates and induces anabolic resistance to protein ingestion. *American Journal of Physiology Endocrinology and Metabolism.* 2015:ajpendo.00227.02015.

22. Oates BR, Glover EI, West DW, Fry JL, Tarnopolsky MA, Phillips SM. Low-volume resistance exercise attenuates the decline in strength and muscle mass associated with immobilization. *Muscle and Nerve.* 2010;42:539-546.

23. Glover EI, Phillips SM, Oates BR, et al. Immobilization induces anabolic resistance in human myofibrillar protein synthesis with low and high dose amino acid infusion. *Journal of Physiology.* 2008.

24. Skeletal muscle atrophy during short-term disuse: Implications for age-related sarcopenia, Ageing Research Reviews(2013).

25. Wall BT, Snijders T, Senden JMG, et al. Disuse impairs the muscle protein synthetic response to protein ingestion in healthy men. *Journal of Clinical Endocrinology and Metabolism.* 2013;98:4872-4881.

26. de Boer MD, Selby A, Atherton P, et al. The temporal responses of protein synthesis, gene expression and cell signalling in human quadriceps muscle and patellar tendon to disuse. *The Journal of physiology.* 2007;585:241-251.

27. Gibson JN, Halliday D, Morrison WL, et al. Decrease in human quadriceps muscle protein turnover consequent upon leg immobilization. *Clinical science.* 1987;72:503-509.

28. Suetta C, Hvid LG, Justesen L, et al. Effects of aging on human skeletal muscle after immobilization and retraining. *Journal of applied physiology (Bethesda, Md : 1985).* 2009;107:1172-1180.

29. Hvid L, Aagaard P, Justesen L, et al. Effects of aging on muscle mechanical function and muscle fiber morphology during short-term immobilization and subsequent retraining. *Journal of Applied Physiology.* 2010;109:1628-1634.

30. Hortobágyi T, Dempsey L, Fraser D, et al. Changes in muscle strength, muscle fibre size and myofibrillar gene expression after immobilization and retraining in humans. *The Journal of physiology.* 2000;524 Pt 1:293-304.

31. Yasuda N, Glover EI, Phillips SM, Isfort RJ, Tarnopolsky MA. Sex-based differences in skeletal muscle function and morphology with short-term limb immobilization. *Journal of Applied Physiology.* 2005.

32. Chen Y-W, Gregory C, Ye F, et al. Molecular signatures of differential responses to exercise trainings during rehabilitation. *Biomedical Genetics and Genomics.* 2017.

33. Biolo G, Fleming RYD, Maggi SP, Wolfe RR. Transmembrane transport and intracellular of amino acids in human skeletal muscle kinetics. *American Journal of Physiology Endocrinology and Metabolism.* 1995;268:E75-E84.

34. Burd Na, Tang JE, Moore DR, Phillips SM. Exercise training and protein metabolism: influences of contraction, protein intake, and sex-based differences. *Journal of applied physiology (Bethesda, Md : 1985).* 2009;106:1692-1701.

35. Jackson RJ, Hellen CU, Pestova TV. The mechanism of eukaryotic translation initiation and principles of its regulation. *Nat Rev Mol Cell Biol.* 2010;11(2):113-127.

36. Hara K, Yonezawa K, Kozlowski MT, et al. Regulation of eIF-4E BP1 phosphorylation by mTOR. *J Biol Chem.* 1997;272(42):26457-26463.

37. Gingras AC, Gygi SP, Raught B, et al. Regulation of 4E-BP1 phosphorylation: a novel two-step mechanism. *Genes Dev.* 1999;13(11):1422-1437.

38. Burnett PE, Barrow RK, Cohen NA, Snyder SH, Sabatini DM. RAFT1 phosphorylation of the translational regulators p70 S6 kinase and 4E-BP1. *Proc Natl Acad Sci U S A.* 1998;95(4):1432-1437.

39. Dorrello NV, Peschiaroli A, Guardavaccaro D, Colburn NH, Sherman NE, Pagano M. S6K1- and betaTRCP-mediated degradation of PDCD4 promotes protein translation and cell growth. *Science.* 2006;314(5798):467-471.

40. Dennis MD, Jefferson LS, Kimball SR. Role of p70S6K1-mediated phosphorylation of eIF4B and PDCD4 proteins in the regulation of protein synthesis. *J Biol Chem.* 2012;287(51):42890-42899.

41. Hannan KM, Brandenburger Y, Jenkins A, et al. mTOR-dependent regulation of ribosomal gene transcription requires S6K1 and is mediated by phosphorylation of the carboxy-terminal activation domain of the nucleolar transcription factor UBF. *Mol Cell Biol.* 2003;23(23):8862-8877.

42. Mayer C, Zhao J, Yuan X, Grummt I. mTOR-dependent activation of the transcription factor TIF-IA links rRNA synthesis to nutrient availability. *Genes Dev.* 2004;18(4):423-434.

43. Ben-Sahra I, Hoxhaj G, Ricoult SJH, Asara JM, Manning BD. mTORC1 induces purine synthesis through control of the mitochondrial tetrahydrofolate cycle. *Science.* 2016;351(6274):728-733.

44. Ben-Sahra I, Howell JJ, Asara JM, Manning BD. Stimulation of de novo pyrimidine synthesis by growth signaling through mTOR and S6K1. *Science.* 2013;339(6125):1323-1328.

45.   Stec MJ, Kelly NA, Many GM, Windham ST, Tuggle SC, Bamman MM. Ribosome biogenesis may augment resistance training-induced myofiber hypertrophy and is required for myotube growth in vitro. *Am J Physiol Endocrinol Metab.* 2016;310(8):E652-E661.

46.   Figueiredo VC, McCarthy JJ. Regulation of Ribosome Biogenesis in Skeletal Muscle Hypertrophy. *Physiology (Bethesda).* 2019;34(1):30-42.

47.   Figueiredo VC, Wen Y, Alkner B, et al. Genetic and epigenetic regulation of skeletal muscle ribosome biogenesis with exercise. *J Physiol.* 2021;599(13):3363-3384.

48.   Murach KA, Fry CS, Dupont-Versteegden EE, McCarthy JJ, Peterson CA. Fusion and beyond: Satellite cell contributions to loading-induced skeletal muscle adaptation. *FASEB J.* 2021;35(10):e21893.

49.   Rock KL, Gramm C, Rothstein L, et al. Inhibitors of the proteasome block the degradation of most cell proteins and the generation of peptides presented on MHC class I molecules. *Cell.* 1994;78(5):761-771.

50.   Schwartz AL, Ciechanover A. The ubiquitin-proteasome pathway and pathogenesis of human diseases. *Annu Rev Med.* 1999;50:57-74.

51.   Nakayama KI, Nakayama K. Ubiquitin ligases: cell-cycle control and cancer. *Nat Rev Cancer.* 2006;6(5):369-381.

52.   Bodine SC, Latres E, Baumhueter S, et al. Identification of ubiquitin ligases required for skeletal muscle atrophy. *Science (New York, NY).* 2001;294:1704-1708.

53.   Solomon V, Goldberg AL. Importance of the ATP-ubiquitin-proteasome pathway in the degradation of soluble and myofibrillar proteins in rabbit muscle extracts. *J Biol Chem.* 1996;271(43):26690-26697.

54.   Du J, Wang X, Miereles C, et al. Activation of caspase-3 is an initial step triggering accelerated muscle proteolysis in catabolic conditions. *J Clin Invest.* 2004;113(1):115-123.

55.   Volodin A, Kosti I, Goldberg AL, Cohen S. Myofibril breakdown during atrophy is a delayed response requiring the transcription factor PAX4 and desmin depolymerization. *Proc Natl Acad Sci U S A.* 2017;114(8):E1375-E1384.

56.   Mizushima N, Komatsu M. Autophagy: renovation of cells and tissues. *Cell.* 2011;147(4):728-741.

57.   Schoenheimer R, Ratner S, Rittenberg D. Studies in protein metabolism. X. The metabolic activity of body proteins investigated with l(-)-Leucine containing two isotopes. *J Biol Chem.* 1939;130:703-732.

58.   Schoenheimer R, Ratner S, Rittenberg D. The Process of Continuous Deamination and Reamination of Amino Acids in the Proteins of Normal Animals. *Science.* 1939;89(2308):272-273.

59.   Ussing HH. The Rate of Protein Renewal in Mice and Rats Studied by Means of Heavy Hydrogen. *Acta Physiologica Scandinavica.* 1941;2(3-4):209-221.

60.   Rennie MJ. An introduction to the use of tracers in nutrition and metabolism. *Proc Nutr Soc.* 1999;58(4):935-944.

61. Gasier HG, Fluckey JD, Previs SF. The application of 2H2O to measure skeletal muscle protein synthesis. *Nutr Metab (Lond).* 2010;7:31.

62. Zhang XJ, Chinkes DL, Wolfe RR. Measurement of muscle protein fractional synthesis and breakdown rates from a pulse tracer injection. *Am J Physiol Endocrinol Metab.* 2002;283(4):E753-764.

63. Zhang XJ, Chinkes DL, Sakurai Y, Wolfe RR. An isotopic method for measurement of muscle protein fractional breakdown rate in vivo. *Am J Physiol.* 1996;270(5 Pt 1):E759-767.

64. Kumar V, Atherton P, Smith K, Rennie MJ. Human muscle protein synthesis and breakdown during and after exercise. *J Appl Physiol (1985).* 2009;106(6):2026-2039.

65. Phillips SM, Tipton KD, Aarsland A, Wolf SE, Wolfe RR. Mixed muscle protein synthesis and breakdown after resistance exercise in humans. *The American journal of physiology.* 1997;273:E99-107.

66. Atherton PJ, Etheridge T, Watt PW, et al. Muscle full effect after oral protein: time-dependent concordance and discordance between human muscle protein synthesis and mTORC1 signaling. *Am J Clin Nutr.* 2010;92(5):1080-1088.

67. Greenhaff PL, Karagounis LG, Peirce N, et al. Disassociation between the effects of amino acids and insulin on signaling, ubiquitin ligases, and protein turnover in human muscle. *Am J Physiol Endocrinol Metab.* 2008;295(3):E595-604.

68. Bohe J, Low JF, Wolfe RR, Rennie MJ. Latency and duration of stimulation of human muscle protein synthesis during continuous infusion of amino acids. *J Physiol.* 2001;532(Pt 2):575-579.

69. Burd NA, West DW, Moore DR, et al. Enhanced amino acid sensitivity of myofibrillar protein synthesis persists for up to 24 h after resistance exercise in young men. *J Nutr.* 2011;141(4):568-573.

70. Wilkinson SB, Phillips SM, Atherton PJ, et al. Differential effects of resistance and endurance exercise in the fed state on signalling molecule phosphorylation and protein synthesis in human muscle. *Journal of Physiology.* 2008.

71. Tang JE, Perco JG, Moore DR, Wilkinson SB, Phillips SM. Resistance training alters the response of fed state mixed muscle protein synthesis in young men. *Am J Physiol Regul Integr Comp Physiol.* 2008;294(1):R172-178.

72. Damas F, Phillips SM, Libardi CA, et al. Resistance training-induced changes in integrated myofibrillar protein synthesis are related to hypertrophy only after attenuation of muscle damage. *Journal of Physiology.* 2016.

73. Reidy PT, Borack MS, Markofski MM, et al. Post-absorptive muscle protein turnover affects resistance training hypertrophy. *European Journal of Applied Physiology.* 2017.

74. Chesley A, MacDougall JD, Tarnopolsky Ma, Atkinson Sa, Smith K. Changes in human muscle protein synthesis after resistance exercise. *Journal of applied physiology.* 1992;73:1383-1388.

75. Gundermann DM, Walker DK, Reidy PT, et al. Activation of mTORC1 signaling and protein synthesis in human muscle following blood flow restriction exercise is

inhibited by rapamycin. *Am J Physiol Endocrinol Metab.* 2014;306(10):E1198-1204.

76.   Drummond MJ, Fry CS, Glynn EL, et al. Rapamycin administration in humans blocks the contraction-induced increase in skeletal muscle protein synthesis. *J Physiol.* 2009;587(Pt 7):1535-1546.

77.   Song Z, Moore DR, Hodson N, et al. Resistance exercise initiates mechanistic target of rapamycin (mTOR) translocation and protein complex co-localisation in human skeletal muscle. *Sci Rep.* 2017;7(1):5028.

78.   Bickel CS, Slade J, Mahoney E, Haddad F, Dudley GA, Adams GR. Time course of molecular responses of human skeletal muscle to acute bouts of resistance exercise. *J Appl Physiol (1985).* 2005;98(2):482-488.

79.   Brook MS, Wilkinson DJ, Mitchell WK, et al. Skeletal muscle hypertrophy adaptations predominate in the early stages of resistance exercise training, matching deuterium oxide-derived measures of muscle protein synthesis and mechanistic target of rapamycin complex 1 signaling. *FASEB J.* 2015;29(11):4485-4496.

80.   Haddad F, Baldwin KM, Tesch PA. Pretranslational markers of contractile protein expression in human skeletal muscle: effect of limb unloading plus resistance exercise. *J Appl Physiol (1985).* 2005;98(1):46-52.

81.   Figueiredo VC, Caldow MK, Massie V, Markworth JF, Cameron-Smith D, Blazevich AJ. Ribosome biogenesis adaptation in resistance training-induced human skeletal muscle hypertrophy. *Am J Physiol Endocrinol Metab.* 2015;309(1):E72-83.

82.   Mobley CB, Haun CT, Roberson PA, et al. Biomarkers associated with low, moderate, and high vastus lateralis muscle hypertrophy following 12 weeks of resistance training. *PLoS One.* 2018;13(4):e0195203.

83.   Phillips SM, McGlory C. CrossTalk proposal: The dominant mechanism causing disuse muscle atrophy is decreased protein synthesis. *J Physiol.* 2014;592(24):5341-5343.

84.   Reid MB, Judge AR, Bodine SC. CrossTalk opposing view: The dominant mechanism causing disuse muscle atrophy is proteolysis. *J Physiol.* 2014;592(24):5345-5347.

85.   Rennie MJ, Selby A, Atherton P, et al. Facts, noise and wishful thinking: muscle protein turnover in aging and human disuse atrophy. *Scand J Med Sci Sports.* 2010;20(1):5-9.

86.   Bodine SC, Latres E, Baumhueter S, et al. Identification of ubiquitin ligases required for skeletal muscle atrophy. *Science.* 2001;294(5547):1704-1708.

87.   Schakman O, Kalista S, Barbe C, Loumaye A, Thissen JP. Glucocorticoid-induced skeletal muscle atrophy. *Int J Biochem Cell Biol.* 2013;45(10):2163-2172.

88.   Gibson JN, Halliday D, Morrison WL, et al. Decrease in human quadriceps muscle protein turnover consequent upon leg immobilization. *Clin Sci (Lond).* 1987;72(4):503-509.

89.   Paddon-Jones D, Sheffield-Moore M, Cree MG, et al. Atrophy and impaired muscle protein synthesis during prolonged inactivity and stress. *J Clin Endocrinol Metab.* 2006;91(12):4836-4841.

90.   Figueiredo VC, D'Souza RF, Van Pelt DW, et al. Ribosome biogenesis and degradation regulate translational capacity during muscle disuse and reloading. *J Cachexia Sarcopenia Muscle.* 2021;12(1):130-143.

91.   Phillips SM, Glover EI, Rennie MJ. Alterations of protein turnover underlying disuse atrophy in human skeletal muscle. *Journal of applied physiology (Bethesda, Md : 1985).* 2009;107:645-654.

92.   Tesch PA, von Walden F, Gustafsson T, Linnehan RM, Trappe TA. Skeletal muscle proteolysis in response to short-term unloading in humans. *J Appl Physiol (1985).* 2008;105(3):902-906.

93.   Gustafsson T, Osterlund T, Flanagan JN, et al. Effects of 3 days unloading on molecular regulators of muscle size in humans. *Journal of Applied Physiology.* 2010;109:721-727.

94.   Lagirand-Cantaloube J, Offner N, Csibi A, et al. The initiation factor eIF3-f is a major target for atrogin1/MAFbx function in skeletal muscle atrophy. *The EMBO journal.* 2008;27:1266-1276.

95.   Lagirand-Cantaloube J, Cornille K, Csibi A, Batonnet-Pichon S, Leibovitch MP, Leibovitch SA. Inhibition of atrogin-1/MAFbx mediated MyoD proteolysis prevents skeletal muscle atrophy in vivo. *PLoS One.* 2009;4(3):e4973.

96.   Hinnebusch AG. eIF3: a versatile scaffold for translation initiation complexes. *Trends Biochem Sci.* 2006;31(10):553-562.

97.   Csibi A, Cornille K, Leibovitch MP, et al. The translation regulatory subunit eIF3f controls the kinase-dependent mTOR signaling required for muscle differentiation and hypertrophy in mouse. *PLoS One.* 2010;5(2):e8994.

98.   Pillon NJ, Gabriel BM, Dollet L, et al. Transcriptomic profiling of skeletal muscle adaptations to exercise and inactivity. *Nat Commun.* 2020;11(1):470.

99.   Robinson MM, Dasari S, Konopka AR, et al. Enhanced Protein Translation Underlies Improved Metabolic and Physical Adaptations to Different Exercise Training Modes in Young and Old Humans. *Cell metabolism.* 2017;25:581-592.

100.   Hoffman NJ, Parker BL, Chaudhuri R, et al. Global Phosphoproteomic Analysis of Human Skeletal Muscle Reveals a Network of Exercise-Regulated Kinases and AMPK Substrates. *Cell Metab.* 2015;22(5):922-935.

101.   Potts GK, McNally RM, Blanco R, et al. A map of the phosphoproteomic alterations that occur after a bout of maximal-intensity contractions. *J Physiol.* 2017;595(15):5209-5226.

102.   Clarke K, Ricciardi S, Pearson T, et al. The Role of Eif6 in Skeletal Muscle Homeostasis Revealed by Endurance Training Co-expression Networks. *Cell Rep.* 2017;21(6):1507-1520.

103.   Stokes T, Timmons JA, Crossland H, et al. Molecular Transducers of Human Skeletal Muscle Remodeling under Different Loading States. *Cell Rep.* 2020;32(5):107980.

104.   Miller BF, Konopka AR, Hamilton KL. The rigorous study of exercise adaptations: why mRNA might not be enough. *J Appl Physiol (1985).* 2016;121(2):594-596.

105.   Schwanhausser B, Busse D, Li N, et al. Global quantification of mammalian gene expression control. *Nature.* 2011;473(7347):337-342.

106.   Li JJ, Bickel PJ, Biggin MD. System wide analyses have underestimated protein abundances and the importance of transcription in mammals. *PeerJ.* 2014;2:e270.

107.   Camera DM, Burniston JG, Pogson MA, Smiles WJ, Hawley JA. Dynamic proteome profiling of individual proteins in human skeletal muscle after a high-fat diet and resistance exercise. *FASEB J.* 2017;31(12):5478-5494.

108.   Timmons JA, Atherton PJ, Larsson O, et al. A coding and non-coding transcriptomic perspective on the genomics of human metabolic disease. *Nucleic Acids Research.* 2018;46:7772-7792.

109.   Srisawat K, Hesketh K, Cocks M, et al. Reliability of Protein Abundance and Synthesis Measurements in Human Skeletal Muscle. *Proteomics.* 2020;20(7):e1900194.

110.   Phillips BE, Williams JP, Gustafsson T, et al. Molecular Networks of Human Muscle Adaptation to Exercise and Age. *PLoS Genetics.* 2013;9.

111.   Stepto NK, Coffey VG, Carey AL, et al. Global gene expression in skeletal muscle from well-trained strength and endurance athletes. *Med Sci Sports Exerc.* 2009;41(3):546-565.

112.   Chapman MA, Arif M, Emanuelsson EB, et al. Skeletal Muscle Transcriptomic Comparison between Long-Term Trained and Untrained Men and Women. *Cell Rep.* 2020;31(12):107808.

113.   Raue U, Trappe TA, Estrem ST, et al. Transcriptome signature of resistance exercise adaptations: mixed muscle and fiber type specific profiles in young and old adults. *Journal of applied physiology (Bethesda, Md : 1985).* 2012;112:1625-1636.

114.   Schönbrodt FD, Perugini M. At what sample size do correlations stabilize? *Journal of Research in Personality.* 2013;47:609-612.

115.   Okada M, Hozumi Y, Ichimura T, et al. Interaction of nucleosome assembly proteins abolishes nuclear localization of DGKzeta by attenuating its association with importins. *Exp Cell Res.* 2011;317(20):2853-2863.

116.   You JS, Dooley MS, Kim CR, et al. A DGKzeta-FoxO-ubiquitin proteolytic axis controls fiber size during skeletal muscle remodeling. *Sci Signal.* 2018;11(530).

117.   Abadi A, Glover EI, Isfort RJ, et al. Limb immobilization induces a coordinate down-regulation of mitochondrial and other metabolic pathways in men and women. *PLoS ONE.* 2009.

118.   Chopard A, Lecunff M, Danger R, et al. Large-scale mRNA analysis of female skeletal muscles during 60 days of bed rest with and without exercise or dietary protein supplementation as countermeasures. *Physiol Genomics.* 2009;38(3):291-302.

119.   Alibegovic AC, Sonne MP, Hojbjerre L, et al. Insulin resistance induced by physical inactivity is associated with multiple transcriptional changes in skeletal muscle in young men. *Am J Physiol Endocrinol Metab.* 2010;299(5):E752-763.

120.   McGlory C, Von Allmen MT, Stokes T, et al. Failed recovery of glycemic control and myofibrillar protein synthesis with 2 wk of physical inactivity in overweight, prediabetic older adults. *Journals of Gerontology - Series A Biological Sciences and Medical Sciences.* 2018;73.

121. Rullman E, Fernandez-Gonzalo R, Mekjavic IB, Gustafsson T, Eiken O. MEF2 as upstream regulator of the transcriptome signature in human skeletal muscle during unloading. *Am J Physiol Regul Integr Comp Physiol.* 2018;315(4):R799-R809.

122. Fernandez-Gonzalo R, Tesch PA, Lundberg TR, Alkner BA, Rullman E, Gustafsson T. Three months of bed rest induce a residual transcriptomic signature resilient to resistance exercise countermeasures. *FASEB J.* 2020;34(6):7958-7969.

123. Lin J, Handschin C, Spiegelman BM. Metabolic control through the PGC-1 family of transcription coactivators. *Cell Metab.* 2005;1(6):361-370.

124. Brocca L, Cannavino J, Coletto L, et al. The time course of the adaptations of human muscle proteome to bed rest and the underlying mechanisms. *J Physiol.* 2012;590(20):5211-5230.

125. Xu R, Andres-Mateos E, Mejias R, et al. Hibernating squirrel muscle activates the endurance exercise pathway despite prolonged immobilization. *Exp Neurol.* 2013;247:392-401.

126. Pearen MA, Muscat GE. Minireview: Nuclear hormone receptor 4A signaling: implications for metabolic disease. *Mol Endocrinol.* 2010;24(10):1891-1903.

127. Samuel VT, Shulman GI. Mechanisms for insulin resistance: common threads and missing links. *Cell.* 2012;148(5):852-871.

128. Phillips SM, McGlory C. CrossTalk proposal: The dominant mechanism causing disuse muscle atrophy is decreased protein synthesis. *The Journal of Physiology.* 2014;592:5341-5343.

129. Kenny HC, Tascher G, Ziemianin A, et al. Effectiveness of Resistive Vibration Exercise and Whey Protein Supplementation Plus Alkaline Salt on the Skeletal Muscle Proteome Following 21 Days of Bed Rest in Healthy Males. *J Proteome Res.* 2020.

130. Csibi A, Leibovitch MP, Cornille K, Tintignac LA, Leibovitch SA. MAFbx/Atrogin-1 controls the activity of the initiation factor eIF3-f in skeletal muscle atrophy by targeting multiple C-terminal lysines. *J Biol Chem.* 2009;284(7):4413-4421.

131. Sweeney TE, Haynes WA, Vallania F, Ioannidis JP, Khatri P. Methods to increase reproducibility in differential gene expression via meta-analysis. *Nucleic Acids Res.* 2017;45(1):e1.

132. Timmons JA, Szkop KJ, Gallagher IJ. Multiple sources of bias confound functional enrichment analysis of global -omics data. *Genome Biol.* 2015;16:186.

133. Timmons JA, Knudsen S, Rankinen T, et al. Using molecular classification to predict gains in maximal aerobic capacity following endurance exercise training in humans. *J Appl Physiol (1985).* 2010;108(6):1487-1496.

134. Haun CT, Vann CG, Roberts BM, Vigotsky AD, Schoenfeld BJ, Roberts MD. A Critical Evaluation of the Biological Construct Skeletal Muscle Hypertrophy: Size Matters but So Does the Measurement. *Front Physiol.* 2019;10:247.

135. Heymsfield SB, Adamek M, Gonzalez MC, Jia G, Thomas DM. Assessing skeletal muscle mass: historical overview and state of the art. *J Cachexia Sarcopenia Muscle.* 2014;5(1):9-18.

136. Janssen I, Heymsfield SB, Baumgartner RN, Ross R. Estimation of skeletal muscle mass by bioelectrical impedance analysis. *J Appl Physiol (1985).* 2000;89(2):465-471.
137. Proctor DN, O'Brien PC, Atkinson EJ, Nair KS. Comparison of techniques to estimate total body skeletal muscle mass in people of different age groups. *Am J Physiol.* 1999;277(3):E489-495.
138. Parker L, Nazarian LN, Carrino JA, et al. Musculoskeletal imaging: medicare use, costs, and potential for cost substitution. *J Am Coll Radiol.* 2008;5(3):182-188.
139. Franchi MV, Longo S, Mallinson J, et al. Muscle thickness correlates to muscle cross-sectional area in the assessment of strength training-induced hypertrophy. *Scandinavian Journal of Medicine and Science in Sports.* 2018.
140. Franchi MV, Raiteri BJ, Longo S, Sinha S, Narici MV, Csapo R. Muscle Architecture Assessment: Strengths, Shortcomings and New Frontiers of in Vivo Imaging Techniques. *Ultrasound Med Biol.* 2018;44(12):2492-2504.
141. McKendry J, Stokes T, McLeod JC, Phillips SM. Resistance Exercise, Aging, Disuse, and Muscle Protein Metabolism. *Compr Physiol.* 2021;11(3):2249-2278.
142. Wolfe RR. The underappreciated role of muscle in health and disease 1 2 3. 2006:475-482.
143. Clark RV, Walker AC, O'Connor-Semmes RL, et al. Total body skeletal muscle mass: estimation by creatine (methyl-d3) dilution in humans. *J Appl Physiol (1985).* 2014;116(12):1605-1613.
144. Madden KM, Feldman B, Arishenkoff S, Meneilly GS. A rapid point-of-care ultrasound marker for muscle mass and muscle strength in older adults. *Age Ageing.* 2021;50(2):505-510.
145. Berger J, Bunout D, Barrera G, et al. Rectus femoris (RF) ultrasound for the assessment of muscle mass in older people. *Arch Gerontol Geriatr.* 2015;61(1):33-38.
146. Hammond K, Mampilly J, Laghi FA, et al. Validity and reliability of rectus femoris ultrasound measurements: Comparison of curved-array and linear-array transducers. *J Rehabil Res Dev.* 2014;51(7):1155-1164.
147. Reeves ND, Maganaris CN, Narici MV. Ultrasonographic assessment of human skeletal muscle size. *European Journal of Applied Physiology.* 2004.
148. MacGillivray TJ, Ross E, Simpson HA, Greig CA. 3D freehand ultrasound for in vivo determination of human skeletal muscle volume. *Ultrasound Med Biol.* 2009;35(6):928-935.
149. Sipila S, Suominen H. Muscle ultrasonography and computed tomography in elderly trained and untrained women. *Muscle Nerve.* 1993;16(3):294-300.
150. Rutten IJ, van Dijk DP, Kruitwagen RF, Beets-Tan RG, Olde Damink SW, van Gorp T. Loss of skeletal muscle during neoadjuvant chemotherapy is related to decreased survival in ovarian cancer patients. *J Cachexia Sarcopenia Muscle.* 2016;7(4):458-466.
151. Puthucheary ZA, Rawal J, McPhail M, et al. Acute skeletal muscle wasting in critical illness. *JAMA.* 2013;310(15):1591-1600.

152. Ahtiainen JP, Hoffren M, Hulmi JJ, et al. Panoramic ultrasonography is a valid method to measure changes in skeletal muscle cross-sectional area. *Eur J Appl Physiol.* 2010;108(2):273-279.
153. Franchi MV, Fitze DP, Hanimann J, Sarto F, Sporri J. Panoramic ultrasound vs. MRI for the assessment of hamstrings cross-sectional area and volume in a large athletic cohort. *Sci Rep.* 2020;10(1):14144.
154. Hernandez-Belmonte A, Martinez-Cava A, Pallares JG. Panoramic ultrasound requires a trained operator and specific evaluation sites to maximize its sensitivity: A comprehensive analysis of the measurement errors. *Physiol Behav.* 2022:113737.
155. Scott JM, Martin DS, Ploutz-Snyder R, et al. Reliability and validity of panoramic ultrasound for muscle quantification. *Ultrasound Med Biol.* 2012;38(9):1656-1661.
156. Scott JM, Martin DS, Ploutz-Snyder R, et al. Panoramic ultrasound: a novel and valid tool for monitoring change in muscle mass. *J Cachexia Sarcopenia Muscle.* 2017;8(3):475-481.
157. Earp JE, Newton RU, Cormie P, Blazevich AJ. Inhomogeneous Quadriceps Femoris Hypertrophy in Response to Strength and Power Training. *Med Sci Sports Exerc.* 2015;47(11):2389-2397.
158. Franchi MV, Atherton PJ, Reeves ND, et al. Architectural, functional and molecular responses to concentric and eccentric loading in human skeletal muscle. *Acta Physiol (Oxf).* 2014;210(3):642-654.
159. Mangine GT, Redd MJ, Gonzalez AM, et al. Resistance training does not induce uniform adaptations to quadriceps. *PLoS One.* 2018;13(8):e0198304.
160. Infantolino BW, Gales DJ, Winter SL, Challis JH. The validity of ultrasound estimation of muscle volumes. *J Appl Biomech.* 2007;23(3):213-217.
161. Nordez A, Jolivet E, Sudhoff I, Bonneau D, de Guise JA, Skalli W. Comparison of methods to assess quadriceps muscle volume using magnetic resonance imaging. *J Magn Reson Imaging.* 2009;30(5):1116-1123.
162. Goodpaster BH, Thaete FL, Kelley DE. Thigh adipose tissue distribution is associated with insulin resistance in obesity and in type 2 diabetes mellitus. *Am J Clin Nutr.* 2000;71(4):885-892.
163. Goodpaster BH, Theriault R, Watkins SC, Kelley DE. Intramuscular lipid content is increased in obesity and decreased by weight loss. *Metabolism.* 2000;49(4):467-472.
164. Visser M, Kritchevsky SB, Goodpaster BH, et al. Leg muscle mass and composition in relation to lower extremity performance in men and women aged 70 to 79: the health, aging and body composition study. *J Am Geriatr Soc.* 2002;50(5):897-904.
165. Brook MS, Wilkinson DJ, Mitchell WK, et al. Synchronous deficits in cumulative muscle protein synthesis and ribosomal biogenesis underlie age-related anabolic resistance to exercise in humans. *Journal of Physiology.* 2016.
166. Narici MV, Roi GS, Landoni L, Minetti AE, Cerretelli P. Changes in force, cross-sectional area and neural activation during strength training and detraining of the human quadriceps. *Eur J Appl Physiol Occup Physiol.* 1989;59(4):310-319.

167. Beyer KS, Fukuda DH, Boone CH, et al. Short-Term Unilateral Resistance Training Results in Cross Education of Strength Without Changes in Muscle Size, Activation, or Endocrine Response. *J Strength Cond Res.* 2016;30(5):1213-1223.

168. Timmons JA. Variability in training-induced skeletal muscle adaptation. *J Appl Physiol (1985).* 2011;110(3):846-853.

169. Kim JS, Petrella JK, Cross JM, Bamman MM. Load-mediated downregulation of myostatin mRNA is not sufficient to promote myofiber hypertrophy in humans: a cluster analysis. *J Appl Physiol (1985).* 2007;103(5):1488-1495.

170. Miotto PM, McGlory C, Bahniwal R, Kamal M, Phillips SM, Holloway GP. Supplementation with dietary ω-3 mitigates immobilization-induced reductions in skeletal muscle mitochondrial respiration in young women. *The FASEB Journal.* 2019.

171. Willis CRG, Gallagher IJ, Wilkinson DJ, et al. Transcriptomic links to muscle mass loss and declines in cumulative muscle protein synthesis during short-term disuse in healthy younger humans. *FASEB J.* 2021;35(9):e21830.

172. Kon M, Ohiwa N, Honda A, et al. Effects of systemic hypoxia on human muscular adaptations to resistance exercise training. *Physiol Rep.* 2015;3(1).

173. Porter C, Reidy PT, Bhattarai N, Sidossis LS, Rasmussen BB. Resistance Exercise Training Alters Mitochondrial Function in Human Skeletal Muscle. *Med Sci Sports Exerc.* 2015;47(9):1922-1931.

174. Tang JE, Hartman JW, Phillips SM. Increased muscle oxidative potential following resistance training induced fibre hypertrophy in young men. *Appl Physiol Nutr Metab.* 2006;31(5):495-501.

175. Salvadego D, Domenis R, Lazzer S, et al. Skeletal muscle oxidative function in vivo and ex vivo in athletes with marked hypertrophy from resistance training. *J Appl Physiol (1985).* 2013;114(11):1527-1535.

176. Larsen S, Nielsen J, Hansen CN, et al. Biomarkers of mitochondrial content in skeletal muscle of healthy young human subjects. *J Physiol.* 2012;590(14):3349-3360.

177. Diebold LP, Gil HJ, Gao P, Martinez CA, Weinberg SE, Chandel NS. Mitochondrial complex III is necessary for endothelial cell proliferation during angiogenesis. *Nature Metabolism.* 2019.

178. Holloway TM, Snijders T, Van Kranenburg J, Van Loon LJC, Verdijk LB. Temporal Response of Angiogenesis and Hypertrophy to Resistance Training in Young Men. *Medicine and Science in Sports and Exercise.* 2018.

179. Snijders T, Nederveen JP, Joanisse S, et al. Muscle fibre capillarization is a critical factor in muscle fibre hypertrophy during resistance exercise training in older men. *Journal of Cachexia, Sarcopenia and Muscle.* 2017;8:267-276.

180. Copley Salem C, Ulrich C, Quilici D, Schlauch K, Buxton ILO, Burkin H. Mechanical strain induced phospho-proteomic signaling in uterine smooth muscle cells. *Journal of Biomechanics.* 2018;73:99-107.

181. Hsia DA, Mitra SK, Hauck CR, et al. Differential regulation of cell motility and invasion by FAK. *J Cell Biol.* 2003;160(5):753-767.

182. Brugnera E, Haney L, Grimsley C, et al. Unconventional Rac-GEF activity is mediated through the Dock180-ELMO complex. *Nat Cell Biol.* 2002;4(8):574-582.

183. Kiyokawa E, Hashimoto Y, Kobayashi S, Sugimura H, Kurata T, Matsuda M. Activation of Rac1 by a Crk SH3-binding protein, DOCK180. *Genes Dev.* 1998;12(21):3331-3336.

184. Moore CA, Parkin CA, Bidet Y, Ingham PW. A role for the Myoblast city homologues Dock1 and Dock5 and the adaptor proteins Crk and Crk-like in zebrafish myoblast fusion. *Development.* 2007;134(17):3145-3153.

185. Ratushnyy AY, Buravkova LB. Expression of focal adhesion genes in mesenchymal stem cells under simulated microgravity. *Dokl Biochem Biophys.* 2017;477(1):354-356.

186. McDonald MLN, Won S, Mattheisen M, et al. Body mass index change in gastrointestinal cancer and chronic obstructive pulmonary disease is associated with Dedicator of Cytokinesis 1. *Journal of Cachexia, Sarcopenia and Muscle.* 2017;8:428-436.

187. Tan W, Palmby TR, Gavard J, Amornphimoltham P, Zheng Y, Gutkind JS. An essential role for Rac1 in endothelial cell function and vascular development. *FASEB J.* 2008;22(6):1829-1838.

188. Benson CE, Southgate L. The DOCK protein family in vascular development and disease. *Angiogenesis.* 2021;24(3):417-433.

189. Crossland H, Atherton PJ, omberg A, Gustafsson T, Timmons JA. A reverse genetics cell-based evaluation of genes linked to healthy human tissue age. *FASEB Journal.* 2017;31:96-108.

190. *Exploring the reproducibility of probabilistic causal molecular network models* 2017.

191. Tian B, Hu J, Zhang H, Lutz CS. A large-scale analysis of mRNA polyadenylation of human and mouse genes. *Nucleic Acids Res.* 2005;33(1):201-212.

192. Mayr C. Regulation by 3 -Untranslated Regions. *Annual Review of Genetics.* 2017;51:171-194.

193. Kozak M. An analysis of 5'-noncoding sequences from 699 vertebrate messenger RNAs. *Nucleic Acids Res.* 1987;15(20):8125-8148.

194. Bohlen J, Fenzl K, Kramer G, Bukau B, Teleman AA. Selective 40S Footprinting Reveals Cap-Tethered Ribosome Scanning in Human Cells. *Mol Cell.* 2020;79(4):561-574 e565.

195. Van den Plas D, Merregaert J. Constitutive overexpression of the integral membrane protein Itm2A enhances myogenic differentiation of C2C12 cells. *Cell Biol Int.* 2004;28(3):199-207.

196. Namkoong S, Lee KI, Lee JI, et al. The integral membrane protein ITM2A, a transcriptional target of PKA-CREB, regulates autophagic flux via interaction with the vacuolar ATPase. *Autophagy.* 2015;11(5):756-768.

197. Page DJ, Thuret R, Venkatraman L, Takahashi T, Bentley K, Herbert SP. Positive Feedback Defines the Timing, Magnitude, and Robustness of Angiogenesis. *Cell Rep.* 2019;27(11):3139-3151 e3135.

198. Ghadiali RS, Guimond SE, Turnbull JE, Pisconti A. Dynamic changes in heparan sulfate during muscle differentiation and ageing regulate myoblast cell fate and FGF2 signalling. *Matrix Biology.* 2017;59:54-68.
199. Mayr C, Bartel DP. Widespread shortening of 3'UTRs by alternative cleavage and polyadenylation activates oncogenes in cancer cells. *Cell.* 2009;138(4):673-684.
200. Gruber AR, Martin G, Muller P, et al. Global 3' UTR shortening has a limited effect on protein abundance in proliferating T cells. *Nat Commun.* 2014;5:5465.
201. Gallagher IJ, Scheele C, Keller P, et al. Integration of microRNA changes in vivo identifies novel molecular features of muscle insulin resistance in type 2 diabetes. *Genome Medicine.* 2010;2:9.
202. Gruber AJ, Zavolan M. Alternative cleavage and polyadenylation in health and disease. *Nat Rev Genet.* 2019;20(10):599-614.
203. Hoque M, Ji Z, Zheng D, et al. Analysis of alternative cleavage and polyadenylation by 3' region extraction and deep sequencing. *Nat Methods.* 2013;10(2):133-139.
204. Vinel C, Lukjanenko L, Batut A, et al. The exerkine apelin reverses age-associated sarcopenia. *Nature Medicine.* 2018;24:1360-1371.
205. Son JS, Chae SA, Wang H, et al. Maternal Inactivity Programs Skeletal Muscle Dysfunction in Offspring Mice by Attenuating Apelin Signaling and Mitochondrial Biogenesis. *Cell Rep.* 2020;33(9):108461.
206. Hammarstrom D, Ofsteng SJ, Jacobsen NB, Flobergseter KB, Ronnestad BR, Ellefsen S. Ribosome accumulation during early phase resistance training in humans. *Acta Physiol (Oxf).* 2022:e13806.
207. Goel AJ, Rieder MK, Arnold HH, Radice GL, Krauss RS. Niche Cadherins Control the Quiescence-to-Activation Transition in Muscle Stem Cells. *Cell Rep.* 2017;21(8):2236-2250.
208. Lundberg TR, Martinez-Aranda LM, Sanz G, et al. Early accentuated muscle hypertrophy is strongly associated with myonuclear accretion. *Am J Physiol Regul Integr Comp Physiol.* 2020;319(1):R50-R58.
209. Angleri V, Damas F, Phillips SM, et al. Resistance training variable manipulations is less relevant than intrinsic biology in affecting muscle fiber hypertrophy. *Scand J Med Sci Sports.* 2022.
210. Dou GR, Wang YC, Hu XB, et al. RBP-J, the transcription factor downstream of Notch receptors, is essential for the maintenance of vascular homeostasis in adult mice. *FASEB J.* 2008;22(5):1606-1617.
211. Biolo G, Williams BD, Fleming RY, Wolfe RR. Insulin action on muscle protein kinetics and amino acid transport during recovery after resistance exercise. *Diabetes.* 1999;48(5):949-957.
212. Biolo G, Tipton KD, Klein S, Wolfe RR. An abundant supply of amino acids enhances the metabolic effect of exercise on muscle protein. *Am J Physiol.* 1997;273(1 Pt 1):E122-129.
213. Borsheim E, Tipton KD, Wolf SE, Wolfe RR. Essential amino acids and muscle protein recovery from resistance exercise. *Am J Physiol Endocrinol Metab.* 2002;283(4):E648-657.

214. Phillips SM, Tipton KD, Ferrando AA, Wolfe RR. Resistance training reduces the acute exercise-induced increase in muscle protein turnover. *Am J Physiol.* 1999;276(1):E118-124.
215. Damas F, Phillips S, Vechin FC, Ugrinowitsch C. A review of resistance training-induced changes in skeletal muscle protein synthesis and their contribution to hypertrophy. *Sports Med.* 2015;45(6):801-807.
216. Phillips SM, Parise G, Roy BD, Tipton KD, Wolfe RR, Tamopolsky MA. Resistance-training-induced adaptations in skeletal muscle protein turnover in the fed state. *Can J Physiol Pharmacol.* 2002;80(11):1045-1053.
217. Kim PL, Staron RS, Phillips SM. Fasted-state skeletal muscle protein synthesis after resistance exercise is altered with training. *J Physiol.* 2005;568(Pt 1):283-290.
218. Abou Sawan S, Hodson N, Malowany JM, et al. Trained Integrated Post-Exercise Myofibrillar Protein Synthesis Rates Correlate with Hypertrophy in Young Males and Females. *Med Sci Sports Exerc.* 2022.
219. Wall BT, Dirks ML, Snijders T, Senden JMG, Dolmans J, Van Loon LJC. Substantial skeletal muscle loss occurs during only 5 days of disuse. *Acta Physiologica.* 2014;210:600-611.
220. Kilroe SP, Fulford J, Holwerda AM, et al. Short-term muscle disuse induces a rapid and sustained decline in daily myofibrillar protein synthesis rates. *Am J Physiol Endocrinol Metab.* 2020;318(2):E117-E130.
221. Ferrando AA, Lane HW, Stuart CA, Davis-Street J, Wolfe RR. Prolonged bed rest decreases skeletal muscle and whole body protein synthesis. *Am J Physiol.* 1996;270(4 Pt 1):E627-633.
222. Symons TB, Sheffield-Moore M, Chinkes DL, Ferrando AA, Paddon-Jones D. Artificial gravity maintains skeletal muscle protein synthesis during 21 days of simulated microgravity. *J Appl Physiol (1985).* 2009;107(1):34-38.
223. Reid MB, Judge AR, Bodine SC. CrossTalk opposing view: The dominant mechanism causing disuse muscle atrophy is proteolysis. *The Journal of physiology.* 2014;592:5345-5347.
224. Urso ML, Scrimgeour AG, Chen YW, Thompson PD, Clarkson PM. Analysis of human skeletal muscle after 48 h immobilization reveals alterations in mRNA and protein for extracellular matrix components. *J Appl Physiol (1985).* 2006;101(4):1136-1148.
225. Sandri M, Barberi L, Bijlsma AY, et al. Signalling pathways regulating muscle mass in ageing skeletal muscle. the role of the IGF1-Akt-mTOR-FoxO pathway. *Biogerontology.* 2013;14:303-323.
226. Lin KH, Wilson GM, Blanco R, et al. A deep analysis of the proteomic and phosphoproteomic alterations that occur in skeletal muscle after the onset of immobilization. *J Physiol.* 2021;599(11):2887-2906.
227. Drummond MJ, Dickinson JM, Fry CS, et al. Bed rest impairs skeletal muscle amino acid transporter expression, mTORC1 signaling, and protein synthesis in response to essential amino acids in older adults. *American journal of physiology Endocrinology and metabolism.* 2012;302:E1113-1122.

228. Peterson TR, Laplante M, Thoreen CC, et al. DEPTOR is an mTOR inhibitor frequently overexpressed in multiple myeloma cells and required for their survival. *Cell.* 2009;137(5):873-886.

229. Kazi AA, Hong-Brown L, Lang SM, Lang CH. Deptor knockdown enhances mTOR Activity and protein synthesis in myocytes and ameliorates disuse muscle atrophy. *Mol Med.* 2011;17(9-10):925-936.

230. Catena V, Fanciulli M. Deptor: not only a mTOR inhibitor. *J Exp Clin Cancer Res.* 2017;36(1):12.

231. Gamrin L, Berg HE, Essen P, et al. The effect of unloading on protein synthesis in human skeletal muscle. *Acta Physiol Scand.* 1998;163(4):369-377.

232. Miyazaki M, Shimozuru M, Tsubota T. Skeletal muscles of hibernating black bears show minimal atrophy and phenotype shifting despite prolonged physical inactivity and starvation. *PLoS One.* 2019;14(4):e0215489.

233. Molenaars M, Janssens GE, Williams EG, et al. A Conserved Mito-Cytosolic Translational Balance Links Two Longevity Pathways. *Cell Metab.* 2020;31(3):549-563 e547.

234. Deane CS, Willis CRG, Phillips BE, et al. Transcriptomic meta-analysis of disuse muscle atrophy vs. resistance exercise-induced hypertrophy in young and older humans. *J Cachexia Sarcopenia Muscle.* 2021;12(3):629-645.

235. Adams CM, Ebert SM, Dyle MC. Role of ATF4 in skeletal muscle atrophy. *Curr Opin Clin Nutr Metab Care.* 2017;20(3):164-168.

236. Ebert SM, Bullard SA, Basisty N, et al. Activating transcription factor 4 (ATF4) promotes skeletal muscle atrophy by forming a heterodimer with the transcriptional regulator C/EBPbeta. *J Biol Chem.* 2020;295(9):2787-2803.